THE UNIVERSITY
of EDINBURGH

Novel regulators of cancer stem cell biology in acute myeloid leukaemia

Jasmin Paris

A thesis submitted in fulfilment of the requirements for the degree of Doctor of Philosophy

University of Edinburgh

2019

Author's declaration

This is to certify that that the work contained within has been composed by me and is entirely my own work. No part of this thesis has been submitted for any other degree or professional qualification.

Jasmin Paris

August 2019

Abstract

Lifelong haematopoiesis depends critically on a small population of bone marrow resident haematopoietic stem cells (HSCs), which possess unique self-renewal capacity and multilineage differentiation potential, ultimately replenishing all blood lineages. In view of these properties, HSC transplantation (HSCT) is an effective treatment for a wide range of bone marrow disorders. However, owing to the rarity of HSCs in adult haematopoiesis, and our inability to effectively expand HSCs *in vitro*, the clinical need for HSCT vastly exceeds HSC availability.

Acute myeloid leukaemia (AML) is an aggressive clonal disorder of haematopoietic stem and progenitor cells (HSPCs), in which the acquisition of mutations by HSPCs results in a block in their myeloid differentiation, and the generation of self-renewing leukaemic stem cells (LSCs). LSCs initiate and propagate the disease, and given that they are treatment-resistant, often fuel disease relapses. The two major challenges in the field of haematopoiesis currently, are therefore to expand HSCs for transplantation, and to identify novel therapeutic targets to eliminate LSCs.

In the last decade, epitranscriptomics has developed as a novel layer of regulation of gene expression. RNA N^6-methyladenosine (m^6A) is the most abundant internal mRNA modification. m^6A is installed on mRNA by methyltransferase complexes known as writers and removed by demethylases defined as erasers. The m^6A modification is recognised by reader proteins, including those belonging to the YTH domain family (YTHDF1, YTHDF2, YTHDF3, YTHDC1, YTHDC2). While writers and erasers have been implicated in several cancers, including AML, the roles of m^6A readers in normal and malignant haematopoiesis remains unexplored.

This thesis describes the study of the YTHDF2 m^6A reader in normal haematopoiesis and AML. Using the *Vav-iCre* system to conditionally delete *Ythdf2* from the haematopoietic system of mice, we observed a significant increase in the number of haematopoietic stem and progenitor cells (HSPCs) compared to controls. In primary and secondary long-term competitive transplantation assays, *Ythdf2*-deficient HSCs reconstituted multilineage haematopoiesis and showed an increased capacity to rapidly repopulate the myeloid lineage. Furthermore, bone marrow analysis 4 months after transplantation revealed an increased contribution of *Ythdf2*-deficient cells to the

HSPC compartments of transplanted mice compared to controls. To study the role of *Ythdf2* in AML, we compared the ability of *Ythdf2*-deficient and control pre-LSCs to generate leukaemia in a murine retroviral AML model. We showed that constitutive (*Vav-iCre*) and inducible (*Mx1-Cre*) genetic deletion of *Ythdf2* severely compromises the development and propagation of leukaemia driven by a range of oncogenes, including *Meis1/Hoxa9*, *Mll-AF9*, *PML-RARA* and *MOZ-TIF2*. Mechanistically, we showed that loss of *Ythdf2* inhibits degradation of multiple m^6A-modified transcripts, including *Tnfrsf2*, whose upregulation sensitizes *Ythdf2*-deficient LSCs to TNF-induced apoptosis.

In summary, we demonstrated that inhibition of *Ythdf2* specifically compromises LSC development and propagation, but simultaneously expands HSCs and enhances their myeloid reconstitution upon transplantation. We therefore propose YTHDF2 as a unique therapeutic target whose inhibition selectively targets LSCs while promoting HSC expansion.

Lay summary

In healthy humans, blood is produced throughout life from a rare population of bone marrow stem cells. These cells can be used to treat a variety of diseases, but are currently in very short supply. Acute myeloid leukaemia is an aggressive cancer of white blood cells, with a poor long-term survival owing to frequent recurrence of disease after treatment. The research of our group is therefore aimed towards these two major areas; identifying new strategies for the expansion of blood stem cells, and finding ways to eliminate cancer cells in acute myeloid leukaemia.

In an attempt to answer these questions, we have focused on a novel area of research, which studies how RNA is processed and broken down. RNA is a code which allows genes to be translated into proteins, ultimately guiding all biological processes. However, it is now known that certain modifications, for example methylation, can determine how well and how long RNA functions for. For example, YTHDF2 is a protein which recognises methylated RNA and targets it for breakdown in the cell. In the course of my PhD, I have studied the role of YTHDF2 in normal blood formation, and also in acute myeloid leukaemia.

Using a mouse model, I showed high levels of YTHDF2 in the cells which give rise to the blood system. I also showed that deletion of the gene *Ythdf2* specifically within the blood system results in an expansion of the primitive, founder bone marrow stem cells. Finally, I showed that *Ythdf2*-deficient cells generate leukaemia in mice with a significant delay compared to control cells, indicating that YTHDF2 is required for leukaemia development.

Overall, the results summarised in this thesis show that YTHDF2 inhibition might allow us to expand the cells which generate blood, and simultaneously eliminate those which drive blood cancer. In this case, YTHDF2 could become a very important treatment target.

Table of contents

Author's declaration *3*

Abstract *5*

Lay summary *7*

Table of contents *9*

Table of figures *13*

Table of tables *15*

Related publications *17*

Abbreviations *19*

Acknowledgements *23*

Chapter 1: Introduction *25*

1.1 Haematopoiesis **25**

1.1.1 The haematopoietic hierarchy 25

1.1.2 Immunophenotypic characterisation of murine HSCs and progenitor cells 30

1.1.3 Functional characterisation of murine HSCs and progenitor cells 32

1.1.4 Developmental origins of the haematopoietic system 33

1.1.5 Properties of HSCs 35

1.1.6 The HSC niche 36

1.1.7 Haematopoietic transcription factors 39

1.1.8 HSC expansion *ex vivo* 41

1.2 Leukaemia **43**

1.2.1 Acute myeloid leukaemia (AML) 44

1.2.2 Epidemiology of AML 44

1.2.3 Classification of AML 45

1.2.4 Pathophysiology of AML 47

1.2.5 Cytogenetics of AML 49

1.2.5.1 t(15;17) PML-RARA 49

1.2.5.2 t(8;21) AML1-ETO 49

1.2.5.3 Inv(16) CBFβ-MYH11 50

1.2.5.4 MLL-fusions 50

1.2.5.5 Meis1/Hoxa9 51

1.2.5.6 MOZ-TIF2 52

1.2.6 Molecular abnormalities of AML 52

1.2.7 Clinical presentation of AML 56

1.2.8 Diagnosis of AML 56

1.2.8.1 Immunophenotyping 57

1.2.9 Treatment of AML 58

1.2.10 Prognosis of AML 60

1.3 Epitranscriptomics as a novel layer of regulation of gene expression **61**

1.3.1 RNA modifications 61

1.3.1.1 2'-O-methylation (Nm) 63

1.3.1.2 5-methylcytosine (m^5C) and 5-hydroxymethylcytosine (hm^5C) 63

1.3.1.3 N^1-Methyladenosine (m^1A) 64

1.3.1.4 Pseudouridine (ψ) 64

1.3.1.5 N^6-methyladenosine (m^6A) 65

1.3.2 m^{6}A regulators 65
1.3.2.1 m^{6}A writers 66
1.3.2.2 m^{6}A erasers 68
1.3.2.3 m^{6}A readers 69
1.3.3 YTHDF2 71
1.3.4 Roles of m^{6}A 73
1.3.5 m^{6}A in cancer 74
1.4 Hypothesis and aims 77
Chapter 2: Methods 79
2.1 Mouse strains 79
2.2 Mouse husbandry 79
2.3 Genotyping 79
2.3.1 DNA extraction 79
2.3.2 PCR primers and programmes 80
2.3.2.1 *Vav-iCre* PCR 80
2.3.2.2 *Mx1-Cre* PCR 80
2.3.2.3 *Ythdf2* flox PCR 81
2.3.2.4 Sexing PCR 81
2.3.3 Gel electrophoresis 82
2.4 Cell lines and primary murine cells 82
2.4.1 HEK 293/HEK 293T 82
2.4.2 Platinum-E (Plat-E) 83
2.4.3 NIH3T3 83
2.4.4 Primary murine cells 83
2.5 Cell culture 83
2.5.1 Freezing cells 84
2.6 Blood sampling 84
2.7 Preparation of bone marrow, spleen, thymus and foetal liver cell suspensions 85
2.8 Immunophenotypic characterisation of white blood cells (WBCs) 85
2.9 Transformation and maxiprep of plasmid DNA 88
2.10 Retrovirus/lentivirus production 88
2.10.1 Lentiviral constructs 90
2.10.2 Retroviral constructs 90
2.10.3 Packaging virus 91
2.11 Isolation of murine foetal liver HSPCs 92
2.12 Transduction of murine HSPCs 93
2.13 Colony forming assay 95
2.13.1 Methylcellulose preparation 95
2.13.2 Colony culture assays in 3231 methylcellulose 95
2.13.3 Colony culture assays in 3434 methylcellulose 96
2.14 Cell sorting 96
2.15 Transplantation assays 97
2.15.1 Non-leukaemic transplantation assays 97
2.15.2 Leukaemic transplantation assays 98

2.15.3 Monitoring of mice transplanted with non-leukaemic haematopoietic cells..... 98
2.15.4 Leukaemic monitoring 100

2.16 Preparation and administration of polyinosinic-polycytidylic acid (Poly(I:C))..... 101

2.17 shRNA-mediated *Tnfrsf1b* knockdown 102

2.18 RNA extraction for Affymetrix and m^{6}A meRIP-Seq (TRIzol™ Method)..... 102

2.19 Affymetrix..... 103

2.20 m^{6}A meRIP-Seq..... 103

2.21 SLAM-Seq..... 103
2.21.1 S4U cytotoxicity assay.....104
2.21.2 S4U catabolic kinetics assay 106

2.22 RIBO-Seq..... 107

2.23 Generation of Figure 5.4.6B. 108

2.24 Statistical analyses..... 109

2.25 Accession 110

Chapter 3: The role of YTHDF2 in normal haematopoiesis 111

3.1 Introduction..... 111
3.1.1. The role of RNA N^6-methyladenosine in normal haematopoiesis 111

3.2 Aims..... 118

3.3 Outline of experiments described in Chapter 3 118

3.4. Results 119
3.4.1 Expression of *Ythdf2* in the HSPC compartment 119
3.4.2 Generation and validation of *Ythdf2*$^{fl/fl}$;*Vav-iCre* mice.....122
3.4.3 Ablation of *Ythdf2* affects cell distribution within stem and progenitor cell compartments 125
3.4.4 *Ythdf2* loss affects myeloerythroid progenitor numbers, but not *in vitro* differentiation capacity 127
3.4.5 *Ythdf2* loss affects T lymphocyte cell homeostasis.....131
3.4.6 Ablation of *Ythdf2* enhances HSC function – FL HSC transplantation.....134
3.4.7 Ablation of *Ythdf2* enhances HSC function – BM HSC transplantation.....139

3.5 Discussion..... 144

Chapter 4: The role of YTHDF2 in malignant haematopoiesis 149

4.1 Introduction..... 149
4.1.1 The role of m^{6}A in acute myeloid leukaemia.....149
4.1.2 Leukaemia models.....153
4.1.2.1 Meis1/Hoxa9.....154
4.1.2.2 Mll-AF9 155
4.1.2.3 PML-RARA.....155
4.1.2.4 MOZ-TIF2.....156

4.2 Aims..... 156

4.3 Outline of experiments described in Chapter 4 156

4.4 Results 156
4.4.1 Ythdf2 is required for leukaemic transformation in vitro 157

4.4.2 Immunophenotypic characterisation of transformed colonies 160
4.4.3. *Ythdf2* inactivation compromises development of *Meis1/Hoxa9* leukaemia *in vivo* 162
4.4.4. *Ythdf2* inactivation may compromise development of *Mll-AF9* leukaemia *in vivo* 166
4.4.5 Acute deletion of *Ythdf2* impairs LSC development and AML propagation in mice 168
4.4.5.1 Acute deletion of *Ythdf2* in pre-LSCs slows leukaemic engraftment 169
4.4.5.2 Acute deletion of Ythdf2 in LSCs impairs maintenance and propagation of AML 170

4.5 Discussion 175

Chapter 5: Mechanisms of YTHDF2 function in leukaemogenesis 179

5.1 Introduction 179
5.1.1 Mechanisms of m^{6}A machinery in AML 179
5.1.2 Molecular methods used to investigate the mechanism of YTHDF2 in AML 180
5.1.2.1 RNA microarray 180
5.1.2.2 m^{6}A meRIP-Seq 181
5.1.2.3 SLAM-Seq 181
5.1.2.4 RIBO-Seq 182

5.2 Aims 183

5.3 Outline of experiments described in Chapter 5 183

5.4 Results 184
5.4.1 Loss of *Ythdf2* results in deregulated gene expression 184
5.4.2 m^{6}A methylated transcripts are upregulated in *Ythdf2*-deficient pre-leukaemic cells 187
5.4.3 m^{6}A methylated transcripts in pre-leukaemic cells are also upregulated in *Ythdf2*-deficient leukaemic cells 189
5.4.4 *Ythdf2* loss increases half-life of methylated transcripts 191
5.4.5 *Ythdf2* loss does not alter translational efficiency 193
5.4.6 Interrogation of *Ythdf2* molecular pathways 194
5.4.7 *Tnfrsf1b* knockdown does not fully rescue impaired leukaemic transformation potential of *Ythdf2*-deficient cells *in vitro*, or delayed leukaemic development *in vivo* 200

5.5 Discussion 203

Chapter 6: Conclusions and future work 209

Appendix: Supplementary tables relating to Chapter 5 213

References 241

Table of figures

Figure	Title
1.1.1	Classical and revised representations of the haematopoietic hierarchy
1.1.2	Cell surface markers used for the immunophenotypic characterisation of murine and human haematopoietic stem and progenitor cells
1.1.4	Sites of haematopoiesis during mouse development
1.1.5	Haematopoietic stem cell fates
1.1.6	The adult BM HSC niche
1.2	Schematic overview of the main types of leukaemia
1.2.2	UK incidence of AML by sex and age, for the period from 2010 to 2015
1.2.4	Leukaemic stem cells propagate AML and are difficult to eradicate
1.2.6	Driver gene mutations in AML
1.3.1	Common chemical modifications in eukaryotic mRNA transcripts
1.3.2	m^6A writers, erasers and readers
2.10	Lentiviral production schematic
2.12	The hypothesized mechanism of RetroNectin® mediated transduction
2.15.3.1	Syngeneic model that allows tracking of transplanted haematopoietic cells (normal or leukaemic) in recipient mice
2.15.3.2	Two methods of evaluating engraftment of $CD45.2^+$ donor cells within recipient mice
2.21.1	S4U cytotoxicity curves for (A) *Ythdf2*$^{fl/fl}$ and (B) *Ythdf2*$^{fl/fl}$;*Vav-iCre* pre-LSC cells
3.4.1	*YTHDF2* expression within the haematopoietic system
3.4.2	Generation and validation of *Ythdf2*$^{fl/fl}$;*Vav-iCre* mice
3.4.3	Ablation of *Ythdf2* affects cell distribution within stem and progenitor cell compartments
3.4.4	*Ythdf2* loss affects myeloerythroid progenitor numbers, but not *in vitro* differentiation capacity
3.4.5	*Ythdf2* loss results in altered T cell homeostasis
3.4.6	Ablation of *Ythdf2* enhances the function of FL HSCs
3.4.7	Ablation of *Ythdf2* enhances the function of BM HSCs
4.1.1	The role of m^6A regulators in AML
4.4.1	*Ythdf2*-deficient c-Kit^+ cells show reduced transformation capacity *in vitro*
4.4.2	Immunophenotypic characterisation reveals no differences between *Ythdf2*-deficient and control *Meis1*/*Hoxa9* transformed pre-LSCs
4.4.3	*Ythdf2* inactivation compromises development of leukaemia in a *Meis1*/*Hoxa9* murine AML model

4.4.4 *Ythdf2* inactivation may compromise development of leukaemia in a *Mll-AF9* murine AML model

4.4.5 Acute deletion of *Ythdf2* impairs LSC development and AML propagation in mice

5.1.2.3 SLAM-Seq workflow

5.4.1 Acute deletion of *Ythdf2* impairs LSC development and AML propagation in mice

5.4.2 m^6A methylated transcripts are upregulated in *Ythdf2*-deficient pre-leukaemic cells

5.4.3 m^6A methylated transcripts in pre-leukaemic cells are also upregulated in *Ythdf2*-deficient leukaemic cells

5.4.4 *Ythdf2* loss increases half-life of methylated transcripts

5.4.5 *Ythdf2* loss does not alter translational efficiency

5.4.6 *TNFRSF1B* gene expression is decreased in different AML subtypes and negatively correlates with LSC activity

5.4.7 The impact of *Tnfrsf1b* knockdown on *Ythdf2*-deficient pre-leukaemic cell colony formation *in vitro* and engraftment *in vivo*

6 The effect of targeting *Ythdf2* on normal and malignant haematopoiesis

Table of tables

Table	Title
1.1.7	Haematopoietic transcription factors
1.2.3A	Summary of the FAB classification of AML
1.2.3B	Summary of the WHO classification of AML
1.2.6	Recurrent gene mutations in AML
1.2.8.1	Two step immunophenotyping process for AML
1.2.9	Novel therapies for AML, additional to cytarabine / anthracycline treatment
1.2.10	Risk stratification in AML
1.3.2.1	Components of the m^6A writer complex and their functions
1.3.2.3	m^6A readers and their functions
1.3.5	The role of m^6A regulators in cancer
2.3.3	Gel electrophoresis resolution of specific PCR products
2.8.1	Biotin-conjugated lineage antibody cocktails
2.8.2	Flow cytometry antibodies
2.12	Selection markers for transfer plasmids used during viral production
2.17	shRNA for *Tnfrsf1b* knockdown
2.21.1	S4U dilution series used for cytotoxicity assay
2.21.2	S4U half-maximal inhibitory concentration (IC_{50}) and experimental working concentration (IC_{10}) in *Ythdf2*$^{fl/fl}$ and *Ythdf2*$^{fl/fl}$;*Vav-iCre* pre-LSC cells
3.1.1	Summary of studies targeting m^6A regulators in haematopoiesis
3.4.5	Peripheral blood counts of 8-10 week old *Ythdf2*$^{fl/fl}$ and *Ythdf2*$^{fl/fl}$;*Vav-iCre* mice

Related publications

Vukovic M., Sepulveda C., Subramani C., Guitart A. V., Mohr J., Allen L., Panagopoulou T. I., **Paris J.**, Lawson H., Villacreces A., Armesilla-Diaz A., Gezer D., Holyoake T. L., Ratcliffe P. J. and Kranc K. R. (2016). Adult hematopoietic stem cells lacking Hif-1α self-renew normally. *Blood*, *127* (23), 2841–2846.

Guitart A., Panagopoulou P., Villacreces A., Vukovic M., Sepulveda C., Allen L., Carter R., van de Lagemaat L., Morgan M., Giles P., Sas Z., Gonzalez M., Lawson H., **Paris J.**, Edwards-Hicks J., Schaak K., Subramani C., Gezer D., Armesilla-Diaz A., Wills J., Easterbrook A., Coman D., So C., O'Carroll D., Vernimmen D., Rodrigues N., Pollard P., Morton N., Finch A and Kranc K. R. (2017). Fumarate hydratase is a critical metabolic regulator of haematopoietic stem cell functions. *JEM*, *214* (3), 719.

O'Duibhir O., **Paris J.**, Lawson H., Vukovic M., Sepulveda C., Shenton D., Carragher N and Kranc K. R. (2018). Machine learning enables live label-free phenotypic screening in three dimensions. *ASSAY and Drug Development Technologies*, *16* (1).

Paris J., Morgan M., Campos J., Spencer G. J., Shmakova A., Ivanova I., Mapperley C., Lawson H., Wotherspoon D. A., Sepulveda C., Vukovic M., Allen L., Sarapuu A., Tavosanis A., Guitart A. V., Villacreces A., Much C., Choe J., Azar A., van de Lagemaat L. N., Vernimmen D., Nehme A., Mazurier F., Somervaille T. C. P., Gregory R. I., O'Carroll D., Kranc K. R. (2019). Targeting the RNA m6A Reader YTHDF2 Selectively Compromises Cancer Stem Cells in Acute Myeloid Leukemia. *Cell stem cell*. 25 (1):137-148.

Abbreviations

ψ	Pseudouridine
5-FU	5-Fluorouracil
AGM	Aorta-gonad mesonephros
ALKBH	Alkylation repair homolog
AHR	Aryl hydrocarbon receptor
ALL	Acute lymphocytic leukaemia
AML	Acute myeloid leukaemia
BCL-2	B-cell lymphoma 2
bHLH	Basic helix-loop-helix
BM	Bone marrow
bp	base pairs
BRD4	Bromodomain containing protein 4
BrdU	5-bromo-2'-deoxyuridine
CEBPA	CCAAT/enhancer binding protein alpha
CFC	Colony-forming cell
CFU-S	Colony-forming unit spleen
c-Kit	Tyrosine-protein kinase (mast/stem cell growth factor receptor (SCFR) or CD117)
CLIP	UV crosslinking and immunoprecipitation
CLL	Chronic lymphocytic leukaemia
CLP	Common lymphoid progenitor
CML	Chronic myeloid leukaemia
CMP	Common myeloid progenitor
CMRP	Common myeloid cell restricted MyRP
CRM1	Chromosome maintenance protein 1
CTLA4	Cytotoxic T-lymphocyte associated protein 4
CXCL12	CXC motif chemokine 12
DGCR8	DiGeorge syndrome chromosomal [or critical] region 8
dHSC	Definitive haematopoietic stem cell
DMEM	Dulbecco's modified eagle's medium
DNMT3	DNA (cytosine-5)-methyltransferase 3
dpc	Days post coitum
E	Embryonic day
EDTA	Ethylenediaminetetraacetic acid
EGFR	Epidermal growth factor receptor
EHT	Endothelial-to-haematopoietic transition
eIF3	Eukaryotic initiation factor 3
ENL	Eleven–nineteen-leukaemia gene
ER	Endoplasmic reticulum
ETS	E26 transformation specific
EZH1	Enhancer of zeste 1 polycomb repressive complex 2 subunit
f^6A	N^6-formyladenosine
FAB	French-American-British classification

FACS	Fluorescence-activated cell sorting
FBS	Foetal bovine serum
FISH	Fluorescence in situ hybridization
FL	Foetal liver
FLT3	Fms related tyrosine kinase 3
FMR1	Fragile X mental retardation 1
FOXO1	Forkhead Box O1
FSC	Forward scatter
FTO	Fat mass and obesity associated
GATA	GATA binding protein
GFP	Green fluorescent protein
GM	Granulocyte/macrophage
GM-CSF	Granulocyte-macrophage colony-stimulating factor
GMP	Granulocyte/macrophage progenitor
GO	Gene ontology
Gy	Gray
HDC	Histone deacetylase complex
HIF	Hypoxia inducible factor
HIV	Human immunodeficiency virus
HLA-DR	Human Leukocyte Antigen – DR isotype
hm^5C	5-hydroxymethylcytosine
hm^6A	N^6-hydroxymethyladenosine
HOX	Homeobox
HPC-1	Haematopoietic progenitor cell-1
HPC-2	Haematopoietic progenitor cell-2
HSC	Haematopoietic stem cell
HSCT	Haematopoietic stem cell transplant
HSPC	Haematopoietic stem and progenitor cell
hUCB	Human umbilical cord blood
IAA	Iodoacetamide
iCre	Improved Cre recombinase
IDH 1/2	Isocitrate dehydrogenase1/2
IGF2BP	Insulin-like growth factor 2 mRNA-binding protein
IL	Interleukin
IMDM	Iscove's modified dulbecco's medium
ITD	Internal tandem mutation
IT-HSC	Intermediate-term haematopoietic stem cell
KD	Knockdown
KO	Knockout
LB	Lysogeny broth
LDA	Limiting dilution assay
Lineage (Lin^-)	Haematopoietic cell population that does not express mature haematopoietic markers
LK	$Lineage^-$ $c\text{-}Kit^+$
LMO2	LIM domain only 2
LMPP	Lymphoid-primed multipotent progenitors

LSC	Leukaemic stem cell
LSK	Lineage$^-$ Sca-1$^+$ c-Kit$^+$
LT-HSC	Long-term haematopoietic stem cell
LTR	Long terminal repeat
m^1A	N^1-methyladenosine
m^1G	1-methylguanosine
m^5C	5-methylcytosine
m^5U	5-methyluridine
m^6A_m	N^6,2'-O-dimethyladenosine
m^7G	7-methylguanosine
MAT2A	Methionine adenosyltransferase 2A
$mcm5s^2U$	5-methoxycarbonyl-methyl-2-thiouridine
MDS	Myelodysplastic syndrome
MEIS	Myeloid ectopic insertion site
MEP	Megakaryocyte/erythroid progenitors
MERP	Megakaryocyte-erythroid restricted MyRP
METTL	Methyltransferase like
Mk	Megakaryocyte
MkRP	Megakaryocyte restricted MyRP
MLL	Mixed lineage leukaemia
MLL-AF9	Mixed lineage leukaemia translocated AF9 protein
MPO	Myeloperoxidase
MPP	Multipotent progenitor
mRNA	Messenger RNA
MS	Mass spectrometry
MSC	Mesenchymal stem cell
MSCV	Murine stem cell virus
MSPC	Mesenchymal stem progenitor cell
MX1	Myxovirus resistance 1
MyRP	Myeloid restricted progenitor with long term repopulating capacity
Nm	2'-O-methylation
NMP1	Nucleophosmin 1
OPN	Osteopontin
P300/CBP	P300/Creb-binding protein
PCR	Polymerase chain reaction
PB	Peripheral blood
P-bodies	Processing bodies
PBS	Phosphate-buffered saline
PD-1	Programmed cell death protein 1
PLT	Platelet
PNK	Polynucleotide kinase
Poly(I:C)	Polyinosinic-polycytidylic acid
Pre-LSCs	Pre-leukaemic stem cells
PU.1	Purine-rich sequence 1
qPCR	Quantitative polymerase chain reaction
RB1	Retinoblastoma gene

RBC	Red blood cell
RBM15	RNA-binding protein 15
RBP	RNA binding protein
RIBO-Seq	Ribosome profiling
RIP	RNA immunoprecipitation
rRNA	Ribosomal RNA
RT	Reverse transcription
RT-PCR	Reverse transcriptase polymerase chain reaction
RUNX1	Runt-related transcription factor 1
S4U	4-Thiouridine
SAM	S-adenosyl methionine
SCA-1	Stem cell antigen-1
SCF	Stem cell factor
SCL	Stem cell leukaemia
shRNA	short-hairpin RNA
SLAM	Signalling lymphocyte activation molecule
snoRNA	Small nucleolar RNA
SOCS2	Suppressor of cytokine signalling 2
SOX2	Sex determining region Y-box 2
SR1	StemRegenin 1
SSC	Side scatter
STAT3	Signal transducer and activator of transcription 3
ST-HSC	Short-term haematopoietic stem cell
TALE	Three amino acids loop extension
TdT	Terminal deoxynucleotidyl transferase
TET	Ten-eleven-translocation gene
TIE2	Tyrosine protein kinase receptor Tie-2
TF	Transcription factor
TGF	Transforming growth factor
tRNA	Transfer RNA
UTR	Untranslated region
UV	Ultraviolet
VCAM1	Vascular cell adhesion protein 1
VEGF	Vascular endothelial growth factor
VIRMA	Vir like m^6A methyltransferase associated
WBC	White blood cell
WHO	World Health Organisation
WT1	Wilm's tumour 1
WTAP1	Wilms tumour 1 associated protein
XIST	X-inactive specific transcript
YTHDF	YTH-domain containing family
ZC3H13	Zinc finger CCCH domain-containing protein 13
ZFP217	Zinc finger protein 217

Acknowledgements

Firstly, I would like to express my sincere gratitude to my supervisor Prof Kamil Kranc, for his support throughout my PhD study, his patience and encouragement, and his great generosity in time, resources and knowledge. I was truly lucky to find a place in your group.

Besides my supervisor, I would like to thank the rest of my thesis committee: Prof Elaine Dzierzak and Prof Charlie Gourley, for their time, encouragement and insight.

To all my Kranc group lab-mates, a huge thank you for all the fun: the afternoon tea-and-cake days, the vegetable patch attempts, and the endless laughs. With your help, big experiments lasted a day rather than two, and science chat came to make sense. Before I joined you, an ECAT colleague told me, 'The Kranc group are an amazing team to be part of', they could not have been more right.

To Fiona Rossi and Claire Cryer of the FACS lab, thank you so much for all your help, and for going above and beyond on countless occasions to fit my experiments in.

To my own little family of Konrad, Rowan and Moss, thank you for making me the happiest mummy, and letting me be a scientist and a runner too, I am so lucky to have you.

Lastly, and most importantly, thank you to my parents Jeff and Alena, for the most wonderful childhood, for teaching me to love learning, and for showing me how to find happiness in nature and in kindness. I will always aspire to make you proud.

Chapter 1: Introduction

1.1 Haematopoiesis

The term ‘haematopoiesis’, originating from the Greek words ‘haima’ (blood) and ‘poiēsis’ (to make something) refers to the production of all cellular components of blood. Haematopoiesis depends critically on a relatively rare population of bone marrow resident haematopoietic stem cells (HSCs) which possess unique self-renewal ability and multilineage differentiation potential, ultimately replenishing all blood lineages (Orkin and Zon 2008).

1.1.1 The haematopoietic hierarchy

The classical model of haematopoiesis is a stepwise hierarchy, in which multipotent HSCs reside at the apex and generate oligopotent progenitors, which in turn give rise to lineage committed unipotent progenitors, and finally mature blood cells. However, it is now widely accepted that this classical model is an oversimplification, prompting several recent revisions to the haematopoietic hierarchy (Zhang, Gao et al. 2018).

The existence of the haematopoietic stem cell, and the hierarchical organisation of haematopoiesis, was first proposed by Maximov, in 1909. In the 1950s, researchers showed that injection of allogeneic bone marrow (BM) into guinea pigs and mice was able to rescue them from the effects of lethal irradiation (Jacobson, Simmons et al. 1951, Lorenz, Congdon et al. 1952). In 1960s the *in vivo* colony forming unit spleen (CFU-S) assay was used to demonstrate that single haematopoietic precursors were capable of multilineage differentiation potential (Till and McCulloch 1961, Becker, McCulloch et al. 1963, Wu, Till et al. 1967). In 1980s, cell surface markers were identified for the isolation of murine HSCs, after which transplantation of these cells was shown to reconstitute all blood lineages. This was followed by the sequential characterisation of HSCs and their progenies (Spangrude, Heimfeld et al. 1988, Kondo, Weissman et al. 1997, Akashi, Traver et al. 2000) to generate the classical haematopoietic hierarchy, with revisions as required when new cell types were identified (Adolfsson, Månsson et al. 2005, Wilson, Laurenti et al. 2008).

Until recently, two classes of HSCs were defined; long-term HSCs (LT-HSCs) capable of permanently reconstituting the haematopoietic system following lethal irradiation,

but rare and quiescent under stable conditions, and short term-HSCs (ST-HSCs), capable of rapidly differentiating to multipotent progenitors (MPPs) and reconstituting the haematopoietic system for 8-12 weeks following irradiation (Morrison, Wandycz et al. 1997, Yang, Bryder et al. 2005).

In the classical model of haematopoiesis (**Figure 1.1.1A**), LT-HSCs sit above ST-HSCs at the apex of the hierarchy. HSCs give rise to MPPs, which generate common myeloid progenitors (CMPs) or common lymphoid progenitors (CLPs). CLPs generate lymphocytes, whilst CMPs give rise to megakaryocyte/erythroid progenitors (MEPs), or granulocyte/macrophage progenitors (GMPs). MEPs generate megakaryocytes and erythrocytes, whereas GMPs generate granulocytes, macrophages, and dendritic cells (Akashi, Traver et al. 2000).

In the last decade, several developments have altered our understanding of haematopoiesis. Firstly, the advent of single cell genomic, transcriptomic and proteomic technologies has revealed marked heterogeneity in HSCs, a population of cells previously considered homogeneous based on their cell surface marker expression. For example, a subset of HSCs has been shown to express *Hdc*, which encodes histidine decarboxylase, and this population has been shown to have a bias towards myeloid differentiation *in vivo* (Chen, Deng et al. 2017). Similarly, differential expression of the SLAM markers CD150 and CD229 has been shown to separate HSCs with varying lineage potential; $CD150^{high}$ (myeloid bias), $CD150^{low}$ (lymphoid bias), CD229 negative (myeloid bias), and CD229 positive (lymphoid bias) (Beerman, Bhattacharya et al. 2010, Oguro, Ding et al. 2013).

Secondly, novel lineage tracing strategies have revealed clonal relationships between haematopoietic cells, demonstrating that lineage segregation is derived principally from HSCs, and occurs in a continuous fashion, rather than the stepwise model of classical haematopoiesis. It has been shown that megakaryocytes can develop directly from HSCs, bypassing intermediate differentiation stages (Notta, Zandi et al. 2016). Accordingly, high expression of the megakaryocyte marker von Willebrand factor has been identified in HSCs (Månsson, Hultquist et al. 2007), and these cells have been shown to depend on thrombopoietin, a cytokine essential for megakaryocytic development (de Sauvage, Carver-Moore et al. 1996, Sanjuan-Pla, Macaulay et al. 2013).

Thirdly, several new cell types have been identified prompting modification of the haematopoietic hierarchy. In addition to LT-HSCs and ST-HSCs, intermediate-term HSCs (IT-HSCs) have been identified with a self-renewal capacity midway between the two (Benveniste, Frelin et al. 2010). Furthermore, several sub-classes of MPPs have been identified (MPP1-4), with MPP1 cells having a similar role to that of ST-HSCs, and MPP2, MPP3 and MPP4 working in parallel directly downstream, with MPP2 and MPP3 predominantly generating CMPs (Wilson, Laurenti et al. 2008, Pietras, Reynaud et al. 2015). Finally, lymphoid-primed multipotent progenitors (LMPPs) have been described as a subpopulation of HSCs with high expression of *Flt3*, and a cell surface marker profile similar to that of MPP4 cells (Adolfsson, Borge et al. 2001, Adolfsson, Månsson et al. 2005, Forsberg, Serwold et al. 2006, Boyer, Schroeder et al. 2011). The revised haematopoietic hierarchy includes IT-HSCs and the four subpopulations of MPPs (**Figure 1.1.1B**).

Finally, significant plasticity has been demonstrated in the haematopoietic system in recent years, particularly in response to stress. In 2014, Sun et al. used a novel transposon tagging system for in situ labelling and clonal tracking of haematopoietic stem cells in mice, to demonstrate that in the steady state, haematopoiesis is maintained by a large number of long-lived progenitors, rather than a small number of multipotent HSC (Sun, Ramos et al. 2014). In 2015, Busch et al. reported HSC lineage tracing and outputs from a mouse model with inducible genetic labelling of primitive $Tie2^{+}$ HSCs (Busch, Klapproth et al. 2015). Consistent with the findings of Sun et al., Busch reported that steady state haematopoiesis is dependent on ST-HSCs, rather than LT-HSCs, but also concluded that long-term (>1 year), the ST-HSC compartment does require continuous input from LT-HSCs (estimate of 150 HSCs feeding in per day). Busch et al. also showed however, that under conditions of haematopoietic stress, for example 5-fluorouracil (5-FU) treatment, LT-HSCs can enter the cell cycle and proliferate rapidly to facilitate haematopoietic reconstitution (Busch, Klapproth et al. 2015).

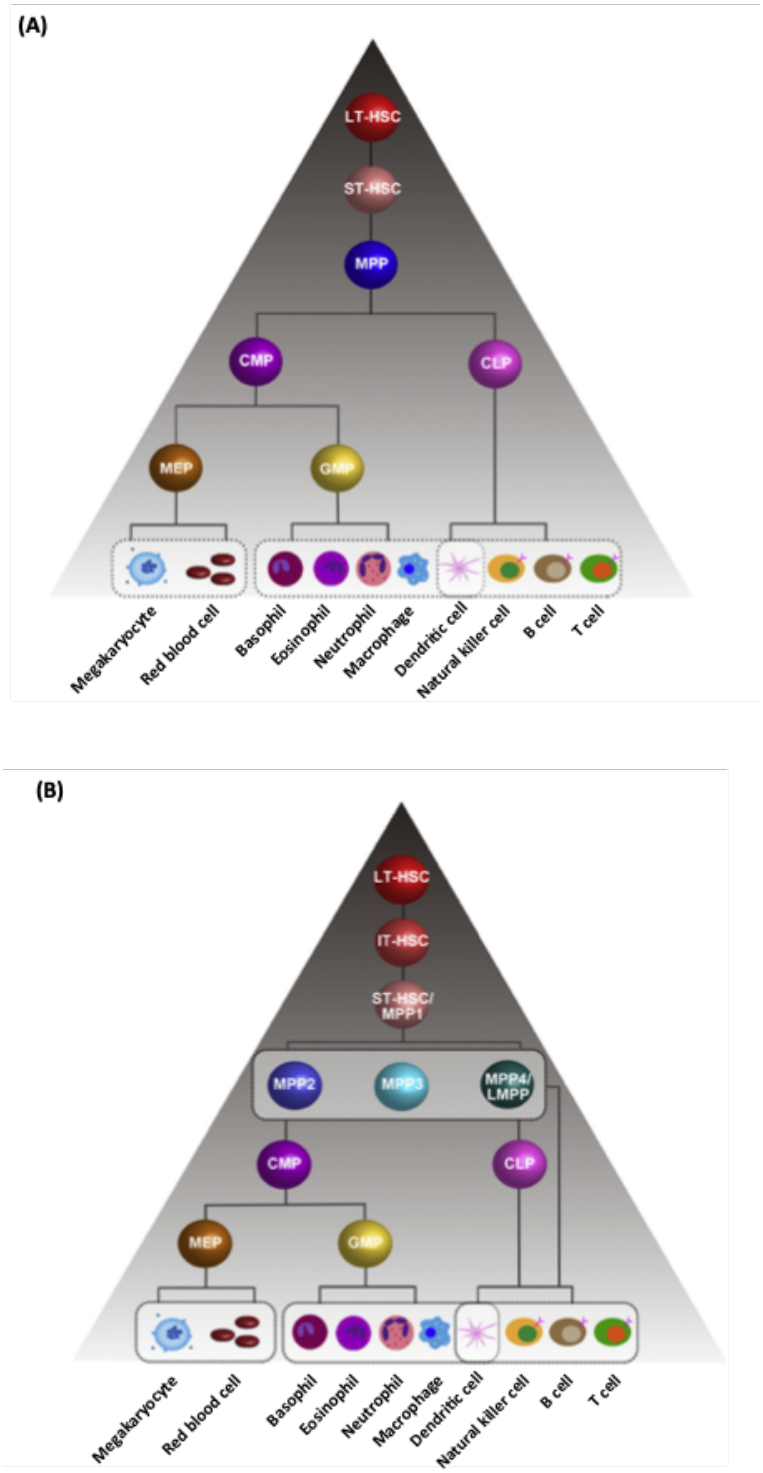

Figure 1.1.1 Classical and revised representations of the haematopoietic hierarchy. (**A**) Classical haematopoietic hierarchy, with LT-HSCs and ST-HSCs giving rise to MPPs, and then diverging to CMP or CLP progenitors. Subsequently, CLPs give rise directly to lymphoid cells, whereas CMPs generate MEPs and GMPs. MEPs generate megakaryocytes and erythrocytes, whilst GMPs generate

granulocytes, macrophages and dendritic cells. (**B**) Revised haematopoietic hierarchy, with the addition of IT-HSCs, MPP subclasses 1-4, and LMPPs. Adapted from 'Haematopoietic Hierarchy - An Updated Roadmap' (Zhang, Gao et al. 2018).

The advent of single cell RNA sequencing (scRNA-Seq) was a turning point in our understanding of the haematopoietic hierarchy. Prior to this, haematopoietic research had long focused on single cells, through colony forming assays *in vitro*, and single cell transplantation as the gold standard assay for HSCs *in vivo*. However, molecular techniques such as bulk RNA-Seq, were compromised by an inability to detect specific gene expression changes occurring at a single cell level, which is of particular importance in a heterogeneous cell population. The advent of scRNA-Seq has allowed us to study molecular heterogeneity in a systematic fashion across the entire haematopoietic system (Laurenti and Göttgens 2018). Whilst this rapidly expanded knowledge (Velten, Haas et al. 2017, Hay, Ferchen et al. 2018, Zheng, Papalexi et al. 2018), it also generated new controversies. For example, a scRNA-Seq study by Velten et al. suggested that unilineage-restricted cells emerge directly from a 'continuum of low-primed undifferentiated HSPCs' (Velten, Haas et al. 2017). In contrast, more recent scRNA-Seq studies together with assays of chromatin stability have supported a structured hierarchy (Buenrostro, Corces et al. 2018, Pellin, Loperfido et al. 2019), including lineage directed stem cell precursors in mice (Sanjuan-Pla, Macaulay et al. 2013, Carrelha, Meng et al. 2018), the presence of sequential lymphoid progenitors in humans (Karamitros, Stoilova et al. 2018), and a previously unidentified basophil haematopoietic branchpoint (Pellin, Loperfido et al. 2019).

The concept of HSC heterogeneity has come not only from scRNA-Seq, but also from functional studies. For example, Knapp et al. performed serial transplantation assays of single human cord blood cells and showed that it is possible to prospectively isolate a population of human cord blood cells ($CD33^{+}CD34^{+}CD38^{-}CD45RA^{-}CD90^{+}CD49F^{+}$) with serially transplantable but wide-ranging cell outputs (Knapp, Hammond et al. 2018). By measuring mitogenic response, DNA methylation, 40-protein content and transcriptional profile at the single cell level, they were able to demonstrate heterogeneity both within and across cell populations (Knapp, Hammond et al. 2018). Another example is the work by Yamamoto et al., who combined a single cell transplantation system and marker mice to demonstrate the existence of myeloid restricted progenitors with long term repopulating capacity (MyRPs) in the

phenotypically defined HSC compartment (Yamamoto, Morita et al. 2013). They showed that these MyRPs are lineage committed to megakaryocytes, megakaryocyte-erythroid cells, or common myeloid cells (MkRPs, MERPs, or CMRPs, respectively). When these authors combined their single cell transplantation assays with paired daughter cell assays, they showed that HSCs can undergo symmetric division to generate two daughter HSCs, or asymmetric division to yield HSC-MkRP or HSC-CMRP pairs. These direct differentiation pathways were described as 'myeloid bypass' pathways, potentially essential for fast responses to ablation stress (Yamamoto, Morita et al. 2013).

1.1.2 Immunophenotypic characterisation of murine HSCs and progenitor cells

Our understanding of the haematopoietic hierarchy has expanded significantly in the last 30 years thanks to the immunophenotypic characterisation of murine haematopoietic stem and progenitor cells (HSPCs). In 1988, Weissman's group showed that a population of haematopoietic cells with ST-HSC activity could be isolated from BM based on the expression of stem cell antigen-1 (Sca-1), low expression of Thy1.1, and a lack of expression of lineage markers (Spangrude, Heimfeld et al. 1988). Subsequent work by the same group showed that this lineage negative (Lin^-), $Sca\text{-}1^+$, Thy1.1 low population also contained LT-HSCs (Uchida and Weissman 1992). However, a major disadvantage of the staining technique was that Thy1.1 is not expressed in all strains of mice, critically not in C57/BL6 mice, which are used widely for haematopoietic transplantation studies (Spangrude and Brooks 1992).

In 1992, Ikuta et al. showed that 5-10% of all BM cells express the stem cell growth factor receptor CD117, also referred to as c-Kit (Ikuta and Weissman 1992). The same year, Okada et al. showed that by combining c-Kit and stem cell antigen-1 (Sca-1) staining, a population of HSPCs could be isolated from the lineage negative fraction of BM (Lin^- $Sca\text{-}1^+$ $c\text{-}Kit^+$ cells, LSK cells) (Okada, Nakauchi et al. 1992). LSK staining thus provided a valuable tool for HSPC isolation, which is still widely used.

Further characterisation of the HSPC compartment was reported in 2001 and 2005, through the staining of LSK cells with antibodies against CD34 and Flt3. These studies showed that LT-HSCs reside within the double negative $CD34^-$ $Flt3^-$ fraction of LSK cells, and subsequently acquire these markers during the process of

differentiation, with ST-HSCs expressing CD34 (LSK $CD34^+$ $Flt3^-$), and LMPPs expressing both CD34 and Flt3 (LSK $CD34^+Flt3^+$) (Adolfsson, Borge et al. 2001, Yang, Bryder et al. 2005).

An alternative approach for isolation of HSCs is through staining with vital dyes, for example the mitochondrial binding dye rhodamine 123 (Rh123) or DNA-binding dye Hoescht 33342 (Ho 33342) (Goodell, Brose et al. 1996). Upon staining, HSCs retain very little of these dyes, owing to the high expression of drug efflux pumps in these cells. More typically however, Ho 33342 staining is used to detect a 'side population of cells' based on dual wavelength emission. Unfortunately, this method can be affected by slight changes in technique and is not as sensitive for HSCs as CD34/Flt3 staining.

Another approach for defining the HSPC compartment is through SLAM staining. SLAM proteins are a family of cell surface glycoproteins in the immunoglobulin superfamily. Kiel et al. showed that a combination of CD150, CD48 and CD224 staining can identify LT-HSC (LSK $CD150^+CD224^-CD48^-$), MPPs (LSK $CD150^-CD224^+CD48^-$), HPC-1 ($CD150^-CD224^+CD48^+$) and HPC-2 (LSK $CD150^+CD224^+CD48^+$) from murine BM (Kiel, Yilmaz et al. 2005). Kim et al. showed that the same combination of markers can be used to isolate HSPC compartments from foetal liver (Kim, He et al. 2006). In contrast to CD34/Flt3 staining, SLAM staining is not significantly affected by age, or transplantation (Yilmaz, Kiel et al. 2006). Recently, Oguro et al. showed that the combination of CD150, CD48, CD224 and CD229 can be used to identify 7 functionally distinct haematopoietic populations, including HSCs, MPPs and restricted progenitors, in a functional hierarchy which displays stepwise reductions in cell cycle quiescence, differentiation potential, and self renewal (Oguro, Ding et al. 2013).

The markers currently used to define the murine haematopoietic hierarchy are shown in **Figure 1.1.2**. Staining for CD34 and Flt3 or SLAM CD150 and CD48 is used most commonly to define HSPC populations within the LSK compartment (Guitart, Subramani et al. 2013, Takubo, Nagamatsu et al. 2013, Vukovic, Sepulveda et al. 2016, Guitart, Panagopoulou et al. 2017, Paris, Morgan et al. 2019). More differentiated progenitors can be identified and isolated based on additional cell

surface markers, such as CD16/32, CD41, CD105, and CD127 (Pronk, Rossi et al. 2007, Kent, Copley et al. 2009, Morita, Ema et al. 2010).

Human long term HSCs have been phenotypically defined as $Lin^{-}CD34^{+}CD38^{-}CD45RA^{-}CD90^{+}Rho^{lo}CD49F^{+}$, whilst human MPPs have been defined as $CD34^{+}CD38^{-}CD45RA^{-}CD90^{-}$ $CD49F^{-}$ (Majeti, Park et al. 2007, Notta, Doulatov et al. 2011). Further discussion of HSCs in this thesis will focus predominantly on murine HSCs, given that the majority of work was carried out in this species.

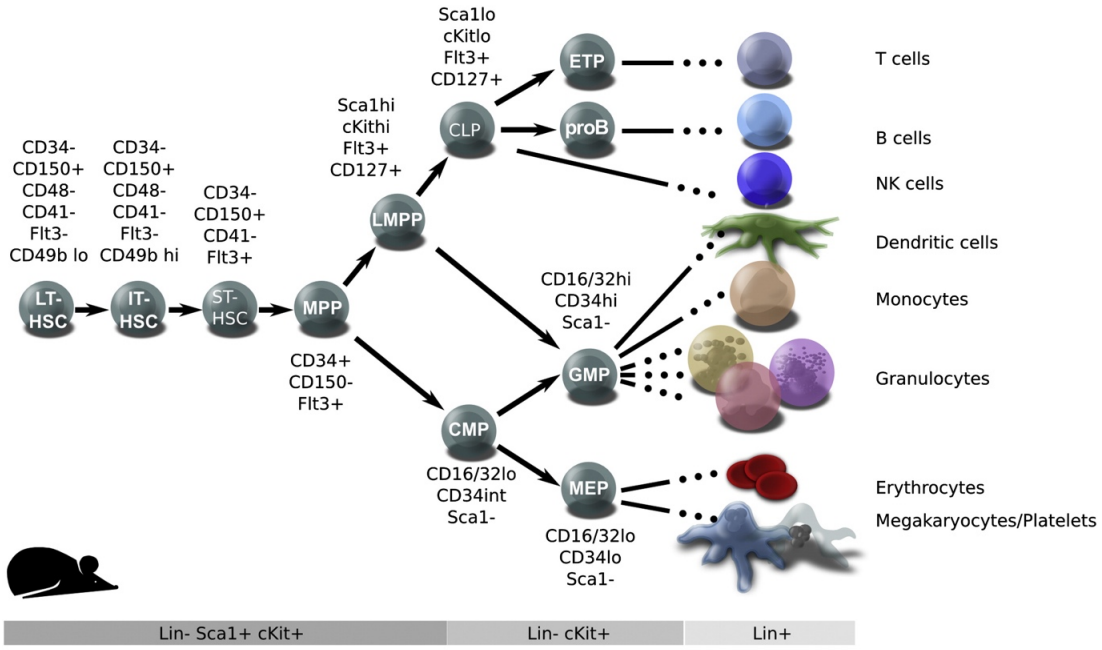

Figure 1.1.2 Cell surface markers used for the immunophenotypic characterisation of murine haematopoietic stem and progenitor cells. Figure adapted from Doulatov et al. 2012 (Doulatov, Notta et al. 2012).

It is important to note that characterising HSCs on the basis of cell surface expression cannot be considered synonymous with functional studies, which are discussed in the next section.

1.1.3 Functional characterisation of murine HSCs and progenitor cells

Colony forming cell (CFC) assays are used as an *in vitro* measure of haematopoietic progenitor cells in a given population. These assays are carried out using semi-solid

agar, or commercially available methylcellulose preparations. Colonies are scored 12 days after plating, and are largely lineage restricted, although the most immature (multipotent) do contain a mixture of granulocytes, macrophages, erythrocytes and sometimes megakaryocytes (Miller and Lai 2005).

The colony forming unit-spleen (CFU-S) assay measures the ability of transplanted haematopoietic cells to rescue an irradiated recipient mouse by colonisation of ablated haematopoietic tissue. Within 2 weeks of transplantation, CFU-S cells seed into the spleen and generate colonies of differentiating haematopoietic cells. Macroscopically visible colonies can thus be counted to give a CFU-S assay result (Till 1964). Importantly, this assay measures early engrafting cells, typically ST-HSCs, or downstream progenitors. To accurately evaluate LT-HSCs, the gold standard long-term repopulating assay should be used.

The most common form of long-term repopulating assay is the competitive transplantation assay, in which the HSC potential of a given sample is measured against that of an established source (typically whole bone marrow of congenic wild type mice) (Harrison 1980). A variation of this assay involves the successive dilution of the test sample compared with the known source (limiting dilution assay), so as to establish HSC frequency (Taswell 1981, Szilvassy, Lansdorp et al. 1989, Szilvassy, Humphries et al. 1990).

1.1.4 Developmental origins of the haematopoietic system

Multiple waves of haematopoiesis take place during development (Orkin and Zon 2008). In mammals, the initial transient waves of haematopoiesis occur in the yolk sac, through haematopoietic differentiation of mesodermal cells. The first and most primitive of these waves generates mainly large nucleated erythrocytes, which provide oxygen carrying capacity to support the needs of the growing embryo. Megakaryocytes and macrophages are also generated, which contribute to tissue remodelling in the embryo (Silver and Palis 1997, Palis, Robertson et al. 1999, Tober, Koniski et al. 2007). The second wave (‘pro-definitive’ wave) follows shortly afterwards, consisting of erythromyeloid and lymphoid progenitors. There is now substantial evidence that these erythromyeloid progenitors give rise to lifelong tissue resident macrophages at many sites throughout the body, including the brain (Ginhoux, Greter et al. 2010), and possibly the liver and lung (Ginhoux and Guilliams

2016, Perdiguero and Geissmann 2016). The third wave of haematopoiesis occurs within the embryo itself, and produces the first definitive HSCs (dHSCs), i.e. HSCs capable of permanently reconstituting the haematopoietic system of an irradiated recipient. These dHSCs first appear in the ventral wall of the dorsal aorta (Müller, Medvinsky et al. 1994, De Bruijn, Ma et al. 2002) in an area known as the aorta-gonad-mesonephros (AGM) region, which is capable of autonomous production of dHSCs, as shown in explant cultures (Medvinsky and Dzierzak 1996). AGM dHSCs go on to seed multiple organs throughout the embryo, including the foetal liver, spleen, thymus and BM.

The origin of HSCs is an area of significant debate, in particular the relationship between primitive and definitive haematopoiesis. In both cases, there exists a close relationship between vascular and haematopoietic cells. The presence of yolk sac blood islands - clusters of haematopoietic precursor cells surrounded by angioblasts – first suggested that haematopoietic and endothelial cells might share a common precursor cell. Consistent with this, recent studies in bH1eGFP transgenic mouse embryos (reporter mice for embryonic globin) have shown that primitive erythroblasts emerge from haemogenic endothelial cells (Stefanska, Batta et al. 2017) or 'haemogenic angioblasts' (Lacaud and Kouskoff 2017). Similarly, definitive haematopoiesis in the AGM of the embryo has been shown to occur through a process of endothelial to haematopoietic transition (EHT) (Jaffredo, Gautier et al. 1998). Studies by North et al. have shown that expression of the haematopoietic transcription factor *Runx1* in haemogenic endothelial cells is essential for EHT to take place (North, Gu et al. 1999, North, De Bruijn et al. 2002).

A schematic for murine haematopoiesis during development is shown in **Figure 1.1.4**. In mice, primitive haematopoiesis starts around E7.5, whilst definitive haematopoiesis begins around E10.5. At this time, and for several days afterwards, HSCs are also found in the mouse placenta, although their contribution to lifelong haematopoiesis is uncertain (Gekas, Dieterlen-Lièvre et al. 2005, Ottersbach and Dzierzak 2005). By E12.5, dHSCs from the AGM have migrated to the foetal liver, and this has become the major site of foetal haematopoiesis (Morrison, Hemmati et al. 1995, Kumaravelu, Hook et al. 2002). Subsequently, haematopoiesis also takes place in the spleen, thymus and ultimately the BM (from E18.5). Postnatally and for the remainder of life, the BM is the major site of haematopoiesis (Zanjani, Ascensao et al. 1993, Clapp, Freie et al. 1995).

It has recently been shown that the definitive haematopoietic program is repressed in early embryogenesis through epigenetic silencing, and that reversal of this repression can elicit multipotency in otherwise lineage restricted haematopoietic progenitors (Vo, Kinney et al. 2018). In this study, the authors investigated the role of EZH1, which mediates methylation on histone H3 lysine 27 (Shen, Liu et al. 2008). They showed that reduced expression of *EZH1* enhances multi-lymphoid output from human pluripotent stem cells, whilst *Ezh1* deficiency in mouse embryos results in precocious emergence of functional dHSCs *in vivo* (Vo, Kinney et al. 2018).

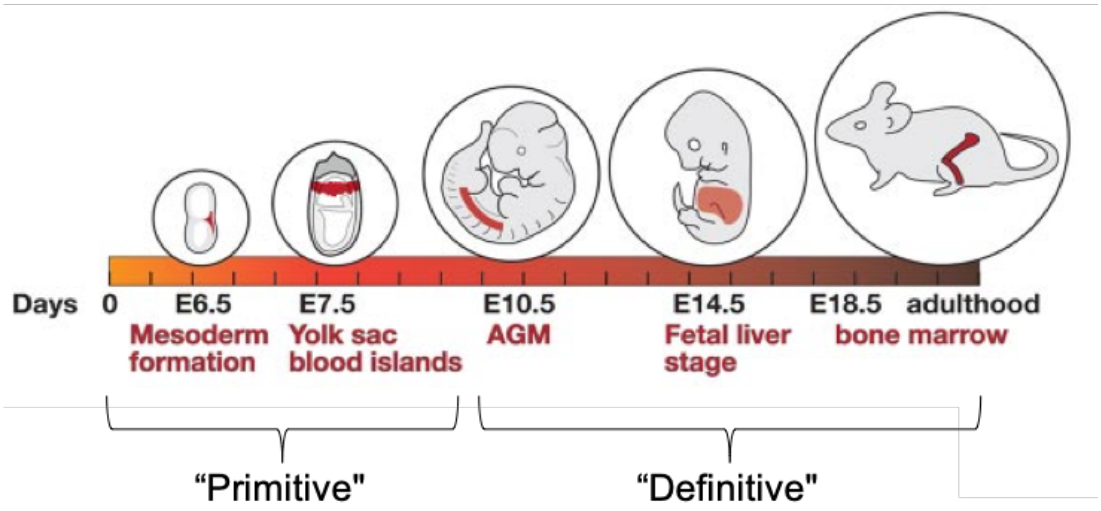

Figure 1.1.4 Sites of haematopoiesis during mouse development. Mesoderm formation (around E6.5) is followed by development of yolk sac blood islands (E7.5) which are responsible for primitive haematopoiesis. Definitive haematopoiesis begins with the emergence of HSCs in the AGM region (E10.5) and continues in the foetal liver (from E14.5), and subsequently in the BM (from E18.5 in the foetus, and then postnatally into adulthood). Adapted from Baron et al. 2012 (Baron, Isern et al. 2012).

1.1.5 Properties of HSCs

HSCs are defined by their capacity for both self-renewal and multilineage differentiation. By this definition, every time that an HSC divides, at least one of its daughter cells must become an HSC itself. Symmetric division results in expansion of the HSC pool, for example in cases of haematopoietic stress, such as transplantation or after haematopoietic injury. In contrast, asymmetric division maintains the HSC pool and multilineage differentiation under steady-state conditions

(Blank, Karlsson et al. 2008). The unique properties of HSCs make it possible for one HSC to reconstitute an entire haematopoietic system. As a result, HSC transplantation (HSCT) is a highly valued treatment modality for a range of bone marrow pathologies (Copelan 2006).

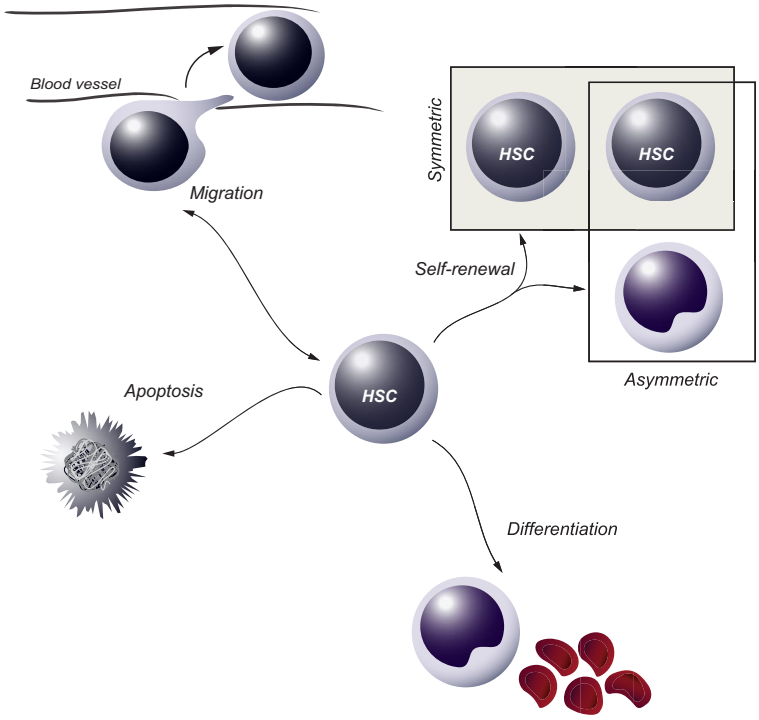

Figure 1.1.5 Haematopoietic stem cell fates. Taken from Blank et al. 2008 (Blank, Karlsson et al. 2008).

Strict regulation of HSC fate choices (**Figure 1.1.5**) is essential for the orderly maintenance of normal haematopoiesis, the ability to respond to episodes of haematopoietic stress, and the avoidance of leukaemic transformation. As in other organ systems, HSC fates are determined by a complex interplay of external stimuli (regulated by the HSC niche, see section **1.1.6**) and intracellular regulatory programs (see section **1.1.7**).

1.1.6 The HSC niche

The concept of the HSC niche was first introduced in a seminal paper by R. Schofield in 1978 (Schofield 1978), referring to the cellular, vascular and neural regulatory unit which maintains and directs HSC self-renewal and differentiation. The adult HSC

bone marrow niche is known to comprise a mixture of cell types, including osteoblasts, macrophages, megakaryocytes, endothelial cells, sympathetic nervous system cells, perivascular and perisinusoidal mesenchymal stromal/stem cells (Boulais and Frenette 2015). Complex cellular interactions are therefore likely to be involved in regulating HSC fate decisions (Wohrer, Knapp et al. 2014).

The localisation of HSCs with the BM niche remains an area of intense debate, beyond the scope of this summary (Morrison and Scadden 2014). Whilst there is a significant body of evidence to suggest that HSCs reside in a perivascular niche, supported by perivascular stromal cells and endothelial cells (Kobayashi, Butler et al. 2010, Ding, Saunders et al. 2012, Ding and Morrison 2013, Greenbaum, Hsu et al. 2013, Poulos, Guo et al. 2013), there is debate as to whether HSCs are localised primarily around sinusoids (Kiel, Yilmaz et al. 2005, Kiel, Radice et al. 2007, Nombela-Arrieta, Pivarnik et al. 2013), or near bone surfaces (Kunisaki, Bruns et al. 2013). An alternative explanation, that HSCs are uniformly distributed within the BM space, was recently published by a group which used catulin and KIT expression to identify HSCs in optically cleared BM (Acar, Kocherlakota et al. 2015).

Various BM cell types have been implicated in the regulation of HSCs within the niche. Early studies implicated an important role for osteoblasts, given their (then believed) co-localisation with HSCs in the endosteal region, as well as the decrease in lymphoid, erythroid and myeloid progenitors following conditional osteoblastic ablation (Visnjic, Kalajzic et al. 2004). Conversely, increasing the number of osteoblasts through enforced parathyroid hormone signalling, or through inactivation of bone morphogenic protein receptor type IA resulted in HSC expansion (Zhang, Niu et al. 2003). However, attempts to uncover a mechanism for the regulation of HSPCs by osteoblasts were unsuccessful, including studies of two critical cytokines known to be non-cell-autonomously required for HSC maintenance, CXC-chemokine ligand 12 (CXCL12) and stem cell factor (SCF). Conditional ablation of these cytokines in osteoblastic cells did not significantly affect HSCs (Ding, Saunders et al. 2012, Ding and Morrison 2013, Greenbaum, Hsu et al. 2013). Since then, 3D imaging studies have shown that HSCs do not significantly associate with osteoblasts in BM (Kunisaki, Bruns et al. 2013), and it is now believed that mature osteoblasts do not significantly regulate HSCs within the BM niche, but that immature osteo-lineage cells do regulate haematopoietic lymphoid progenitor cells.

Perivascular cells have been shown to play an important role in regulating HSC functions in the BM, specifically mesenchymal stem cells (MSCs), a stromal stem cell population capable of differentiation into bone, fat or cartilage. MSCs have been shown to organise niche structures capable of supporting HSCs *in vitro* and *in vivo* (Frenette, Pinho et al. 2013), within the BM and also in ectopic locations such as the renal capsule (Chan, Chen et al. 2009). Mesenchymal stem and progenitor cells (MSPCs) have been shown to express high levels of factors involved in HSC regulation, including CXCL12, SCF, ANGPT1, OPN and VCAM1 (Pinho and Frenette 2019). In this context, MSCs (enriched in a population of cells expressing GFP from regulatory elements of the *Nes* promoter) have been reported as the cell type responsible for potentiating sympathetic nervous system induced HSC mobilisation by CXCL12 (Méndez-Ferrer, Michurina et al. 2010).

Other cells involved in regulation of the HSC niche include endothelial cells, HSC descendants (macrophages, T regulatory cells, megakaryocytes) and adipocytes. Endothelial cells have been shown to regulate the HSC niche through the production of factors such as Notch ligands, CXCL12, SCF and pleiotrophin, and by promoting haematopoietic injury following regeneration (Pinho and Frenette 2019). Under stable conditions, megakaryocytes are responsible for maintaining HSC quiescence, through secretion of cell cycle regulators thrombopoietin, TGFβ1 and CXCL4 (Bruns, Lucas et al. 2014, Nakamura-Ishizu, Takubo et al. 2014, Zhao, Perry et al. 2014). In response to haematopoietic stress however, megakaryocytes secrete FGF1 and downregulate TGFβ1, resulting in expansion of the HSC pool (Zhao, Perry et al. 2014).

The complexity of the cellular interactions within the BM niche is depicted in **Figure 1.1.6**.

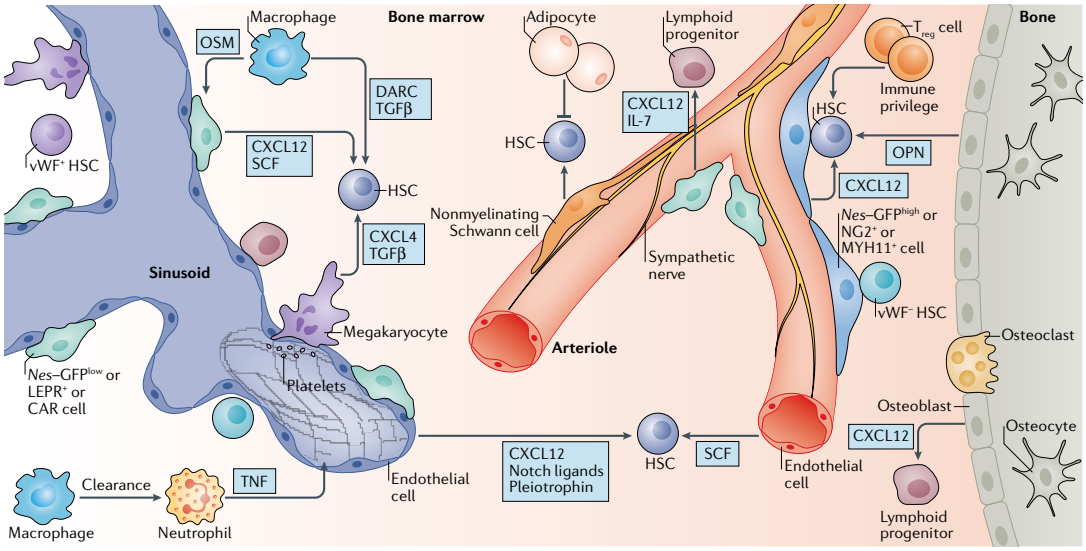

Figure 1.1.6 The adult BM HSC niche. Figure taken from Pinho et al. 2019 (Pinho and Frenette 2019).

1.1.7 Haematopoietic transcription factors

Intracellular decision making is strongly influenced by the co-ordinated action of transcriptional regulatory networks, which are composed of transcription factors (TFs) and the gene regulatory DNA sequences they bind to.

TFs can act as dominant or negative regulators of haematopoiesis. Historically, the chicken model developed by Graf et al. facilitated many of the discoveries which underlie our current understanding of haematopoiesis. In this system, multipotent progenitor cells from chickens are transformed with retrovirus containing *myb* and *ets* oncogenes. Forced expression of the transcription factor *GATA1* in these cells induces reprogramming to erythroid, eosinophil, or thromboblast (chicken megakaryocyte) lineages (Kulessa, Frampton et al. 1995). On the other hand, forced expression of *PU.1* induces myeloid differentiation (Nerlov and Graf 1998), whilst the combination *PU.1*, *GATA1* and *C/EBP* induces eosinophilic differentiation (Nerlov, McNagny et al. 1998). The concentration of TFs was also shown to be important, for example low *GATA1* expression resulted in eosinophilic differentiation, whilst high *GATA1* expression induced erythroid and megakaryocytic differentiation (Kulessa, Frampton et al. 1995). Concentration dependent haematopoietic TF effects have also been demonstrated in the mouse, where a decrease in *GATA1* concentration

interferes with the maturation of erythroid cells (McDevitt, Shivdasani et al. 1997). Whilst the aforementioned TFs act in a dominant positive way to regulate haematopoiesis, others exert negative effects, for example *Pax5* is required for B cell commitment and differentiation, and in the absence of *Pax5*, progenitors fail to restrict their lineage choice (Nutt, Heavey et al. 1999).

Whilst these studies clearly demonstrate the importance of TFs in regulation of haematopoiesis, the *in vivo* situation is significantly more complex. Recent work has therefore focused on defining more complex haematopoietic regulatory network models, with the aid of genome-wide technologies, and advanced computational analyses (Sive and Göttgens 2014). For example, Wilson et al. evaluated ten key regulators of HSPCs (Scl, Lyl1, Lmo2, Gata2, Runx1, Meis1, Pu.1, Erg, Fli-1, Gfi1b) in a murine multipotent progenitor cell line, and identified a previously unrecognized interaction between seven TFs (Scl, Lyl1, Lmo2, Gata2, Runx1, Erg and Fli1) (Wilson, Foster et al. 2010).

A summary of major haematopoietic transcription factors and their functions is provided in **Table 1.1.7**.

Transcription Factor	**Role in haematopoiesis**
Stem Cell Leukaemia (SCL)	A basic helix-loop-helix (bHLH) TF which is required for specification of haematopoiesis during development, adult HSC survival and quiescence, and terminal maturation of erythroid, megakaryocyte, and mast cell lineages (Porcher, Chagraoui et al. 2017).
Runt-related transcription factor 1 (RUNX1)	First identified as a critical regulator of haematopoiesis (Okuda, Van Deursen et al. 1996, Wang, Stacy et al. 1996). RUNX1 is a core binding factor required for the emergence of HSCs in the yolk sac, and development of HSCs throughout adulthood (de Bruijn and Dzierzak 2017).
Mixed lineage leukaemia (MLL)	MLL has a critical role in foetal and adult HSC self-renewal (McMahon, Hiew et al. 2007), and is a common translocation partner in leukaemia (Hess 2004). MLL encodes a SET-domain containing a histone methyltransferase region, which is shown to be active in chromatin remodelling, activating *Hox* genes (Milne, Briggs et al. 2002).
Lim only domain 2 (LMO2)	Member of the large zinc-finger protein LMO family (Kadrmas and Beckerle 2004). Required for definitive haematopoiesis, and commitment to the erythroid lineage (Yamada, Warren et al. 1998).

Globin transcription factor 2 (GATA2)	Member of the GATA family of zinc-finger TFs, essential for foetal and adult haematopoiesis, with a broad expression across all haematopoietic cells (Tsai, Keller et al. 1994). Involved in the production and expansion of HSCs in the AGM, and the proliferation of HSCs in the BM (Ling, Ottersbach et al. 2004).
Purine-rich sequence 1 (PU.1)	An ETS-family TF that functions in myeloid and B lymphoid lineage differentiation (Laslo, Spooner et al. 2006, Gupta, Gurudutta et al. 2009). Also binds RNA and may modulate pre-mRNA splicing (Guillouf, Gallais et al. 2006).
Homeobox A9 (HOXA9)	Member of the HOX family of homeobox genes, best recognised for their role in axial patterning (Krumlauf 1994). *HOXA9* is highly expressed in HSPCs, and its expression decreases with differentiation (Sauvageau, Lansdorp et al. 1994, Pineault, Helgason et al. 2002).
Myeloid ecotropic viral integration site 1 (MEIS1)	Member of the TALE (three amino acid loop extension) family of homeodomain transcription factors (Moskow, Bullrich et al. 1995). Regulates growth and differentiation during vertebrate development (Moens and Selleri 2006). Highly expressed in the primitive compartment, and downregulated in differentiated cells (Pineault, Helgason et al. 2002).
Leucine zipper CCAAT-enhancer binding protein α (C/EPBα)	Essential TF for neutrophilic differentiation and for the development of acute myeloid leukaemia (AML) (Avellino and Delwel 2017).

Table 1.1.7 Haematopoietic transcription factors.

Notably, more than half of all haematopoietic transcription factors identified to date were discovered first as chromosomal translocation partners in the context of leukaemia. Clearly therefore, the excessive cell proliferation and differentiation block which characterises this malignancy is not a non-specific effect but involves the disruption of critical pathways of haematopoietic transcriptional control.

1.1.8 HSC expansion *ex vivo*

HSCT can provide a new haematopoietic system and restore blood cell production in recipients (Osawa, Hanada et al. 1996, Copelan 2006, Notta, Doulatov et al. 2011). As such, HSCT is a valuable treatment modality for a variety of disorders, including cancers, bone marrow failure syndromes, and also in gene therapy settings (Copelan 2006). However, human HSCs are rare, only constituting around 0.01% of adult BM (Seita and Weissman 2010), and this limits the clinical application of HSCT therapy.

The outcome of HSCT is directly correlated with the number of HSCs transplanted. For HSCT to be successful, approximately 3-4 x 10^6/kg of recipient bodyweight HSCs are required (Al-Anazi 2012, Remberger, Törlén et al. 2015). Efficient expansion of HSCs *ex-vivo*, from human BM or umbilical cord blood, is therefore a key area of research.

Several advancements have been made in this area over the past decade. The advent of high throughput screening libraries of low molecular weight compound libraries has revealed promising new chemical compounds for *ex-vivo* HSC expansion. For example, Boitano et al. screened 100 000 small molecules and identified a purine derivative, StemRegenin 1 (SR1), capable of promoting a 50-fold *ex vivo* expansion of human cord blood-derived $CD34^+$ cells. SR1 has been showed to antagonise the aryl hydrocarbon receptor (AHR). A recent clinical trial using SR1 expanded HSCs (treated for 15 days *ex-vivo*) showed better engraftment and earlier recovery of recipient neutrophil and platelet counts compared to control HSCs. Similarly, Fares et al. screened a library of 5280 low molecular weight compounds and 300 analogues to identify a pyrimidoindole derivative UM171, which induces HSC expansion in an AHR-independent manner, and is more effective at doing so with primitive human $CD34^+CD45RA$ cells compared with SR1 (Fares, Chagraoui et al. 2014).

Another approach for ex-vivo HSC expansion has focused on engineering an appropriate ex-vivo HSC niche, through provision of cytokines, extracellular matrix components, and structural 3D architectures. For example, co-culturing human $CD34^+$ cord blood cells with mesenchymal stromal cells resulted in a 30-fold expansion of $CD34^+$ cells, and subsequently faster neutrophil engraftment times in transplanted recipients, compared to those who received control $CD34^+$ cells (De Lima, McNiece et al. 2012).

There is also growing evidence that targeting HSC metabolic pathways and endoplasmic reticulum (ER) stress pathways might potentiate improved HSC expansion *ex-vivo*. For example, it is known that FL HSCs undergo very rapid expansion *in vivo*, without showing ER stress (Sigurdsson, Takei et al. 2016). With this is mind, it is interesting that chemical chaperones capable of reducing ER stress, for example tauroursodeoxycholic acid (TUDCA) have been shown to support the

engraftment of HSCs following transplantation (Miharada, Sigurdsson et al. 2014). In terms of metabolic pathways, treatment of murine LSK cells with alexidine dihydrochloride (which inhibits mitochondrial phosphatase Ptpmt1 and can shift mitochondrial aerobic metabolism to glycolysis) was shown to triple the transplantation efficiency in a competitive transplant setting relative to control cells (Liu, Zheng et al. 2015). Active mitophagy also seems to be a mechanism for inducing HSC self-renewal, as opposed to differentiation (Ito, Turcotte et al. 2016).

Most recently, a study by Wilkinson et al. reported long term *ex-vivo* HSC expansion using a defined, albumin-free culture system. They identified a synergistic combination of thrombopoietin and low levels of fibronectin and stem cell factor to induce HSC self-renewal, and replaced serum albumin in the culture system with polyvinyl alcohol, to reduce biological contaminants. Using this approach, the authors showed between 236- and 899-fold expansions of functional HSCs over 1 month (Wilkinson, Ishida et al. 2019).

In spite of these, and many other, significant advances in the field of *ex-vivo* HSC expansion, much work remains to bring HSC availability in line with HSCT demand. Of particular importance will be to determine the relative contributions of stem cell intrinsic and niche factors in HSC self-renewal, as well as the role of hypoxia and reactive oxygen species in the ex-vivo setting (Kumar and Geiger 2017).

1.2 Leukaemia

The term ‘leukaemia’, originating from the Greek words ‘leukos’ (white) and ‘haima’ (blood) refers to a malignant proliferation of immature white blood cells. The condition typically originates in the bone marrow, and proceeds to involve the peripheral blood and extramedullary organs. Leukaemias are broadly divided into four main types, depending on the cell type of origin and its state of differentiation; acute myeloid (or myelogenous) leukaemia (AML), chronic myeloid (or myelogenous) leukaemia (CML), acute lymphocytic (or lymphoblastic) leukaemia (ALL), and chronic lymphocytic leukaemia (CLL). Polycythaemia vera and essential thrombocythaemia also fall under the umbrella classification of myeloid leukaemia. AML itself may arise *de novo* or may be preceded by a myelodysplastic phase (myelodysplastic syndrome, MDS). A schematic overview of these leukaemia subtypes is illustrated in **Figure 1.2**. The work

presented in this thesis focused on AML, as this is the commonest leukaemia affecting adult patients, and has been the focus of work in our lab for several years.

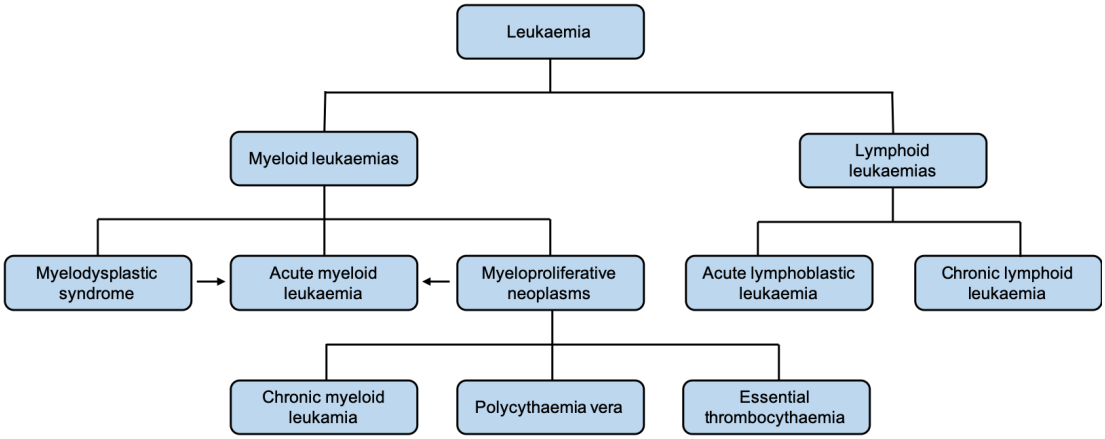

Figure 1.2 Schematic overview of the main types of leukaemia. AML can arise *de novo*, or from a pre-existing myelodysplastic syndrome. On rare occasions, AML develops from myeloproliferative neoplasia. Adapted from 'Acute Myeloid Leukaemia' (Khwaja, Bjorkholm et al. 2016).

1.2.1 Acute myeloid leukaemia (AML)

AML is an aggressive malignant disorder of haematopoietic stem and progenitor cells, characterised by a clonal expansion of poorly differentiated myeloid precursor cells at the expense of normal haematopoiesis.

1.2.2 Epidemiology of AML

AML is the commonest form of leukaemia in adults, accounting for 80% of cases in this group (Yamamoto and Goodman 2008). In contrast, AML only accounts for about 20% of leukaemia cases in paediatric patients (Puumala, Ross et al. 2013). Although AML can affect any age group, it is most common in older people, with the median age of diagnosis around 70 years (Bennett, Catovsky et al. 1976, Juliusson, Antunovic et al. 2009). The incidence of AML increases gradually from the age of 40-50 years, and more steeply from the age of 60 years, as shown by Cancer Research UK data (**Figure 1.2.2)**. In the western world, AML is slightly more common in males compared

with females, with a male to female ratio of 1.1 to 1.3, increasing to 1.8 at 80-84 years of age (Dores, Devesa et al. 2012) (**Figure 1.2.2**). People who have received cytotoxic chemotherapy or radiation therapy for a primary malignancy are at a greater risk for subsequent AML development, as are those with myelodysplastic conditions. Treatment with alkylating agents (chlorambucil, cyclophosphamide, melphalan) or topoisomerase II inhibitors (for example, etoposide, mitoxantrone, anthracyclines) is especially linked to development of therapy-related AML (Bueso-Ramos, Kanagal-Shamanna et al. 2015). In addition, AML is known to have a strong ethnic component, with Asian Americans having a significantly lower lifetime risk compared with white Americans, regardless of birth place (Pang, Cook et al. 2002). Finally, certain inherited disorders are associated with a high risk of AML, including Down syndrome, Fanconi anaemia, Bloom syndrome, ataxia-telangiectasia, Diamond-Blackfan anaemia, Schwachman-Diamond syndrome and severe congenital neutropenia (Seif 2011).

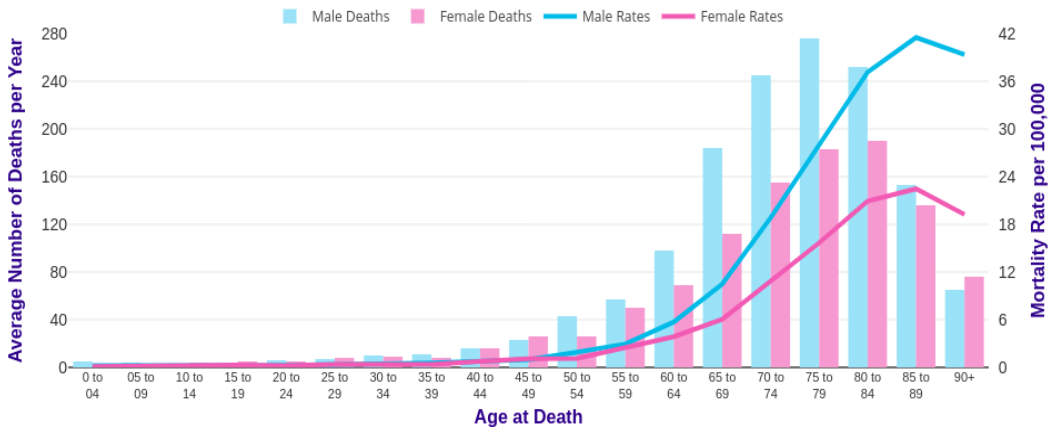

Figure 1.2.2 UK incidence of AML by sex and age, for the period from 2010 to 2015. Figure adapted from Cancer Research UK incidence statistics (*Cancer Research UK* [online], http://www.cancerresearchuk.org/health-professional/ cancer-statistics/statistics-by-cancer-type/leukaemia- aml/incidence (accessed June 2019)).

1.2.3 Classification of AML

A variety of classification systems have been used historically for AML. In the 1970s, AML was classified according to the French American British (FAB) system (Bennett, Catovsky et al. 1976). This system initially defined six major AML subtypes (M1-M6,

see **Table 1.2.3A**) based on cell morphology and the use of α-naphthyl acetate esterase (ANAE) to discriminate monoblasts from myeloblasts (Bennett, Catovsky et al. 1976). Later, immunological markers were used to define two additional AML subtypes; acute myeloblastic leukaemia with minimal differentiation (AML-M0) (Lee, Pollak et al. 1987) and acute megakaryocytic leukaemia (AML-M7) (see **Table 1.2.3A**). In 2001, the WHO issued a replacement classification system for haematological malignancy, incorporating cytogenetic and molecular analysis results for more accurate sub-grouping of the diseases (Vardiman, Harris et al. 2002). Updates to the WHO classification system were published in 2008 (Vardiman, Thiele et al. 2009), and 2016 (Arber, Orazi et al. 2016), to take into account the expanding knowledge in the area of cancer genomics. The most recent classification system, from 2016, is summarised in **Table 1.2.3B**.

FAB subtype	Name
M0	Acute myeloblastic leukaemia with minimal differentiation
M1	Acute myeloblastic leukaemia without maturation
M2	Acute myeloblastic leukaemia with maturation
M3	Promyelocytic leukaemia
M4	Acute myelomonocytic leukaemia
M5	Acute monocytic leukaemia
M6	Acute erythroid leukaemia
M7	Acute megakaryocytic leukaemia

Table 1.2.3A Summary of the FAB classification of AML

Acute myeloid leukaemia and related neoplasms
AML with recurrent genetic abnormalities • AML with t(8;21)(q22;q22.1); RUNX1-RUNX1T1 • AML with inv(16)(p13.1q22) or t(16;16)(p13.1;q22);CBFB-MYH11 • APL with PML-RARA • AML with t(9;11)(p21.3;q23.3);MLLT3-KMT2A • AML with t(6;9)(p23;q34.1);DEK-NUP214 • AML with inv(3)(q21.3q26.2) or t(3;3)(q21.3;q26.2); GATA2, MECOM • AML (megakaryoblastic) with t(1;22)(p13.3;q13.3);RBM15-MKL1

• Provisional entity: AML with BCR-ABL1 • AML with mutated NPM1 • AML with biallelic mutations of CEBPA • Provisional entity: AML with mutated RUNX1
AML with myelodysplasia-related changes
Therapy related myeloid neoplasms
AML not otherwise specified (NOS) • AML with minimal differentiation • AML without maturation • AML with maturation • Acute myelomonocytic leukaemia • Acute monoblastic/monocytic leukaemia • Pure erythroid leukaemia • Acute megakaryoblastic leukaemia • Acute basophilic leukaemia • Acute panmyelosis with myelofibrosis
Myeloid sarcoma
Myeloid proliferations related to Down syndrome • Transient abnormal myelopoiesis (TAM) • Myeloid leukaemia associated with Down syndrome

Table 1.2.3B Summary of the WHO classification of AML. Adapted from 'The 2016 revision to the World Health Organization classification of myeloid neoplasms and acute leukemia' (Arber, Orazi et al. 2016).

1.2.4 Pathophysiology of AML

AML results from the malignant transformation of a haematopoietic stem cell, or a primitive haematopoietic progenitor cell which has re-acquired stem cell properties, generating a leukaemic stem cell (LSC). This leukaemic stem cell divides to generate leukaemic progenitor cells, which acquire additional mutations, leading to the characteristic karyotypic and molecular heterogeneity of AML. Critically, leukaemic stem cells are both rare and quiescent, making them relatively resistant to the standard therapies used to eliminate bulk cancer cells. As a result, they may survive and go on to fuel relapse upon cessation of treatment (**Figure 1.2.4**).

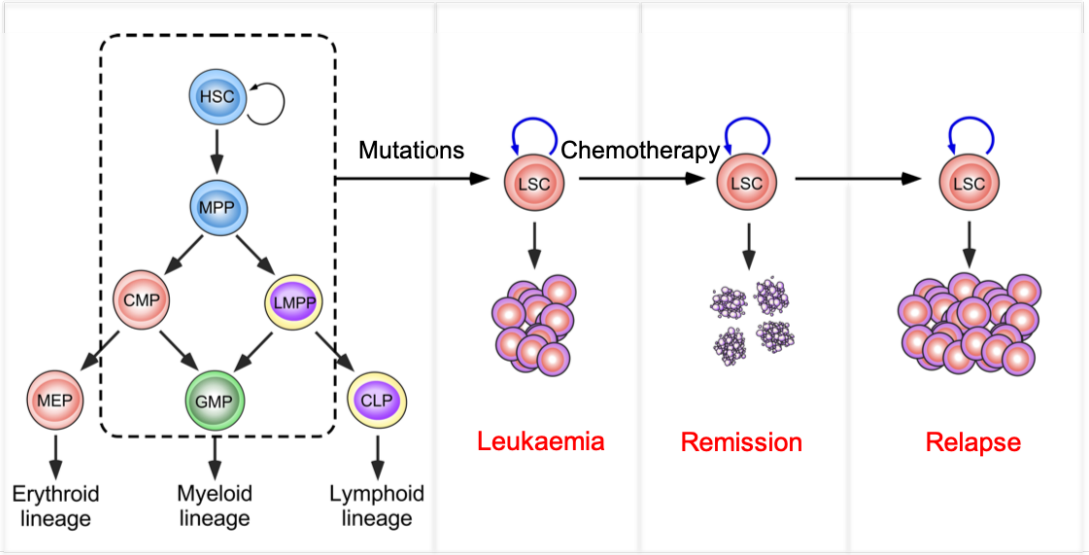

Figure 1.2.4 Leukaemic stem cells propagate AML and are difficult to eradicate. HSPCs (within dashed box) acquire mutations to generate LSCs, which give rise to the bulk of cancer cells. LSCs are rare and quiescent, therefore relatively resistant to standard therapies. Residual LSCs therefore fuel AML relapse upon cessation of treatment.

Approximately half of all human AML patients have gross structural cytogenetic abnormalities, including balanced translocations and chromosomal gains or losses (Byrd, Mrózek et al. 2002). These cytogenic abnormalities are well established as causal genetic events in AML, and strongly influence disease course as well as treatment response. In addition, almost all AML patients are found to have at least one oncogenic driver mutation, whilst two or more oncogenic drivers are identified in at least 86% of cases (Papaemmanuil, Gerstung et al. 2016). The commonest cytogenetic abnormalities and oncogenic mutations in AML are discussed in further detail in sections **1.2.5** and **1.2.6** respectively.

Work conducted in mouse models has shown a ‘two hit’ model for AML, whereby a single gene mutation is insufficient to cause leukaemia in isolation, instead initial and secondary mutations are required (Kelly and Gilliland 2002, Papaemmanuil, Gerstung et al. 2016). This is supported by the observation that the risk of AML increases with age (Short, Rytting et al. 2018), in line with the acquisition of mutations by haematopoietic stem and progenitor cells. Studies of clinically healthy humans have

shown that clonal haematopoiesis (defined as clonal expansion of HSCs harbouring mutations) increases with age, with a sharp rise in incidence between the ages of 50 and 65 years (Jaiswal, Fontanillas et al. 2014, Score, Chase et al. 2015). Mutations in genes that encode epigenetic modifiers, *DNMT3A*, *TET2*, *ASXL1* and *IDH1/2* are frequently identified in elderly people with clonal haematopoiesis and carry an increased risk of haematopoietic malignancy (Jaiswal, Fontanillas et al. 2014, Xie, Lu et al. 2014). However, given that these mutations are consistently identified within the founding AML clone, and are almost never found in isolation (Papaemmanuil, Gerstung et al. 2016), it seems likely that they require additional, co-operating mutations in order to initiate leukaemia.

1.2.5 Cytogenetics of AML

Cytogenetic abnormalities are known to be the most important independent prognostic factor in AML (Mrózek, Marcucci et al. 2012, Estey 2013) and are present in approximately half of all AML patients (Byrd, Mrózek et al. 2002). Although over 740 recurrent balanced aberrations have been identified in AML (Mitelman, Johansson et al. 2002), four translocations occur most frequently, namely *PML-RARA*, *AML1-ETO*, *CBFβ-MYH11* and *MLL*-fusions. These common onco-fusions are discussed in further detail below, as are the critical downstream effectors of *MLL*-fusions, *Meis1* and *Hoxa9,* and the oncogenic fusion *MOZ-TIF2*.

1.2.5.1 t(15;17) PML-RARA

PML-RARA is a fusion oncogene present in more than 95% of human acute promyelocytic leukaemia (APL; FAB-M3) cases, and in 10% of total human AML cases (Martens and Stunnenberg 2010). PML-RARA is the product of a t(15;17) chromosomal translocation, which fuses the promyelocytic leukaemia gene (PML) to the gene encoding retinoic acid receptor α (RARA) (de Thé, Chomienne et al. 1990). The resulting PML-RARα fusion impairs the normal function of RARα in neutrophil differentiation, and ultimately induces APL.

1.2.5.2 t(8;21) AML1-ETO

The *AML1*-ETO fusion is present in approximately 10% of AML cases (Martens and Stunnenberg 2010). The fusion protein is formed of the conserved runt homology

domain (rhd) from the critical haematopoietic transcription factor RUNX1 (formerly termed AML1, encoded on chromosome 21), joined to the majority of the ETO repressor protein (encoded on chromosome 8). AML1-ETO retains the ability to bind DNA sequences through the rhd of RUNX1, and to recruit transcriptional corepressors through ETO, therefore acting as a transcriptional repressor of RUNX1 target genes. More recently, additional roles for AML1-ETO have been documented in AML, namely increased HSC/MPP self-renewal through activation of the Wnt and Notch signalling pathways, and inhibition of lineage commitment through interaction with the haematopoietic transcription factors, GATA-1, PU.1, C/EBPa and E2A (Elagib and Goldfarb 2007).

1.2.5.3 Inv(16) CBFβ-MYH11

The CBFβ-MYH11 fusion is present in approximately 8% of AML cases (Martens and Stunnenberg 2010). This fusion protein results from the pericentric inversion of chromosome 16, thereby fusing core binding factor β (CBFβ) to the C-terminal coiled-coil region of a smooth muscle myosin heavy chain (*MYH11*) (Liu, Tarle et al. 1993). In normal haematopoiesis, CBFβ binds to RUNX1, forming the core binding factor (CBF), an essential transcription factor for haematopoiesis and myeloid differentiation. The CBFβ-MYH11 fusion disrupts the binding of CBFB to RUNX1, leading to repression of CBF-target genes, and ultimately a block in differentiation (Lutterbach, Hou et al. 1999). Expression of CBFβ-MYH11 in isolation is insufficient to generate leukaemia, and co-operating mutations are required for leukaemic transformation (Castilla, Garrett et al. 1999).

1.2.5.4 MLL-fusions

The Mixed Lineage Leukaemia gene (*MLL*) on chromosome 11q23 is the human homologue of *Drosophila melanogaster* trithorax, and is a frequent target for chromosomal translocations in human acute leukaemias of both lymphoblastic and myeloid varieties. *MLL*, which encodes a histone methyltransferase (Milne, Briggs et al. 2002, Nakamura, Mori et al. 2002), is involved in the regulation of homeotic genes during embryonic development (Benjamin, Hess et al. 1995) and is also required for the development and maintenance of normal haematopoiesis (Yagi, Deguchi et al. 1998, Ernst, Mabon et al. 2004, Jude, Climer et al. 2007). *MLL* translocations are present in more than 70% of infant leukaemias (either lymphoblastic or myeloid), 10%

of adult leukaemias (myeloid), and also occur following therapy with topoisomerase II inhibitors for other malignancies (Muntean and Hess 2012). Overall, *MLL* rearrangements are present in approximately 10% of human leukaemias, and are often associated with a poor prognosis (Krivtsov and Armstrong 2007). In *MLL*-rearranged leukaemias, the N terminal of MLL is fused to one of over 60 fusion partners. The most common translocation in AML is t(9;11), which encodes the oncogenic fusion protein MLL-AF9, and is typically associated with the FAB-M4 or M5 subtypes of human AML (Swansbury, Slater et al. 1998).

1.2.5.5 Meis1/Hoxa9

Homeobox A9 (*HOXA9*) belongs to the HOX family of homeobox genes, best recognised for their role in axial patterning (Krumlauf 1994). *HOXA9* is highly expressed in HSCs and primitive haematopoietic progenitors, and its expression decreases with differentiation (Sauvageau, Lansdorp et al. 1994, Pineault, Helgason et al. 2002). *HOXA9* is frequently upregulated in human AML samples, particularly when MLL fusions are present, and is associated with a negative prognosis (Golub, Slonim et al. 1999, Kawagoe, Humphries et al. 1999, Lawrence, Rozenfeld et al. 1999). In a cancer classification study based on gene microarrays, an attempt to identify genes linked with clinical outcome highlighted *HOXA9* from amongst 6817 genes as the single most highly correlated gene overexpressed in patients with treatment failure (Golub, Slonim et al. 1999).

MEIS1 belongs to the TALE (three amino acid loop extension) family of homeodomain transcription factors (Moskow, Bullrich et al. 1995). Like *HOXA9*, *MEIS1* is known to play an important role in regulating growth and differentiation during vertebrate development (Moens and Selleri 2006). Furthermore, *MEIS1* expression mirrors that of *HOXA9* during haematopoiesis, with high levels of expression in early progenitors and progressive downregulation during differentiation (Pineault, Helgason et al. 2002). In the context of AML, both Meis1 and Hoxa9 are directly upregulated by MLL-fusion proteins (Milne, Briggs et al. 2002, Zeisig, Milne et al. 2004), and are also highly expressed in non MLL-rearranged leukaemias, where they carry a negative prognosis (Lawrence, Rozenfeld et al. 1999). Meis1 is reported to be an essential and rate-limiting regulator of MLL leukemia stem cell potential (Wong, Iwasaki et al. 2007), and is also an important and well-established co-factor of HOXA9 in leukaemic development.

1.2.5.6 MOZ-TIF2

The *MOZ-TIF2* fusion is associated with AML with inv(8)(p11q13) (Carapeti, Aguiar et al. 1999), and is a less common oncogenic fusion in human AML, accounting for fewer than 1% of cases (Martens and Stunnenberg 2010). MOZ (monocytic leukaemia zinc finger) is a MYST family histone acetyltransferase (HAT), which was first cloned as a fusion partner of CBP as a consequence of t(8;16)(p11;p13) associated with the FAB M4/M5 subtype of AML (Borrow, Stanton et al. 1996). TIF2 is a member of the p160 nuclear receptor transcriptional coactivator family (Glass, Rose et al. 1997), which stimulates gene expression by facilitating the assembly of basal transcription factors into a stable preinitiation complex (Klein-Hitpass, Tsai et al. 1990). MOZ-TIF2 was first identified by Carapeti et al., who reported that this fusion retains the histone acetyltransferase homology domains of both proteins and also the CBP binding domain of TIF2 (Carapeti, Aguiar et al. 1998, Carapeti, Aguiar et al. 1999).

1.2.6 Molecular abnormalities of AML

Approximately 48% of primary AML patients present with no gross structural chromosomal changes (Byrd, Mrózek et al. 2002). These cytogenetically normal AML (CN-AML) cases are the result of gene mutations and altered gene expression, driving changes in the proliferation and differentiation of HSPCs. The advent of high throughput next generation sequencing technologies has fuelled a rapid expansion in our understanding of the AML genomic landscape and has highlighted the marked heterogeneity and complexity that exists there (Network 2013, Metzeler, Herold et al. 2016, Papaemmanuil, Gerstung et al. 2016). In 2013, the Cancer Genome Atlas Research Network published a comprehensive analysis of the genetic abnormalities (genomic, transcriptomic and epigenomic) from 200 adult AML patients. In this study, whole genome sequencing of 50 patients and exome sequencing of 150 patients revealed more than 2,000 different mutated genes, of which 23 were defined as frequently mutated genes. On average there were 13 gene mutations per sample, 5 of those in frequently mutated genes. Only 3 genes were mutated in >25% of patients; *FMS-related tyrosine kinase 3* (*FLT3*), *nucleophosmin 1* (*NPM1*) and *DNA methyltransferase 3A* (*DNMT3A*) (Network 2013). *FLT3*, *NPM1* and *DNMT3A* were also reported as the most frequently mutated genes (occurring in 39%, 33% and 31%

of patients respectively) in a 2016 paper by Metzeler et al. who sequenced 68 recurrently mutated genes in a cohort of 664 adult AML patients (**Figure 1.2.6**) (Metzeler, Herold et al. 2016). In the same year, Pappermuil et al. reported the results of cytogenetic analysis, and sequencing of 111 cancer genes, from 1540 AML patients enrolled in three high intensity treatment trials (Papaemmanuil, Gerstung et al. 2016). This study identified 5234 driver mutations across 76 genes or genomic regions, with at least one driver mutation identified in 96% of AML patients, and at least 2 found in 86% AML patients. Importantly, the large sample size of this study meant that the authors were able to use allele fractions of point mutations to infer clonal relationships. In this way, they showed that mutations in genes encoding epigenetic modifiers (*DNMT3A*, *TET2*, *ASXL1*, *IDH1* and *IDH2*) are often acquired early in the course of the disease and require additional mutations to induce leukaemia (Papaemmanuil, Gerstung et al. 2016). Our expanding understanding of AML gene mutations, and their implications for prognosis and treatment, has resulted in the amendment of the WHO classification system (Arber, Orazi et al. 2016), and the introduction of molecular screening as a routine component of AML classification at the time of diagnosis.

The cooperating mutations in AML can be categorized into functional groups reflecting distinct cellular activities. Broad categories of mutations are those affecting 1) transcription factors regulating stem cell self-renewal and differentiation, 2) cell signalling pathways regulating cell proliferation and survival and 3) epigenetic modifiers regulating gene expression. More recently, the importance of cohesin complex and spliceosome mutations has also become apparent (Papaemmanuil, Gerstung et al. 2016). For example, splicesome mutations including SRSF2, SF3B1, U2AF1 and ZRSR2 are now regarded as pathognomic for AML secondary to MDS (Cazzola, Della Porta et al. 2013). Similarly, somatic cohesion complex mutations, including STAG2, TAD21 and SMC3 have been identified in approximately 20% of high risk MDS and secondary AML, and are associated with an adverse prognosis (Thota, Viny et al. 2014).

A summary of the most commonly mutated genes in AML is presented in **Table 1.2.6**.

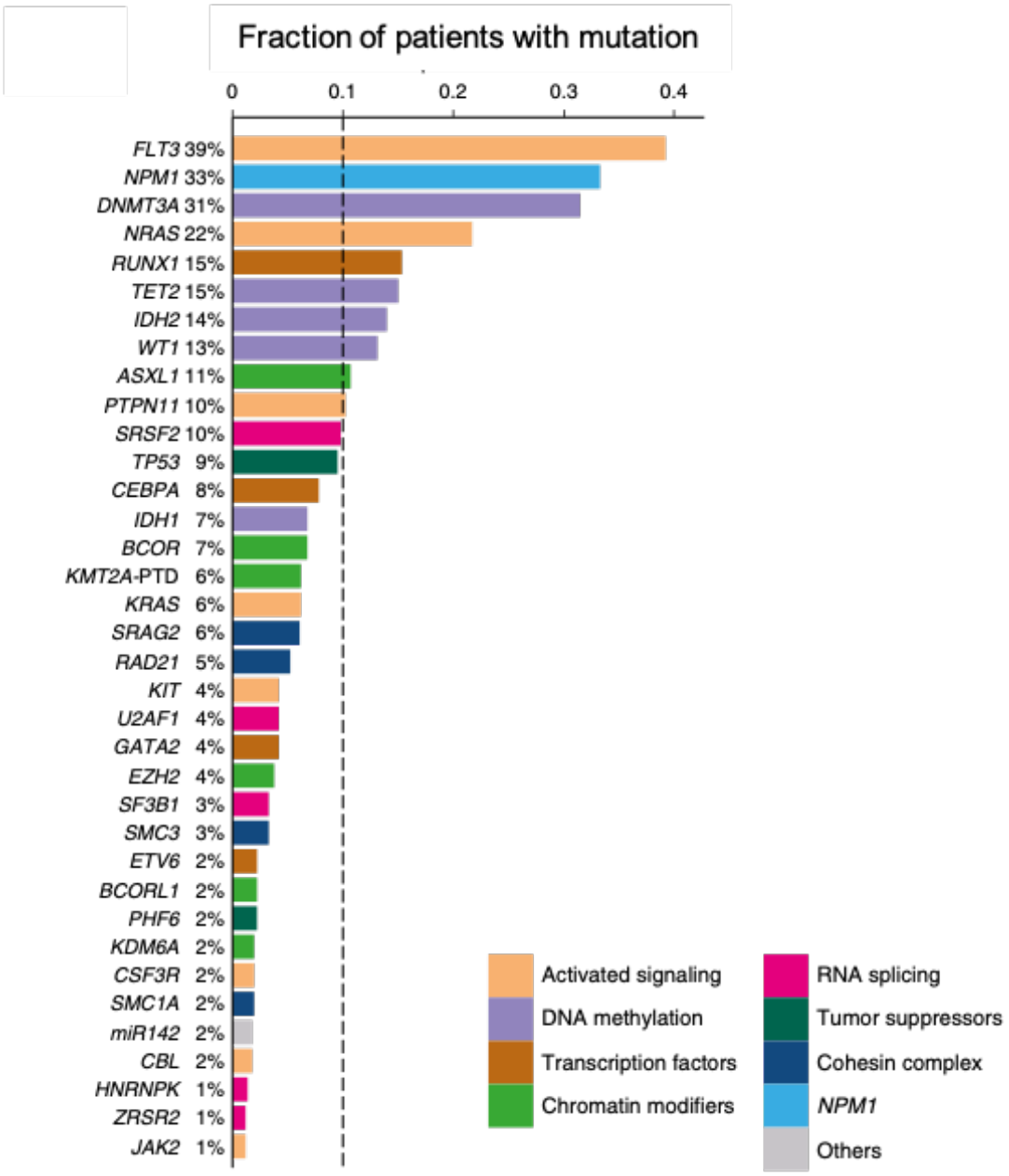

Figure 1.2.6 Driver gene mutations in AML. Adapted from 'Spectrum and prognostic relevance of driver gene mutations in acute myeloid leukaemia' (Metzeler, Herold et al. 2016).

Gene and Category	Prevalence	Description	Prognosis
***Nucleophosmin 1* (*NPM1*)**	25-30% of AML Female bias	Expression of NPM1 protein in the cytoplasm instead of the nucleus, causing myeloid proliferation and leukaemogenesis. Associated with monocytic AML morphology.	Favourable
***DNA Methyltransferase 3A* (*DNMT3A*)** • Epigenetic modification	18-22% of AML 34% of CN-AML	*DNMT3A* mutations are identified frequently in clonal haematopoiesis, and as preleukaemic mutations. May persist during remission.	Adverse
***FMS-like Tyrosine Kinase 3* (*FLT3*)** • Proliferation	20% of AML 30-45% of CN-AML	Internal tandem duplications (ITDs) in the juxta membrane domain, or mutations in the second tyrosine kinase domain (TKD), causing constitutive activation of *FLT3* and blast proliferation.	ITDs adverse TKDs unclear
Isocitrate Dehydrogenase* (*IDH*) *1* and *2 • Epigenetic modification	15-20% AML 25-30% CN-AML	Gain of function mutations, replacing physiological IDH enzyme function with the ability to convert α-ketoglutarate into 2-hydroxyglutarate.	Variable
***Ten-Eleven Translocation 2* (*TET2*)** • Epigenetic modification and differentiation	9-23% AML	Loss of function mutations. Commoner in older patients. Mutually exclusive with *IDH1*, *IDH2* and *WT1* mutations.	Adverse or none
***Runt-Related Transcription Factor* (*RUNX1*)** • Transcriptional regulation	5-13% AML	More common in older patients and secondary AML.	Adverse
***CCAAT Enhancer Binding Protein α* (*CEBPA*)** • Differentiation and stem cell self-renewal	6-10% AML 15-19% CN-AML	Critical transcription factor controlling gene expression during haematopoiesis. Biallelic mutations (usually N terminal plus C terminal) predict favourable outcome.	Biallelic favourable in absence of *FLT3-ITDs* and *DNMT3A* mutations
***Additional Sex Comb-Like* (*ASXL1*)** • Epigenetic modification	5-11% AML	Loss of function mutations, commoner in older patients and secondary AML.	Adverse
***Mixed Lineage Leukaemia* (*MLL*)** • Differentiation and stem cell self-renewal	11% CN-AML	Partial in tandem duplications associated with a poorer prognosis.	Adverse
***Tumour Protein p53* (*TP53*)** • Tumour suppression	8-14% AML	Occurs in AML with a complex karyotype, rare in the absence of chromosomal deletions. Associated with chemoresistance. More common in older patients and secondary AML.	Very adverse
***Receptor Tyrosine Kinase* (*c-Kit*)**	<5% AML	Constitutive activation and aberrant downstream signalling.	Adverse

• Proliferation	22-29% in AML with t(8;21) or inv(16)		
NRAS* and *KRAS • Proliferation	12% AML (NRAS) 5% AML (KRAS)	Missense mutations affecting membrane localisation. Aberrant downstream signalling.	None
Wilms Tumour 1 (WT1) • Epigenetic modification and differentiation	7% AML	Predominantly normal karyotype. Mutually exclusive with *IDH1*, *IDH2* and *TET2* mutations.	Adverse

Table 1.2.6 Recurrent gene mutations in AML. Combined data from Khwaja et al., Saultz et al., and Short et al. (Khwaja, Bjorkholm et al. 2016, Saultz and Garzon 2016, Short, Rytting et al. 2018).

1.2.7 Clinical presentation of AML

AML patients present with signs reflecting the accumulation of malignant and poorly differentiated myeloid cells in the BM, peripheral blood, and occasionally also other organs. Non-specific symptoms are common, including a decreased appetite, weight loss, fatigue and fever. Signs of BM failure are frequently present, specifically thrombocytopenia causing bleeding tendencies, anaemia, and infection. Lymphadenopathy (enlarged lymph nodes) and hepatosplenomegaly (enlargement of the liver and spleen) may be present (Khwaja, Bjorkholm et al. 2016). In rare AML patients, hyperleukocytosis, which is defined as a leukocyte count of > 100 x 10^9 WBC/l, can lead to capillary occlusion, and potentially multi-organ failure and death (Röllig and Ehninger 2015). Another infrequent complication of AML is spontaneous tumour lysis syndrome, which can occur in patients with a high tumour burden, particularly upon initiation of treatment (Montesinos, Lorenzo et al. 2008).

1.2.8 Diagnosis of AML

Diagnosis of AML requires the identification of at least 20% myeloid blast cells (myeloblasts, monoblasts, megakaryoblasts) during examination of the BM (samples obtained by aspirate and/or core biopsy) or peripheral blood (Döhner, Estey et al. 2010). Notable exceptions to this rule are isolated extramedullary AML (myeloid sarcoma), or the presence of recurrent karyotypic or molecular abnormalities which are pathognomic for AML, i.e., t(8;21), inv(16) and t(15;17) (Vardiman, Thiele et al. 2009). Immunophenotyping of patient samples by flow cytometry confirms the myeloid

origin of the malignancy and facilitates further categorisation of AML subtype. Positive myeloperoxidase staining, or the documentation of Auer rods (azurophilic cytoplasmic inclusion bodies seen commonly in APL, acute myelomonocytic leukaemia, and the majority of AML with t(8;21)), are also consistent with a myeloid malignancy (De Kouchkovsky and Abdul-Hay 2016). Following a diagnosis of AML, cytogenetic analysis (through karyotyping and fluorescent in situ hybridisation, FISH), and screening for commonly identified gene mutations and rearrangements are carried out, to facilitate accurate AML classification. This information is used to provide prognostic information and to guide the optimal therapeutic approach.

1.2.8.1 Immunophenotyping

Immunophenotyping is used for lineage specification (differentiation of AML from ALL), and for sub-classification of AML subtypes in a 2-step approach, as outlined in **Table 1.2.8.1**. AML can be confirmed if myeloblasts are positive for at least 2 of the following myeloid markers; MPO, CD13, CD33, CDw65 and CD117, with MPO being the most specific (Bene, Castoldi et al. 1995). Notably, lymphoid antigens are detected in around 25% of AML patient samples, with T cell marker CD7 reported in 10-30% of cases, and B cell marker CD19 reported in 3% of cases.

Step 1: Lineage specification	
B lineage	CD19, cyCD22 and cyCD79a
T lineage	cyCD3, CD2 and CD7
Myeloid lineage	MPO, CD13, CD33 and CDw65
Progenitor cell antigens	CD34, TdT, HLA-DR, CD10 and CD117
Step 2: Subtype specification in myeloid leukaemia	
Monocytic	CD14, CD11b, CD4
Erythroid	CD71, CD36, CD235a
Megakaryoblastic	CD41a, CD61
Granulocytic	CD65, (CD15)

Table 1.2.8.1 Two step immunophenotyping process for AML. Cy, cytoplasmic; HLA-DR, human leukocyte antigen-antigen D related; MPO, myeloperoxidase; TdT,

terminal deoxynucleotidyltransferase. Adapted from 'Acute Myeloid Leukaemia' (Khwaja, Bjorkholm et al. 2016).

1.2.9 Treatment of AML

The treatment for AML has changed little in the last 40 years. However, since 2017 several new drugs have been introduced, building on an increased understanding about the genomic landscape of AML, and the rationale for targeted and specific therapies. Nevertheless, the core of therapy remains the same currently; cytarabine and an anthracycline for induction, followed by consolidation chemotherapy with cytarabine, or haematopoietic stem cell transplantation (HSCT) (Short, Rytting et al. 2018). The intensity of the regime is chosen based on the patient's ability to tolerate treatment. Where possible, high intensity induction therapy is administered, with 7 days of cytarabine at 100-200 mg/m^2 intravenously plus 3 days of an anthracycline i.e. daunorubicin or idarubicin (Short, Rytting et al. 2018). With this treatment, 'complete *morphological* remission' (see **1.2.10** for discussion) is reported in 60-85% of patients under the age of 60 years, and in 40-60% of patients 60 years of age and above (Döhner, Weisdorf et al. 2015). Assuming complete remission is achieved with induction therapy, the next choice is whether to follow this up with consolidation chemotherapy, or proceed directly to HSCT, which carries a greater risk of treatment related mortality, but reduces the risk of relapse in high risk AML disease (Schlenk 2014). Consolidation chemotherapy is generally recommended at first remission for AML patients with favourable risk disease. Standard of care is a cytarabine-based regimen, 1.5-3 g/m^2 (dose depending on AML subtype) every 12 hours for 3 days per cycle, with 4 cycles administered in total (Short, Rytting et al. 2018). In general, HSCT is recommended at the first remission where the risk of relapse is considered to exceed 35% i.e. in high risk cases, and in some intermediate risk cases. Allogeneic HSCT benefits AML patients via a two-part mechanism; leukaemic cells are targeted first by the high-dose cytotoxic pre-conditioning regimen, and then by engrafted donor T cells, which exert an important 'graft versus host leukaemia' effect (Gupta, Tallman et al. 2011).

In recent years, several new drugs have been introduced for the treatment of AML, to complement or replace standard cytarabine - anthracycline therapy, depending on

patient factors and the molecular and cytogenetic features of their disease. These various therapies, and the rationale for their use, are summarised in **Table 1.2.9**.

Therapy	Mechanism	Usage	References
Gemtuzumab ozogamicin	Anti-CD33 antibody drug conjugate that carries calicheamicin, a potent DNA damaging toxin.	Beneficial effect in most AML subgroups, particularly those with high CD33 expression, and in patients with favourable/intermediate risk disease. Used in combination with standard therapy (particularly effective in paediatric leukaemia), or as a single agent in patients unable to tolerate standard therapy.	(Godwin, Gale et al. 2017)
FLT3 inhibitors	Midostaurin is an oral multitargeted kinase inhibitor. Further examples include Sorafenib, Quizartinib, Crenolanib.	Midostaurin significantly improves survival in AML patients with *FLT3 ITD* or *FLT3* kinase domain mutations (51.4 versus 44.3% 4-year overall survival when used in combination with standard therapy).	(Stone, Mandrekar et al. 2017)
Mutant IDH2 inhibitors	Enasidenib is an oral selective inhibitor of mutant *IDH2*, which induces blast cell differentiation.	Suitable for AML patients with *IDH2* mutations (10-20% AML cases). Overall response rate of around 40%, complete remission of 20%, median survival time 9.3 months.	(Stein, DiNardo et al. 2017)
Clofarabine	Second generation purine nucleoside analogue.	Single agent or as combination therapy, overall response rates around 40%. Well tolerated addition to low dose cytarabine in patients not suitable for high intensity treatment.	(Kantarjian, Erba et al. 2009, Burnett, Russell et al. 2013)
Hypomethylating agents	Inhibition of DNA methylation, resulting in re-expression of tumour suppressor genes. Examples include azacytidine and decitabine.	Used in MDS and AML. Response rates of 20-30%. Well tolerated addition to low dose cytarabine in patients not suitable for high intensity treatment.	(Kantarjian, Thomas et al. 2012, Dombret, Seymour et al. 2015)
All-trans-retinoic acid (ATRA) and arsenic trioxide (ATO)	Induce differentiation of promyelocytes into neutrophils.	Used in APL. Should be administered immediately, decreases risk of bleeding diathesis and death.	(Lo-Coco, Avvisati et al. 2013)

Table 1.2.9 Novel therapies for AML, additional to cytarabine / anthracycline treatment.

Several novel therapies are currently in development for AML, offering new hope to patients with high risk or relapsed disease, or those unfit for standard therapy. For

example, reversible inhibitors of the major nuclear export receptor chromosome region maintenance 1 (CRM1) (which mediates export and inactivation of tumour suppressors including p53, RB1, p21, p73, FOXO1), have shown strong anti-leukaemic effects in pre-clinical studies (Ranganathan, Yu et al. 2012, Etchin, Sun et al. 2013). Other drugs under investigation for treatment of AML include STAT3 small molecule inhibitors, monoclonal antibodies against CD123, bromodomain and extra terminal protein inhibitors, B-cell lymphoma 2 (BCL-2) inhibitors, checkpoint inhibitors e.g. anti-CTLA4 and anti-PD1 monoclonal antibodies, and novel chimeric antigen receptor T cell therapies that target epitopes highly expressed on AML blasts (Gill, Tasian et al. 2014, Grosso, Hess et al. 2015).

1.2.10 Prognosis of AML

In 2010, the European Leukaemia Net (ELN) classification scheme was created in an attempt to standardise risk stratification in adult AML patients by combining details of cytogenetic and molecular abnormalities (Döhner, Estey et al. 2010, Mrózek, Marcucci et al. 2012). Using this scheme, patients were divided into 1 of 4 groups favourable, intermediate 1, intermediate 2 and adverse (see **Table 1.2.10**).

Genetic group	Subsets
Favourable	t(8;21)(q22;q22); *RUNX1-RUNX1T1*
	inv(16)(p13.1q22) or t(16;16)(p13.1;q22); *CBFB-MYH11*
	Mutated *NPM1* without *FLT3*-ITD (normal karyotype)
	Mutated *CEBPA* (normal karyotype)
Intermediate I	Mutated *NPM1* and *FLT3*-ITD (normal karyotype)
	Wild-type *NPM1* and *FLT3*-ITD (normal karyotype)
	Wild-type *NPM1* without *FLT3*-ITD (normal karyotype)
Intermediate II	t(9;11)(p22;q23); *MLLT3-MLL*
	Cytogenetic abnormalities not classified as favourable or adverse
Adverse	inv(3)(q21q26.2) or t(3;3)(q21;q26.2); *RPN1-EVI1*
	t(6;9)(p23;q34); *DEK-NUP214*
	t(v;11)(v;q23); *MLL* rearranged
	−5 or del(5q); −7; abnl(17p); complex karyotype

Table 1.2.10 Risk stratification in AML (Döhner, Estey et al. 2010).

Morphological complete remission of AML is defined as fewer than 5% of blasts on a BM aspirate sample with marrow spicules and with a count of at least 200 nucleated cells, alongside an absolute neutrophil count of > 1000/μl and a PLT count of ≥ 100,000/μl. There should also be no blasts with Auer rods, and no persistence of extramedullary disease (Cheson, Bennett et al. 2003). However, with the advent of next generation high throughput sequencing methods, it has become increasingly clear that *morphological* complete remission fails to detect minimal residual disease, which can subsequently serve as a foundation for leukaemic relapse (Chen, Xie et al. 2015). Prognostic information is therefore likely to change significantly as methods for detection of minimal residual disease become mainstream, for example multiparameter flow cytometry, and quantitative real-time PCR (Kern, Haferlach et al. 2008). At present, with standard cytarabine/anthracycline chemotherapy, long term survival for patients with AML is achieved in only 35-40% of those younger than 60 years of age. The prognosis for patients of 60 years and above is even poorer, with a long-term survival of only 10-15% (Döhner, Estey et al. 2017). The reason for the inferior prognosis in older patients is twofold, they are less likely to tolerate intensive chemotherapy (Podoltsev, Stahl et al. 2017), and they are more likely to have higher risk disease, with less favourable cytogenetic and molecular characteristics (Lindsley, Mar et al. 2015, Creutzig, Zimmermann et al. 2016). In contrast, the prognosis for paediatric AML is more favourable, with cure rates approaching 70% (Kolb and Meshinchi 2015).

1.3 Epitranscriptomics as a novel layer of regulation of gene expression

Genomic, transcriptomic and epigenomic pathways controlling AML have been recognised for many years, and continue to be well studied (**1.2.5** and **1.2.6**). However, in the last decade, the field of epitranscriptomics has emerged as a novel layer of regulation of gene expression, with significant effects on normal and malignant stem cell biology. With the advent of next generation and high throughput sequencing technologies, and liquid chromatography/mass spectroscopy techniques, the extent of these modifications and their biological significance is becoming increasingly apparent.

1.3.1 RNA modifications

Over 170 RNA modifications have been identified to date. These modifications are listed and regularly updated in the comprehensive MODOMICS database (Boccaletto, Machnicka et al. 2017). Through the addition of polar, charged, aliphatic or aromatic moieties, these modifications affect the functions of the four basic ribonucleotide residues of RNA; adenine (A), uracil (U), guanine (G) and cytosine (C), providing a post transcriptional layer of regulation for gene expression. Compared to transcriptional regulation of mRNA, regulatory pathways at the post transcriptional level have the advantage of providing fine-tuned and localised control, which can be rapidly adapted to changing circumstances.

In the process of protein synthesis, messenger RNA (mRNA) is translated into protein through the combined actions of transfer RNA (tRNA) and ribosomal RNA (rRNA), which associates with specific proteins to form ribosomes. The most abundant cellular RNA is rRNA, whereas the most extensively modified is tRNA (Pan 2018). Common rRNA modifications include 2'-O-methylation (Nm) of the ribose and isomeration of uridine to pseudouridine (ψ), and these typically occur adjacent to functionally important sites (Sloan, Warda et al. 2017). Modifications of tRNA are highly diverse, and include 5-methylcytosine (m^5C), N^1-methyladenosine (m^1A), pseudouridine (ψ), 5-methyluridine (m^5U), 1-methylguanosine (m^1G), 7-methylguanosine (m^7G), inosine (I), and also more complex multistep modifications such as 5-methoxycarbonyl-methyl-2-thiouridine ($mcm5s^2U$) (Pan 2018).

The 5' cap and 3' poly(A) tail are well characterised modifications of mRNA, and both contribute to transcript stability, nuclear export and translation initiation (Sachs 1990, Ghosh and Lima 2010). The mRNA 5' cap also assists polyadenylation, and pre-mRNA splicing. In addition to the 5'cap and 3' poly(A) tail, a number of internal mRNA modifications have also been identified (**Figure 1.3.1**), the best characterised of which is N^6-methyladenosine (m^6A).

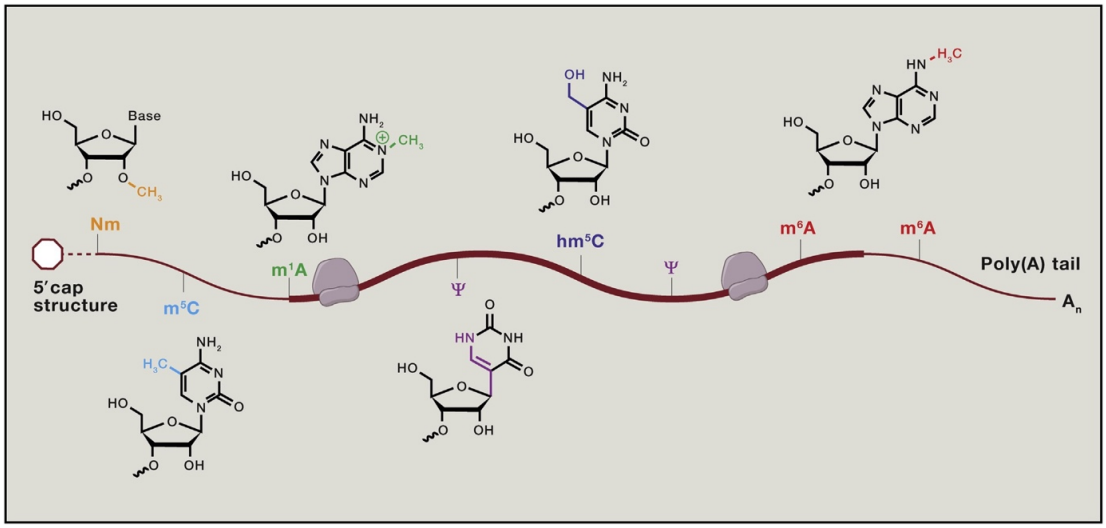

Figure 1.3.1 Common chemical modifications in eukaryotic mRNA transcripts. Nm (2'-O-methylation); m^5C (5-methylcytosine); m^1A (N^1-methyladenosine); ψ (pseudouridine); hm^5C (5-hydroxymethylcytosine), m^6A (N^6-methyladenosine). Figure taken from Roundtree et al. (Roundtree, Evans et al. 2017).

1.3.1.1 2'-O-methylation (Nm)

2'-O-methylation (Nm) is a co- or post-transcriptional modification of RNA in which a methyl group (CH_3) is added to the 2' hydroxyl (OH) of the ribose moiety. This abundant and highly conserved modification is found at multiple sites on tRNA, rRNA, mRNA and small non-coding RNAs (ncRNAs). Amongst other roles, Nm modification can affect structure and RNA/protein interactions of RNA (Dimitrova, Teysset et al. 2019).

1.3.1.2 5-methylcytosine (m^5C) and 5-hydroxymethylcytosine (hm^5C)

Methylation at the 5 position of cytosine in mRNA was first identified more than 40 years ago (Desrosiers, Friderici et al. 1974, Dubin and Taylor 1975), but it was only recently, with the advent of bisulfide m^5C sequencing, that the abundance and extent of this modification in mRNA and ncRNA became apparent (Squires, Patel et al. 2012). Recent work has shown that m^5C is recognised by the mRNA export adaptor protein ALYREF, suggesting that it plays a role in the nuclear export of m^5C-modified transcripts (Yang, Yang et al. 2017). 5-hydroxymethylcytosine (hm^5C) is the oxidation

product of m^5C, catalysed by the ten-eleven translocation (TET) family of enzymes (Fu, Guerrero et al. 2014).

1.3.1.3 N^1-Methyladenosine (m^1A)

Methylation at the N^1 position of adenosine (m^1A) occurs in mammalian mRNA at low levels, with m^1A/A ratios ranging from 0.015% to 0.16% in cells and tissues (Dominissini, Nachtergaele et al. 2016). Nevertheless, because m^1A occurs at the Watson Crick interface it generates a positively charged base and can therefore markedly affect RNA secondary structure (Dominissini, Nachtergaele et al. 2016, Li, Xiong et al. 2016). m^1A is enriched around translation initiation start sites in coding transcripts and is thought to function primarily in translation, and RNA-RNA interactions (Dominissini, Nachtergaele et al. 2016, Li, Xiong et al. 2016). To date, two AlkB family proteins have been found to demethylate m^1A; ALKBH3 (Li, Xiong et al. 2016) and ALKBH1 (Liu, Clark et al. 2016). Levels of m^1A are dynamic, changing in response to nutrient starvation and heat shock (Dominissini, Nachtergaele et al. 2016, Li, Xiong et al. 2016).

1.3.1.4 Pseudouridine (ψ)

Pseudouridine (ψ), isomerisation of the uridine base, was the first RNA modification discovered (Cohn and Volkin 1951) and was quickly established as an abundant component of rRNA and tRNA (Cohn 1960). In the last 5 years, sequencing technologies including PseudoU-Seq and ψ-Seq have facilitated transcriptome-wide quantitative mapping of pseudouridine, revealing hundreds of ψ-modified human mRNAs (Carlile, Rojas-Duran et al. 2014, Schwartz, Bernstein et al. 2014). Furthermore, quantitative mass spectroscopy analysis has shown that ψ is much more prevalent in mammalian mRNA than previously thought, occurring at a ψ/U ratio of 0.2-0.6% (Li, Zhu et al. 2015). Pseudouridylation, which is catalysed by pseudouridine synthases, alters RNA secondary structure due to improved base stacking (Davis 1995), and has been shown to affect many cellular processes including translation efficiency, splicing, telomere maintenance and regulation of gene expression (Mochizuki, He et al. 2004, Carlile, Rojas-Duran et al. 2014, Schwartz, Bernstein et al. 2014). In addition, pseudouridylation of any of the three translation termination codons (all of which contain a uridine at the first position) has been shown

to prevent translation termination in a process termed stop codon read through (Karijolich and Yu 2011, Fernández, Ng et al. 2013).

1.3.1.5 N^6-methyladenosine (m^6A)

Methylation at the N^6 position of adenosine (m^6A) is the most prevalent internal modification on eukaryotic mRNA and has been identified in the transcripts of over 7000 human genes (Meyer, Saletore et al. 2012, Dominissini, Moshitch-Moshkovitz et al. 2013). m^6A was first discovered in 1974 (Desrosiers, Friderici et al. 1974, Perry and Kelley 1974), but received limited attention until the discovery of the demethylase enzymes FTO (Jia, Fu et al. 2011) and ALKBH5 (Zheng, Dahl et al. 2013), which indicated that the modification was reversible, and might therefore act in a regulatory role. Around the same time, the development of high throughput sequencing technologies provided transcriptome-wide maps of modification sites on mRNA, long non-coding RNAs, and later also small nucleolar RNAs (snoRNAs) (Meyer, Saletore et al. 2012, Dominissini, Moshitch-Moshkovitz et al. 2013), revealing the prevalence of m^6A, and prompting studies of its functional significance.

The ratio of m^6A to A in total cellular RNA is reported to be around 0.1-0.5% (Desrosiers, Friderici et al. 1974, Dubin and Taylor 1975, Jia, Fu et al. 2011, Zheng, Dahl et al. 2013). N^6-methyladenosine marks are preferentially located near stop codons and 3′ untranslated regions (Meyer, Saletore et al. 2012, Dominissini, Moshitch-Moshkovitz et al. 2013), and occur in the consensus motifs G(m^6A)C (70%) or A (m^6A)C (30%) (Wei and Moss 1977).

We now know that m^6A plays a fundamental role in key biological processes, and that aberrations in m^6A regulators drive a wide range of pathologies, including cancer. The regulation of m^6A, and its role in health and disease is discussed below.

1.3.2 m^6A regulators

m^6A methylation is installed by methyltransferase complexes (writers) and removed by demethylases (erasers). The effects of m^6A methylation are mediated by reader proteins.

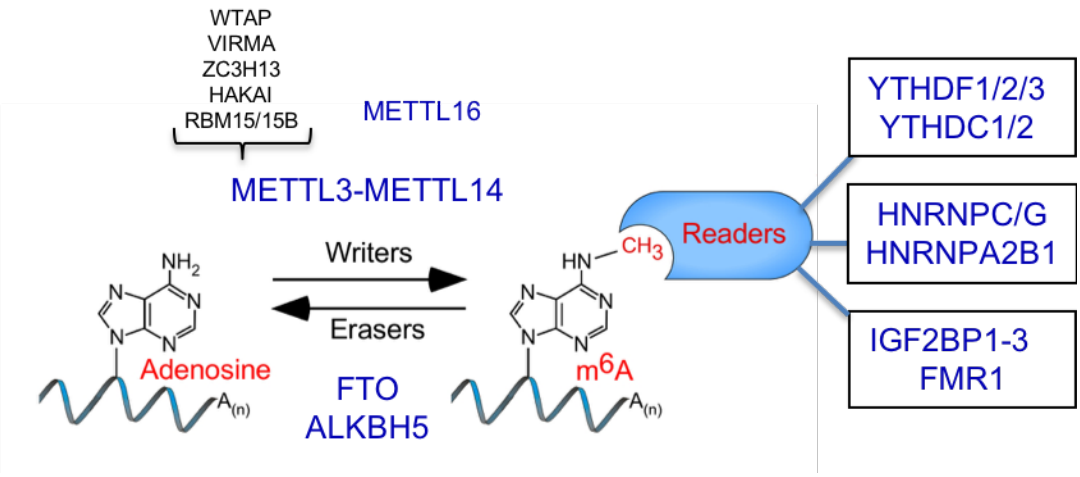

Figure 1.3.2 m^{6}A writers, erasers and readers. ***m^{6}A writers****:* m^{6}A is predominantly installed on mRNA in the consensus sequence RR(m^{6}A)CH (R = A or G; H = A, C or U) by a methyltransferase complex with a METTL3-METTL14 core, and associated adaptor proteins including WTAP, VIRMA, ZC3H13, HAKAI, RBM15/15B. METTL16 is a recently identified m^{6}A writer, which installs m^{6}A in the consensus sequence UAC(m^{6}A)GAGAA on transcript *MAT2A*. ***m^{6}A erasers***: m^{6}A is removed by either of the two demethylases, FTO or ALKBH5. ***m^{6}A readers***: m^{6}A modified mRNA is bound by 3 classes of reader proteins a) YTH family proteins, which bind via a well-defined YTH domain b) HNRNPC/G and HNRNPA2B1, which bind following a 'structural switch' of RNA, which is initiated by m^{6}A modification c) RNA binding proteins IGF2BP1-3 and FMR1, which bind via an unknown mechanism.

1.3.2.1 m^{6}A writers

m^{6}A is installed on mRNA co-transcriptionally by a methyltransferase writer complex. At the core of this complex is methyltransferase 3 (METTL3), which is the catalytically active subunit (Bokar, Shambaugh et al. 1997), bound to methyltransferase 14 (METTL14), which facilitates RNA binding (Wang, Doxtader et al. 2016, Wang, Feng et al. 2016). The METTL3-METTL14 core is associated with several additional proteins, including WTAP, VIRMA, ZC3H13, HAKAI and RBM15/15B. The function of the METTL3-METTL14 writer complex proteins is summarised in **Table 1.3.2.1**.

Subunit	Role	References
METTL3	Catalytic subunit	(Bokar, Shambaugh et al. 1997)

METTL14	Critical to support METTL3 structurally and for recognition of RNA substrates but weak methyltransferase activity itself	(Liu, Yue et al. 2014, Wang, Doxtader et al. 2016, Wang, Feng et al. 2016)
WTAP	METTL3/14 localisation and substrate recruitment	(Ping, Sun et al. 2014)
VIRMA	Mediates preferential mRNA methylation in 3′UTR and near stop codon	(Yue, Liu et al. 2018)
ZC3H13	Facilitates nuclear localisation of the writer complex	(Wen, Lv et al. 2018)
HAKAI	Interacts with core components to facilitate m^6A methylation	(Horiuchi, Kawamura et al. 2013, Růžička, Zhang et al. 2017)
RBM15 RBM15B	Associate with METTL3-WTAP, facilitating binding to certain mRNAs and *XIST*	(Patil, Chen et al. 2016)

Table 1.3.2.1 Components of the m^6A writer complex and their functions.

The METT3-METTL14-WTAP complex is predominantly localised in the nucleus (Bokar, Shambaugh et al. 1997, Ping, Sun et al. 2014), but can be found in the cytoplasm in some malignant cells, for example in AML (Barbieri, Tzelepis et al. 2017), and breast cancer (Alarcón, Lee et al. 2015).

METTL3 has been shown to be essential for a wide range of biological processes, including yeast meiosis and sporulation (Clancy, Shambaugh et al. 2002), differentiation of murine embryonic stem cells (Batista, Molinie et al. 2014, Geula, Moshitch-Moshkovitz et al. 2015), sex determination in fruit flies (Haussmann, Bodi et al. 2016) and spermatogenesis (Xu, Yang et al. 2017). In addition, METTL3 is known to respond to stress, for example heat shock results in radical re-localisation of Mettl3 to heat-shock genes, where it acts together with Dgcr8 to co-transcriptionally mark mRNAs for subsequent RNA degradation, ultimately ensuring rapid clearance of heat shock transcripts (Knuckles, Carl et al. 2017). Similarly, UV radiation causes rapid re-localisation of the heterodimer METTL3/METTL14 to areas of damage, and subsequently increased m^6A at these sites. This m^6A is required for effective recruitment of the enzyme DNA polymerase kappa, ultimately facilitating DNA repair (Xiang, Laurent et al. 2017).

Within the cytoplasm, METTL3 may function as a reader, thereby promoting translation. For example, in lung cancer cells, the interaction between METTL3 and EIF3 (which is overexpressed in many cancers) results in the increased translation of transcripts bound to the 3'UTR of METTL3 (Lin, Choe et al. 2016).

Although the majority of m^6A mRNA methylation is installed by the METTL3-METTL14 complex, METTL16 has recently been identified as the methyltransferase which modifies U6 spliceosomal RNA (Pendleton, Chen et al. 2017, Warda, Kretschmer et al. 2017). In addition, METTL16 is also responsible for the regulation of *MAT2A*, the human gene encoding S-adenosylmethionine (SAM)-synthetase. In this way, METTL16 controls the production of SAM, an essential methyl donor for numerous biological processes. METTL16 may function as an m^6A reader, directing alternative splicing of *MAT2A* in response to low SAM levels (Pendleton, Chen et al. 2017), or may regulate MAT2A mRNA stability through YTHDC1 mediated m^6A mRNA degradation (Shima, Matsumoto et al. 2017).

1.3.2.2 m^6A erasers

To date, two m^6A mRNA demethylases have been identified; fat mass and obesity-associated protein (FTO) and ALKBH5, both of which are members of the α-ketoglutarate (αKG)-dependent dioxygenase enzyme family.

FTO was the first m^6A mRNA demethylase discovered (Jia, Fu et al. 2011). Subsequently, the same group showed that FTO oxidation of m^6A occurs in a stepwise manner, from m^6A to N^6-hydroxymethyladenosine (hm^6A), and then to f^6A. In doing so, they demonstrated that FTO can bind hm^6A as well as m^6A substrates (Fu, Jia et al. 2013). Subsequent to this, Mauer et al. showed that FMO selectively demethylates the first encoded nucleotide adjacent to the 7-methylguanosine cap in mRNA, termed N^6,2'-O-dimethyladenosine (m^6A_m). These authors showed that FTO preferentially demethylates m^6A_m rather than m^6A. Most recently, however, Wei et al. used cross linking immunoprecipitation sequencing (CLIP-Seq) to investigate the spectrum of FTO substrates, and concluded that FTO exhibits effective demethylation activity toward m^1A in specific tRNAs, m^6A_m in some snRNAs, and internal m^6A and cap-m^6A_m in mRNA (Wei, Liu et al. 2018). These authors also showed that FTO mediates mRNA m^6A and cap-m^6A_m demethylation in the cytoplasm, but mainly mRNA m^6A demethylation in the nucleus. Although FTO was initially reported as a nuclear protein, Wei et al. showed that in some AML cell lines a large amount of FTO is located within the cytoplasm, and consequently, up to 40% of mRNA m^6A is subjected to demethylation by FTO (in contrast to common cell lines such as HeLa and HEK, where FTO is largely nuclear, therefore only 5-10% of mRNA m^6A is subject to its demethylation activity) (Wei, Liu et al. 2018). Roles of FTO reported to date

include response to heat shock (Zhou, Wan et al. 2015), cardiac remodelling and repair (Mathiyalagan, Adamiak et al. 2019), stress related psychiatric disorders (Engel and Chen 2018), adipogenesis (Wu, Liu et al. 2018) and cancer (Tan, Dang et al. 2015, Li, Weng et al. 2017, Yang, Wei et al. 2019).

ALKBH5 was the second demethylase of m^{6}A to be discovered (Zheng, Dahl et al. 2013). Zheng et al. reported that the demethylation activity of ALKBH5 affects mRNA export and RNA metabolism, as well as the assembly of mRNA processing factors in nuclear speckles. These authors showed that *Alkbh5* is widely expressed in mouse tissues, with particularly high expression levels in the testes. They went on to show that targeted deletion of *Alkbh5* results in male specific infertility in mice, due to apoptosis affecting meiotic metaphase-stage spermatocytes (Zheng, Dahl et al. 2013).

1.3.2.3 m^{6}A readers

Several families of reader proteins for m^{6}A have been identified, which bind m^{6}A modified mRNA through different mechanisms. The YT521-B homology (YTH) domain containing family of proteins bind m^{6}A mRNA directly via the highly conserved YTH domain (Xu, Wang et al. 2014), whereas heterogeneous nuclear ribonucleoproteins (HNRNPs) rely upon the 'structural switch' induced by m^{6}A modification to access and bind specific RNA (Liu, Dai et al. 2015). Most recently, insulin-like growth factor 2 mRNA binding proteins (IGF2BPs; including IGF2BP1/2/3) have been identified as a third class of m^{6}A mRNA binding proteins (Huang, Weng et al. 2018), through an as yet unknown mechanism. A summary of m^{6}A readers and their functions is listed in **Table 1.3.2.3**.

m^{6}A reader	Functional role
YTHDF1	Promotes translation of target transcripts by recruitment of translation initiation factors (Wang, Zhao et al. 2015)
YTHDF2	Targets m^{6}A mRNA for decay, partially by recruitment of the CCR4-NOT deadenylase complex (Du, Zhao et al. 2016)
YTHDF3	Promotes translation and decay of m^{6}A mRNA (Shi, Wang et al. 2017)
YTHDC1	Regulates mRNA splicing (Xiao, Adhikari et al. 2016), mRNA export (Roundtree, Luo et al. 2017), decay of selected mRNA transcripts (Shima, Matsumoto et al. 2017), and function of *XIST,* a long non coding RNA involved in X-chromosome inactivation (Patil, Chen et al. 2016)

YTHDC2	Facilitates the switch from mitosis to meiosis in male and female gametogenesis (Bailey, Batista et al. 2017, Hsu, Zhu et al. 2017, Wojtas, Pandey et al. 2017, Jain, Puno et al. 2018)
HNRNPC/G HNRNPA2B1	Regulate alternative splicing or processing of target transcripts (Alarcón, Goodarzi et al. 2015, Liu, Dai et al. 2015, Liu, Zhou et al. 2017, Wu, Su et al. 2018)
IGF2BPs	Promote stability and storage of target m^{6}A mRNAs (Huang, Weng et al. 2018)
Proline rich coiled-coil 2A (Prrc2a)	Recently discovered, reported to stabilise a critical m^{6}A modified transcript required for myelination (Wu, Li et al. 2019)
Fragile X mental retardation 1 (FMR1)	Affects RNA translation and RNA stability likely through interplay with YTHDF1 and YTHDF2 (Edupuganti, Geiger et al. 2017, Zhang, Kang et al. 2018)
Eukaryotic initiation factor 3 (eIF3)	Participates in translation initiation, and allows for cap-independent translation of mRNAs with m^{6}A modified 5′ UTR (Meyer, Patil et al. 2015)

Table 1.3.2.3 m^{6}A readers and their functions.

In humans, the YTH domain family of proteins includes five members; cytoplasmic YTHDF1, YTHDF2, YTHDF3 and YTHDC2, and nuclear YTHDC1. Although YTHDF1, YTHDF2 and YTHDF3 have been shown to have their own unique target mRNAs, there is also a set of common mRNA targets which they share (Wang, Zhao et al. 2015, Shi, Wang et al. 2017). YTHDF1 has been shown to promote mRNA translation, by delivering more cellular mRNAs to translation machinery, and also by increasing mRNA translation efficiency (Wang, Zhao et al. 2015). In contrast, YTHDF2 has been shown to affect the stability of m^{6}A-modified mRNAs by localising them to mRNA decay sites, such as processing bodies (Wang, Lu et al. 2014). The opposing roles of YTHDF1 and YTHDF2, and the overlap of their mRNA targets, indicate a degree of complexity in the overall function of m^{6}A on mRNA. Interestingly, Wang et al. reported that shared mRNA targets are first bound by YTHDF1, and subsequently by YTHDF2, and proposed that the two reader proteins might be playing complementary roles to provide a tight level of control (i.e. a rapid but short-lived response of sufficient magnitude) of gene expression at the post transcriptional level (Wang, Zhao et al. 2015).

Further complexity is evident in the opposing roles of YTHDF2 and IGFBP2 on m^{6}A mRNA stability. In 2016, Du et al. showed that YTHDF2 recruits the CCR4-NOT complex by a direct interaction between the YTHDF2 N terminus and the SH domain of the CNOT1 subunit, thereby targeting m^{6}A containing mRNAs for deadenylation by CAF1 and CCR4, and subsequent degradation (Du, Zhao et al. 2016). In contrast, Huang et al. showed in 2018 that IGF2BPs promote the stability and storage of their target mRNAs (for example, *MYC*) in an m^{6}A dependent manner under normal and

stress conditions. One explanation for the differential outcome following m^6A mRNA binding by YTHDF2 and IGF2BPs is their differential binding sites on mRNA; whilst YTHDF2 favours the 3' UTR, IGFBPs preferentially bind to the coding sequence (Huang, Weng et al. 2018).

Very recently, Ries et al. published a study showing that the cytosolic m^6A-binding proteins YTHDF1, YTHDF2 and YTHDF3 undergo liquid-liquid phase separation *in vitro* and in cells (Ries, Zaccara et al. 2019). These authors showed that polymethylated mRNAs act as a multivalent scaffold for the binding of the low complexity domain YTHDF proteins, ultimately resulting in phase separated YTHDF–m^6A–mRNA complexes in cells. As a result, the number and location of m^6A sites on mRNA (which varies according to disease state and cell type) determines the composition of the phase separated transcriptome, which in turn influences partitioning into intracellular compartments for example P-bodies, stress granules, or neuronal granules. Thus, the pattern of m^6A mRNA methylation is important in determining phase separation and therefore the outcome of m^6A mRNA modification (Ries, Zaccara et al. 2019).

1.3.3 YTHDF2

The *YTHDF2* gene (located on chromosome 1) encodes a 579-residue protein, which is identified in the Swiss-Prot database with the accession number Q9Y5A9. Synonyms for YTHDF2 include High-Glucose-Regulated Protein 8, Renal Carcinoma Antigen NY-REN-2, and CLL-Associated Antigen KW-14. BLAST analysis has shown that the *YTHDF2* gene spans 32 kilobases and consists of 5 exons (Cardelli, Marchegiani et al. 2006). The YTHDF2 protein is highly conserved across vertebrates, with a stretch of 546 residues in the human protein which are 99.7% identical to that of the mouse, and a stretch of 518 residues which show significant similarity (89.8%) to that of the zebrafish (Cardelli, Marchegiani et al. 2006).

The YTHDF2 C-terminal YTH domain is responsible for specifically binding m^6A containing mRNA, with a preference for transcripts containing a consensus motif of G(m^6A)C (Wang, Lu et al. 2014). The crystal structure of YTHDF2 has been reported by two groups, revealing the mechanism for recognition of m^6A (Li, Zhao et al. 2014, Zhu, Roundtree et al. 2014). Zhu et al. reported that YTH domains are highly conserved across YTH-domain containing proteins (YTHDF1-3, YTHDC1-2) and

species, implying an important function. Through fluorescence polarization assays and electrophoretic mobility shift assays, they showed that YTHDF2 binds m^6A RNA with a significantly higher affinity than unmodified RNA. Crystal structure analysis of YTHDF2 revealed a globular fold with a central core of 4-stranded β-sheets surrounded by 4 α helices and flanking regions on two sides. Subsequently, these authors showed the basic residues K416 and R527 on the surface of YTHDF2 are involved in binding to the RNA backbone, whilst the residues W432 and W486 within an adjacent hydrophobic pocket contribute to the specific recognition of m^6A (Zhu, Roundtree et al. 2014). Similarly, Li et al. also showed that YTHDF2 binds m^6A via a hydrophobic pocket, and went on to show that the m^6A mononucleotide is positioned in an aromatic cage of three aromatic amino acids, of which Trp486 from β4-β5 loop forms the base, and Trp432 from β2 strand and Trp491 from β4-β5 loop form the walls (Li, Zhao et al. 2014).

In the mouse, *Ythdf2* is highly expressed in a wide range of tissues, including testis, ovary, spleen, liver, thymus (Ivanova, Much et al. 2017). In a study from 2017, YTHDF2 deletion in mice was reported to be partially permissive, with approximately half of expected *Ythdf2* knock out mice observed at weaning. Viable *Ythdf2* knock out mice in that study were outwardly indistinguishable from their wild type or heterozygous litter mates, but females were sterile. Through a maternal conditional deletion strategy, this sterility was shown to be due to a lack of *Ythdf2* within the germline, resulting in failure of maternal RNA degradation and stalled oocyte development (Ivanova, Much et al. 2017). In contrast, a study from 2018 used a different knock out mouse strain in which *Ythdf2* deletion was found to be embryonic lethal, with the majority of lethality occurring between E14.5 and E18.5 (Li, Zhao et al. 2018). Analysis of dissected knock out and heterozygous embryos (the latter showed semi-lethality) revealed abnormal cortical development in the absence of *Ythdf2.* Mechanistically, the authors attributed this to reduced degradation of neuron differentiation-related m^6A-containing mRNAs in *Ythdf2* deficient embryos (Li, Zhao et al. 2018).

It has been shown that YTHDF2 can relocate from the cytoplasm to the nucleus in response to stress, for example following heat shock (Zhou, Wan et al. 2015). In this study, the authors showed that YTHDF2 competes with FTO in the nucleus to prevent 5'UTR demethylation of heat shock response genes. The increased 5'UTR

methylation enables cap-independent translation initiation, providing a mechanism for selective mRNA translation under heat shock stress.

A polymorphism of *YTHDF2* located in an Alu-Rich Genomic Domain is known to be associated with human longevity (Cardelli, Marchegiani et al. 2006), and *YTHDF2* has been described as a novel *RUNX1* translocation partner gene in human AML (Nguyen, Ma et al. 2006).

1.3.4 Roles of m^6A

Given the wide range of m^6A reader functions (**1.3.2.3**), it is not surprising that m^6A has been shown to play a critical role in almost all major biological processes, many of which have been presented already, in the context of m^6A regulators (see **1.3.2.1-3**).

m^6A has also been shown to regulate the pace of circadian RNA processing, and therefore control circadian clock speed (Fustin, Doi et al. 2013). Fustin et al. initially showed that a non-specific inhibitor of methylation, 3-deazaadenosine (DAA), lengthens the circadian period in cultured cell lines and in mice. High throughput sequencing and m^6A immunoprecipitation revealed a number of circadian RNAs marked by m^6A and downregulated by DAA. Fustin et al. subsequently showed that siRNA *Mettl3* inhibition extended the duration of the circadian period, and delayed the nuclear exit of mature *Per2* and *Bmal1* (*Arntl*) circadian clock gene mRNA (Fustin, Doi et al. 2013).

A recurring theme in the reported roles of m^6A mRNA methylation is its ability to regulate the transition between cell states. For example, early work by Geula et al. showed that m^6A-dependent regulation of the transcript stability of pluripotency regulators determines the transition between naïve pluripotency and differentiation in mouse embryonic stem cells (Geula, Moshitch-Moshkovitz et al. 2015). More recently, a study by Zhao et al. highlighted the role of m^6A in maternal-to-zygotic transition in zebrafish (Zhao, Wang et al. 2017). In this study, Zhao et al. crossed *Ythdf2*-deficient female zebrafish to wild type males, creating offspring lacking maternal *Ythdf2*. Loss of maternal *Ythdf2* slowed the rate of decay of maternal mRNAs, impeding zygotic genome activation. Similarly, the loss of *Ythdf2* has been reported to inhibit oocyte

development (Ivanova, Much et al. 2017) and cortical development in mice (Li, Zhao et al. 2018). In both cases, failure of transition was attributed to persistence of mRNAs associated with the existing cell state.

1.3.5 m^{6}A in cancer

Given the critical role that m^{6}A plays in both self-renewal and differentiation in cells, it is not surprising that m^{6}A also plays a regulatory role in the context of cancer. Investigations into the effect of dysregulated m^{6}A methylation machinery (writers, erasers or readers) show that m^{6}A regulators can act as tumour suppressors or oncogenes, depending on the context. A summary of these studies is shown in **Table 1.3.5**.

Cancer Type	Enzyme	Role	Pathway(s) affected	References
Hepatocellular carcinoma	YTHDF2	Tumour suppressor	MEK/ERK	(Zhong, Liao et al. 2019)
	YTHDF2	Oncogene	miR145	(Yang, Li et al. 2017)
	METTL3	Oncogene	SOCS2	(Chen, Wei et al. 2018)
	METTL14	Tumour suppressor	miR126	(Ma, Yang et al. 2017)
Glioblastoma	ALKBH5	Oncogene	FOXM1	(Zhang, Zhao et al. 2017)
	METTL3/14	Tumour suppressors	ADAM19, EPHA3, KLF4	(Cui, Shi et al. 2017)
	METLL3	Oncogene	SOCS2	(Visvanathan, Patil et al. 2018)
Endometrial cancer	METTL3/14	Tumour suppressors	AKT	(Liu, Eckert et al. 2018)
Breast cancer	ALKBH5	Oncogene	NANOG	(Zhang, Samanta et al. 2016)
Cervical cancer	FTO	Oncogene	Unknown	(Wang, Li et al. 2017)
Pancreatic cancer	YTHDF2	Oncogene Tumour suppressor	AKT/GSK3ß/CyclinD1 EMT/YAP	(Chen, Sun et al. 2017)
Gastric cancer	METTL3	Oncogene	AKT/ p70S6K/CyclinD1	(Lin, Liu et al. 2019)
	YTHDF2	Oncogene	Unknown	(Zhang, Pi et al. 2017)
Lung adenocarcinoma	METTL3	Oncogene	miR-33-a	(Lin, Choe et al. 2016)
Prostate cancer	YTHDF2	Oncogene	Unknown	(Li, Meng et al. 2018)
Acute myeloid leukaemia	METTL3	Oncogene	CEBPZ, c-MYC, SP1, SP2	(Barbieri, Tzelepis et al. 2017)
	METTL3	Oncogene	c-MYC, BCL2, PTEN	(Vu, Pickering et al. 2017)
	METTL3	Oncogene	MYB, MYC	(Weng, Huang et al. 2018)
	METTL14	Oncogene	MYB, MYC	(Weng, Huang et al. 2018)
	FTO	Oncogene	ASB2, RARA	(Li, Weng et al. 2017)

	FTO	Oncogene	MYC/CEBPA	(Su, Dong et al. 2018)
	IGF2BP	Oncogene	MYC	(Huang, Weng et al. 2018)

Table 1.3.5 The role of m^{6}A regulators in cancer. Adapted (and modified) from Fitzimmons and Batista (Fitzsimmons and Batista 2018).

The role of m^{6}A in hepatocellular carcinoma (HCC) is controversial. In 2017, Yang et al. reported that YTHDF2 levels are increased in HCC, and are negatively correlated with prognosis. They also showed that microRNA (miR)-145 levels are decreased in HCC, and that overexpression of *miR-145* decreases YTHDF2 expression at both the mRNA and protein levels, by targeting the 3' UTR of *YTHDF2* mRNA (Yang, Li et al. 2017). Whilst this study indicated an oncogenic role for YTHDF2 in HCC, a recent study proposed that YTHDF2 acts as a tumour suppressor in this tumour instead (Zhong, Liao et al. 2019). Zhong et al. reported that *YTHDF2* is specifically induced by hypoxia in HCC, and suppresses cell proliferation, tumour growth, and activation of MEK and ERK in HCC cells. Mechanistically, the authors showed that m^{6}A-dependent YTHDF2 binding to the 3'UTR of *EGFR* mRNA results in degradation of *EGFR* mRNA in HCC cells, and therefore suppression of cell proliferation and growth.

In contrast, a study into the role of METTL3 in HCC showed that m^{6}A-dependent YTHDF2-mediated mRNA degradation promotes tumour progression (Chen, Wei et al. 2018). Chen et al. showed that *METTL3* levels and m^{6}A methylation levels are increased in HCC and are correlated with a negative prognosis. These authors demonstrated decreased HCC tumorigenicity and lung metastasis *in vivo* following *METTL3* knock out, and conversely, increased HCC growth *in vitro* and *in vivo* in response to *METTL3* overexpression. Mechanistically, they identified suppressor of cytokine signalling 2 (SOCS2) as a target of METTL3 m^{6}A modification, and showed that m^{6}A targets *SOCS2* mRNA for degradation via YTHDF2 (Chen, Wei et al. 2018). The findings of Chen et al. were surprising in view of earlier work by Ma et al., who reported decreased m^{6}A methylation levels in HCC, alongside a reduction in *METTL14* expression (Ma, Yang et al. 2017). These authors reported that METTL14 suppresses the metastatic potential of hepatocellular carcinoma by modulating m^{6}A-dependent primary microRNA processing. Specifically, they identified *miR-126* as a critical target of METTL14 in metastatic HCC, and showed that depletion of *METTL14* decreased *miR-126* expression by modulating binding of the microprocessor protein DGCR8 to primary *miR126* in an m^{6}A dependent manner (Ma, Yang et al. 2017).

In glioblastoma, as in HCC, the role of m^{6}A methylation is a subject of debate. In 2017, Zhang et al. showed that *ALKBH5* is highly expressed in glioblastoma stem cells (GSCs), and is associated with a poor prognosis. Mechanistically, increased *ALKBH5* expression was reported to increase demethylation of *FOXM1* mRNA, and therefore decrease m^{6}A-mediated *FOXM1* mRNA degradation, ultimately increasing FOXM1 levels (Zhang, Zhao et al. 2017). In the same year, Cui et al. reported that knockdown of *METTL3* or *METTL14* dramatically promotes GSC growth, self-renewal and tumorigenesis, whilst *METTL3* overexpression, or inhibition of *FTO* suppresses GSC growth and self-renewal. Mechanistically, Cui et al. showed that these effects depended on m^{6}A mRNA modification of target oncogenes including *ADAM19*, *EPHA3*, and *KLF4* (Cui, Shi et al. 2017). More recently however, Visvanathan et al. reported an opposing role for METTL3 in glioblastoma. These authors showed that m^{6}A modification is increased in GSCs and that METTL3-dependent m^{6}A modification is crucial for GSC maintenance. Mechanistically, they identified *SOX2* mRNA as a downstream target of METTL3, whose stability is increased following m^{6}A modification in a Human antigen R-dependent fashion (Visvanathan, Patil et al. 2018).

In tumours of female reproductive organs, m^{6}A methylation has repeatedly been associated with tumour suppression. Liu et al. reported that up to 70% of endometrial tumours have decreased m^{6}A methylation compared to matched normal endometrial tissue, due to a hotspot R298P mutation in *METTL14*, or a reduction in *METTL3* expression (Liu, Eckert et al. 2018). Mechanistically, these authors showed that reductions in m^{6}A methylation lead to decreased expression of the negative AKT regulator *PHLPP2* and increased expression of the positive AKT regulator *mTORC2*, ultimately increasing proliferation and tumorigenicity of endometrial cancer cells (Liu, Eckert et al. 2018). Reductions in m^{6}A methylation have also been implicated in breast cancer pathogenesis. Zhang et al. reported that hypoxia stimulates hypoxia-inducible factor (HIF)-1α- and HIF-2α-dependent expression of *ALKBH5* in breast cancer cells. This increased *ALKBH5* expression decreases m^{6}A methylation of *NANOG* mRNA, which increases NANOG levels, and the breast cancer stem cell phenotype (Zhang, Samanta et al. 2016). Finally, decreased m^{6}A methylation is also reported to drive cervical cancer progression. Wang et al. reported decreased m^{6}A methylation in cervical cancer cells compared to adjacent normal tissue, and showed that increased m^{6}A methylation (through knockdown of *FTO*/*ALKBH5* demethylases, or overexpression of *METTL3*/*METTL14* methyltransferases) suppressed cervical tumour development *in vitro* and *in vivo* (Wang, Li et al. 2017).

m^{6}A regulators have also been implicated in tumours of the gastrointestinal tract, pancreas and lungs. Increased *YTHDF2* expression in pancreatic cancer has been reported to promote proliferation, whilst inhibiting migration and invasion (so called 'migration proliferation dichotomy') (Chen, Sun et al. 2017). In gastric cancer, both *METTL3* and *YTHDF2* have been reported to act as oncogenes (Zhang, Pi et al. 2017, Lin, Liu et al. 2019), and in pulmonary adenocarcinoma, METTL3 promotes tumour growth, survival and invasion through enhanced translation of certain mRNAs, including *TAZ* and *EGFR* (Lin, Choe et al. 2016).

In addition to its role in solid tumours, m^{6}A modification is known to play a critical role in haematological malignancies, in particular AML. Analysis of datasets from the Cancer Genome Atlas Research Network (TCGA) revealed that mutations or copy number variations of m^{6}A regulatory genes are strongly associated with *TP53* mutations in AML, and predict a poorer prognosis in these patients (Kwok, Marshall et al. 2017). Studies in mice and human cells have shown an essential requirement for the methyltransferases METTL3 and METTL14 (Barbieri, Tzelepis et al. 2017, Li, Weng et al. 2017, Vu, Pickering et al. 2017, Weng, Huang et al. 2018) and the demethylase FTO (Li, Weng et al. 2017) in AML. However, the role of the YTH-family of m^{6}A readers in AML, including that of YTHDF2, has not been investigated previously.

1.4 Hypothesis and aims

Given the critical role that m^{6}A plays in both self-renewal and differentiation in cells, and the rapidly accumulating evidence of its function in cancer, we hypothesized that the m^{6}A reader YTHDF2 would play a significant role in normal and malignant haematopoiesis.

The aims of this thesis were therefore to establish the requirement for YTHDF2 in normal haematopoiesis and in the context of AML. By characterizing the role of YTHDF2 in HSC fate decisions, we hoped to identify potential novel therapies with which to eliminate leukaemic stem cells in AML, and therefore improve the prognosis for what is currently still a devastating disease.

Chapter 2: Methods

2.1 Mouse strains

All mice were on the C57BL/6 genetic background. *Ythdf2*$^{fl/fl}$ transgenic mice were generated by Ivanova et al. (Ivanova, Much et al. 2017). *Vav-iCre* (de Boer, Williams et al. 2003) and *Mx1-Cre* (Kuhn, Schwenk et al. 1995) mice were purchased from the Jackson Laboratory. Conditional knock out mice were generated by crossing *Ythdf2*$^{fl/fl}$ mice with *Vav-iCre* mice. Inducible knock out mice were generated by crossing *Ythdf2*$^{fl/fl}$ mice with *Mx1-Cre* mice. All transgenic and knockout mice were CD45.2^{+}. Congenic recipient mice were CD45.1^{+}/CD45.2^{+}.

2.2 Mouse husbandry

All experiments were performed with Home Office approval, under the project licence 70/8417 and the personal licence I9FC1E63F. Mice were housed in a dedicated specific pathogen free facility, and every effort was made to comply with the 3Rs principles in the course of their use. Mice were used for breeding from 6-8 weeks of age, and were housed as pairs or triplets. Pups were weaned at 3 weeks of age, at which time they were ear notched for identification purposes. The tissue obtained during the notching process was used for subsequent genotyping. Stock mice were caged in sex-matched groups of ≤ 6 mice.

2.3 Genotyping

Polymerase chain reaction (PCR) was used to genotype all transgenic mice. PCR is a method which uses thermal cycling for exponential amplification of small amounts of DNA. The process involves 20-40 cycles of three basic steps: denaturation of double-stranded DNA into single strands, annealing of specific primers, and DNA replication by DNA polymerase.

2.3.1 DNA extraction

Genomic DNA was extracted from ear notching tissue or haematopoietic cells using the PCR Direct Genotyping Kit (Cat. B40015-BIT, Bimake) according to the manufacturer's instructions. Samples were placed into 1.5 ml centrifuge tubes. In a

separate tube, a protease mixture was prepared using Buffer L (100 μl per sample) and Protease Plus (2 μl per sample). The mixture was added to the sample tubes and incubated for 15 minutes at 55°C. The digested samples were incubated for a further 5 minutes at 95°C, after which the lysates were ready for use as a PCR template.

2.3.2 PCR primers and programmes

A PCR Mix was prepared using PCR Super Master Mix™ (Cat. B46018, Bimake) or Mango Mix™ (Cat. BIO-25033, Bioline), each of which contained DNA Polymerase, $MgCl_2$ and dNTPs. Water, primers and extracted genomic DNA were added to this mix, as detailed below. All primers were made up at 100 μM.

2.3.2.1 *Vav-iCre* PCR

***Vav-iCre* PCR Mix**	
2 μl DNA	DNA
0.1 μl	CCGAGGGGCCAAGTGAGAGG
0.1 μl	GGAGGGCAGGCAGGTTTTGGTG
10 μl	PCR Super Master Mix™
7.8 μl	Nuclease free H_20

The PCR programme consisted of 5 minutes at 95°C (initialisation); 30 cycles of 94°C for 30 seconds, 64°C for 40 seconds, 72°C for 30 seconds (denaturation, primer annealing and elongation); then 72°C for 5 minutes (final elongation), and finally the samples were held at 10°C. The expected band (Cre) was 400 bp.

2.3.2.2 *Mx1-Cre* PCR

***Mx1-Cre* PCR Mix**	
2 μl	DNA
0.1 μl	CGTTTTCTGAGCATACCTGGA
0.1 μl	ATTCTCCCACCGTCAGTACG
10 μl	PCR Super Master Mix™
7.8 μl	Nuclease free H_20

The PCR programme consisted of 5 minutes at 95°C (initialisation); 39 cycles of 95°C for 30 seconds, 67°C for 45 seconds, 72°C for 1 minute (denaturation, primer annealing and elongation); then 72°C for 5 minutes (final elongation), and finally the samples were held at 10°C. The expected band (Cre) was 400 bp.

2.3.2.3 *Ythdf2* flox PCR

YTHDF2 flox PCR Mix	
2 μl	DNA
0.1 μl	GGGGAAAGGACCTTTCCGAA
0.1 μl	CAGTGTATTGGCTCCTTCGAA
10 μl	PCR Super Master Mix™
7.8 μl	Nuclease free H_20

The PCR programme consisted of 5 minutes at 95°C (initialisation); 34 cycles of 95°C for 30 seconds, 60°C for 1 minute, 72°C for 40 seconds (denaturation, primer annealing and elongation); then 72°C for 5 minutes (final elongation), and finally the samples were held at 10°C. The expected bands were: Wild Type (294 bp) and Flox (340 bp).

2.3.2.4 Sexing PCR

Sexing PCR Mix	
2 μl	DNA
0.1 μl	AATAAATGTTTTACAACTCCTGATTCC
0.1 μl	TGCATAGACGTGTAAAACCTGC
0.1 μl	GAGAGCATGGAGGGCCAT
0.1 μl	CCACTCCTCTGTGACACT
10 μl	PCR Super Master Mix™
7.6 μl	Nuclease free H_20

The PCR programme consisted of 3 minutes at 95°C (initialisation); 34 cycles of 95°C for 30 seconds, 60°C for 30 seconds, 72°C for 30 seconds (denaturation, primer annealing and elongation); then 72°C for 2 minutes (final elongation), and finally the samples were held at 12°C. The expected bands were: 195 bp (X) and 266 bp (Y).

2.3.3 Gel electrophoresis

PCR products were separated according to molecular size using gel electrophoresis. Agarose gels were prepared by dissolving agarose (Cat. AG500, Thistle) in 1X TAE buffer (40 mM Tris acetate, pH 8.3, 1 mM EDTA) (Cat. 161-0773, Biorad) and Sybr™ Safe DNA Gel Stain (Cat. S33102, Life Technologies), which is a less hazardous alternative to ethidium bromide for visualisation of DNA in agarose gels, was added at 0.0001X. Gels were run at 90 V in 1X TAE buffer, and DNA band length was measured against a standard ladder (Easy Ladder I, Cat. BIO-33046, Bioline). The agarose percentage of the gel and the running time were tailored to achieve optimal resolution of PCR products (see **Table 2.3.3**).

PCR	Agarose (%)	Gel running time (minutes)
Vav-iCre	2	40
Mx1-Cre	2	40
Ythdf2 flox	2.5	120
Sexing PCR	2	40

Table 2.3.3 Gel electrophoresis resolution of specific PCR products.

2.4 Cell lines and primary murine cells

Two packaging cell lines were used for virus production, one for lentiviral production (HEK 293T) and one for retroviral production (Platinum E).

2.4.1 HEK 293/HEK 293T - HEK 293 cells are a packaging cell line established from primary embryonic human kidney transformed with sheared human adenovirus type 5 DNA. These cells are straightforward to grow in culture and highly transfectable by various techniques, including the calcium phosphate method. A variant of this cell line

is HEK 293T, which additionally contain the SV40 Large T-antigen that allows for episomal replication of transfected plasmids containing the SV40 origin of replication.

2.4.2 Platinum-E (Plat-E) - these cells are a retrovirus packaging cell line based on the HEK 293T cell line. These cells express *gag*, *pol* and *env* genes under the control of an EF1α promoter, allowing for retroviral packaging with a single plasmid transfection, and ensuring longer stability and high-yield structural protein expression. An IRES (internal ribosome entry site) potentiates expression of blasticidin and puromycin selection markers.

2.4.3 NIH3T3 - murine fibroblast cell line used for testing virus.

2.4.4 Primary murine cells - pre-leukaemic stem cells (pre-LSCs) were generated by retroviral transformation of foetal liver (FL) haematopoietic stem and progenitor cells (HSPCs) followed by serial re-plating (see section **2.13**). Leukaemic stem cells (LSCs) were harvested from the bone marrow of leukaemic recipient mice.

2.5 Cell culture

Pre-LSCs and LSCs were cultured in Iscove's Modified Dulbecco's Medium (IMDM) (Cat. 12440061, Life Technologies) with 10% foetal bovine serum (FBS), 2.0 mM L-glutamine, 1% penicillin/streptomycin (100 Units/ml penicillin and 100 mg/ml streptomycin) and cytokines favouring myeloid differentiation: IL-3 20 ng/ml, IL-6 20 ng/ml, and SCF 40 ng/ml (IL-3 Cat. 575506; IL-6 Cat. 575706; SCF Cat. 579708, all from Biolegend). Cells were cultured in an incubator at 5% CO_2 and 37°C. Cells were passaged every 2-3 days at 200 000 cells/ml.

HEK293, Plat-E and NIH3T3 cells were all cultured in Dulbecco's Modified Eagle Medium (DMEM) (Cat. 41965062, Life Technologies) supplemented with 10% FBS, 2.0 mM L-glutamine and 1% penicillin/streptomycin (100 Units/ml penicillin and 100 mg/ml streptomycin). Cells were cultured in an incubator at 5% CO_2 and 37°C. Cells were passaged in a 1:10 split ratio once they reached 80% confluency, which was approximately every 3-4 days.

The number and viability of cells in culture was determined by staining a 10 μl aliquot of cell suspension with Trypan Blue (Cat. T8154, Sigma Aldrich), and counting live (unstained) versus dead (stained blue) cells with a haemocytometer.

2.5.1 Freezing cells

To freeze harvested cells (either cell lines or primary murine cells), cells in the exponential phase of cell growth were centrifuged (500 g for 5 minutes) and the pellet was re-suspended in cold freezing mix (i.e. FBS containing 10% DMSO (Sigma)) and aliquoted to pre-chilled 1.8 ml cryovials. Each vial contained approximately 0.5-3 x 10^6 cells. These cryovials were transferred to a freezer box (Cat 5100-0001, Thermo Fisher Scientific, allows slow cooling at the rate of - 1°C/min) and placed into the -80°C freezer overnight. The cells were then moved to liquid nitrogen for long-term preservation. In order to culture cells from liquid nitrogen, cells in the cryovials were thawed in a water bath at 37°C and swiftly transferred into a conical tube containing 10 ml of standard culture media (containing 10% FBS), pre-warmed at 37°C. The cells were centrifuged (300 g for 3 minutes) and then cultured as described above.

2.6 Blood sampling

Peripheral blood samples were obtained from the tail vein for haematopoietic multilineage assessment. Mice were warmed in a heat box at 38°C to induce vasodilation. Individual mice were then identified based on ear notches, and placed into a restraining tube. Blood samples were collected from the lateral tail vein by puncturing the vein with a needle (25g 5/8 inch) before applying the tip of an EDTA collection tube (Microvette® CB 300 K2E, Cat. 16.444, Sarstedt) and allowing blood to enter via capillary action. A maximum of 200 μl of blood was collected per sampling, although typically the volume of blood collected was less than 50 μl.

For preparation of blood samples, 12μl of EDTA anti-coagulated blood was added to 600 μl of NH_4Cl and mixed thoroughly. The samples were incubated at room temperature for 10 minutes, then centrifuged at 400 g for 8 minutes. The supernatant was removed, and the cells were resuspended in pre-prepared antibody mix (see section **2.8**).

2.7 Preparation of bone marrow, spleen, thymus and foetal liver cell suspensions

To retrieve BM, tibias and femurs of both hind legs were taken from 8-12-week-old adult mice and crushed with a pestle and mortar to achieve a homogeneous cell suspension. BM cells were collected in PBS 2% FBS and filtered through a 70 μm nylon strainer (Cat. 22363548, Fisherbrand). Spleen, thymus and FL cell suspensions were all generated by mashing of the tissue with a 5 ml syringe plunger, and flushing through a 70 μm nylon strainer with PBS 2% FBS. Cell counts were obtained using an automatic cell counter (Celltac α MEK-6500K, Nihon Kohden) for use in subsequent assays.

2.8 Immunophenotypic characterisation of white blood cells (WBCs)

HSC staining: 12 x 10^6 BM or FL cells were centrifuged (500 g for 5 minutes) and resuspended in 50 μl of CD16/CD32 antibody (Fc Block) in cold phosphate-buffered saline (PBS, Sigma) supplemented with 2% heat-inactivated foetal bovine serum (PBS 2% FBS), then incubated at 4°C in the dark for 5 minutes. Next, 50 μl of 2X antibody mix containing Sca-1, c-Kit, CD48, CD150 and a biotin conjugated lineage cocktail (see **Table 2.8.1**) was added, and the sample was incubated for 30 minutes in the dark at 4°C. The cells were then washed in cold PBS 2% FBS, centrifuged (500 g for 5 minutes) and the pellet was resuspended in 100 μl of Streptavidin conjugated antibody. After 15 minutes of incubation in the dark at 4°C, the cells were washed in cold PBS 2% FBS, centrifuged (500 g for 5 minutes), resuspended in 500 μl cold PBS 2% FBS and filtered through 35 μm mesh into capped FACS tubes.

Myeloid progenitor cell staining (Pronk and Bryder 2011): 8 x 10^6 BM cells were centrifuged (500 g for 5 minutes) and resuspended in 100 μl of antibody mix containing Sca-1, c-Kit, CD150, CD16/32, CD41, CD105 and a biotin conjugated lineage cocktail (BM GMP lineage cocktail, see **Table 2.8.1**). The cells were incubated for 30 minutes in the dark at 4°C. The cells were then washed in cold PBS 2% FBS, centrifuged (500 g for 5 minutes) and the pellet was resuspended in 100 μl of Streptavidin conjugated antibody. After 15 minutes of incubation in the dark at 4°C, the cells were washed in cold PBS 2% FBS, centrifuged (500 g for 5 minutes),

resuspended in 500 μl cold PBS 2% FBS and filtered through 35 μm mesh into capped FACS tubes.

Lineage cocktail	Antibodies
FL SLAM lineage cocktail	CD4, CD5, CD8a, B220, Ter119, Gr-1
BM SLAM lineage cocktail	CD4, CD5, CD8a, B220, Ter119, Gr-1, CD11b
BM GMP lineage cocktail	CD4, CD5, CD8a, B220, Gr-1, CD11b

Table 2.8.1 Biotin-conjugated lineage antibody cocktails

Lineages staining: 2 x 10^5 cells (BM, spleen or thymus) were incubated for 20 minutes in the dark at 4°C with antibody mix as follows: myeloid cells (Gr-1$^+$, CD11b$^+$), B cells (B220$^+$, CD19$^+$), T cells (CD4$^+$, CD8$^+$), erythroid cells (Ter119$^+$, CD71$^+$). The cells were then centrifuged (500 g for 5 minutes), resuspended in 200 μl PBS 2% FBS and filtered through 35 μm mesh into capped FACS tubes.

Leukaemic cell staining: 2 x 10^5 BM cells were incubated for 20 minutes in the dark at 4°C with antibody mix as follows: CD45 markers (CD45.1, CD45.2), myeloid cells (Gr-1, CD11b), and c-Kit cells. The cells were then centrifuged (500 g for 5 minutes), resuspended in 200 μl PBS 2% FBS and filtered through 35 μm mesh into capped FACS tubes.

Antibody	Conjugate	Concentration	Cat #	Clone	Manufacturer
Anti-Mouse CD4	Biotin	0.3125 μg/mL	553649	H129.19	BD Biosciences
Anti-Mouse CD5	Biotin	0.625 μg/mL	553019	53-7.3	BD Biosciences
Anti-Mouse CD8a	Biotin	0.625 μg/mL	553029	53-6.7	BD Biosciences
Anti-Mouse CD11b	Biotin	2.5 μg/mL	553309	M1/70	BD Biosciences
Anti-Mouse CD45R/B220	Biotin	2.5 μg/mL	553086	RA3-6B2	BD Biosciences
Anti-Mouse Ter119	Biotin	10 μg/mL	553672	TER-119	BD Biosciences
Anti-Mouse Gr-1/Ly-6G/C	Biotin	5 μg/mL	553125	RB6-8C5	BD Biosciences

Anti-Mouse c-Kit/CD117	APC-Cy7	1 µg/mL	105826	2B8	Biolegend
Anti-Mouse c-Kit/CD117	APC	1 µg/mL	105812	2B8	Biolegend
Anti-Mouse Sca-1	PB	2.5 µg/mL	122520	E13-161.7	Biolegend
Anti-Mouse Sca-1	APC-Cy7	1 µg/mL	122513	E13-161.7	Biolegend
Anti-Mouse CD48	PE	0.25 µg/mL	103406	HM48-1	Biolegend
Anti-Mouse CD150	PE-Cy7	1 µg/mL	115914	12F12.2	Biolegend
Anti-Mouse CD45R/B220	PerCP	0.4 µg/mL	103236	RA3-6B2	Biolegend
Anti-Mouse CD19	APC-Cy7	0.2 µg/mL	6D5	115530	Biolegend
Anti-Mouse CD11b	PB	0.5 µg/mL	M1/70	101224	Biolegend
Anti-Mouse CD11b	PE	0.2 µg/mL	M1/70	101208	Biolegend
Anti-Mouse CD11b	APC	0.2 µg/mL	M1/70	101212	Biolegend
Anti-Mouse Gr-1/Ly-6G/C	PE-Cy7	0.1 µg/mL	RB6-8C5	108416	Biolegend
Anti-Mouse CD8a	APC	0.2 µg/mL	53-6.7	100712	Biolegend
Anti-Mouse CD8a	PE	0.2 µg/mL	53-6.7	100708	Biolegend
Anti-Mouse CD4	PE	0.05 µg/mL	H129.19	130310	Biolegend
Anti-Mouse CD45.1	BV711	0.4 µg/mL	A20	110739	Biolegend
Anti-Mouse CD45.2	PB	0.5 µg/mL	104	109820	Biolegend
Anti-Mouse Ter119	APC	0.2 µg/mL	TER-119	17-5921	eBiosciences
Anti-Mouse CD120b/TNFRII	PE	1 µg/mL	TR75-89	113405	Biolegend
Annexin-V (PE conjugated)	PE	1/100 dilution	-	556421	BD Biosciences
Streptavidin	PerCP	1.3 µg/mL	-	405213	Biolegend
Fc Block	None	10 µg/mL	2.4G2	553142	BD Biosciences

Table 2.8.2 Flow cytometry antibodies

For all analyses, cells were acquired on a FACS Fortessa (BD). Data were acquired through BD FACS Diva (BD Biosciences) and analysed by Flowjo software (Tree Star Inc., USA). TO-PRO™-3 Iodide (Cat. T3605, Life Technologies) or DAPI (4' ,6-Diamidino-2-Phenylindole, Dihydrochloride) (Cat. D1306, Life Technologies) were used for dead cell exclusion.

2.9 Transformation and maxiprep of plasmid DNA

Bacteria (α-Select Chemically Competent Cells, Cat. BIO-85027, Bioline) were transformed with plasmids. For this, 1.5 μl of plasmid was mixed with 20 μl of competent bacteria in a 1.5 ml centrifuge tube. After 5 minutes of incubation on ice, the tube was placed in a water bath at 42°C for 30 seconds followed by 2 minutes of incubation on ice. The mix was streaked onto a Lysogeny Broth (LB) agar plate containing 100 μg/ml of ampicillin and incubated overnight at 37°C. An individual colony from the LB agar plate was selected and cultured in 5 ml of LB broth (starter culture) with ampicillin (100 μg/ml) for 6 hours at 37°C in the bacterial shaker.

Maxiprep of plasmids was carried out using the HiSpeed Plasmid Maxi Kit (Cat. 12663, Qiagen), according to the manufacturer's instructions. Briefly, the starter culture was added to 250 mL of LB broth and incubated in a shaker overnight at 37°C. The following day the bacteria were harvested by centrifugation at 6000 g for 15 minutes at 4°C. The resultant bacterial pellet was re-suspended in 10 ml of Buffer P1 (lysis step). Following addition of 10 ml Buffer P2, the mixture was incubated at room temperature for 5 minutes. 10 ml of pre-chilled Buffer P3 were then added and the lysate was transferred into the QIAfilter Cartridge and incubated at room temperature for 10 minutes. The lysate was then filtered through the QIAfilter Cartridge outlet nozzle into the equilibrated HiSpeed tip and left to enter the resin by gravity flow. The HiSpeed tip was then washed with 60 ml of Buffer QC and DNA was eluted with 15 ml of Buffer QF. DNA was precipitated by adding 10.5 ml isopropanol, and then isolated by filtering the mixture through a QIAprecipitator Module. Following a 70% ethanol wash, DNA was eluted from the QIAprecipitator Module in a final volume of 0.4 ml of nuclease free water. The concentration of the eluted DNA was measured by nanodrop spectrometer (Nanodrop ND1000 Spectrophotometer; Labtech International Ltd, East Sussex, UK). The DNA purity was assessed through the ratio of absorbance at 260 nm and 280 nm. DNA with an A260/A280 ratio of 1.7 - 1.9 was considered pure.

2.10 Retrovirus/lentivirus production

Both lentiviral and retroviral vectors were used during this project. In contrast to y-retroviruses, which can only infect mitotically active cell types, lentiviruses (a subtype of retrovirus) are able to infect non-diving and actively dividing cell types. Retroviruses

were therefore used to deliver oncogenes to transform HSPCs (e.g. *Meis1/Hoxa9*), and lentiviruses were used as vectors during rescue experiments for shRNA delivery (*Tnfrsf1b* knock-down).

The constructs used in the respective systems are listed below, and illustrated in **Figure 2.10**. In both cases, a transfer plasmid is used to deliver the transgene, sgRNA, or shRNA of interest. The transgene sequence is flanked by long terminal repeat sequences (LTRs), which facilitate integration of the plasmid sequences into the host genome.

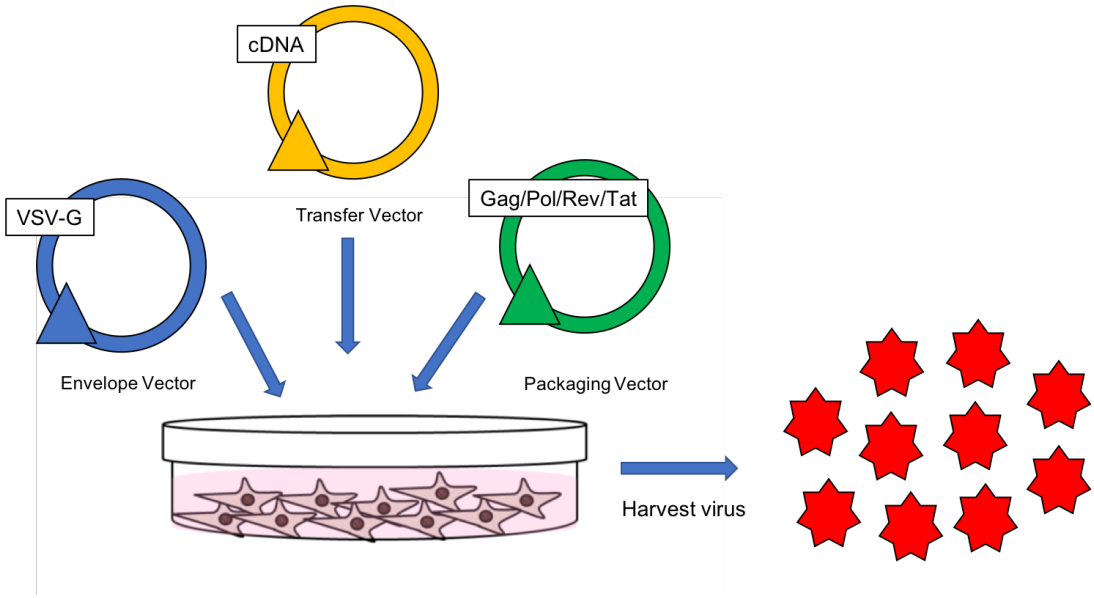

Figure 2.10 Lentiviral production schematic. Retrovirus was produced in the same way, but without the packaging vector. Adapted from https://www.addgene.org/viral-vectors/lentivirus/lenti-guide/.

For lentiviral production, a second-generation system was used (see **Figure 2.10**), consisting of 3 plasmids; the lentiviral transfer plasmid encoding the insert of interest, the envelope plasmid VSV-G, and the packaging plasmid psPAX2, which encodes the *gag*, *pol*, *rev*, and *tat* genes. Since retrovirus was produced in Plat-E cells, which express *gag*, *pol* and *env* genes, only the transfer plasmid was required in that case. Nevertheless, the pantropic envelope plasmid VSVG was also added because Plat-E cells express an ecotropic envelope protein (able to infect only mouse and rat cells), which is less stable when compared to VSVG pseudotyped virus.

2.10.1 Lentiviral constructs

pLKO.1 puro - third generation transfer plasmid (HIV-based). This is a recommended vector for cloning and expressing new shRNA sequences, and is being used by the RNAi Consortium to produce their shRNA library (https://portals.broadinstitute.org/gpp/public/). This plasmid was used to package shRNA for knockdown of *Tnfrsf1b* (see section **2.17**). Selection is based on puromycin resistance.

psPAX2 - lentiviral packaging plasmid encoding the *rev*, *pol*, *gag* and *tat* genes, and therefore suitable for both second and third generation lentiviral systems. Viral structural proteins are encoded by *gag* (group specific antigen) and *pol* (DNA polymerase), whereas essential regulatory elements are encoded by *re*v (regulator of expression of virion proteins) and *tat* (HIV trans-activator).

- **Gag** is the major strutural protein of retroviruses, contributing to the matrix, capsid and nucleocapsid.
- **Pol** is a precursor protein to reverse transcriptase, integrase and protease viral enzymes.
- **Tat** facilitates the activation of transcription from the LTR promoter.
- **Rev** binds to the Rev response element in order to facilitate nuclear export.

VSV-G - Vesicular stomatitis virus G glycoprotein is an envelope plasmid encoding the *env* gene. VSV-G is commonly used in lentiviral particle production because it confers broad tropism over a range of species and cell types.

2.10.2 Retroviral constructs

MSCV – Murine Stem Cell Virus transfer plasmid used for retroviral packaging. This plasmid is optimized for introducing and expressing target genes in pluripotent cells, including murine haematopoietic cells.

PGK – the phosphoglycerate kinase (PGK) promoter drives the expression of antibiotic resistance genes thus enabling selection of infected cells on the basis of antibiotic resistance.

MSCV-*Meis1-puro* – Mouse *Meis1a* cDNA cloned into the EcoRI and HpaI site of the MSCV- PGK-PAC retroviral vector. The LTR region controls the expression of the *Meis1* gene and the PGK promoter drives the puromycin resistance cassette (Kroon, Krosl et al. 1998).

MSCV-*HoxA9-neo* – Mouse *HoxA9* cDNA inserted in the BamHI-XhoI site of the pMSCVneo vector (neomycin (G418) resistance) (Kroon, Krosl et al. 1998). The LTR region controls the expression of the *HoxA9* gene and the PGK promoter drives the neomycin resistance cassette.

MSCV-*MOZ-TIF2-GFP* – This plasmid was a gift from Brian Huntly (Deguchi, Ayton et al. 2003). To construct the expression vector *MOZ-TIF2*, the breakpoint region was PCR amplified from patient cDNA (Carapeti, Aguiar et al. 1998) and ligated to 5 *MOZ* fragment obtained from *pBS-MOZ* (kindly provided by J. Borrow) and 3 *TIF2* fragment obtained from *pSG5-TIF2* (kindly provided by H. Gronemeyer) by two step ligation. The full-length cDNA was subcloned from pcDNA to *MSCV2.2* GFP into the XhoI-EcoRI sites.

MSCV-PML-RARA-neo – This plasmid was a gift from Eric So (Esposito, Zhao et al. 2015). The LTR region controls the expression of the *PML-RARA* gene and the PGK promoter drives the neomycin resistance cassette.

MSCV-MII-AF9 GFP – This plasmid was a gift from Neil Rodrigues. Selection is based on GFP fluorescence (Krivtsov, Twomey et al. 2006).

2.10.3 Packaging virus

Plat-E cells and HEK 293T cells were used to package MSCV constructs and lentiviral vectors respectively. Transfection was carried out using the calcium phosphate method, which relies upon formation of a calcium phosphate-DNA precipitate to facilitate DNA binding to the cell surface, and ultimately entry of DNA to the cell by (Kingston, Chen et al. 2003).

For viral production, 10 cm tissue culture dishes were coated with 0.1% sterile gelatin for 20 minutes at room temperature. HEK 293T or Plat-E cells were trypsinised with care to obtain a single cell suspension, and 2 x 10^6 cells in 8 ml of supplemented DMEM (see section **2.5**) were plated as evenly as possible into each dish, then

incubated at 37°C and 5% CO_2 overnight. The following morning dishes suitable for transfection were selected based on the degree of cell confluency and evenness of plating. Culture media was removed from these dishes and replaced with DMEM supplemented with 10% FBS and 2.0 mM L-glutamine. 25 μM chloroquine (Cat. C6628-25G, Sigma) was added to increase transfection efficiency through preservation of transfected DNA integrity (Luthman and Magnusson 1983).

For transfection (quantities given per 10 cm dish), 12.5 μg of plasmid DNA, 4 μg of VSV-G envelope plasmid, 6 μg HIV packaging plasmid (lentiviral production only) and 62.5 μl 2M $CaCl_2$ were diluted in sterile H_20 to a total volume of 500 μl in a 2 ml Bijou tube (mixture henceforth referred to as 'DNA mix'). In a separate Bijou tube, 500 μl of Hank's Balanced Salt Solution (HBSS, Cat. H6648, Sigma) was bubbled continuously using a 5 ml pipette, and the DNA mix was then added dropwise to the HBSS solution. The transfection mixture (total 1 ml) was incubated at room temperature for 20 minutes, then added dropwise to the pre-prepared dish of HEK 293T/Plat-E cells. The dishes were incubated for 6 hours at 37°C and 5% CO_2, then washed 4 times with 8 ml un-supplemented DMEM, to remove calcium phosphate crystals which might inhibit cell growth. The media was replaced with fully supplemented DMEM, and the cells were incubated once again. Supernatant (containing viral particles) was collected 12 and 24 hours after this media change, filtered through a 0.45 μm non-protein binding filter (Merck) and snap frozen in dry ice in 1 ml aliquots, which were then stored at -80°C for future use.

In order to test virus efficiency, NIH3T3 cells were plated in 6-well plates (1 x 10^5 cells per well) and incubated with virus for 12 hours. The efficacy of infection was assessed by comparing the number of live infected and non-infected cells after antibiotic selection or based on the fluorescence signal determined by flow cytometry.

2.11 Isolation of murine foetal liver HSPCs

Cells were extracted from FL as described in section **2.7**. The cells were pelleted by centrifugation (500 g for 5 minutes) and resuspended in 100 μl PBS 2% FBS containing 5 μl of CD117 MicroBeads (Cat. 130-091-224, Miltenyi Biotec). The cells were incubated at 4°C in the dark for 20 minutes, then washed in PBS 2% FBS, centrifuged (500 g for 5 minutes), and resuspended in 3 ml of PBS 2% FBS. Cells

bound to magnetic CD117 MicroBeads were obtained by positive selection using LS Columns (Cat. 130-042-401, Miltenyi Biotec) positioned in the magnetic field of a QuadroMACS™ Separator (Cat. 130-090-976, Miltenyi Biotec). A filter was placed into the top of each column and the system was primed with 3 ml PBS 2% FBS. The cell suspension was loaded into the column, and magnetically labelled cells were subsequently retained, whilst unlabelled cells passed through. The column was washed three times with 3 ml PBS 2% FBS, then removed from the separator and the magnetically retained $CD117^+$ cells were eluted with the aid of a plunger in 8 ml PBS 2% FBS (5 ml then 3 ml). The eluted cells were centrifuged (500 g for 5 minutes) and resuspended at a concentration of 200,000 cells/ml in IMDM supplemented with cytokines favouring myeloid differentiation (IL-3, IL-6 and SCF, see section **2.5**).

2.12 Transduction of murine HSPCs

Murine HSPCs were transduced using the RetroNectin® (Cat. T100A, TaKaRa) bound virus method (**Figure 2.12**). RetroNectin® reagent is a 63 kD recombinant human fibronectin fragment (rFN-CH-296) composed of three functional domains: the cell-binding domain (C-domain), the heparin-binding domain (H-domain), and the CS-1 sequence. RetroNectin® enhances gene transduction by potentiating co-localisation of target cells and virions (Hanenberg, Xiao et al. 1996). Virus particles interact with the H-domain, whilst target cells bind through interaction of cell surface integrin receptor VLA-5 and VLA-4 with the fibronectin C-domain and CS-1 site, respectively.

For transduction of one sample, 200 µl of RetroNectin® was placed into one well of a 48-well non-tissue culture treated plate, and incubated at 4°C for 12 hours, or at 20°C for 2 hours. The RetroNectin® was removed (and frozen at -20°C for subsequent re-use) and 1 ml viral supernatant (produced as described in section **2.10.3**) was placed into the well. The plate was then centrifuged at high speed (2000 g) for 90 minutes at 32°C. The viral supernatant was carefully removed and replaced by 200,000 HSPCs in 1 ml of supplemented IMDM (see section **2.5**). The plate was centrifuged a second time, at 300 g for 3 minutes, to settle the cells at the bottom of the well. The plate was then incubated overnight at 37°C and 5% CO_2. The whole process was repeated 3 times in total, with a 12-hour gap between each cycle. After the final round of

transduction, the cells were incubated for 24 hours, and then selected based on antibiotic resistance, or GFP positivity (**Table 2.12**).

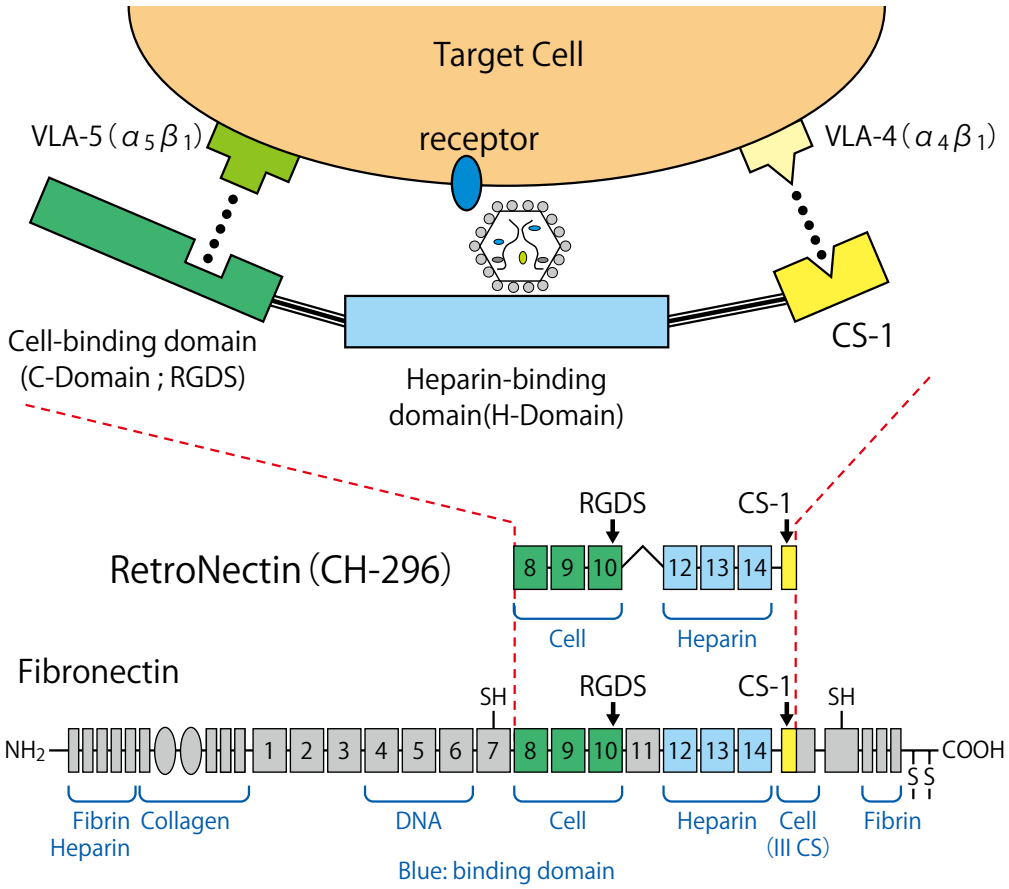

Figure 2.12 The hypothesized mechanism of RetroNectin® mediated transduction. From the TaKaRa RetroNectin® Product Manual. The cell binds to the CS-1 site via VLA-4 and the C-domain via VLA-5. The viral particle can bind to the H-domain of RetroNectin®. The interactions increase the localised concentrations of cells and viral particles, ultimately enhancing gene transduction.

Transfer plasmid	**Selection**
MSCV-Meis1	Puromycin 1.5 μg/ml
MSCV-Hoxa9	Neomycin 1 mg/ml
MSCV-Mll-AF9	GFP
MSCV-PML-RARA	Neomycin 1 mg/ml

MSCV-MOZ-TIF2	GFP
pLKO.1	Puromycin 2 μg/ml

Table 2.12 Selection markers for transfer plasmids used during viral production.

2.13 Colony forming assay

2.13.1 Methylcellulose preparation

3231 methylcellulose was prepared by combining 20 ml IMDM, 80 ml MethoCult™ M3231 (Cat. 3231, STEMCELL Technologies), 1 ml penicillin/streptomycin (100 Units/ml penicillin and 100 mg/ml streptomycin) and cytokines favouring myeloid differentiation: 20 ng/ml SCF, 10 ng/ml IL-3, 10 ng/ml IL-6 and 10 ng/ml GM-CSF (GM-CSF Cat. 576306, Biolegend). The methylcellulose was vortexed and allowed to settle, then dispensed in 2.25 ml aliquots into 15 ml conical tubes. The aliquots were frozen at -20°C and defrosted as required.

3434 methylcellulose (MethoCult™ GF M3434, Cat. 03434, STEMCELL Technologies) was dispensed in 2.25 ml aliquots into 15 ml conical tubes. The aliquots were frozen at -20°C and defrosted as required.

2.13.2 Colony culture assays in 3231 methylcellulose

Leukaemic colony forming assays were carried out using MethoCult™ 3231 methylcellulose medium. Selected cells were suspended in fresh IMDM at a concentration of 8,000 cells/ml (*Meis1/Hoxa9* transformed cells) or 20,000 cells/ml (*Mll-AF9, PML-RARA* and *MOZ-TIF2* transformed cells), and added to the prepared aliquots (see section **2.13.1**) of methylcellulose (2.25 ml each) at a ratio of 1: 9 (i.e. 250 μl was added to each methylcellulose aliquot, therefore 2,000 (*Meis1/Hoxa9*) or 5,000 (*Mll-AF9 PML-RARA* and *MOZ-TIF2*) cells per plate). Where applicable, selection of transformed cells was continued during the colony forming assay, through addition of antibiotics (*Meis1/Hoxa9* transformed cells: neomycin (1 mg/ml) and puromycin (1.5 μg/ml); *PML-RARA* transformed cells: neomycin (1 mg/ml) *pLKO.1* transduced cells puromycin (2 μg/ml)), in which case the concentration of the cell

suspension was adjusted accordingly to maintain the total volume of 2.5 ml. The methylcellulose samples were vortexed and allowed to settle, then divided equally into the two central wells of a 6-well plate using an 18 g needle and a 2.5 ml syringe. The outer four wells were filled with PBS in order to minimise evaporation of the semi-solid medium, and the plate was incubated at 37°C and 5% CO_2. After 4-5 days (*Meis1/Hoxa9* transformed cells) or 6-7 days (*Mll-AF9, PML-RARA* and *MOZ-TIF2* transformed cells) the primary colonies (CFC1) were counted, and re-plated to secondary colonies (CFC2). For this, 5 ml of IMDM was drawn into a syringe and 2.5 ml was dispensed onto the surface of each colony-containing well. The media and methylcellulose were syringed up and down to resuspend the colonies, and the resultant mixture was combined in a 15 ml conical tube. The process was repeated with a second 5 ml syringe of IMDM. The IMDM/cell/methylcellulose suspension was centrifuged at 500 g for 10 minutes. The supernatant was removed, and the cells were resuspended in 1 ml IMDM, counted, and plated into secondary colonies as for CFC1.

2.13.3 Colony culture assays in 3434 methylcellulose

Non leukaemic CFC assays were carried out using MethoCult™ M3434 methylcellulose medium. Selected cells were suspended in fresh IMDM at a concentration of 100,000 cells/ml and added to the prepared aliquots of methylcellulose (2.25 ml each) at a ratio of 1: 9 i.e. 25,000 cells per plate. The methylcellulose samples were vortexed and allowed to settle, then divided equally into the two central wells of a 6-well plate using an 18 g needle and a 2.5 ml syringe. The outer four wells were filled with PBS in order to minimise evaporation of the semi-solid medium, and the plate was incubated at 37°C and 5% CO_2. After 10 days the primary colonies (CFC1) were counted.

In order to test virus efficiency, NIH3T3 cells were plated in 6-well plates (1×10^5 cells per well) and incubated with virus for 12 hours. The efficacy of infection was assessed by comparing the number of live infected and non-infected cells after antibiotic selection or based on the fluorescence signal determined by flow cytometry.

2.14 Cell sorting

Cells were isolated from the BM and FL as described in **2.7**. Isolated BM or FL cells were enriched for HSPCs (c-Kit^+ cells) using magnetic beads and LS columns, as

described in section **2.11**, and antibody staining was carried out as described in section **2.8**. Cell sorting was performed using a BD FACS Aria (BD Biosciences).

2.15 Transplantation assays

2.15.1 Non-leukaemic transplantation assays

Irradiation details: 8-12-week-old mice (minimum bodyweight 20 g) were subjected to whole body *gamma* irradiation (Gammacell 40 Executor unit, Serial number 59R (Best Theratronics); source: Cesium 137). A total dose of 11 Gy (lethal irradiation) was delivered in two separate doses of 5.5 Gy each using a 33% attenuator (0.59 Gy/min). A 4-hour break was applied between irradiations. Where possible female mice were used for long term assays, as the chance of needing to cull mice due to fighting was significantly smaller. All animal experiments were authorized by the UK Home Office.

Primary transplants: Lethally irradiated (11 Gy) $CD45.1^+/CD45.2^+$ syngeneic recipient mice were transplanted with 100 (FL) or 200 (BM) $CD45.2^+$ HSCs ($Lin^-c\text{-}Kit^+Sca\text{-}1^+CD48^-CD150^+$) together with 200 000 unfractionated WT BM support cells ($CD45.1^+$) via the tail vein in a total volume of 200 μl. The HSCs were obtained by sorting E14.5 dpc FL, or BM of 8-12-week-old adult mice, as previously described (see section **2.14**). Monitoring of transplanted mice was carried out as described in section **2.15.3**. All recipient mice were culled and analyzed 16-20 weeks post-transplantation.

Secondary transplants: Lethally irradiated (11 Gy) $CD45.1^+/CD45.2^+$ syngeneic recipient mice were transplanted with 2,000 (secondary from FL) or 3,000 (secondary from BM) $CD45.2^+$ LSKs ($Lin^-c\text{-}Kit^+Sca\text{-}1^+$) together with 200,000 unfractionated WT BM support cells ($CD45.1^+$) via the tail vein in a total volume of 200 μl. The LSKs were obtained by sorting BM of primary recipient mice (see section **2.14**) 4 months after transplantation. Monitoring of transplanted mice was carried out as described in section **2.15.3**. All recipient mice were culled and analyzed 16-20 weeks post-transplantation.

Tertiary transplants: Lethally irradiated (11 Gy) $CD45.1^+/CD45.2^+$ syngeneic recipient mice were transplanted with 4M unfractionated $CD45.2^+$ BM cells via the tail vein in a total volume of 200 μl. The $CD45.2^+$ BM cells were obtained from secondary recipient

mice 4 months after transplantation. Monitoring of transplanted mice was carried out as described in section **2.15.3**. All recipient mice were culled and analyzed 16-20 weeks post-transplantation.

2.15.2 Leukaemic transplantation assays

For primary transplantation, knock-out and wild type pre-LSCs from CFC3 (see section **2.13.2**) were harvested and counted. 100,000 live pre-LSCs ($CD45.2^+$) were mixed with 200,000 support bone marrow cells ($CD45.1^+$) and injected into the tail vein of lethally irradiated (11 Gy) syngeneic recipient mice ($CD45.1^+/CD45.2^+$) in a total volume of 200 μl. Leukaemic development was monitored as described in section **2.15.4**.

For secondary transplantation, knock-out and wild type LSCs from culled leukaemic primary recipient mice were defrosted, passaged through one CFC (see section **2.13.2**), harvested and counted. 10,000-50,000 live LSCs ($CD45.2^+$) were mixed with 200,000 support bone marrow cells ($CD45.1^+$) and injected into the tail vein of lethally irradiated (11 Gy) syngeneic recipient mice ($CD45.1^+/CD45.2^+$) in a total volume of 200 μl. Leukaemic development was monitored as described in section **2.15.4**.

2.15.3 Monitoring of mice transplanted with non-leukaemic haematopoietic cells

Engraftment of transplanted cells was followed by tracking $CD45.2^+$ cell chimerism in the peripheral blood (**Figure 2.15.3.1**). Mice were bled every 4 weeks from the tail vein, and WBCs were stained for flow cytometry: $CD45.1^+$ (WT support/competitor total bone marrow cells), $CD45.2^+$ (cells under study) and $CD45.1^+/CD45.2^+$ (recipient BM cells remaining following irradiation). Engraftment was evaluated based on the proportion of $CD45.2^+$ cells within the total transplanted cell population ($CD45.2^+/(CD45.1^+ + CD45.2^+)$). In addition, differentiation of transplanted cells was evaluated by staining for myeloid cells ($Gr1^+$, $CD11b^+$), B cells ($CD19^+$) and T cells ($CD4^+$, $CD8^+$). The contribution of each differentiated cell type to the total $CD45.2^+$ cell population was calculated, as was the proportion of $CD45.2^+$ cells within each differentiated cell type (e.g. $CD45.2^+$ B cells/$CD45.1^+$ B cells + $CD45.2^+$ B cells) (**Figure 2.15.3.2**).

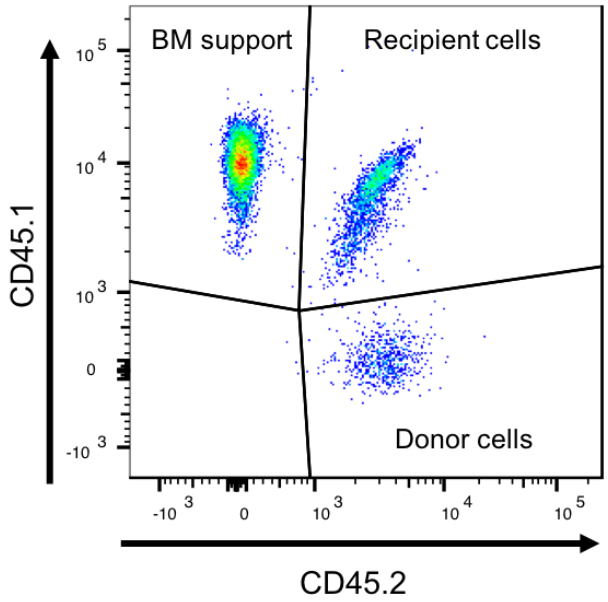

Figure 2.15.3.1 Syngeneic model that allows tracking of transplanted haematopoietic cells (normal or leukaemic) in recipient mice. Peripheral blood samples are stained with antibodies against CD45.1 and CD45.2, and evaluated by flow cytometry. Populations are $CD45.1^+$ (WT support/competitor total bone marrow cells), $CD45.2^+$ (donor cells under study) and $CD45.1^+/CD45.2^+$ (recipient BM cells remaining following irradiation).

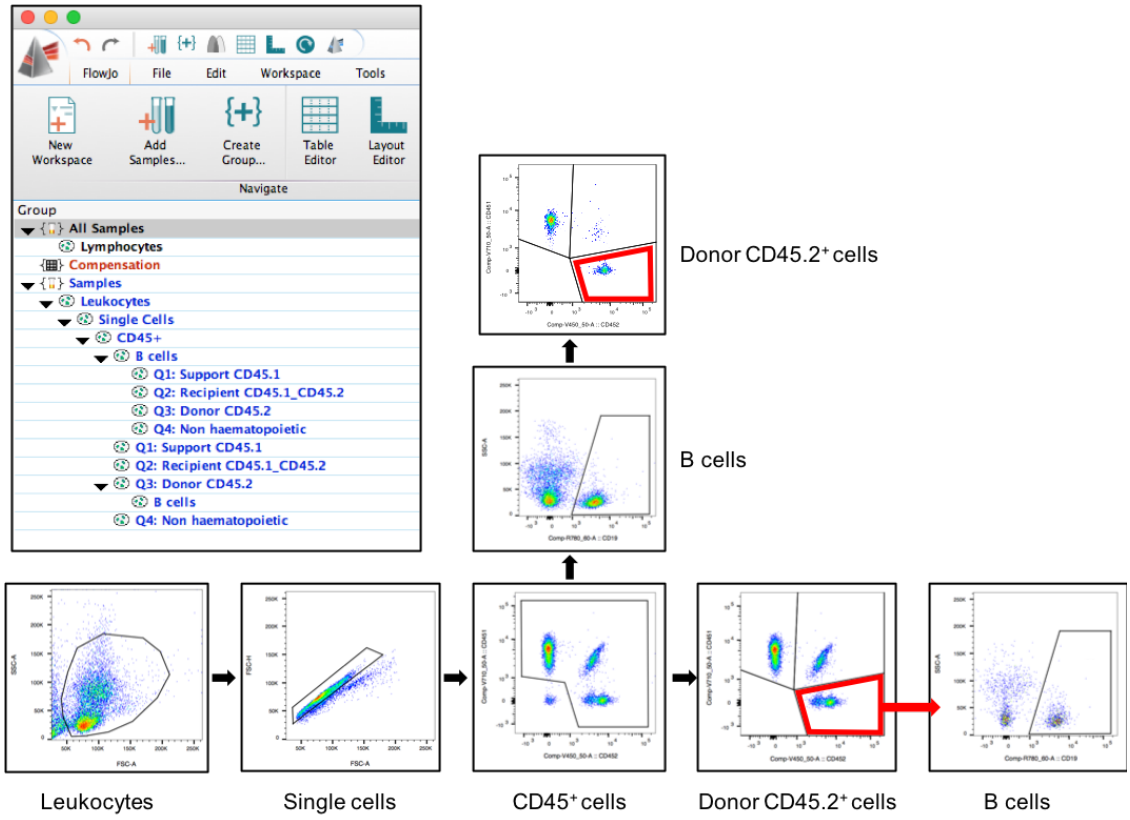

Figure 2.15.3.2 Two methods of evaluating engraftment of CD45.2$^+$ donor cells within recipient mice. The contribution of each differentiated cell type to the total CD45.2$^+$ cell population is calculated, as is the proportion of CD45.2$^+$ cells within each differentiated cell type (e.g. CD45.2$^+$ B cells/CD45.1$^+$ B cells + CD45.2$^+$ B cells).

2.15.4 Leukaemic monitoring

For all leukaemic mice models, AML development was followed by tracking CD45.2$^+$ cell chimerism in the peripheral blood (Figure **2.15.3.1**). Mice were bled every 2-4 weeks from the tail vein, and WBCs were stained for flow cytometry: CD45.1$^+$ (WT support/competitor total bone marrow cells), CD45.2$^+$ (cells under study) and CD45.1$^+$/CD45.2$^+$ (recipient BM cells remaining following irradiation). Leukaemic engraftment was evaluated based on the proportion of CD45.2$^+$ cells within the total transplanted cell population (CD45.2$^+$/(CD45.1$^+$ + CD45.2$^+$) (Figure **2.15.3.1**). In addition, immunophenotypic characterisation of the developing leukaemia was carried out by staining for myeloid cells (Gr1$^+$, CD11b$^+$), HSPCs (c-Kit$^+$), and in the case of the *Mll-AF9* knock in model, also B cells (CD19$^+$) and T cells (CD4$^+$, CD8$^+$). Mice were weighed weekly and monitored daily. Upon developing clinical signs of

leukaemia (for example: loss of weight, reduced movement, hunched posture, staring coat, pale paws and tachypnoea indicative of anaemia) the mice were culled. One hind leg (tibia and femur) and the spleen were harvested and processed as described in section **2.7**. Bone marrow WBCs were stained for flow cytometry as described above for leukaemic monitoring, and additional BM samples were frozen at -80°C for future use. Spleens were photographed and weighed. WBC counts were obtained from peripheral blood, or from harvested BM and spleen using an automatic cell counter (Celltac α MEK-6500K, Nihon Kohden).

2.16 Preparation and administration of polyinosinic-polycytidylic acid (Poly(I:C))

Polyinosinic-polycytidylic acid (Poly(I:C)) (Cat. 27-4732-01, GE Healthcare) was used to induce gene deletion in the *Mx1-Cre* system. Poly(I:C) is a synthetic double stranded RNA which acts as a natural stimulant of Toll-like receptor 3 (TLR3) (Matsumoto and Seya 2008), and therefore induces type I interferon (IFN) inflammatory cytokine/chemokine production. Since the *Mx1-Cre* promotor is activated in an interferon dependent manner, administration of poly(I:C) ultimately results in *Mx-1Cre* induction, and deletion of the floxed allele in *Mx1-Cre* mice (Kuhn, Schwenk et al. 1995).

To prepare 1 mg/ml of poly(I:C) solution, 100 ml of sterile PBS was added to 265 mg of lyophilised poly(I:C) and dissolved at 50°C for 2-3 hours. 165 ml of pre-warmed PBS was added to the poly(I:C) solution to make the volume up to 265 ml. The solution was placed at 50°C for one additional hour until the poly(I:C) had fully dissolved. The solution was allowed to cool overnight at room temperature and 2-5 ml aliquots of 1 mg/ml concentration were prepared and stored at -20°C.

To induce *Mx1-Cre* mediated gene deletion, 200-300 μl poly(I:C) (1 μg/μl) was administered to transplanted mice by intra-peritoneal injection once every other day for a total of 6 doses. Mice transplanted with *Mx1-Cre* negative cells were used as controls.

2.17 shRNA-mediated *Tnfrsf1b* knockdown

Meis1/Hoxa9 transformed *Ythdf2*$^{fl/fl}$ and *Ythdf2*$^{fl/fl}$;*Vav-iCre* pre-LSCs were transduced with lentiviruses expressing shRNA for *Tnfrsf1b* (shRNA1-3), or control shRNA (shRNA CTL) (**Table 2.17**) as described in section **2.12**. Transduced pre-LSCs were selected by culture in the presence of 2 μg/ml puromycin.

	TRC number	Clone ID	Manufacturer
shRNA 1	TRCn0000012320	NM_011610.1-264s1c1	Sigma
shRNA 2	TRCn0000012321	NM_011610.1-929s1c1	Sigma
shRNA 3	TRCn0000012322	NM_011610.1-814s1c1	Sigma
shRNA CTL		Custom cloned	

Table 2.17 shRNA for *Tnfrsf1b* knockdown

2.18 RNA extraction for Affymetrix and m^{6}A meRIP-Seq (TRIzol™ Method)

Ythdf2$^{fl/fl}$ and *Ythdf2*$^{fl/fl}$;*Vav-iCre* pre-LSCs intended for RNA Extraction were pelleted by centrifugation (500 g for 5 minutes) and resuspended in TRIzol™ Reagent (Cat. 15596026, Life Technologies) in 1.5 ml Eppendorf® DNA LoBind tubes (Cat. 30108051, Sigma). A minimum of 0.75 ml TRIzol™ was used per 5 x 10^6 cells, as per manufacturer's instructions. Samples were briefly vortexed to ensure homogenization, and then snap frozen in dry ice and stored at -80°C for future use.

When ready to proceed, the samples were allowed to defrost at room temperature, then incubated for a further 5 minutes at room temperature. Chloroform (25:24:1 Phenol-Chloroform-Isoamyl Alchohol Mix for DNA Extraction Cat. 77617, Sigma) was then added at a ratio of 200 μl chloroform per 1 ml TRIzol™ and the sample tubes were shaken vigorously by hand for 15 seconds, then incubated at room temperature for 2-3 minutes. The samples were centrifuged at 12000 g for 15 minutes at 4°C, and then the clear upper aqueous layer (containing RNA) was carefully transferred to a new 1.5 ml Eppendorf® DNA LoBind tube. Then 10 μg (stock: 5 mg/ml; 10 μg = 2 μl) of linear acrylamide was then added to each sample to aid recovery of nucleic acids

during alcohol precipitation, after which 500 μl of isopropanol was added to precipitate RNA and samples were mixed by multiple (5 x) inversion. The samples were incubated at room temperature for 10 minutes, then centrifuged at 12000 g for 10 minutes at 4°C. The supernatant was removed and 1 ml of 70% ethanol was added in order to clean the RNA precipitate and remove the remaining isopropanol. Following a brief vortex, the samples were centrifuged at 7500 g for 5 minutes at 4°C. The supernatant was removed and the RNA pellet was resuspended in 20 μl of nuclease-free water. RNA yield was determined using a nanodrop spectrometer (Nanodrop ND1000 Spectrophotometer; Labtech International Ltd, East Sussex, UK).

2.19 Affymetrix

RNA was prepared by Jasmin Paris (see section **2.18**), **further steps were carried out by Marcos Morgan**. Total RNA (4 million cells per sample) was used to synthesize biotinylated cDNA with the Ambion WT Expression kit (Cat. 4491974, Ambion). cDNA was fragmented and labelled with the Affymetrix, WT Terminal and Control Kits (Cat. 901524, Affymetrix) and then hybridized for 16 hours at 45°C on a GeneChip Mouse Gene 2.0 ST Array. The chip was later washed and stained with the Affymetrix Fluidics Station 450. Data were processed and analyzed as described in section **2.24**.

2.20 m^{6}A meRIP-Seq

RNA was prepared by Jasmin Paris (see section 2.18), further steps were carried out by Marcos Morgan and Juhno Choe in collaboration with Richard Gregory. m^{6}A meRIP-Seq library preparation was performed as previously described (Lin, Choe et al. 2016) from *Ythdf2*$^{fl/fl}$ pre-leukaemic cells (50 million cells per sample). Three biological replicates for each condition were used. Data were processed and analyzed as described in section **2.24**.

2.21 SLAM-Seq

First, the SLAMseq Explorer Kit – Cell Viability Titration Module (Cat. No. 059, Lexogen) was used to carry out an initial titration series of experiments of 4-Thiouridine (S4U) to assess cytoxicity and therefore identify the optimal concentration

of S4U for further experiments. The SLAMseq Kinetics Kit – Catabolic Kinetics Module (Cat. No. 062, Lexogen) was subsequently used to prepare samples for SLAM Seq, according to the manufacturer's instructions. This kit is designed for S4U labelling of RNA in cultured cells followed by treatment of cells with unlabelled uridine. In this way, existing RNA is labelled with S4U while newly synthesized RNA is unlabelled.

2.21.1 S4U cytotoxicity assay

Ythdf2$^{fl/fl}$ and *Ythdf2*$^{fl/fl}$*;Vav-iCre* pre-LSC cells were incubated with a dilution series of S4U containing media in order to determine the optimal concentration for the catabolic kinetics experiment. Cells were seeded at 400,000 cells/ml in 0.5 ml of standard culture media (see section **2.5**) in a 24-well plate. Three biological replicates of both *Ythdf2*$^{fl/fl}$ and *Ythdf2*$^{fl/fl}$*;Vav-iCre* pre-LSCs were plated into 12 wells each. Using the same culture media and a stock concentration of 100 mM S4U, a 2X concentrated dilution series was generated starting with 8,000 μM (tube 1) and decreasing twofold for 10 dilutions (tubes 2-11). A control dilution (tube 12) was generated with H_20 in place of S4U. Subsequently, 0.5 ml of each S4U dilution was added to the wells, giving 200,000 cells/ml, at S4U concentrations ranging from 4,000 μM to 0 μM (**Table 2.21.1**).

Cell dilution	Concentration (μM)	Concentration (log2 [μM])
1	4000	11.966
2	2000	10.966
3	1000	9.966
4	500	8.966
5	250	7.966
6	125	6.966
7	62.5	5.966
8	31.25	4.966
9	15.625	3.966
10	7.8125	2.966
11	3.90625	1.966
12	0	0

Table 2.21.1 S4U dilution series used for cytotoxicity assay.

S4U incorporation rates are enhanced when fresh S4U-containing media is added during cell culture. Therefore, after 9 hours, 0.5 ml of media was carefully removed from the surface of each well, and replaced with 0.5 ml of S4U-containing media at the same dilution.

After a further 15 hours (total of 24 hours; the cytotoxicity assay duration should be twice the duration of labelling used for the catabolic kinetics assay), cells were harvested, washed in PBS 2% FBS, and resuspended in 100 μl PBS 2% FBS. DAPI (1:1,000) was added and the percentage of DAPI positive and negative cells was analysed by FACS, as a measure of dead and live cells respectively.

Note: S4U is highly light sensitive and can cross link (Herzog, Reichholf et al. 2017). Tubes and plates with S4U-containing media were therefore wrapped in tin foil, and exposure to light during cell culture was minimised.

In GraphPad Prism, the percentage of dead cells was plotted against S4U concentration (log2 [μM]) to obtain inhibition versus S4U concentration curves for *Ythdf2*$^{fl/fl}$ and *Ythdf2*$^{fl/fl}$*;Vav-iCre* pre-LSC cells (**Figure 2.21.1**). Using these curves, the half-maximal inhibitory concentration (IC_{50}) and experimental working concentration (IC_{10}) were calculated for both pre-LSC cell types (**Table 2.21.2**)

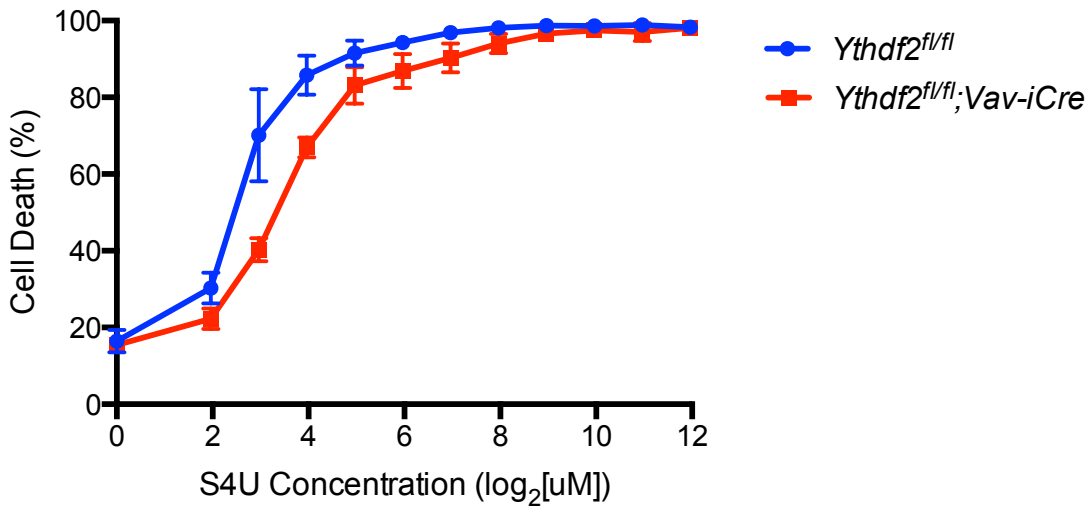

Figure 2.21.1 S4U cytotoxicity curves for (A) *Ythdf2*$^{fl/fl}$ and (B) *Ythdf2*$^{fl/fl}$*;Vav-iCre* pre-LSC cells.

	IC_{10}	IC_{50}
Ythdf2$^{fl/fl}$	2.91	6.69
Ythdf2$^{fl/fl}$*;Vav-iCre*	3.77	12.48

Table 2.21.2 S4U half-maximal inhibitory concentration (IC_{50}) and experimental working concentration (IC_{10}) in *Ythdf2*$^{fl/fl}$ and *Ythdf2*$^{fl/fl}$*;Vav-iCre* pre-LSC cells.

2.21.2 S4U catabolic kinetics assay

Three biological replicates of both *Ythdf2*$^{fl/fl}$ and *Ythdf2*$^{fl/fl}$*;Vav-iCre* pre-LSCs were studied. Initially, 4 million cells were seeded into T75 flasks in a total volume of 18 ml standard culture media (see section **2.5**). After 6 hours, 2 ml of 10X concentrated S4U containing media was added, giving a total volume of 20 ml (200,000 cells/ml), with an S4U concentration of 2.91 μM (the limiting IC_{10}, as determined in the cytotoxicity assay). Since S4U is highly light sensitive, tubes and plates with S4U-containing media were wrapped in tin foil, and exposure to light during cell culture was minimised.

After 9 hours, 10 ml of media was carefully removed from the surface of each flask and replaced with 10 ml fresh 1X S4U media. After a further 3 hours, the cells were centrifuged at 500 g for 5 minutes, and resuspended in 20 ml PBS 2% FBS. An aliquot of 1.4 ml (280 000 cells) was taken into an Eppendorf® DNA LoBind tube (time 0). The remainder of the cells were centrifuged as before, washed in a further 20 ml PBS 2% FBS, centrifuged again, and resuspended in media containing a 100X excess of uridine relative to the original S4U media i.e. 291 μM uridine. Further 1.4 ml (280 000 cells) aliquots were taken from each flask 1 hour (time 1), 3 hours (time 3) and 9 hours (time 9) after addition of uridine media.

All aliquots (time 0, time 1, time 3, time 9) were processed immediately upon collection. In each case the samples were centrifuged at 500 g for 5 minutes at 4°C. The supernatant was removed and the samples were resuspended in 1 ml TRIzol™ Reagent, snap frozen in dry ice, and stored at -80°C.

Further steps were carried out by Marcos Morgan (MRC Centre for Regenerative Medicine, University of Edinburgh). In brief, SLAM-seq libraries were prepared using the Lexogen catabolic kit (Cat. 062.24) and the Lexogen QuantSeq 3′ mRNA-Seq Library Prep Kit FWD for Illumina (Cat. no. 015.24) in both cases following manufacturers' instructions. Libraries were sequenced using an Illumina HiSeq platform in a 50 bp single-end mode. Biological triplicates for both *Ythdf2*$^{fl/fl}$ and *Ythdf2*$^{fl/fl}$*;Vav-iCre* pre-leukaemic cells were used to generate the different libraries sets. Data were processed and analyzed as described in section **2.24**.

2.22 RIBO-Seq

Ythdf2$^{fl/fl}$ and *Ythdf2*$^{fl/fl}$*;Vav-iCre* pre-LSC cells were seeded at 200,000 cells/ml in 10 ml of supplemented IMDM in a T75 flask (2 million cells per sample), and incubated overnight at 37°C 5% CO_2. The following day the contents of each flask was transferred to a 15 ml conical tube and centrifuged (5 minutes at 500 g). The supernatant was removed and the cells were washed with ice cold PBS (2 ml), centrifuged as above, and the supernatant removed. The cells were resuspended in cold PBS (1.4 ml) a second time, transferred to a 1.5 ml Eppendorf® DNA LoBind tube and centrifuged for 2 minutes at 6,000 RPM at 4°C. The supernatant was discarded, and the cell pellet was resuspended in 300 µl of ice-cold lysis buffer containing 1% NP-40, 200 mM KOAc, 25 mM K-HEPES pH 7.2, 10 mM MgCl and 4 mM $CaCl_2$. The cells were incubated on ice for 5 minutes, then centrifuged for 5 minutes at 9,000 RPM at 4°C. The supernatant was collected, taking care not to disturb the pellet. An aliquot of 60 µl (termed 'No nuclease sample') was placed into a 1.5 ml Eppendorf® DNA LoBind tube and lysed with 1 ml TRIzol™ Reagent, then snap frozen in dry ice. The remaining 200 µl were placed into another 1.5 ml Eppendorf® DNA LoBind tube and diluted with 200 µl water to lower the KOAc concentration to 100 mM. Micrococcal nuclease (MNase) was then added to each sample (from a 2 mg/ml stock in 50% glycerol, 1 mM EDTA pH 7, 10 mM Tris pH 8, 50 mM NaCl) (Cat. 10107921001, Roche Appiled Science) to a final concentration of 10 µg/ml. The samples were incubated for 30 minutes at 37°C, then divided equally (100 µl each) between four 1.5 ml Eppendorf® DNA LoBind tubes, lysed with 1 ml TRIzol™, then snap frozen.

The remainder of the preparation was carried out by Marcos Morgan, following a previously described protocol (Reid, Shenolikar et al. 2015). Briefly, digested RNA was extracted with TRIzol™ and later treated with PNK (Cat. M0201S, New England Biolabs) for 30 minutes at 37°C. To isolate ribosome-protected mRNA fragments (RPFs), the PNK-treated RNA was resolved on a 15% Novex TBE-Urea Gel (Cat. EC6885BOX, Thermo Fisher Scientific), and RPFs 25 to 40 nucleotides long were excised and purified. Libraries were then prepared using the NEBNext® Multiplex Small RNA Library Prep Set for Illumina following manufacturer's instructions. For input controls, total RNA was extracted from the pre-leukaemic cell lysates before MNase digestion using TRIzol™. Samples were then depleted of ribosomal RNA using the Epicentre Ribo-zero kit (Cat. MRZH116, Illumina), and libraries were generated using the SENSE Total RNA-Seq Library Prep Kit (Cat. 009.08, Illumina) following manufacturer's instructions. Libraries were sequenced with the Illumina HiSeq platform in a 50 bp single-end mode. Biological triplicates were used to generate libraries for both *Ythdf2*$^{fl/fl}$ and *Ythdf2*$^{fl/fl}$*;Vav-iCre* pre-leukaemic cells. Data were processed and analyzed as described in section **2.24**.

2.23 Generation of Figure 5.4.6B.

These analyses were carried out by Marcos Morgan. To generate **Figure 5.4.6B** the following publicly available datasets were used: GSE10358, GSE52891, GSE61804, GSE68833, GSE12417, GSE13159, GSE15061, GSE15434, GSE16015, GSE19577, and GSE22845 (Metzeler, Hummel et al. 2008, Tomasson, Xiang et al. 2008, Haferlach, Mecucci et al. 2009, Klein, Ruckert et al. 2009, Mills, Kohlmann et al. 2009, Haferlach, Kohlmann et al. 2010, Pigazzi, Masetti et al. 2011, Taskesen, Bullinger et al. 2011, Bachas, Schuurhuis et al. 2015, Metzelder, Michel et al. 2015). Exclusion criteria included datasets with less than 20 samples, samples with undefined tissue of origin, cell type and karyotype, in addition to RAEB samples. A total of 1732 samples were retained for further analysis. The Simpleaffy package from Bioconductor was used to extract quality measurement of microarrays (Gentleman, Carey et al. 2004, Wilson and Miller 2005). RNA degradation was assessed based on 3' to 5' ratio of *GAPDH* and *ACTNB* genes. Samples with NUSE < 1.05 and relative log expression (RLE) < 0.15 were excluded from further analysis (McCall, Murakami et al. 2011). The retained samples were assessed for their homogeneity using the Bioconductor arrayQualityMetrics package (Kauffmann,

Gentleman et al. 2009). Low quality RNA and outlier samples were excluded, while high quality samples retained after quality control were background corrected and normalized using RMAexpress software (http://rmaexpress.bmbolstad.com/). Pairwise comparisons between each karyotype and control were performed using student t-test.

2.24 Statistical analyses

For **cell culture and mouse experimental work**, statistical analyses were performed using GraphPad Prism 6 software (GraphPad Software, Inc.). Depending on whether data assumed a normal distribution or not, P values were calculated using a two-tailed unpaired t-test, or a Mann–Whitney U test respectively. Kaplan-Meier survival curve statistics were determined using the Log-rank (Mantel Cox) test. For mouse analyses or transplantation experiments, I selected group sizes that confer 80-97% power to detect inter-group differences of 50% in a measured parameter whose standard deviation (SD) was approx. 20%, assuming random normal data and a type I error rate of 5%. If initial experiments showed smaller differences than 50%, subtle ~25% inter-group differences (assuming SD of 20%) were assessed using appropriate group sizes of animals to achieve >80% power.

For **Affymetrix**, data were processed and analyzed using the Bioconductor Limma Package (Ritchie, Phipson et al. 2015). Samples were normalized using the rma function and differential expression was assessed using linear modelling. Log2-fold-changes and moderated t-statistics were calculated using the contrasts.fit function.

For **m^{6}A meRIP-Seq**, reads were aligned to the mouse or human reference genome using HISAT2 (Kim, Langmead et al. 2015) and peaks were called using MACS2 (Zhang, Liu et al. 2008). To analyze the distribution of peaks along the transcripts, bedgraph files were converted to bigWig format and used as input for the computeMatrix function of the deepTools package (Ramírez, Dündar et al. 2014). Motif enrichment was done using HOMER selecting a motif length of 6 nucleotides. Background regions were generated by shuffling peaks along the transcriptome using the shuffleBed tool from the BEDtools suite (Quinlan and Hall 2010). Network analysis was performed using the ConsensusPathDB (CPDB) software (Kamburov, Stelzl et al. 2012). For gene set enrichment analysis (GSEA), the GSE76008 dataset (Ng,

Mitchell et al. 2016) was used to rank genes according to the engraftment potential of pre-leukemic cells. The GVIZ bioconductor package was used for peak visualization (Hahne and Ivanek 2016). Correlation with YTHDF2 was measured to determine robust YTHDF2 targets after the knockout (Mansson, Tsapogas et al. 2004). Briefly, Pearson correlation between YTHDF2 and the identified YTHDF2 targets was calculated using the 1732 AML samples described in section **2.23**. Correlation significance was measured using parametric test with length (genes)-2 degrees of freedom (cor.test function, stats package, R project, http://www.R-project.org/), and adjusted for multiple comparisons using Benjamini & Hochberg method (Benjamini and Hochberg 1995). Genes with negative coefficients and adjusted p-value < 0.05 were considered strong targets of YTHDF2.

For **SLAM-Seq**, libraries were analysed as previously described (Herzog, Reichholf et al. 2017). Briefly, T to C conversion rates were obtained using the SlamDunk pipeline. Conversion rates across different time points were normalised to time 0 for each gene and were used to fit a first order decay reaction with the R stats package nls function.

For **Ribo-Seq** analysis, Kallisto (Bray, Pimentel et al. 2016) was used to obtain read counts per gene for the RPF and mRNA libraries. Read counts were then used to calculate the differential translational efficiency between *Ythdf2*$^{fl/fl}$ and *Ythdf2*$^{fl/fl}$*;Vav-iCre* pre-leukaemic cells with Xtail (Xiao, Zou et al. 2016). To estimate the relative translational efficiency for genes in each condition, we compared RPF and mRNA read counts using DESeq2 (Love, Huber et al. 2014).

2.25 Accession

Affymetrix, m^{6}A meRIP-Seq, RIBO-seq and SLAM-seq datasets were deposited in ArrayExpress under the following accession numbers: E-MTAB-6783, E-MTAB-7782, E-MTAB-6791, E-MTAB-7783, E-MTAB-7785 and E-MTAB-7784. Data from human cell lines was obtained from previously published work with the following accession number: GSE87190 (NOMO-1, MA9.3ITD).

Chapter 3: The role of YTHDF2 in normal haematopoiesis

3.1 Introduction

3.1.1. The role of RNA N^6-methyladenosine in normal haematopoiesis

In recent years, RNA N^6-methyladenosine has emerged as a critical regulator of the transition between cell states. For example, m^6A has been shown to affect the transcript stability of pluripotency regulators, facilitating the transition between naïve pluripotency and differentiation in mouse embryonic stem cells. Whilst embryonic stem cells lacking m^6A remain pluripotent in spite of differentiation signals (Batista, Molinie et al. 2014, Geula, Moshitch-Moshkovitz et al. 2015), depletion of m^6A in more differentiated cells results in increased and abnormal differentiation, suggesting that the effect of m^6A is also both cell type and stage specific (Geula, Moshitch-Moshkovitz et al. 2015).

Considering the role of m^6A in regulating cell fates, several recent studies have focused on m^6A in the haematopoietic system. A summary of these studies is presented in **Table 3.1.1**.

m^6A regulator	**Species**	**Targeting strategy**	**Phenotype**	**Reference**
mettl3	Zebrafish	Morpholino Knock out	Failure of endothelial to haematopoietic transition (EHT) in the AGM, decreased HSPC emergence, reduction all blood lineages. Mechanism through reduced *notch1a* and *rhoca* mRNA degradation.	(Zhang, Chen et al. 2017)
Mettl3	Mouse	Conditional knock out (*Vec-Cre*)	Failure of EHT in the AGM. Mechanism through reduced Ythdf2-mediated m^6A-dependent *notch1a* mRNA degradation.	(Lv, Zhang et al. 2018)
METTL3	Human	shRNA $CD34^+$ HSPCs	Decreased proliferation and increased myeloid differentiation *in vitro*.	(Vu, Pickering et al. 2017)
METTL14	Human	shRNA $CD34^+$ HSPCs	Increased myeloid differentiation in vitro, via a mechanism independent of YTHDF1-3.	(Weng, Huang et al. 2018)

Mettl3	Mouse	Conditional knock out (*CD4-Cre*)	Disruption of T cell homeostasis and differentiation.	(Li, Tong et al. 2017)
Mettl3	Mouse	Conditional knock out (*FoxP3-Cre*)	Severe autoimmune disease due to inability of *Mettl3*-deficient regulatory T cells to suppress naïve T cell proliferation.	(Tong, Cao et al. 2018)
Ythdf1	Mouse	Knock out	Increased capacity of *Ythdf1*-deficient dendritic cells to cross-prime $CD8^+$ T cells, resulting in slower growth of B16-OVA tumours.	(Han, Liu et al. 2019)
Mettl3	Mouse	Conditional knock out (*Lysm-Cre*)	No phenotype in mature myeloid cells.	(Lee, Bao et al. 2019)
Mettl3 *Mettl14*	Mouse	Inducible knock out (*Mx1-Cre*)	Large increase in HSCs following *Mettl3* deletion, poor at reconstituting irradiated recipients upon transplantation. Increased cell cycling and reduced expression of HSC quiescence genes in *Mettl3*-deficient HSCs.	(Yao, Sang et al. 2018)
Mettl3	Mouse	Inducible knock out (*Mx1-Cre)* (*Rosa26-CreER*T2)	Increased HSCs and HPC-2s, as a result of decreased differentiation.	(Lee, Bao et al. 2019)
Ythdf2	Mouse Human	Inducible knock out (*Mx1-Cre*) shRNA human umbilical cord (hUCB) HSCs	Marked increase in ST-HSC and LT-HSC. Improved LT-HSC engraftment upon transplantation (no change in multilineage reconstitution capacity). Expansion and increase in function of hUCB HSCs.	(Li, Qian et al. 2018)
Ythdf2	Mouse	Conditional knock out models (*Mx1-Cre*, *ERT-Cre* and *Vav-iCre*)	Increased numbers of LT-HSCs and ST-HSCs, MPPs. Improved LT-HSC engraftment upon transplantation (no change in multilineage reconstitution capacity). 5-FU treatment or repeated ionising radiation increased numbers and	(Wang, Zuo et al. 2018)

			function of LT-HSCs in *Ythdf2*$^{fl/fl}$;*Mx1-Cre* mice compared to controls.	

Table 3.1.1 Summary of studies targeting m^{6}A regulators in haematopoiesis.

Initial studies addressed the role of m^{6}A in the emergence of definitive haematopoeitic stem and progenitor cells (HSPCs) during embryogenesis. In this context, the Liu group showed first in zebrafish (Zhang, Chen et al. 2017), and then in mice (Lv, Zhang et al. 2018), that m^{6}A modulates haematopoietic stem and progenitor cell specification. Zhang et al. published that depletion of the m^{6}A writer Mettl3 by *mettl3* morpholino knockdown in zebrafish resulted in a blockage of endothelial-to-haematopoeitic transition (EHT) in the AGM, resulting in decreased HSPC emergence and a reduction of all blood lineages. Endothelial cells in *mettl3* morphant zebrafish retained endothelial identity and expression of arterial markers *deltaC*, *tbx20*, *hey2*, and *ephrin B2a*. The authors subsequently generated *ythdf2* morphants, which showed a similar phenotype to *mettl3* morphants. They then mutated the binding sites for m^{6}A on zebrafish Ythdf2, thereby showing that the function of Ythdf2 in HSPC development is dependent on its ability to bind m^{6}A. Finally, the authors used a combination of RNA-Seq, m^{6}A-Seq and miCLIP to identify *notch1a* as a target of Mettl3 and Ythdf2, and concluded that reduced Ythdf2-mediated mRNA decay of the arterial genes *notch1a* and *rhoca* contributes to the blocked EHT in *mettl3* morphant zebrafish (Zhang, Chen et al. 2017). In a follow up report, Lv et al. used *Mettl3*$^{fl/fl}$;*Vec-Cre* endothelial specific conditional knock out mice to show that METTL3 is also essential for murine definitive haematopoiesis, and that this too is dependent on *Notch1*. The authors showed that in the absence of METTL3, *Notch1* mRNA is not methylated and therefore NOTCH activity remains high, inhibiting EHT. Finally, they showed that YTHDF2 recognises the m^{6}A peak near the stop codon of *Notch1* mRNA, suggesting that YTHDF2-mediated *Notch1* mRNA decay is responsible for the phenotype observed (Lv, Zhang et al. 2018). In conclusion therefore, the group showed using both zebrafish and mouse models that METTL3 regulates EHT through *Notch1*, whose expression depends upon m^{6}A-directed YTHDF2-mediated mRNA decay.

m^{6}A has also been shown to regulate human stem and progenitor cells. A study of METTL3 in normal and malignant haematopoiesis showed that shRNA-mediated depletion of *METTL3* in cord-blood derived CD34$^+$ HSPCs decreased m^{6}A levels,

decreased proliferation and increased myeloid differentiation in vitro (Vu, Pickering et al. 2017). Another study showed that shRNA-mediated depletion of *METTL14* from human $CD34^+$ HSPCs also increased their myeloid differentiation (Weng, Huang et al. 2018). However, these authors showed no consistent pattern for any YTHDF gene (YTHDF1-3) during differentiation of normal HSPCs, and were unable to demonstrate any effect of YTHDF knockdown on the METTL14 targets, MYB and MYC, which they had identified. The authors argued therefore that the effect of METTL14 on mRNA stability and translation of its target genes was unlikely to be mediated by YTHDF proteins in this instance.

In contrast to early development, the role of m^6A in differentiated adult haematopoiesis is less well defined. Functional studies have been carried out in T cells (Li, Tong et al. 2017, Tong, Cao et al. 2018), dendritic cells (Han, Liu et al. 2019), and to a lesser extent also myeloid cells (Lee, Bao et al. 2019).

Two studies have shown that m^6A modification plays an important role in T cell mediated pathogenesis. In the first, the authors demonstrated that deletion of the m^6A 'writer' *Mettl3* in *Mettl3*$^{fl/fl}$;*CD4-Cre* conditional knock out mice disrupts T cell homeostasis and differentiation (Li, Tong et al. 2017). Although no differences were observed in cell type or numbers at the level of the thymus, the number of naïve T cells in the spleen and lymph nodes of knock out mice was significantly increased compared to wild type mice. Furthermore, in a lymphopenic mouse adoptive transfer model (*Rag2*$^{-/-}$ mice), naïve *Mettl3*-deficient $CD4^+$ T cells failed to undergo homeostatic expansion and remained in the naïve state for up to 12 weeks, thereby preventing colitis. In a follow up paper, the same group showed that deletion of *Mettl3* in *Mettl3*$^{fl/fl}$; *FoxP3-Cre* conditional knock out mice resulted in severe autoimmune disease resulting from an inability of *Mettl3*-deficient regulatory T cells to suppress naïve T cell proliferation (Tong, Cao et al. 2018). In both cases, the mechanism was attributed to increased SOCS family activity, secondary to reduced m^6A-mediated decay of *Socs* mRNAs. Upregulation of *Socs* family genes resulted in inhibition of IL-7 signalling in $CD4^+$ T cells, and the IL2-STAT5 pathway in $FoxP3^+$ T cells, inhibiting activation and suppressive capacity respectively (Li, Tong et al. 2017, Tong, Cao et al. 2018).

In terms of dendritic cells (DCs), Han et al. showed in a melanoma murine tumour model that neoantigen specific immunity is regulated by mRNA m^6A methylation

through the m^{6}A binding protein YTHDF1 (Han, Liu et al. 2019). In this paper, the authors observed slower growth of B16-OVA tumours and prolonged survival in *Ythdf1*-deficient mice and subsequently attributed this to an increased capacity of *Ythdf1*-deficient DCs to cross-prime CD8$^+$ T cells. They also showed enhanced cross-presentation ability by *Mettl14*-deficient DCs compared to wild type DCs, supporting a more general dependence on RNA m^{6}A methylation.

Most recently, Lee et al. conditionally deleted *Mettl3* in myeloid cells by generating *Mettl3*$^{fl/fl}$;*Lysm-Cre* mice, as part of a wider study investigating differentiation defects in *Mettl3*-deficient HSCs (described below) (Lee, Bao et al. 2019). They found no difference in the number of myeloid cells in the peripheral blood, BM or spleens of 6-8 week old *Mettl3*$^{fl/fl}$;*Lysm-Cre* mice compared with controls. Furthermore, macrophages derived from BM of *Mettl3*$^{fl/fl}$;*Lysm-Cre* mice showed normal upregulation of inflammatory cytokines (*Tnfα*, *Il1b*, *Il6*) and normal engulfing activity compared to controls, suggesting that *Mettl3* is not required for the maintenance or function of mature myeloid cells (Lee, Bao et al. 2019).

In the last year, concurrent with the work outlined in the results section below, several publications have emerged supporting a requirement for m^{6}A in haematopoietic stem and progenitor cell function and maintenance.

Multiple studies have documented that expression of *Mettl3* and *Mettl14* is higher in HSPCs compared with differentiated cells in mouse bone marrow, suggesting a potential role in controlling the most primitive haematopoietic compartments (Weng, Huang et al. 2018, Yao, Sang et al. 2018, Lee, Bao et al. 2019). To investigate this possibility, Yao et al. generated inducible *Mx1-Cre*-mediated conditional knock out models to delete *Mettl3*, *Mettl14* or both *Mettl3* and *Mettl14* in mice. The authors treated these mice at 6 weeks of age with pIpC to induce gene deletion, and analysed bone marrow compartments 6 weeks later. As expected, there was a reduction of m^{6}A, although this was greater with *Mettl3* deletion than with *Mettl14* deletion. Notably there was also a large (10 fold) increase in HSCs following deletion of *Mettl3*. In contrast, deletion of *Mettl14*, either in isolation or together with *Mettl3*, had no discernible effect on HSPC compartments. Primary and secondary transplantation of BM from *Mettl3* deleted mice showed reduced engraftment and multilineage reconstitution potential of *Mettl3*-deficient HSCs compared to wild type HSCs. The authors went on to show increased cell cycling and reduced expression of genes

which maintain HSC quiescence in *Mettl3*-deficient HSCs (*Nr4a2*, *p21*, *Bmi-1*, *Prdm16*). They concluded that METTL3 is a pivotal regulator of HSC self-renewal in adult BM, which functions by promoting the expression of genes which maintain HSC quiescence (Yao, Sang et al. 2018).

The publication by Yao et al. was closely followed by another study evaluating the effect of *Mettl3* deletion (Lee, Bao et al. 2019). Lee et al. generated inducible *Mx1-Cre*-mediated and *Rosa26-CreER*T2-mediated conditional knock out models to delete *Mettl3* from mice. They reported a sustained significant increase in HSCs and HPC2 cells following *Mettl3* deletion, a modest increase in HPC1 cells, and no significant difference in MPPs. Changes were also observed in committed progenitor cells (decreases in GMPs and increases in Pre-MegEs and MkPs) and differentiated cells (decreases in platelets, neutrophils and lymphocytes). Based on the results of BrdU incorporation assays, methylcellulose colony forming assays, 5-FU myeloablation treatment of mice, and competitive BM and HSC transplantation assays, the authors concluded that the increase in HSCs following *Mettl3* deletion was a result of reduced differentiation, as opposed to increased self-renewal. They went on to use a combination of meRIP-Seq and RNA-Seq to demonstrate that *Mettl3* deletion decreased m^6A modification of HSC differentiation genes, including *Myc*, *Junb* and *Tet2*. Interestingly RNA-Seq showed little difference in the transcriptome of control versus *Mettl3*-deleted HSCs, and the authors subsequently showed that the effect of m^6A was predominantly on mRNA translation in this case. Lee et al. discussed the discrepancy between their findings and those of Vu et al. and Wang et al. ((Vu, Pickering et al. 2017, Weng, Huang et al. 2018), both of whom reported increases in differentiation following *Mettl* deletion in HSPCs. However, in those cases a mixed population of human cord blood $CD34^+$ cells was used, arguably clouding the interpretation, particularly in light of the cell specific effects reported by Lee at al on HSCs versus progenitor cells following *Mettl3* deletion (minimal effect on progenitor cells, marked effect on HSCs) (Lee, Bao et al. 2019).

The requirement for YTHDF2 in haematopoietic stem and progenitor cell function and maintenance has also been reported in two recent publications (Li, Qian et al. 2018, Wang, Zuo et al. 2018).

Li et al. used an inducible *Mx1-Cre*-mediated conditional knock out model to delete *Ythdf2* in mice. Four weeks after pIpC-mediated *Ythdf2* deletion, the authors observed increased numbers of long-term HSCs (LT-HSCs) and short-term (ST-HSCs), without any change in progenitor or committed lineage cells, in the BM of *Ythdf2*-deleted mice compared to controls. Primary and secondary transplantation of total BM from *Ythdf2*-deleted and control mice showed improved overall engraftment, without any alteration in multilineage reconstitution capacity or likelihood of malignant transformation, for *Ythdf2*-deleted cells. This study also reported that shRNA-mediated depletion of *YTHDF2* led to an ex-vivo expansion of human umbilical cord blood (hUCB) HSCs and an increase in HSC functionality, as measured in a limiting dilution transplantation assay. The authors showed that in *Ythdf2* KO HSPCs and *YTHDF2* KD hUCB HSCs, there was an increase in methylated mRNAs encoding transcription factors essential for stem cell renewal, and attributed this to reduced YTHDF2-mediated decay of m6A modified transcripts (Li, Qian et al. 2018).

Wang et al. used 3 conditional knock out models (*Mx1-Cre*, *ERT-Cre* and *Vav-iCre)* to delete *Ythdf2* in mice (Wang, Zuo et al. 2018). They reported increased numbers of LT-HSCs and ST-HSCs, MPPs and LSK cells in pIpC treated *Ythdf2*$^{fl/fl}$;*Mx1-Cre* mice compared to controls, without any changes in progenitor cell compartments (CMP, CLP, GMP, MEP), or differentiated cells (myeloid cells, B lymphocytes, T lymphocytes). Increased LT-HSCs numbers were also observed in *Ythdf2*$^{fl/fl}$;*Vav-iCre* mice compared to controls. Transplantation of LT-HSCs from pIpC treated *Ythdf2*$^{fl/fl}$;*Mx1-Cre* and control mice showed increased engraftment by *Ythdf2*-deficient cells. Application of haematopoietic stressors, in the form of 5-FU treatment or repeated ionising radiation, resulted in increased numbers and function (based on *in-vitro* colony formation) of LT-HSC in *Ythdf2*$^{fl/fl}$;*Mx1-Cre* mice compared to controls. Mechanistically, the authors used a combination of RNA-Seq, m^{6}A-RIP-qPCR and actinomycin-D treatment to show upregulation of genes in the Wnt signalling pathway, including downstream targets *Myc* and *Axin2*, the mRNAs of which were significantly more methylated in *Ythdf2*-deficient HPSCs, and were also increased following actinomycin-D treatment. Administration of the small-molecule Wnt/β-catenin inhibitor ICG-001 to pIpC treated *Ythdf2*$^{fl/fl}$;*Mx1-Cre* and control mice partially rescued the proliferation and phenotypic expansion of HSCs. The authors concluded that the expression of *Ythdf2* in HSCs facilitates decay of the m^{6}A-modified mRNAs of Wnt target genes, contributing to the repression of Wnt signalling in the steady state, whilst YTHDF2 deficiency simultaneously prevents the degradation of mRNAs of both Wnt

target genes and survival-related genes during hematopoietic stresses (Wang, Zuo et al. 2018).

In summary, the combined data described above supports an important role for m^6A in normal haematopoiesis, and provides the context for the results presented in this chapter.

3.2 Aims

Based on the evidence presented in this introduction, we hypothesised that YTHDF2 would play an important role in haematopoiesis.

The aims of the project were therefore to investigate the requirement for YTHDF2 at different stages of haematopoiesis and to identify molecular mechanisms by which YTHDF2 functions during these processes.

3.3 Outline of experiments described in Chapter 3

To study the functional role of YTHDF2 in haematopoiesis, we made use of the conditional and reporter *Ythdf2*^{fl} mouse allele, in which exon 2 of *Ythdf2* is flanked by *LoxP* sites, and eGFP is inserted into exon 1, generating a fully functional endogenously expressed eGFP-YTHDF2 fusion protein (Ivanova, Much et al. 2017). We analysed eGFP-YTHDF2 expression within the HSPC compartments of 8-12-week old adult *Ythdf2*$^{fl/fl}$ mice, and E14.5 dpc (embryonic 14.5 days post coitum) embryos. We then crossed *Ythdf2*$^{fl/fl}$ mice with *Vav-iCre* mice (de Boer, Williams et al. 2003), in order to delete the gene specifically within the haematopoietic system, and studied the effect of this on HSPC compartments in adult BM and foetal liver (FL), as well as peripheral blood and lymphoid organs of 8-12-week-old adult mice. Finally, to study the function of YTHDF2 in haematopoiesis, we carried out serial transplantation of *Ythdf2*$^{fl/fl}$ and *Ythdf2*$^{fl/fl}$;*Vav-iCre* BM and FL HSCs.

3.4. Results

3.4.1 Expression of *Ythdf2* in the HSPC compartment

To study the role of YTHDF2 in haematopoiesis, we employed a mouse kindly provided by Ivanova et al., in which exon 2 of *Ythdf2* is flanked by *LoxP* sites, and eGFP-PreScission-His6-Flag-HA2 tag is inserted after the start codon of *Ythdf2* within exon 1 (**Figure 3.4.1 A**) (Ivanova, Much et al. 2017). According to these authors., N-terminal tagging of YTHDF2 with GFP-His6-FLAG-HA does not affect the expression (as examined by western blotting) or function of the protein (mice homozygous for *Ythdf2*^{fl} are viable and fertile, with no outward abnormalities in contrast to *Ythdf2*-deficient mice, which display female specific infertility, see section **1.1.3**). Furthermore, c-Kit^{+} stem and progenitor cells from *Ythdf2*$^{fl/fl}$ and *Ythdf2*$^{+/+}$ mice express equal levels of YTHDF2 protein, and *Ythdf2*$^{fl/fl}$ and *Ythdf2*$^{+/+}$ mice display identical numbers of HSCs and downstream progeny (unpublished data from the Kranc lab in London). In this mouse, here referred to as the *Ythdf2*$^{fl/fl}$ mouse, eGFP fluorescence reports YTHDF2 protein levels. For convenience, eGFP will hereafter be referred to as GFP in this text.

In their paper, Ivanova et al. examined HA-YTHDF2 protein levels in tissues of *Ythdf2*$^{fl/fl}$ mice by western blotting. They showed that the HA-YTHDF2 protein was expressed in all tissues analysed, specifically testis, ovaries, liver, spleen, thymus, kidney brain, heart, and lung. Notably, respective tissues expressed differential amounts of YTHDF2, with the highest expression in the testis, ovaries, spleen and thymus (Ivanova, Much et al. 2017).

To investigate *Ythdf2* expression in the HSPC compartment, we evaluated GFP expression in the FL (the major site of definitive haematopoiesis during development) of E14.5 dpc *Ythdf2*$^{fl/fl}$ embryos and BM of 8-12-week-old adult *Ythdf2*$^{fl/fl}$ mice. FL and BM were harvested, stained with antibodies against LSK SLAM markers, and analysed on an LSRFortessa™ (BD) as described in sections **2.7** and **2.8**.

HSPC populations were gated according to the expression of the following surface makers: LK (Lin^{-}Sca-1^{-}c-Kit^{+}); LSK (Lin^{-}Sca-1^{+}c-Kit^{+}); haematopoietic stem cells (HSCs: LSK CD48^{-}CD150^{+}); multipotent progenitors (MPPs: LSK CD48^{-}CD150^{-});

haematopoietic progenitor cells-1 (HPC-1: LSK $CD48^{+}CD150^{-}$); haematopoietic progenitor cells-2 (HPC-2: LSK $CD48^{+}CD150^{+}$), as shown in **Figure 3.4.1 B**.

All hematopoietic cells from the FL and adult BM expressed GFP-YTHDF2 (**Figures 3.4.1 C-D**). Notably, YTHDF2 was highly expressed in $Lin^{-}Sca\text{-}1^{+}c\text{-}Kit^{+}$ (LSK) cells, LSK $CD48^{-}CD150^{+}$ HSCs, LSK $CD48^{-}CD150^{-}$ multipotent progenitors (MPPs), primitive hematopoietic progenitor cells (i.e. LSK $CD48^{+}CD150^{-}$HPC-1 and LSK $CD48^{+}CD150^{+}$ HPC-2 populations), and $Lin^{-}Sca\text{-}1^{-}c\text{-}Kit^{+}$ (LK) myeloid progenitors, and its expression was decreased in differentiated Lin^{+} cells (**Figures 3.4.1 C-D**). The correlation of YTHDF2 expression with primitive cell compartments suggested that it may be involved in maintenance of cells at the top of the haematopoietic hierarchy.

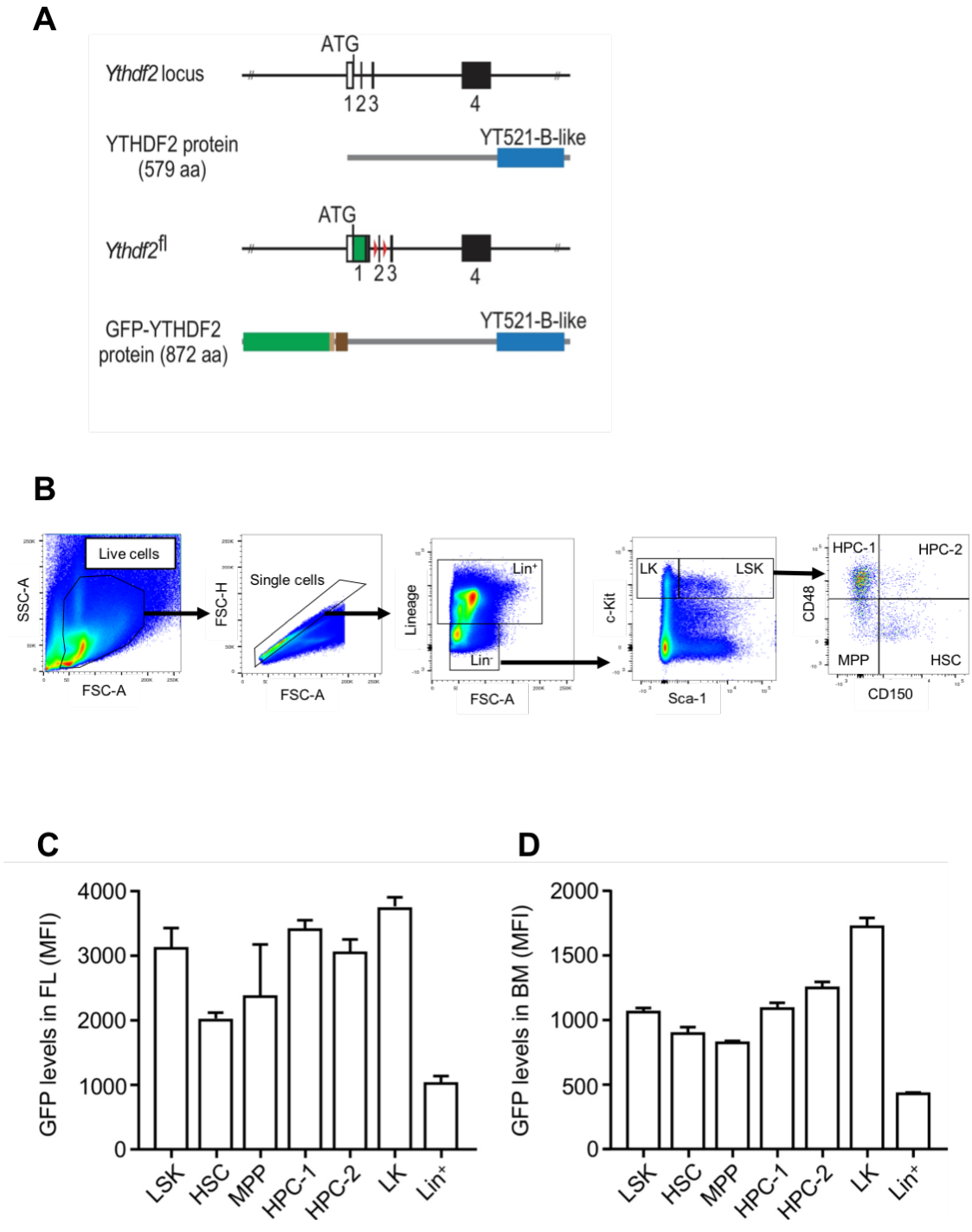

Figure 3.4.1 *Ythdf2* expression within the haematopoietic system. (**A**) The sequences encoding the eGFP-PreScission-His6-Flag-HA2 epitope tag were inserted into exon 1 of the *Ythdf2* locus, and exon 2 was flanked by *LoxP* sites (Ivanova, Much et al. 2017). For simplicity, this allele is referred to as *Ythdf2*^{fl} and codes for eGFP-PreScission-His6-Flag-HA2-YTHDF2 fusion protein (referred to as GFP-YTHDF2 protein). (**B**) LSK SLAM population flow cytometry gating strategy. (**C**) GFP

expression in the indicated FL cell populations from *Ythdf2*$^{fl/fl}$ 14.5 dpc embryos. YTHDF2 is uniformly expressed in FL LSK cells, LSKCD48^{-}CD150^{+} HSCs, LSKCD48^{-}CD150^{-} multipotent progenitors (MPPs), primitive haematopoietic progenitor cells (i.e. LSKCD48^{+}CD150^{-} HPC-1 and LSKCD48^{+}CD150^{+} HPC-2 populations), and Lin^{-}Sca-1^{-}c-Kit^{+} (LK) myeloid progenitors, and its expression is decreased in differentiated Lin^{+} cells. The data represent mean fluorescence intensity (MFI) ± SD (*n* = 3-4 mice per genotype). GFP levels are significantly lower in Lin^{+} compartment compared to all HSPC compartments ($p<0.05$ for MPP, and $p<0.0001$ for all other comparisons, Unpaired t-test). (**D**) GFP expression in the indicated BM cell populations from 8-12-week-old mice. YTHDF2 is expressed at higher levels in HSC/progenitor cells compared to mature cells and its expression is decreased in the more differentiated Lin^{+} cell compartment. The data represent MFI ± SD (*n* = 3-4 mice per genotype). GFP levels are significantly lower in Lin^{+} compartment compared to all HSPC compartments ($p<0.0001$ for each comparison, Unpaired t-test).

3.4.2 Generation and validation of *Ythdf2*$^{fl/fl}$;*Vav-iCre* mice

To reveal the role of YTHDF2 in haematopoiesis, we crossed *Ythdf2*$^{fl/fl}$ mice with *Vav-iCre* mice (de Boer, Williams et al. 2003) to generate *Ythdf2*$^{fl/fl}$;*Vav-iCre* mice, in which *Ythdf2* is specifically ablated within the hematopoietic system shortly after the emergence of definitive HSCs (**Figures 3.4.2 A-C**). In these mice, the *vav* promoter elements direct Cre mediated recombination in all cells of the haematopoietic system, and mammalian codon usage is applied to *Cre-recombinase* (termed Codon-improved Cre-recombinase, or iCre) for improved *Cre* expression, and reduced susceptibility to epigenetic silencing (Shimshek, Kim et al. 2002). This Cre mouse line has been used extensively by multiple groups including our own (Guitart, Subramani et al. 2013, Vukovic, Sepulveda et al. 2016) to delete floxed genes specifically from the haematopoietic system.

Analysis of GFP-YTHDF2 expression by flow cytometry in LSKs derived from *Ythdf2*$^{fl/fl}$;*Vav-iCre* embryos confirmed loss of GFP, and thereby efficient *Ythdf2* deletion (**Figure 3.4.2 B-C**). *Ythdf2*$^{fl/fl}$;*Vav-iCre* mice were subsequently established as a breeding colony. Cre recombinase activity has been reported in the testes of *Vav-iCre* mice (de Boer, Williams et al. 2003, Croker, Metcalf et al. 2004), potentially resulting in germline deletion in some offspring. For this reason, we exclusively mated Cre^{+} females with Cre^{-} males. Upon weaning at 3 weeks of age offspring were ear

notched, and the tissue was used for genotyping PCRs (*Ythdf2* flox and *Vav-iCre*), as described in section **2.3** and as shown in **Figure 3.4.2 D**. We found that *Ythdf2*$^{fl/fl}$;*Vav-iCre* mice were born at normal Mendelian ratios (*Ythdf2*$^{fl/fl}$ X *Ythdf2*$^{fl/fl}$;*Vav-iCre* matings resulted in 65 *Ythdf2*$^{fl/fl}$ and 47 *Ythdf2*$^{fl/fl}$;*Vav-iCre* mice at weaning, P = 0.29, Two-tailed T test **Figure 3.4.2 E**), and matured to adulthood without any observable defects.

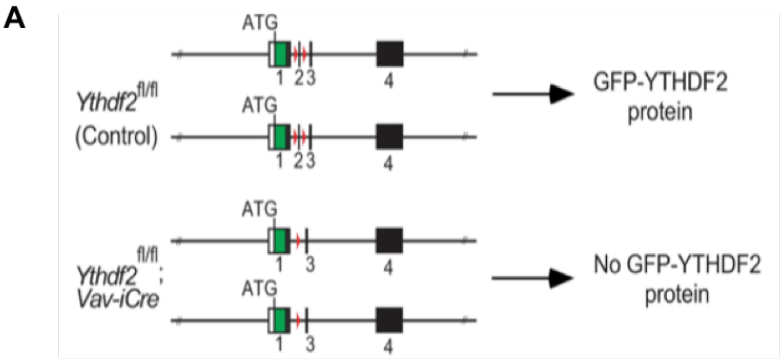
A
ATG
1 2 3
4
Ythdf2fl/fl
(Control)
GFP-YTHDF2
protein
Ythdf2fl/fl;
Vav-iCre
No GFP-YTHDF2
protein

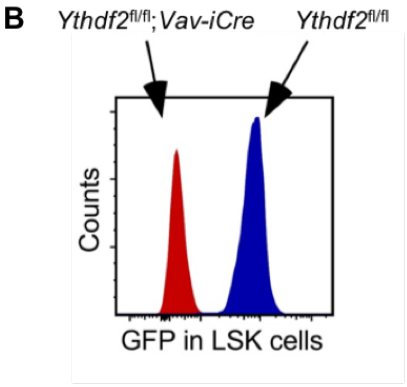
B
Ythdf2fl/fl;Vav-iCre
Ythdf2fl/fl
Counts
GFP in LSK cells

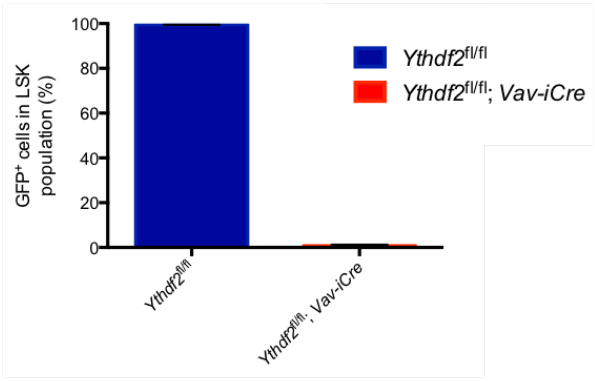
C
GFP+ cells in LSK population (%)
100
80
60
40
20
0
Ythdf2fl/fl
Ythdf2fl/fl; Vav-iCre

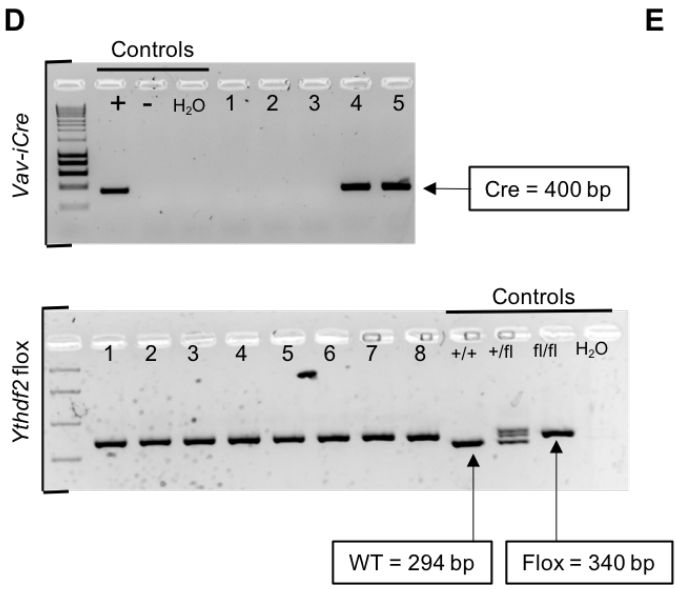
D
Controls
Vav-iCre
+ - H2O 1 2 3 4 5
Cre = 400 bp
Controls
Ythdf2 flox
1 2 3 4 5 6 7 8 +/+ +/fl fl/fl H2O
WT = 294 bp
Flox = 340 bp

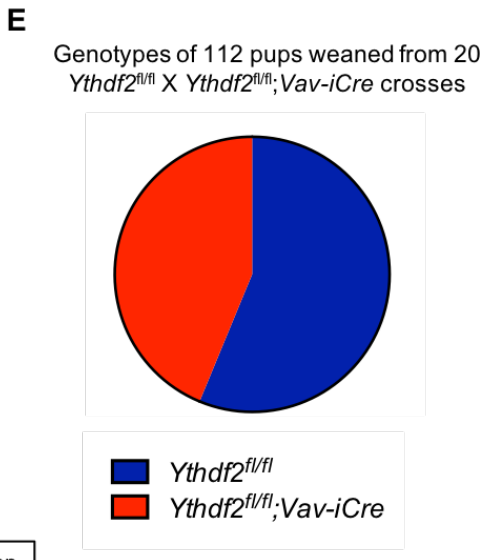
E
Genotypes of 112 pups weaned from 20
Ythdf2fl/fl X Ythdf2fl/fl;Vav-iCre crosses
Ythdf2fl/fl
Ythdf2fl/fl;Vav-iCre

Figure 3.4.2 Generation and validation of *Ythdf2*$^{fl/fl}$;*Vav-iCre* mice. (**A**) Deletion of *Ythdf2* from the haematopoietic system using *Vav-iCre*. FL cells from control E14.5 dpc *Ythdf2*$^{fl/fl}$ embryos produce normal GFP-YTHDF2 protein. In the presence of *iCre*, exon 2 is deleted resulting in a frameshift mutation and a complete loss of the GFP-YTHDF2 protein. (**B**) A representative histogram showing GFP-YTHDF2 protein expression in *Ythdf2*$^{fl/fl}$ FL LSK cells and the lack of GFP-YTHDF2 expression in *Ythdf2*$^{fl/fl}$;*Vav-iCre* FL LSK cells. (**C**) Percentage of GFP-positive cells in the E14.5 dpc FL LSK cell population from FLs of *Ythdf2*$^{fl/fl}$ and *Ythdf2*$^{fl/fl}$;*Vav-iCre* embryos. Data are mean ± s.e.m. (*n* = 5 per genotype). (**D**) Representative gel showing PCR genotyping products for *Ythdf2* flox and *Vav-iCre.* (**E**) Proportion of *Ythdf2*$^{fl/fl}$ and *Ythdf2*$^{fl/fl}$;*Vav-iCre* weaned pups resulting from *Ythdf2*$^{fl/fl}$ X *Ythdf2*$^{fl/fl}$;*Vav-iCre* breeding crosses (*n* = 112 pups from 20 crosses) P = 0.29, Two-tailed T test.

3.4.3 Ablation of *Ythdf2* affects cell distribution within stem and progenitor cell compartments

Given the elevated levels of YTHDF2 in HSCs and progenitor cells compared to differentiated cells (**Figures 3.4.1 C-D**), we investigated the impact of *Ythdf2* deletion on these cell populations.

Haematopoietic stem cells and direct progeny were investigated in FL and BM of *Ythdf2*$^{fl/fl}$ and *Ythdf2*$^{fl/fl}$;*Vav-iCre* E14.5 dpc embryos and adult mice respectively. There was no significant difference in the total WBC count between *Ythdf2*$^{fl/fl}$ and *Ythdf2*$^{fl/fl}$;*Vav-iCre* genotypes in the FL (**Figure 3.4.3 A**) or BM (counts provided per one hind leg i.e. tibia plus femur) (**Figure 3.4.3 B**). The number of Lin^{-}Sca-1^{-}c-Kit^{+} (LK) cells was also unchanged between *Ythdf2*$^{fl/fl}$ and *Ythdf2*$^{fl/fl}$;*Vav-iCre* genotypes, both in the FL (**Figure 3.4.3 C**) and in the adult BM (**Figure 3.4.3 D**). However, there was a significant expansion in both the frequency and the absolute number of LSK stem and progenitor cells in *Ythdf2*$^{fl/fl}$;*Vav-iCre* FL (**Figures 3.4.3 E-F**) and adult BM (**Figures 3.4.3 G-H**) when compared to *Ythdf2*$^{fl/fl}$ controls. LSK, HSC and primitive progenitor (HPC-1 and HPC-2) compartments were all expanded. In adult BM, multipotent progenitor (MPP) numbers were reduced in *Ythdf2*$^{fl/fl}$;*Vav-iCre* mice compared to *Ythdf2*$^{fl/fl}$ controls, however this difference was not observed in FL (**Figures 3.4.3 F (FL)** and **H (BM)**).

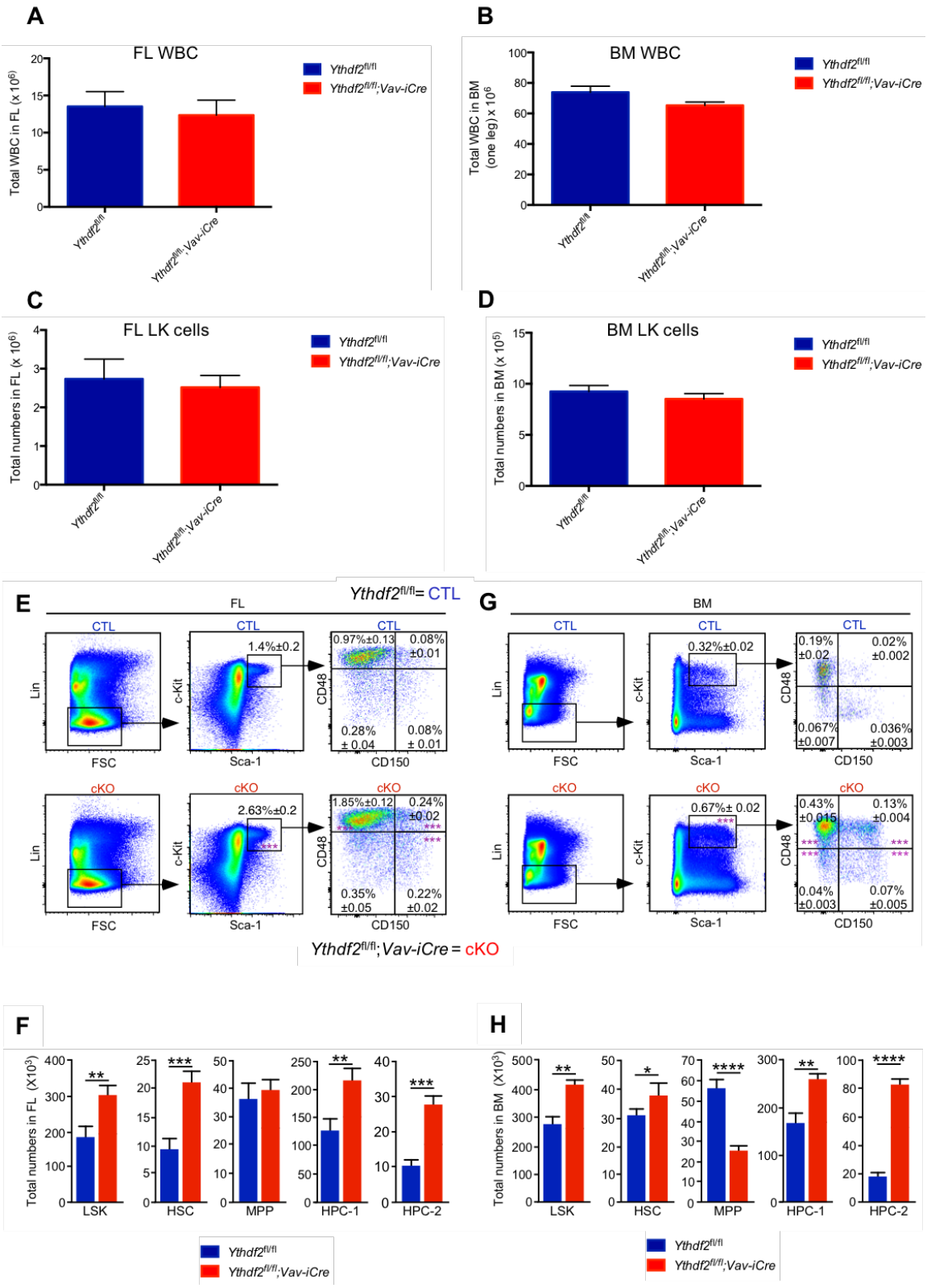

Figure 3.4.3 Ablation of *Ythdf2* affects cell distribution within stem and progenitor cell compartments. (A-B) Total WBC counts in FL **(A)** and BM **(B)** from

Ythdf2$^{fl/fl}$ and *Ythdf2*$^{fl/fl}$;*Vav-iCre* E14.5 dpc embryos and 8-12 week old adult mice respectively. BM counts are given per one hind leg i.e. tibia plus femur. **(C-D)** Total LK numbers in FL **(C)** and BM **(D)** from *Ythdf2*$^{fl/fl}$ and *Ythdf2*$^{fl/fl}$;*Vav-iCre* E14.5 dpc embryos and 8-12 week old adult mice respectively. **(E-F)** Frequencies **(E)** and total numbers **(F)** of LSK, HSC, MPP, HPC-1 and HPC-2 cell populations in FLs from *Ythdf2*$^{fl/fl}$ (control, CTL) and *Ythdf2*$^{fl/fl}$;*Vav-iCre* (conditional knock out, cKO) embryos. **(G-H)** Frequencies **(G)** and total numbers **(H)** in BM from *Ythdf2*$^{fl/fl}$ and *Ythdf2*$^{fl/fl}$;*Vav-iCre* 8-12 week old mice.
Data are mean ± s.e.m. n = 10 (FL) or 7-8 (BM) per genotype. *, P < 0.05; **, P < 0.01, ***, P < 0.001, ****, P < 0.0001, Mann-Whitney U test.

Overall, the SLAM LSK staining data obtained for both adult BM and embryonic FL showed an expansion of HSCs and primitive progenitor cells (HPC-1 and HPC-2) and in the case of adult BM, also a reduction in multipotent progenitor cells.

3.4.4 *Ythdf2* loss affects myeloerythroid progenitor numbers, but not *in vitro* differentiation capacity

In an attempt to further resolve the alterations in the HSPC compartments, myeloerythroid progenitor cell staining and flow cytometry was carried out (see section **2.8**), based on a protocol described by Pronk et al (Pronk and Bryder 2011). This method allows for the identification of immature myeloerythroid progenitor subsets in murine bone marrow, including early bipotent progenitors for the erythroid/megakaryocyte lineages (pre-MegE), early monopotent erythroid (pre-CFU-E and CFU-E) and megakaryocyte progenitors (MkP), and primitive granulocyte/macrophage progenitors (pre-GM and GMP) (**Figure 3.4.4 A**). To facilitate separation of these populations from the LK compartment, Pronk relied upon the detection of signalling lymphocytic activation molecule family member 1 (Slamf1/CD150), Endoglin (Eng/CD105) and Integrin alpha 2b (Itga2b/CD41), in addition to CD16/32FCRII/IIII (**Figure 3.4.4 B**).

Making use of this staining to analyse BM of *Ythdf2*$^{fl/fl}$ and *Ythdf2*$^{fl/fl}$;*Vav-iCre* adult mice (8-12-weeks old), we found lower numbers of pre-GMP cells, and increased numbers of pre-MegE, pre-CFU-E and MkP cells in *Ythdf2*$^{fl/fl}$;*Vav-iCre* mice compared to *Ythdf2*$^{fl/fl}$ controls (**Figure 3.4.4 C**). Nevertheless, lineage restricted progenitors of granulocytes and monocytes (GMP) and also erythroid cells (CFU-E) appeared

unaffected by loss of *Ythdf2* (**Figure 3.4.4 C**), suggesting that the changes were successfully compensated at more differentiated stages. To further characterise the progenitor cell compartment, it would be useful to carry out additional antibody staining for lymphoid primed MPP (LMPP), common lymphoid progenitor (CLP), and common myeloid progenitor (CMP) cell populations, as described by Akashi and colleagues (Kondo, Weissman et al. 1997, Akashi, Traver et al. 2000). This staining was unfortunately not carried out earlier due to challenges faced when optimising a non-FITC conjugated CD34 antibody for use in the protocol (as opposed to the FITC conjugated CD34 antibody specified, which cannot be used in combination with GFP-YTHDF2 mice).

To investigate how the changes in HSPC compartments in *Ythdf2*$^{fl/fl}$;*Vav-iCre* mice relate to self-renewal and differentiation potential *in vitro*, 25 000 FL cells isolated from E14.5 dpc *Ythdf2*$^{fl/fl}$ and *Ythdf2*$^{fl/fl}$;*Vav-iCre* embryos were plated into 3434 methylcellulose (MethoCult™ GF M3434), as described in section **2.13.2**. This is a semi-solid growth medium, optimized for the growth and enumeration of hematopoietic progenitor cells in colony-forming unit assays of mouse bone marrow, spleen, peripheral blood, and foetal liver cells. The medium is formulated to support growth of primitive erythroid progenitor cells (CFU-Red), granulocyte-macrophage progenitor cells (CFU-GM, CFU-G and CFU-M), and multi-potential granulocyte, erythroid, macrophage, megakaryocyte progenitor cells (CFU-GEMM) (Miller and Lai 2005). Enumeration of colonies after 10 days revealed no significant difference in the total colony number or multilineage differentiation potential of *Ythdf2*$^{fl/fl}$;*Vav-iCre* cells compared to *Ythdf2*$^{fl/fl}$ controls (**Figure 3.4.4 D-E**).

In summary, the combined results of *in vitro* 3434 methylcellulose colony assays and *in vivo* myeloerythroid progenitor cell staining suggested that the changes observed in the HSPC LSK SLAM compartments of *Ythdf2*-deficient mice are largely compensated as differentiation of cell lineages progresses, at least under stable conditions.

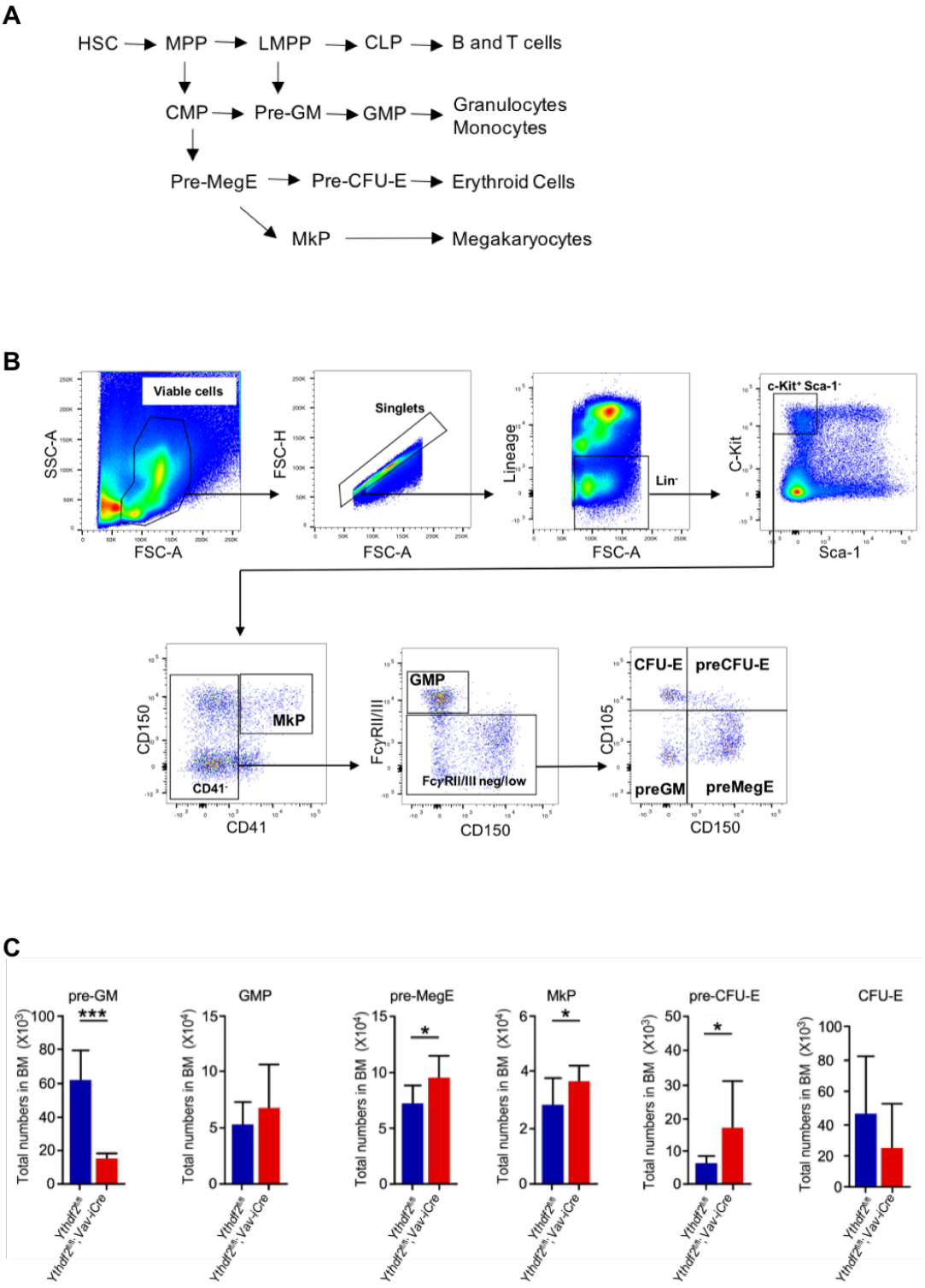
A
HSC
MPP
LMPP
CLP
B and T cells
CMP
Pre-GM
GMP
Granulocytes
Monocytes
Pre-MegE
Pre-CFU-E
Erythroid Cells
MkP
Megakaryocytes
B
Viable cells
SSC-A
FSC-A
Singlets
FSC-H
FSC-A
Lineage
Lin-
FSC-A
c-Kit+ Sca-1-
C-Kit
Sca-1
CD150
MkP
CD41-
CD41
GMP
FcγRII/III neg/low
FcγRII/III
CD150
CFU-E
preCFU-E
preGM
preMegE
CD105
CD150
C
pre-GM
***
GMP
pre-MegE
*
MkP
*
pre-CFU-E
*
CFU-E
Total numbers in BM (X10³)
Total numbers in BM (X10⁴)
Total numbers in BM (X10⁴)
Total numbers in BM (X10⁴)
Total numbers in BM (X10³)
Total numbers in BM (X10³)
Ythdf2fl/fl
Ythdf2fl/fl; Vav-iCre

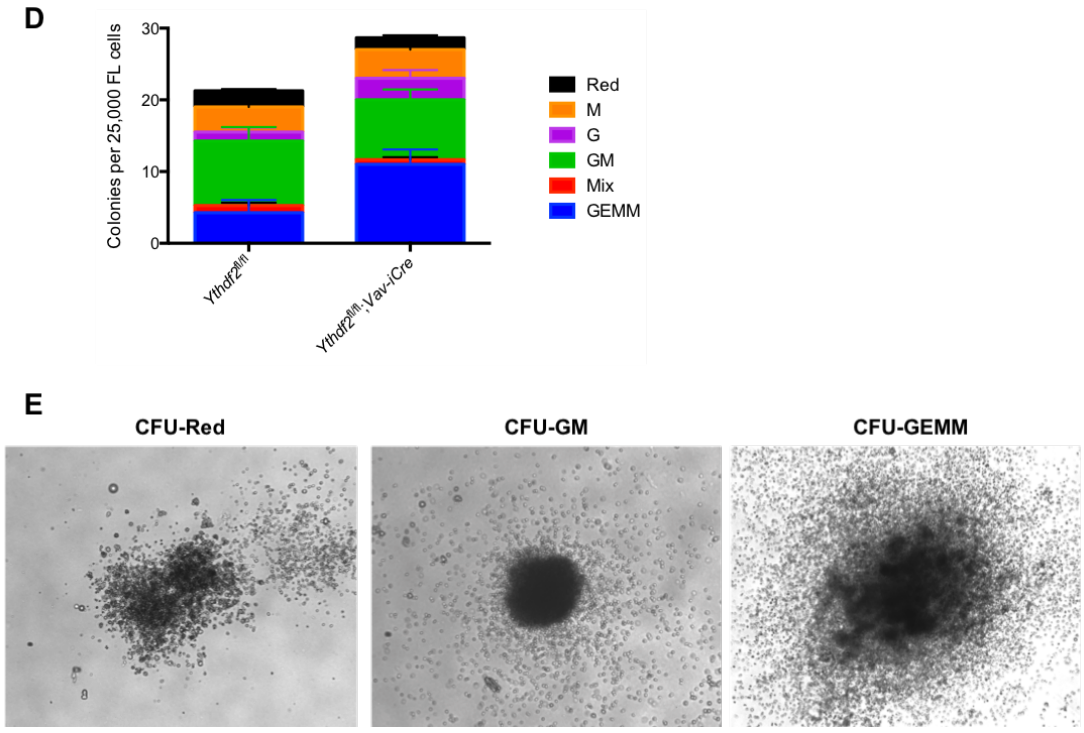

Figure 3.4.4 *Ythdf2* loss affects myeloerythroid progenitor numbers, but not *in vitro* differentiation capacity. (**A**) Schematic overview of the first developmental stages in the differentiation from multipotent HSC to progeny possessing oligo and unilineage differentiation potentials. Adapted from Pronk et al. 2011 (Pronk and Bryder 2011). HSC haematopoietic stem cell, MPP multipotent progenitor, LMPP lymphoid primed MPP, CLP common lymphoid progenitor, CMP common myeloid progenitor, Pre-GM pre-granulocyte/macrophage progenitor, Pre-MegE pre-megakaryocyte/erythrocyte, Pre-CFU-E pre-colony forming unit – erythrocytes, MkP megakaryocyte progenitor. (**B**) Flow cytometry-based strategy for multiparameter fractionation of murine myeloerythroid precursors according to the Pronk protocol. (**C**) Total numbers of committed progenitor cells in the BM of *Ythdf2*$^{fl/fl}$ and *Ythdf2*$^{fl/fl}$*;Vav-iCre* mice. Data are mean ± s.e.m. (*n* = 5-6 mice per genotype). *, P<0.05; ****, P < 0.0001, Unpaired t-test. (**D**) CFU assays performed with BM cells from 8–10-wk-old mice. CFU-Red, CFU-erythroid and/or megakaryocyte; CFU-G, CFU-granulocyte; CFU-M, CFU-monocyte/macrophage; CFU-GM, CFU–granulocyte and monocyte/macrophage; CFU-Mix, at least three of the following: granulocyte, erythroid, monocyte/macrophage, and megakaryocyte. CFU-GEMM, all of the following: granulocyte, erythroid, monocyte/macrophage, and megakaryocyte. Data

are mean ± s.e.m. (*n* = 4 per genotype). (**E**) Representative images of CFU-Red, CFU-GM and CFU-GEMM colonies presented in (**D**). OLYMPUS IX50, 10X magnification.

3.4.5 *Ythdf2* loss affects T lymphocyte cell homeostasis

Having shown that *Ythdf2* loss expands the HSC compartment in the BM and FL of *Ythdf2*$^{fl/fl}$;*Vav-iCre* adult mice and E14.5 dpc embryos, we next characterised differentiated haematopoietic cells in the peripheral blood and lymphoid organs. To do so, we harvested peripheral blood, BM, thymus and spleen from a cohort of 8-10 week old *Ythdf2*$^{fl/fl}$ and *Ythdf2*$^{fl/fl}$;*Vav-iCre* mice for cell counts, antibody staining and flow cytometry (see sections **2.6**, **2.7**, **2.8**).

As shown in **Table 3.4.5**, loss of *Ythdf2* resulted in several significant alterations in the peripheral blood. Mild decreases were seen in white blood cells (WBCs), red blood cells (RBCs), CD8$^+$ T lymphocytes (CD8$^+$ T cells) and B lymphocytes (B cells), and a mild increase was observed in platelets (PLTs). However, with the exception of CD8$^+$ T cell lymphocytes, where the reduction was approximately 2-fold, the peripheral blood changes observed as a result of *Ythdf2* loss were all relatively small.

Analysis of spleens from *Ythdf2*$^{fl/fl}$ and *Ythdf2*$^{fl/fl}$;*Vav-iCre* mice revealed a significant reduction in CD8$^+$ T lymphocytes, but no other abnormalities (**Figures 3.4.5 A-B**). In contrast, at the level of the thymus there was a small increase in overall WBC count and CD4$^+$ T lymphocytes, but no difference in the number of CD8$^+$ or CD4$^+$CD8$^+$ (double positive) T lymphocytes (**Figures 3.4.5 C-D**). The significance of these findings is unclear. Given that the naive T cell pool in mice is almost exclusively sustained by thymic output (den Braber, Mugwagwa et al. 2012), it may be that the reduction in CD8$^+$ T lymphocytes within the peripheral blood and spleen of *Ythdf2* deficient cells is the result of peripheral expansion and/or loss. Nevertheless, there are several caveats to this conclusion, which are discussed further below (see **3.5 Discussion)**.

In summary, analysis of adult *Ythdf2*-deficient and control mice revealed small changes in red and white blood cell parameters, of which the most significant was a

reduction of $CD8^+$ T lymphocytes in the peripheral blood and spleen. Nevertheless, in the unchallenged state, these changes did not appear to be clinically significant.

	***Ythdf2*$^{fl/fl}$**	***Ythdf2*$^{fl/fl}$*;Vav-iCre***	**P value**
WBC (/µl)	9767 ± 935	7214 ± 2292	**0.0479**
RBC (x10^4/µl)	1178 ± 23.61	1071 ± 22.87	**0.0051**
Hb (g/dl)	16.91 ± 0.3513	15.97 ± 0.3803	0.1085
HCT (%)	52.12 ± 0.9812	49.90 ± 1.079	0.1033
MCV (fl)	44.26 ± 0.2271	46.61 ± 0.1924	**< 0.0001**
MCH (pg)	14.37 ± 0.1082	14.92 ± 0.1140	**0.0018**
PLT (x10^4/µl)	80.78 ± 3.896	100.2 ± 5.841	**0.0460**
$CD4^+$ T cells (/µl)	1459 ± 176.7	1161 ± 168.2	0.1135
$CD8^+$ T cells (/µl)	1102 ± 178.6	530.5 ± 92.22	**0.0206**
B cells (/µl) ($CD19^+$)	5226 ± 575.6	3828 ± 182.3	**0.0206**
Granulocytes (/µl) ($Gr1^+CD11b^+$)	2112 ± 458.5	1510 ± 361.7	0.3655
Monocytes (/µl) ($Gr1^-CD11b^+$)	390.8 ± 41.93	442.3± 26.04	0.2320

Table 3.4.5 Peripheral blood counts of 8-10 week old *Ythdf2*$^{fl/fl}$ and *Ythdf2*$^{fl/fl}$*;Vav-iCre* mice. Data are mean ± s.e.m. (*n* = 8-9 mice per genotype). P values are indicated. Mann-Whitney U test.

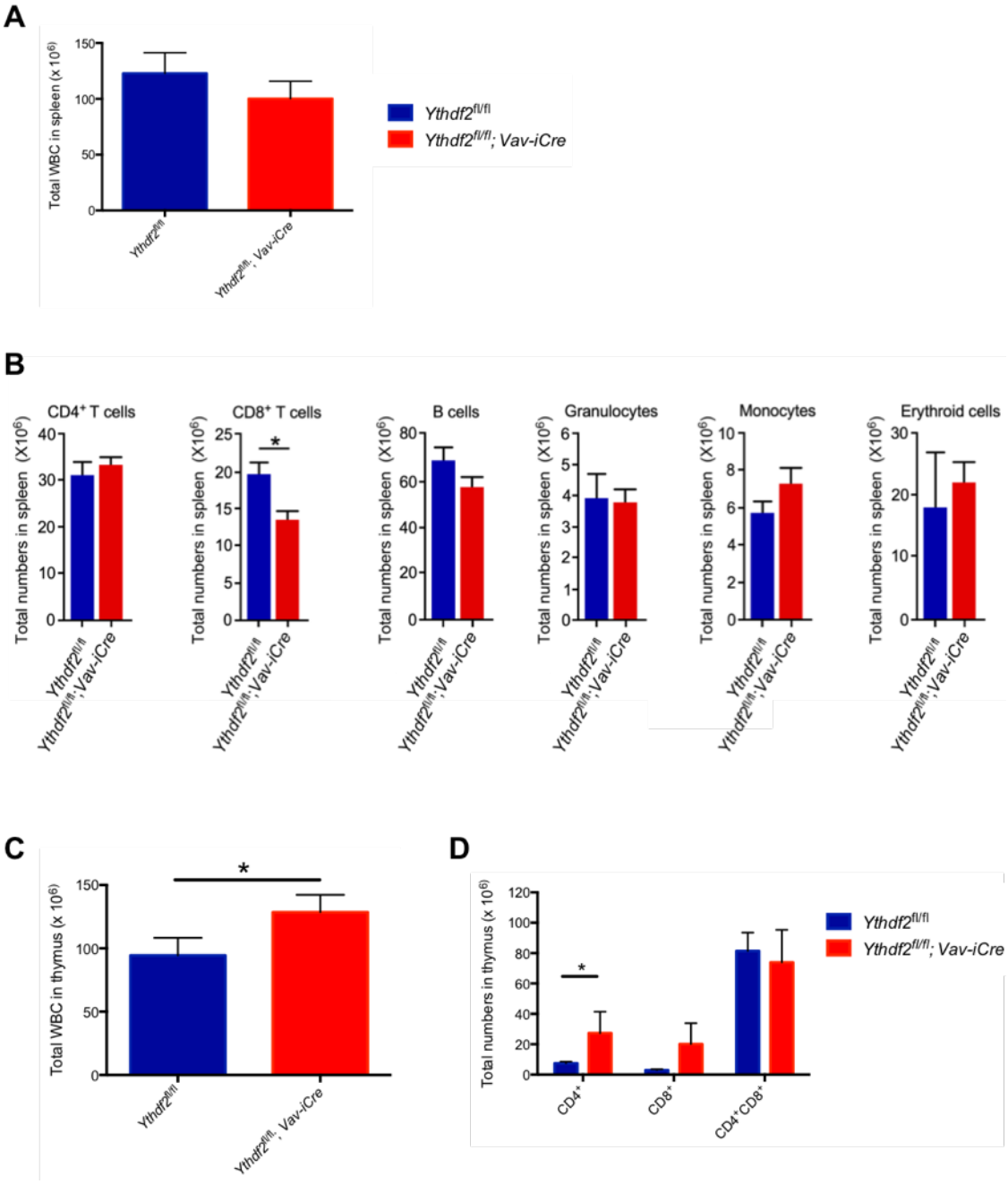

Figure 3.4.5 *Ythdf2* loss results in altered T cell homeostasis. (**A**) Total WBC in spleens of 8-10 week old *Ythdf2*$^{fl/fl}$ and *Ythdf2*$^{fl/fl}$*;Vav-iCre* mice. (**B**) Total numbers of T cells, B cells, granulocytes, monocytes and erythroid cells in spleens from 8-10 week old *Ythdf2*$^{fl/fl}$ and *Ythdf2*$^{fl/fl}$*;Vav-iCre* mice. (**C**) Total WBC in the thymus of 8-10 week old *Ythdf2*$^{fl/fl}$ and *Ythdf2*$^{fl/fl}$*;Vav-iCre* mice. (**D**) Total numbers of CD4$^+$, CD8$^+$ and CD4$^+$CD8$^+$ T cells in the thymus of 8-10 week old *Ythdf2*$^{fl/fl}$ and *Ythdf2*$^{fl/fl}$*;Vav-iCre* mice.

Data are mean ± s.e.m. (*n* = 5-6 mice per genotype). *, P < 0.05, Mann-Whitney U test.

3.4.6 Ablation of *Ythdf2* enhances HSC function – FL HSC transplantation

Having demonstrated that *Ythdf2*$^{fl/fl}$;*Vav-iCre* mice have increased numbers of FL and BM HSCs compared to *Ythdf2*$^{fl/fl}$ mice, we next sought to establish the functional status of these cells. To do so, we used a serial transplantation assay.

We sorted HSCs from E14.5 dpc FL, and transplanted them into irradiated recipient mice, as described in section **2.15.1**, and as shown in **Figure 3.4.6 A**.

Ythdf2$^{fl/fl}$ and *Ythdf2*$^{fl/fl}$;*Vav-iCre* LSKCD48^{-}CD150^{+} HSCs were sorted, and 100 CD45.2^{+} HSCs were transplanted via the tail vein into lethally irradiated (11 Gy) recipient mice (CD45.1^{+} CD45.2^{+}), together with 200 000 unfractionated bone marrow support cells (CD45.1^{+}). Haematopoietic monitoring was carried out as described in section **2.15.3**, with CD45.1 and CD45.2 staining used to monitor engraftment and differentiation of study HSCs against the background of recipient and support bone marrow cells.

Serial peripheral blood analysis of primary transplanted mice showed no significant difference in the engraftment of *Ythdf2*$^{fl/fl}$ and *Ythdf2*$^{fl/fl}$;*Vav-iCre* FL HSCs for at least 16 weeks after transplantation (**Figure 3.4.6 B**). HSCs lacking *Ythdf2* gave equal overall reconstitution compared to control HSCs. Furthermore, whilst *Ythdf2*-deficient HSCs were capable of differentiating into all lineages (**Figure 3.4.6 B**), a skewing was observed, whereby *Ythdf2*-deficient HSCs had enhanced early myeloid lineage reconstitution capacity and compromised T-cell lineage reconstitution capacity when compared to control HSCs (**Figure 3.4.6 B**).

After 16 weeks the mice were culled, and bone marrow was harvested for analysis (see sections **2.7** and **2.8**). Strikingly, *Ythdf2*-deficient HSCs displayed a significantly increased capacity to contribute to the bone marrow LSK, HSC, and HPC-2 compartments (**Figure 3.4.6 C**) of the recipient mice compared to control HSCs. When analysing contribution to BM differentiated cell compartments, there was no difference between recipients transplanted with *Ythdf2*-deficient or control HSCs (**Figure 3.4.6 D**). Based on these findings we concluded that *Ythdf2*-deficient FL

HSCs are at least as good as, and in some cases superior to, control FL HSCs in terms of reconstituting stem and progenitor cell compartments in transplanted mice, and are able to contribute to all lineages, albeit with a bias favouring myeloid over T cell differentiation.

Next, we carried out secondary transplantation. For this, we sorted CD45.2$^+$ LSK (Lin$^-$ Sca-1$^+$c-Kit$^+$) cells from the BM of culled primary recipient mice and transplanted them into irradiated recipient mice, as described in sections **2.14** and **2.15.1**, and as shown in **Figure 3.4.6 A**.

Ythdf2$^{fl/fl}$ and *Ythdf2*$^{fl/fl}$;*Vav-iCre* CD45.2$^+$ LSKs were sorted, and 2000 CD45.2$^+$ LSKs were transplanted via the tail vein into lethally irradiated (11 Gy) recipient mice (CD45.1$^+$ CD45.2$^+$), together with 200 000 unfractionated bone marrow support cells (CD45.1$^+$). Haematopoietic monitoring was carried out as described in section **2.15.3**, with CD45.1 and CD45.2 staining used to monitor engraftment and differentiation of study HSCs against the background of recipient and support bone marrow cells.

Serial peripheral blood analysis of primary transplanted mice showed no significant difference in the engraftment of *Ythdf2*$^{fl/fl}$ and *Ythdf2*$^{fl/fl}$;*Vav-iCre* HSCs for at least 16 weeks after transplantation (**Figure 3.4.6 E**). HSCs lacking *Ythdf2* gave equal overall reconstitution compared to control HSCs. Furthermore, whilst *Ythdf2*-deficient HSCs were capable of differentiating into all lineages, *Ythdf2*-deficient HSCs had enhanced myeloid lineage reconstitution capacity and compromised T-cell lineage reconstitution capacity when compared to control HSCs (**Figure 3.4.6 E**), replicating the pattern observed in primary recipients.

After 16 weeks the mice were culled, and bone marrow was harvested for analysis (see sections **2.7** and **2.8**). Strikingly, *Ythdf2*-deficient HSCs displayed a significantly increased capacity to contribute to the bone marrow LSK, HSC, MPP, HPC-1, HPC-2, LK, Lin$^-$ and Lin$^+$ compartments (**Figure 3.4.6 F**) and myeloid differentiated cell compartments (**Figure 3.4.6 G**) of the recipient mice compared to control HSCs. Based on these findings we concluded that *Ythdf2*-deficient FL HSCs are able to outcompete control HSCs and display enhanced myeloid reconstitution capacity in secondary recipients.

Finally, we carried out tertiary transplantation. For this, we harvested BM from secondary recipients and transplanted 4 million unfractionated and unsorted cells to lethally irradiated tertiary recipients, with no additional BM support. In an ideal world, this tertiary transplantation would have been carried out using a set number (2000-3000) of $CD45.2^+$ LSK cells together with $CD45.1^+$ BM support, however the level of engraftment in the secondary recipients was too low for this to be feasible. To standardise the transplanted BM as much as possible, BM with similar levels of $CD45.2^+$ chimerism was selected for transplantation.

Serial peripheral blood analysis of tertiary transplanted mice showed a significantly higher engraftment in recipients of *Ythdf2*$^{fl/fl}$;*Vav-iCre* HSCs compared with control *Ythdf2*$^{fl/fl}$ HSCs for at least 16 weeks following transplantation (**Figure 3.4.6 H**). The superior reconstitution capacity of *Ythdf2*$^{fl/fl}$;*Vav-iCre* HSCs compared with *Ythdf2*$^{fl/fl}$ HSCs was also apparent within all differentiated cell lineages (granulocytic, monocytic, B lymphocyte), with the exception of T lymphocytes (**Figure 3.4.6 H**), once again mirroring the pattern in primary and secondary transplantation experiments. However, when the tertiary recipients were culled at 16 weeks, BM analysis revealed a very low donor derived cell chimerism at the level of the BM, with $CD45.2^+$ cells comprising less than 1% of the total population in all but one mouse (**Figure 3.4.6 I**). Further BM analyses were therefore not carried out.

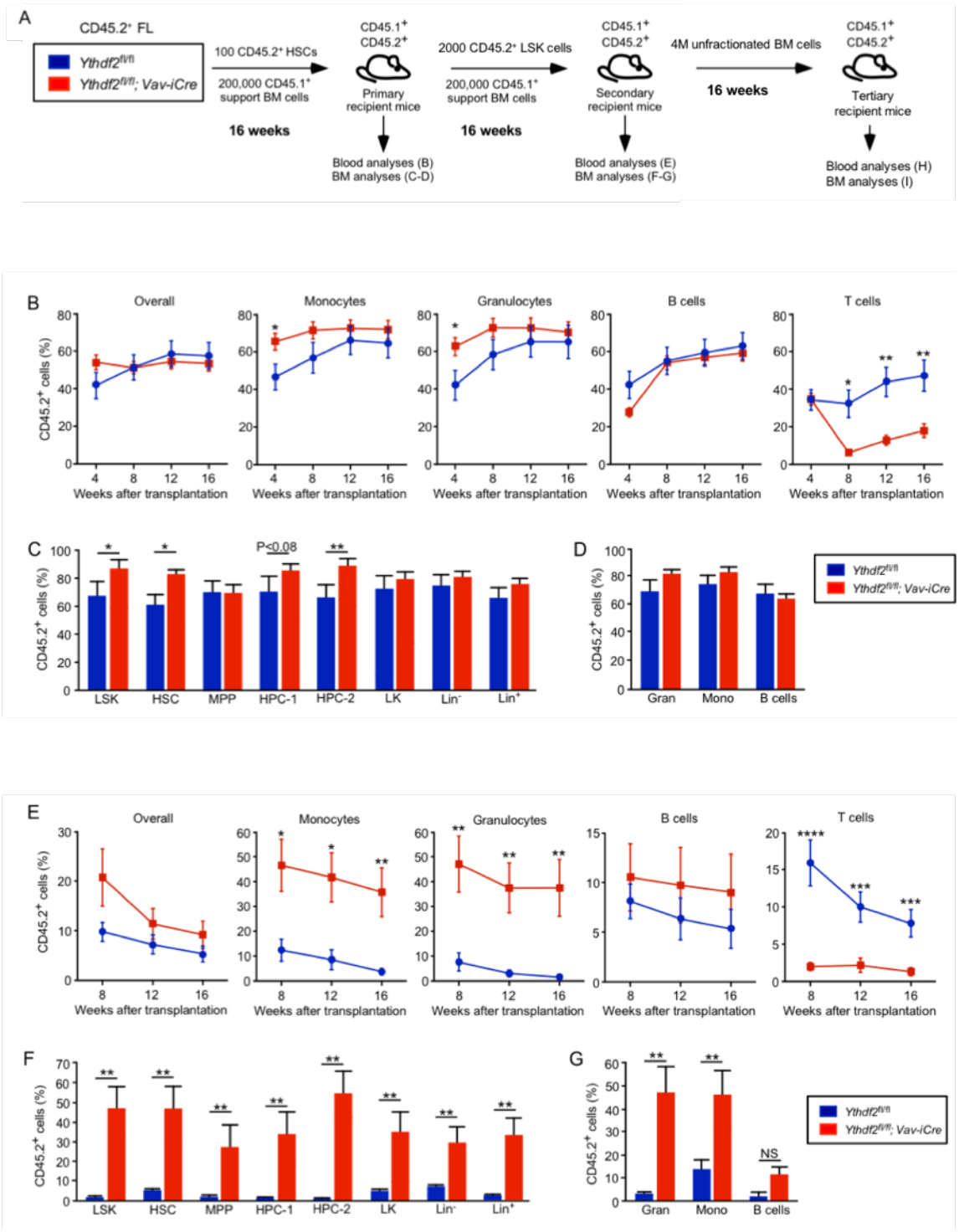
A
CD45.2+ FL
Ythdf2fl/fl
Ythdf2fl/fl; Vav-iCre
100 CD45.2+ HSCs
200,000 CD45.1+ support BM cells
16 weeks
CD45.1+ CD45.2+
Primary recipient mice
Blood analyses (B)
BM analyses (C-D)
2000 CD45.2+ LSK cells
200,000 CD45.1+ support BM cells
16 weeks
CD45.1+ CD45.2+
Secondary recipient mice
Blood analyses (E)
BM analyses (F-G)
4M unfractionated BM cells
16 weeks
CD45.1+ CD45.2+
Tertiary recipient mice
Blood analyses (H)
BM analyses (I)
B
Overall
Monocytes
Granulocytes
B cells
T cells
CD45.2+ cells (%)
Weeks after transplantation
C
CD45.2+ cells (%)
P<0.08
LSK
HSC
MPP
HPC-1
HPC-2
LK
Lin-
Lin+
D
CD45.2+ cells (%)
Gran
Mono
B cells
Ythdf2fl/fl
Ythdf2fl/fl; Vav-iCre
E
Overall
Monocytes
Granulocytes
B cells
T cells
CD45.2+ cells (%)
Weeks after transplantation
F
CD45.2+ cells (%)
LSK
HSC
MPP
HPC-1
HPC-2
LK
Lin-
Lin+
G
CD45.2+ cells (%)
NS
Gran
Mono
B cells
Ythdf2fl/fl
Ythdf2fl/fl; Vav-iCre

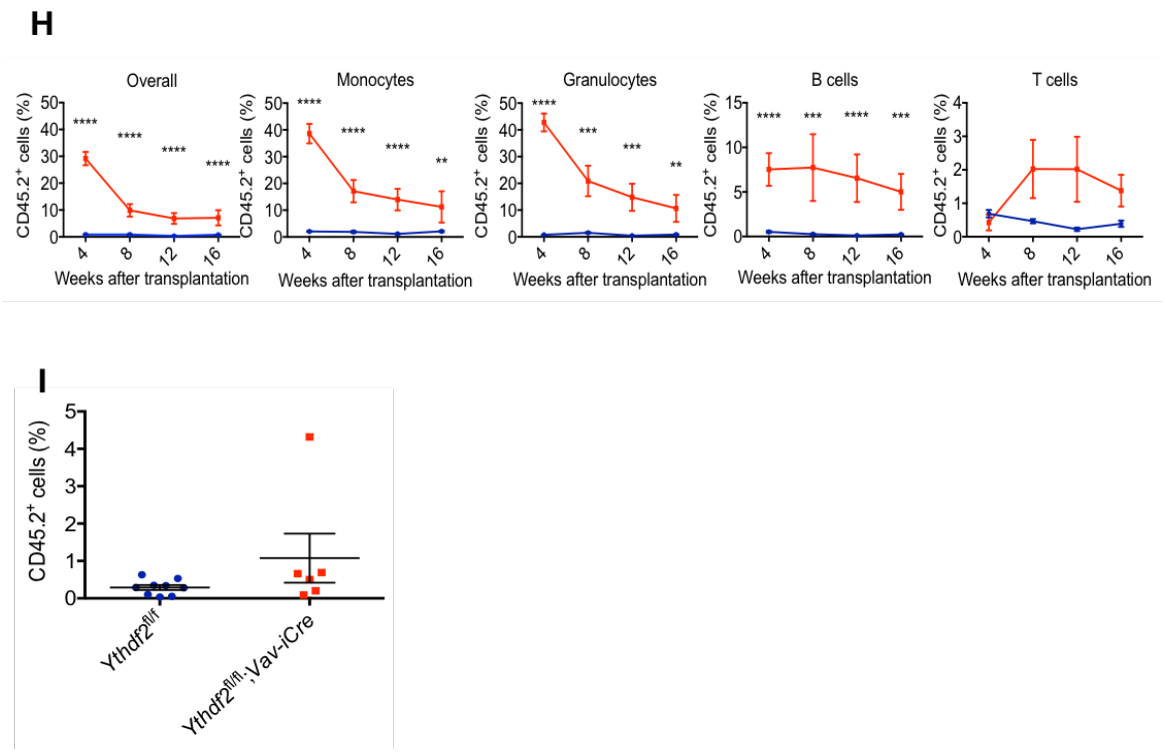

Figure 3.4.6 Ablation of *Ythdf2* enhances the function of FL HSCs. (**A**) Schematic of primary, secondary and tertiary transplantation of HSCs from FL. 100 FL HSCs (from *Ythdf2*$^{fl/fl}$ and *Ythdf2*$^{fl/fl}$*;Vav-iCre* embryos) were transplanted into lethally irradiated 8-10 week old syngeneic CD45.1$^+$/CD45.2$^+$ recipient mice (*n* = 18-27 mice per genotype) together with 2 x 10^5 CD45.1$^+$ competitor BM cells. After 16 weeks primary recipient mice were culled, and 2,000 CD45.2$^+$ BM LSK cells from primary recipients were transplanted into lethally irradiated 8-10-week-old syngeneic CD45.1$^+$/CD45.2$^+$ secondary recipient mice (*n* = 10 mice per genotype) together with 2 x 10^5 CD45.1$^+$ competitor BM cells. After a further 16 weeks, secondary recipient mice were culled, and 4 million (4M) unfractionated BM cells were transplanted into lethally irradiated 8-10-week-old syngeneic CD45.1$^+$/CD45.2$^+$ tertiary recipient mice (*n* = 10 mice per genotype). Peripheral blood was obtained on a monthly basis from all recipient mice up to 4 months, at which stage recipients were culled for BM analysis. (**B**) Percentage of CD45.2$^+$ cells overall in the peripheral blood (PB) and in the monocyte, granulocyte, B cell and T cell compartments of the PB of primary recipients. Data are mean ± s.e.m. *, P<0.05; **, P<0.01, Mann-Whitney U test. (**C-D**) Percentage of CD45.2$^+$ cells in the LSK, HSC, MPP, HPC-1, HPC-2, LK, Lin$^-$ and Lin$^+$ (C) and differentiated (D) cell compartments in the BM of primary recipient mice. Data are mean ± s.e.m. *, P<0.05; **, P<0.01, Mann-Whitney U test. (**E**) Percentage of

$CD45.2^+$ cells overall in the peripheral blood (PB) and in the monocyte, granulocyte, B cell and T cell compartments of the PB of secondary recipients. Data are mean ± s.e.m. *, P<0.05; **, P<0.01; ****, P < 0.0001, Mann-Whitney U test. (**F-G**) Percentage of $CD45.2^+$ cells in the LSK, HSC, MPP, HPC-1, HPC-2, LK, Lin^- and Lin^+ (F) and differentiated (G) cell compartments in the BM of secondary recipient mice. Data are mean ± s.e.m. *, P<0.05; **, P<0.01, Mann-Whitney U test. (**H**) Percentage of $CD45.2^+$ cells overall in the peripheral blood (PB) and in the monocyte, granulocyte, B cell and T cell compartments of the PB of tertiary recipients. Data are mean ± s.e.m. *, P<0.05; **, P<0.01; ***, P < 0.001; ****, P < 0.0001, Mann-Whitney U test. (**I**) Percentage of $CD45.2^+$ cells overall in the BM of tertiary recipients. Data are mean ± s.e.m.

3.4.7 Ablation of *Ythdf2* enhances HSC function – BM HSC transplantation

Next, we sought to corroborate the findings obtained using FL HSCs with BM HSCs. We therefore carried out primary and secondary transplantation assays, as shown in schematic **Figure 3.4.7 A**.

For the primary transplantation, *Ythdf2*$^{fl/fl}$ and *Ythdf2*$^{fl/fl}$;*Vav-iCre* $LSKCD48^-CD150^+$ HSCs were sorted, and 200 $CD45.2^+$ HSCs were transplanted via the tail vein into lethally irradiated (11 Gy) recipient mice ($CD45.1^+$ $CD45.2^+$), together with 200 000 unfractionated bone marrow support cells ($CD45.1^+$) (**Figure 3.4.7 A**). Monitoring was carried out as described previously.

Serial peripheral blood analysis of primary transplanted mice showed a slower initial engraftment of *Ythdf2*-deficient HSCs (**Figure 3.4.7 B week 2**), but thereafter no significant difference in the engraftment of *Ythdf2*$^{fl/fl}$ and *Ythdf2*$^{fl/fl}$;*Vav-iCre* FL HSCs for at least 18 weeks after transplantation (**Figure 3.4.7 B**). Furthermore, whilst *Ythdf2*-deficient HSCs were capable of differentiating into all lineages (**Figure 3.4.7 B**), a skewing was observed, whereby *Ythdf2*-deficient HSCs had enhanced myeloid lineage reconstitution capacity and compromised T-cell lineage reconstitution capacity when compared to control HSCs (**Figure 3.4.7 B**).

After 18 weeks the mice were culled, and bone marrow and spleens were harvested for analysis (see sections **2.7** and **2.8**). Strikingly, *Ythdf2*-deficient HSCs displayed a significantly increased capacity to contribute to the bone marrow LSK, HSC, MPP, HPC-1, HPC-2, LK and Lin^+ compartments (**Figure 3.4.7 C**) of the recipient mice

compared to control HSCs. When analysing contribution to BM differentiated cell compartments, *Ythdf2*-deficient HSCs had enhanced myeloerythroid lineage reconstitution capacity and compromised T-cell lineage reconstitution capacity when compared to control HSCs (**Figure 3.4.7 D**). Based on these findings we concluded that *Ythdf2*-deficient BM HSCs are able to outcompete control HSCs and display enhanced myeloid reconstitution capacity in primary recipients. The findings mirrored those obtained using FL HSCs.

To further characterise the reconstitution capacity of *Ythdf2*$^{fl/fl}$ and *Ythdf2*$^{fl/fl}$;*Vav-iCre* BM HSCs we examined the contribution of individual HSPC compartments to the engrafted CD45.2$^+$ cell population as a whole (**Figure 3.4.7 E**). The results showed that *Ythdf2*-deficient LSK cells formed a greater proportion of CD45.2$^+$ cells compared to control LSK cells, which was the result of greater HPC-1 and HPC-2 contributions to the CD45.2$^+$ cell population as a whole for *Ythdf2*-deficient cells.

We also looked at the contribution of CD45.2$^+$ cells to the differentiated lineages in the spleen of primary recipients (**Figure 3.4.7 F**). This revealed a significant reduction in the donor derived chimerism within the CD8$^+$ T cell population for recipients of *Ythdf2*-deficient cells (**Figure 3.4.7 F**). No other significant differences were observed in the spleens of *Ythdf2*$^{fl/fl}$ and *Ythdf2*$^{fl/fl}$;*Vav-iCre* recipients.

Next we carried out secondary transplantation. For this, we sorted CD45.2$^+$ LSK (Lin$^-$ Sca-1$^+$c-Kit$^+$) cells from the BM of culled primary recipient mice and transplanted them into irradiated recipient mice, as described in sections **2.14** and **2.15.1**, and as shown in **Figure 3.4.7 A**.

Ythdf2$^{fl/fl}$ and *Ythdf2*$^{fl/fl}$;*Vav-iCre* CD45.2$^+$ LSKs were sorted, and 3000 CD45.2$^+$ LSKs were transplanted via the tail vein into irradiated recipient mice (CD45.1$^+$ CD45.2$^+$), together with 200 000 unfractionated bone marrow support cells (CD45.1$^+$). However, at the time this experiment was carried out, a reduced irradiation dose had been implemented (two doses of 4.6 Gy four hours apart, as opposed to two doses of 5.5 Gy four hours apart) in agreement with the Home Office, as an interim response to several unexplained post irradiation mouse deaths in the unit. Unfortunately, the irradiation provided was therefore sub-lethal, resulting in reduced engraftment of transplanted cells.

As a result, serial peripheral blood analysis of these secondary transplanted mice showed limited overall and lineage specific engraftment initially, and a collapse to negligible levels over the 16 weeks of observation (**Figure 3.4.7 G).** No significant difference was observed for mice transplanted with *Ythdf2*$^{fl/fl}$ or *Ythdf2*$^{fl/fl}$;*Vav-iCre* LSKs. After 16 weeks the transplanted mice were culled and bone marrow was analysed, as described previously. In accordance with peripheral blood data, bone marrow engraftment, and contribution to HSPC compartments, was low, and there were no significant differences between *Ythdf2*-deficient and control cells (**Figures 3.4.7 H-I**).

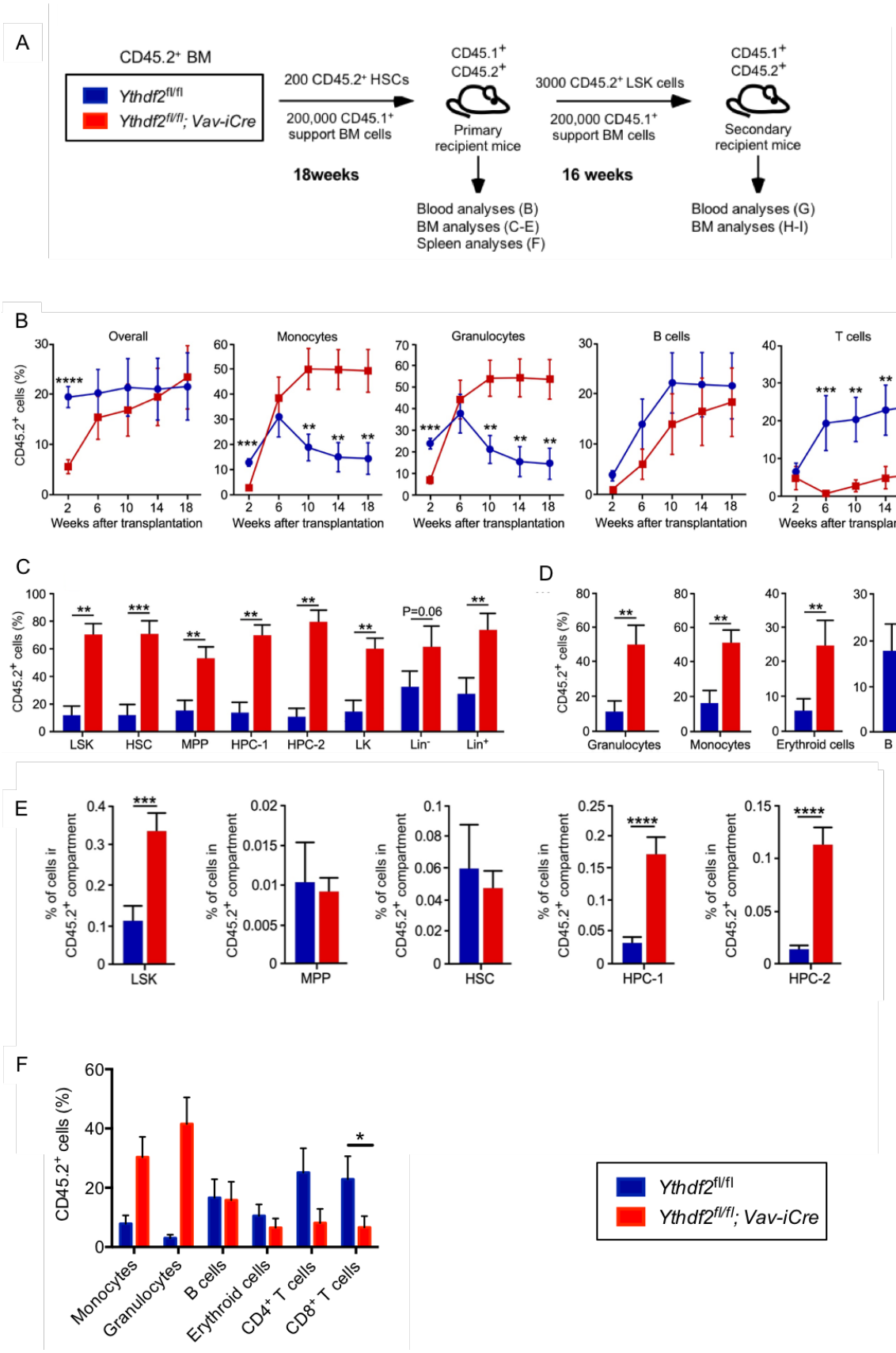
A
CD45.2+ BM
Ythdf2fl/fl
Ythdf2fl/fl; Vav-iCre
200 CD45.2+ HSCs
200,000 CD45.1+ support BM cells
18weeks
CD45.1+ CD45.2+
Primary recipient mice
Blood analyses (B)
BM analyses (C-E)
Spleen analyses (F)
3000 CD45.2+ LSK cells
200,000 CD45.1+ support BM cells
16 weeks
CD45.1+ CD45.2+
Secondary recipient mice
Blood analyses (G)
BM analyses (H-I)
B
Overall
Monocytes
Granulocytes
B cells
T cells
CD45.2+ cells (%)
Weeks after transplantation
C
D
LSK
HSC
MPP
HPC-1
HPC-2
LK
Lin-
Lin+
P=0.06
Granulocytes
Monocytes
Erythroid cells
B cells
E
% of cells ir CD45.2+ compartment
% of cells in CD45.2+ compartment
LSK
MPP
HSC
HPC-1
HPC-2
F
CD45.2+ cells (%)
Monocytes
Granulocytes
B cells
Erythroid cells
CD4+ T cells
CD8+ T cells
Ythdf2fl/fl
Ythdf2fl/fl; Vav-iCre

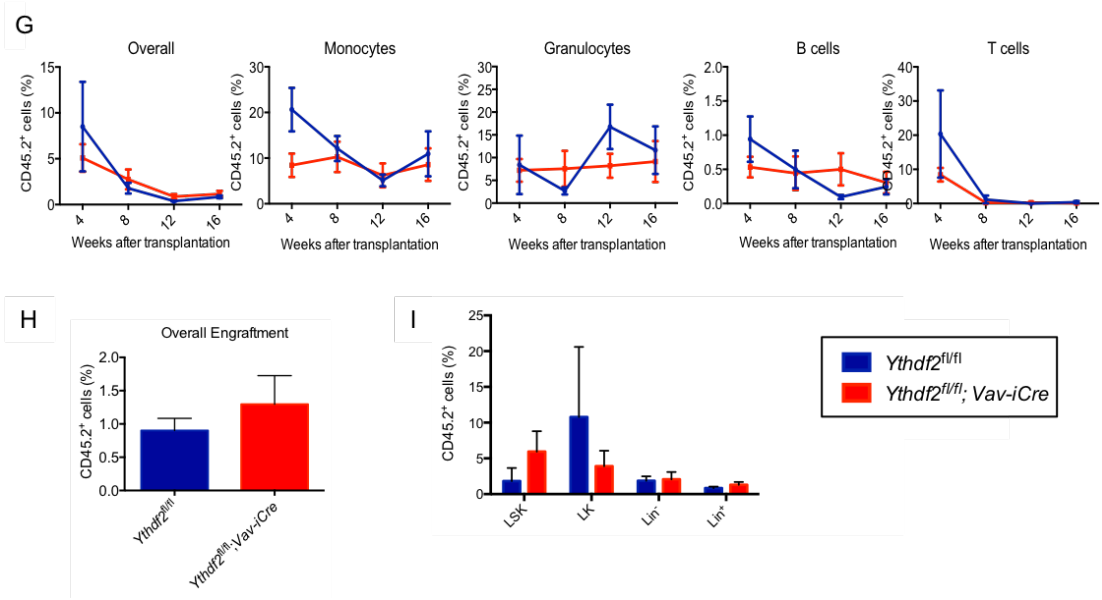

Figure 3.4.7 Ablation of *Ythdf2* enhances the function of BM HSCs. (**A**) Schematic of primary and secondary transplantation of HSCs from BM. 200 BM HSCs (from *Ythdf2*$^{fl/fl}$ and *Ythdf2*$^{fl/fl}$*;Vav-iCre* mice) were transplanted into lethally irradiated 8-10 week old syngeneic CD45.1$^+$/CD45.2$^+$ recipient mice (*n* = 11-13 mice per genotype) together with 2 x 10^5 CD45.1$^+$ competitor BM cells. After 18 weeks primary recipient mice were culled, and 3,000 CD45.2$^+$ BM LSK cells from primary recipients were transplanted into lethally irradiated 8-10-week-old syngeneic CD45.1$^+$/CD45.2$^+$ secondary recipient mice (*n* = 6-14 mice per genotype) together with 2 x 10^5 CD45.1$^+$ competitor BM cells. After a further 16 weeks, secondary recipient mice were culled. Peripheral blood was obtained on a monthly basis from all recipient mice up to 4 months, at which stage recipients were culled for BM analysis. (**B**) Percentage of CD45.2$^+$ cells overall in the peripheral blood (PB) and in the monocyte, granulocyte, B cell and T cell compartments of the PB of primary recipients. Data are mean ± s.e.m. *, P<0.05; **, P<0.01, Mann-Whitney U test. (**C-D**) Percentage of CD45.2$^+$ cells in the LSK, HSC, MPP, HPC-1, HPC-2, LK, Lin$^-$ and Lin$^+$ (C) and differentiated (D) cell compartments in the BM of primary recipient mice. Data are mean ± s.e.m. *, P<0.05; **, P<0.01; ***, P < 0.001; ****, P < 0.0001, Mann-Whitney U test. (**E**) Percentage of LSK, MPP, HSC, HPC-1 and HPC-2 cells within the CD45.2$^+$ cell compartment of BM of primary recipient mice. Data are mean ± s.e.m. ***, P < 0.001; ****, P < 0.0001, Mann-Whitney U test. (**F**) Percentage of CD45.2$^+$ cells overall in the monocyte, granulocyte, B lymphocyte, erythroid, CD4$^+$ T lymphocyte and CD8$^+$ T lymphocyte compartments of the spleen of primary recipients. Data are mean ± s.e.m. *, P<0.05,

Mann-Whitney U test. (**G**) Percentage of CD45.2$^+$ cells overall in the peripheral blood (PB) and in the monocyte, granulocyte, B cell and T cell compartments of the PB of secondary recipients. Data are mean ± s.e.m. (**H**) Percentage of CD45.2$^+$ cells overall in the BM of secondary recipients. Data are mean ± s.e.m. (**I**) Percentage of CD45.2$^+$ cells in the LSK, LK, Lin$^-$ and Lin$^+$ in the BM of secondary recipient mice. Data are mean ± s.e.m.

3.5 Discussion

The results presented in this chapter demonstrate the important role that YTHDF2 plays in normal haematopoiesis. Using the *Ythdf2*$^{fl/fl}$ mouse, in which GFP fluorescence reports YTHDF2 protein levels, we first showed that YTHDF2 is highly expressed by cells at the top of the haematopoietic differentiation hierarchy, suggesting it may play a role in their maintenance. Next, we used *Ythdf2*$^{fl/fl}$; *Vav-iCre* conditional knock out mice to show that haematopoiesis-specific *Ythdf2* deletion results in an expansion of HSPCs in both FL and adult BM, and a reduction in peripheral CD8$^+$ T cells in adult mice. Finally, we used serial transplantation experiments of both FL and adult BM HSCs to demonstrate that *Ythdf2*-deficient HSCs engraft at least as well, if not better than, control HSCs, and retain multilineage differentiation capacity, albeit with a bias towards myeloid lineages and away from T lymphocyte cells.

Our findings correlate well with previous publications about the importance of m^{6}A in haematopoiesis. In particular, two recent studies have also reported an expansion of HSCs following *Ythdf2* deletion in the mouse (Li, Qian et al. 2018, Wang, Zuo et al. 2018). In both cases, the authors used an *Mx1-Cre* inducible mouse model to acutely delete *Ythdf2* through pIpC administration, and subsequently observed increases in LT-HSCs and ST-HSCs. However, in both cases there was no lineage skewing, either in the baseline state or following BM transplantation. In contrast, we observed reduced peripheral CD8$^+$ T lymphocytes in *Ythdf2*-deficient mice and a bias towards myeloid differentiation and away from T cell differentiation, by transplanted *Ythdf2*-deficient HSCs. The cause of this discrepancy is unclear, but may reflect the differences in methodology between the three groups.

Both Li et al. and Wang et al. used a *Mx1-Cre* inducible mouse model to acutely delete *Ythdf2* through pIpC administration, followed by BM analysis (4 weeks later in the case of Li et al., unspecified in the case of Wang et al.) (Li, Qian et al. 2018, Wang,

Zuo et al. 2018). In contrast, we used *Vav-iCre* mice, in which *Ythdf2* is deleted specifically from the haematopoietic system shortly after the emergence of definitive HSCs (de Boer, Williams et al. 2003), and analysed adult mice at 8-10 weeks of age. Given that the *Mx-1 Cre* is activated in many tissues (including the liver, heart, kidney and spleen) upon pIpC treatment (Kuhn, Schwenk et al. 1995), it is possible that *Ythdf2*-deletion in other cell types, for example the stromal cells of the haematopoietic niche (Morrison and Scadden 2014), may have influenced the phenotype observed by Li et al. and Wang et al. Wang et al. did also report increased LT-HSC in *Ythdf2*$^{fl/fl}$; *Vav-iCre* mice, but no mention of multilineage differentiation, or BM transplantation was made in that case.

It is also interesting to note that when Li et al. analysed their mice 5 months after pIpC administration, they detected only a modest increase in LT-HSCs, although they reported persistently greater HSC function in *Ythdf2*-deleted cells (Li, Qian et al. 2018). They did not comment on the presence or absence of lineage skewing 5 months post pIpC.

In agreement with our findings, both Li et al. and Wang et al. reported increased engraftment of *Ythdf2*-deficient cells in BM transplantation experiments, albeit without lineage skewing. Once again however, there were variations in methodology between the groups. Given the differences in baseline HSC numbers between *Ythdf2*$^{fl/fl}$ and *Ythdf2*$^{fl/fl}$;*Vav-iCre* mice, we elected to sort HSCs for primary transplantation (100 FL HSCs, 200 BM HSCs), in order to compare *Ythdf2*$^{fl/fl}$ and *Ythdf2*$^{fl/fl}$;*Vav-iCre* HSC function in an objective manner. In contrast, Li et al. transplanted unfractionated total bone marrow in both primary and secondary transplantations (Li, Qian et al. 2018), whilst Wang also used unfractionated total bone marrow for secondary transplantations (Wang, Zuo et al. 2018).

Although Li et al. did not report any lineage skewing following acute *Ythdf2* deletion, other publications do suggest that m^{6}A plays a role in haematopoietic multilineage differentiation. An increase in myeloid differentiation has been reported following shRNA-mediated depletion of *METTL3* (Vu, Pickering et al. 2017) or *METTL14* (Weng, Huang et al. 2018) in human HSPCs. Furthermore, multiple papers suggest that m^{6}A impacts upon the homeostasis of peripheral white blood cell subsets. Deletion of *Mettl3* has been shown to maintain CD4$^+$ T cells in a naïve state (Li, Tong et al. 2017), and to inhibit the suppressor capacity of FoxP3$^+$ T cells (Tong, Cao et al.

2018), whilst deletion of *Ythdf1* from dendritic cells improves their capacity for $CD8^+$ T cell priming (Han, Liu et al. 2019).

Deletion of *Mettl3* in $CD4^+$ T cells was reported to control T cell homeostasis by targeting the IL-7/STAT5/SOCS pathways (Li, Tong et al. 2017). This is interesting in the context of our own observations, since it is known that Interleukin-7 (IL-7) also mediates the homeostasis of naïve and memory $CD8^+$ T cells (Schluns, Kieper et al. 2000). It is therefore possible that the decreased peripheral $CD8^+$ T cells we observe in *Ythdf2*$^{fl/fl}$;*Vav-iCre* mice may also reflect alterations in IL-7 levels brought about by defective m^6A dependent processes.

Either way, it is clear that this area deserves further work, particularly when the caveats of our immune cell analyses are considered. For example, the *Ythdf2*$^{fl/fl}$;*Vav-iCre* and *Ythdf2*$^{fl/fl}$ mice were analysed at 8-10 weeks of age. It is known that the cellularity of the mouse thymus expands rapidly after birth, reaching a plateau at 4-6 weeks of age, after which the thymus starts to involute (Gray, Seach et al. 2006). For this reason, studies of the mouse thymus generally use 4-6-week-old mice (Bornstein, Nevo et al. 2018). Furthermore, in our experience thymic involution and surrounding fat deposition makes accurate harvesting of the intact thymus challenging in older mice, whilst lower thymic cell counts potentially limit the power of any subsequent conclusions. Finally, CD4 and CD8 antibody staining is only a small component of complete immunophenotypic thymic evaluation, which could also include staining for CD25, CD44, B220, TCR β, CD5 and CD69 (Biosciences and Jose 2012). In summary therefore, the role of *Ythdf2* in T lymphocyte biology is an intruiging subject and warrants further study.

In this chapter, haematopoietic evaluation of both FL and adult BM is presented. The repopulation potential of foetal liver HSCs in mice has been reported to exceed that of their adult BM counterparts (Rebel, Miller et al. 1996). Consistent with this, we observed a greater engraftment of transplanted FL HSCs (53-57% at 4 months) compared to BM HSCs (21-23% at 4 months) in primary recipient mice. Nevertheless, in contrast to some studies, which have reported opposing results in FL and adult BM studies (Kim, Saunders et al. 2007), the general pattern of our results was very similar i.e. increased number and function of HSCs in *Ythdf2*-deficient embryos/adult mice, with a myeloid bias upon transplantation.

In addition to the increase in HSCs we observed in *Ythdf2*-deficient mice, there were also increases in the HPC-1 and HPC-2 compartments. In contrast, MPP cells were either unchanged in number (BM), or decreased (FL) in number. Li et al. also reported increases in LT-HSCs and ST-HSCs, but no change in MPPs, in *Ythdf2*-deficient mice (Li, Qian et al. 2018). The reason for this is unclear, but could reflect a blockage at the HPC stage of differentiation.

HSC transplantation of irradiated primary recipient mice resulted in an equal overall engraftment of *Ythdf2*-deficient cells compared to control cells, with the exception of week 2 for adult BM, when engraftment of *Ythdf2*-deficient HSC engraftment lagged behind that of control HSC engraftment (**Figure 3.4.7 B**). Reduced early engraftment might suggest a homing defect (Szilvassy, Meyerrose et al. 2001, Lapidot, Dar et al. 2005, Liang, Van Zant et al. 2005). However, both Li et al. and Weng et al. found no evidence for homing defects in *Ythdf2*-deficient HSCs (Li, Qian et al. 2018, Wang, Zuo et al. 2018). Furthermore, multiple publications suggest that HSCs with homing defects fail to achieve efficient long-term reconstitution (Ishikawa, Chang et al. 2013, Ruppert, Moser et al. 2015). Given that we demonstrated increased long-term reconstitution of the HSC compartment by *Ythdf2*-deficient HSCs, significant homing effects are considered unlikely.

To further study the effects of *Ythdf2* deletion, additional work is being carried out by our group, including acute deletion in the *Mx1-Cre* model and 5-FU injections to explore the ability of *Ythdf2*-deficient cells to respond to stress. In addition, *Ythdf2*$^{fl/fl}$ and *Ythdf2*$^{fl/fl}$;*Vav-iCre* mice are being aged, in order to evaluate the effect of long term *Ythdf2* deficiency on haematopoiesis and the potential for malignant transformation.

In conclusion, the work presented in this chapter shows that deletion of *Ythdf2* results in an expansion of HSCs which retain the capacity for multilineage reconstitution in serial transplantation assays. This suggests that targeting of YTHDF2, for example through the use of small molecule inhibitors (currently in production, personal communication), may provide a means by which to expand human HSCs *in vitro*, and potentially also *in vivo*, for therapeutic purposes. HSCT is regarded as the optimal treatment for a variety of diseases, including leukaemia, autoimmunity, bone marrow failure syndromes, and also in gene therapy settings (Copelan 2006) but is limited by a shortage of HSCs (see section **1.1.8** for a discussion of current expansion

strategies). In this context, our findings suggest that pharmacological targeting of YTHDF2 may be an exciting future therapeutic strategy for HSCT.

Chapter 4: The role of YTHDF2 in malignant haematopoiesis

4.1 Introduction

4.1.1 The role of m^{6}A in acute myeloid leukaemia

Having characterised the important role of YTHDF2 in normal haematopoiesis, namely in regulating HSC maintenance and myeloid differentiation, we next sought to establish the role of YTHDF2 in the context of malignant haematopoiesis, specifically acute myeloid leukaemia (AML).

In the last few years, it has become clear that m^{6}A plays a critical role in AML. However, the studies to date have focused only on m^{6}A writers or erasers, whilst the role of m^{6}A writers, YTHDF2 included, has not yet been investigated (**Figure 4.1.1** and **Table 1.3.5**).

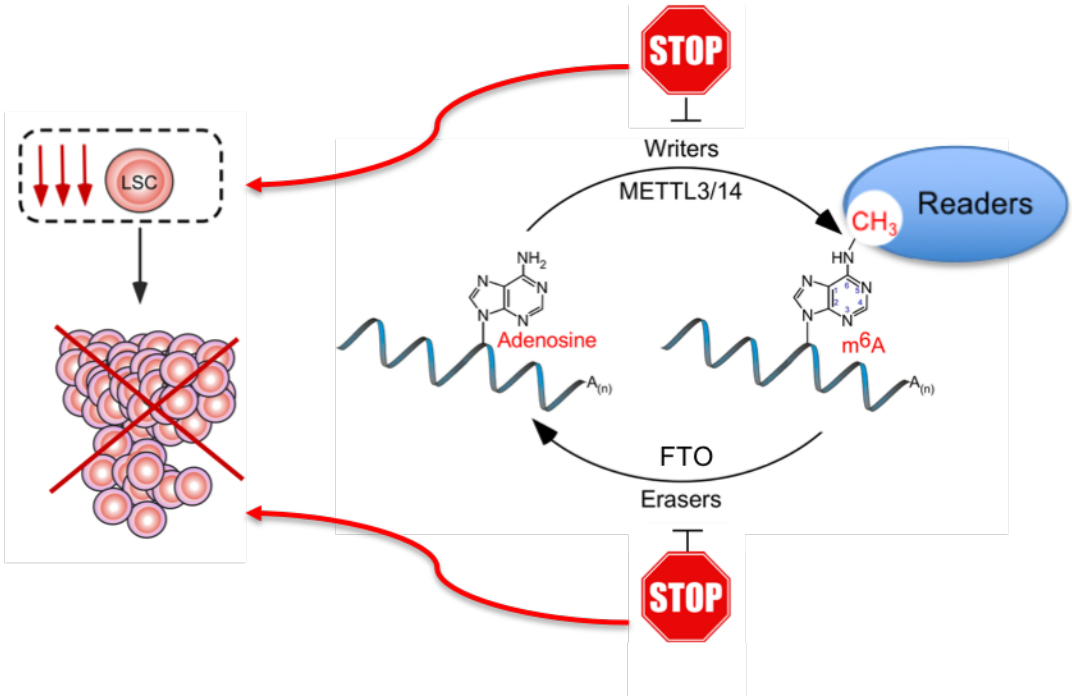

Figure 4.1.1 The role of m^{6}A regulators in AML. Studies have revealed an essential requirement for the m^{6}A writers METTL3 and METTL14, and for the m^{6}A eraser FTO in AML (Barbieri, Tzelepis et al. 2017, Li, Weng et al. 2017, Vu, Pickering et al. 2017,

Su, Dong et al. 2018, Weng, Huang et al. 2018, Yao, Sang et al. 2018). Inhibition of these m^6A regulators inhibits LSCs and AML. However, the role of m^6A readers, including YTHDF2, remains unknown.

Several studies have shown an essential requirement for m^6A writers in acute myeloid leukaemia. According to the Caner Genome Atlas (TCGA; https://cancergenome.nih.gov/) members of the m^6A writer complex, particularly *METTL3*, and *RBM15*, are highly expressed in AML compared to other cancer types (Cerami, Gao et al. 2012, Gao, Aksoy et al. 2013). High expression of *METTL3* and *METTL14* in both human and mouse AML cells has also been reported in several focused studies (Barbieri, Tzelepis et al. 2017, Vu, Pickering et al. 2017, Sorci, Ianniello et al. 2018, Weng, Huang et al. 2018). Furthermore, a genome wide CRISPR based screen to identify genes essential for cell survival using 14 human AML cell lines ranked all members of the writer complex, including *METTL3*, *METTL14*, *WTAP* and *KIAA1429*, amongst the top 10% in the list of essential genes (Vu, Pickering et al. 2017, Wang, Yu et al. 2017).

Barbieri et al. reported similar findings in mouse AML cells (Barbieri, Tzelepis et al. 2017). This study used two distinct genetic screens, both based on the CRISPR Cas9 system (first a genome wide screen, second a focused screen with a custom domain-focused guide RNA library) to identify *Mettl3* as an essential gene for growth of AML cells. Results of both the CRISPR Cas9 screen and shRNA knockdown of *Mettl3* showed that downregulation of *Mettl3* causes cell cycle arrest and differentiation of AML cells (increased expression of CD11b), and failure to establish leukaemia in immunodeficient mice. They went on to show that METTL3, independently of METTL14, associates with chromatin, and localises to the transcriptional start site (TSS) of active genes (most of which have CEBPZ protein present at the TSS, which is required for METTL3 recruitment). They reported that promoter bound METTL3 induces m^6A modification in the coding region of the associated mRNA and enhances its translation by relieving ribosome stalling. In contrast, depletion of *Mettl3* had no effect on transcription of METTL3 bound genes (Barbieri, Tzelepis et al. 2017).

The role of METTL3 has also been reported in human AML cells (Vu, Pickering et al. 2017). Vu et al. showed that METTL3 mRNA and protein are expressed more abundantly in human AML cells versus healthy HSPCs or other tumour types. They also showed that shRNA mediated depletion of *METTL3* in human AML cell lines

leads to apoptosis and differentiation, and delays leukaemogenesis *in vivo*. Using single-nucleotide-resolution mapping of m^{6}A coupled with ribosome profiling, they went on to show that m^{6}A promotes the translation of *c-MYC, BCL2* and *PTEN* mRNAs in the MOLM13 AML cell line. They reported that loss of *METTL3* increases phosphorylated AKT, thereby contributing to differentiation (Vu, Pickering et al. 2017).

METTL14 has also been shown to promote leukaemogenesis via mRNA m^{6}A modification (Weng, Huang et al. 2018). Weng et al. reported impaired colony formation *in vitro* and delayed leukaemia initiation *in vivo* by *Mettl14*-deficient cells (using a murine *Mll-AF9* model). Similar findings were observed in secondary recipients, suggesting that METTL14 is required for both initiation and maintenance of AML. The authors went on to show that *METTL14* depletion also impairs survival and growth of human AML cells (*in vitro* and *in vivo* xenotransplantation assays), and promotes ATRA induced myeloid cell differentiation. Using a combination of RNA-Seq and m^{6}A-Seq, the authors identified METTL14 targets (hypomethylated), including *MYB* and *MYC*. Notably, in the majority of targets, mRNA levels were downregulated upon *METTL14* knockdown. They went on to show that *METTL14* knockdown regulates *MYB* and *MYC* expression by modulating mRNA stability (experiments performed with the transcription inhibitor actinomycin D) and mRNA translation (polysome profiling experiments). Since the authors were unable to identify a consistent pattern for YTHDF genes during drug induced differentiation of AML cells, and knockdown of *YTHDF* genes had no effect on *MYB* and *MYC*, the authors concluded that the effect of METTL14 on mRNA stability and translation of its target genes was unlikely to be mediated by YTHDF proteins (Weng, Huang et al. 2018).

In addition to METTL3 and METTL14, there is evidence that other components of the m^{6}A writer complex also play a role in AML, specifically WTAP and RBM15. WTAP was first identified as an interactor of the Wilms Tumour-1 (WT-1) protein (Little, Hastie et al. 2000). A subsequent study showed that *WTA*P levels are increased in human AML samples when compared to mononuclear blood cells from healthy patients, with elevated *WTAP* expression reported in 32% of newly diagnosed AML patients. Knockdown of *WTAP* reduced proliferation and clonogenic survival in AML cell lines and primary human AML samples *in vitro*, and leukaemogenesis *in vivo* (tumour xenograft experiments in nude mice). In addition, knockdown of *WTAP* also promoted phorbol 12-myristate 13-acetate (PMA)-induced myeloid differentiation

(Bansal, Yihua et al. 2014). More recent work by Sorci et al. showed that *METTL3* levels are essential for WTAP protein homeostasis, with both knockdown and overexpression of *METTL3* resulting in elevated WTAP protein levels (Sorci, Ianniello et al. 2018). Importantly, the authors also showed that upregulation of *WTAP* in the absence of *METTL3* is not sufficient to promote cell proliferation, leading them to conclude that the oncogenic function of WTAP is strictly connected to a functional m^6A methylation complex (Sorci, Ianniello et al. 2018).

RBM15, another component of the m^6A writer complex, has also been implicated in acute myeloid leukaemia. Chromosomal translocations of *RMB15* with the *MAL* gene have been shown to mediate acute megakaryoblastic leukaemia (Gruber and Downing 2015). RBM15 is known to play important roles in controlling HSC quiescence and differentiation of megakaryoblastic leukaemic cells by regulating the splicing of key haematopoietic differentiation genes, including *GATA1*, *RUNX1*, *TAL1* and *c-MPL* (Zhang, Tran et al. 2015). Given that RBM15 is involved in m^6A formation in the transcriptome, the oncogenic effects of *RBM15* overexpression and *RBM15-MAL* translocation might reflect abnormal m^6A formation.

In contrast to m^6A writers, whose requirement in AML is undisputed, the role of m^6A demethylases is currently unclear. An initial study by Li et al. in 2017 reported that FTO plays an oncogenic role in AML as an m^6A demethylase (Li, Weng et al. 2017). These authors showed that *FTO* is highly expressed in AML, particularly in MLL-rearranged AML, and reported that oncogenic transformation of murine bone marrow cells increases the levels of FTO, both at the RNA and protein level. Through *in vitro* overexpression and knockdown studies, they showed that FTO promoted cell transformation and proliferation and reduced apoptosis, whilst forced expression of *FTO in vivo* hastened development of *MLL*-induced leukaemia in recipient mice. Interestingly, when these authors performed m^6A-Seq and RNA-Seq on control cell lines and those overexpressing *FTO*, they found that potential FTO targets (i.e. those whose methylation decreased upon *FTO* overexpression, for example *ASB2* and *RARA*) appeared to be negatively regulated by FTO i.e. their mRNA levels decreased upon *FTO* overexpression. Since this finding was counter-intuitive to the idea of m^6A directed YTHDF2-mediated degradation, the authors proposed that a separate, YTHDF2 independent mechanism, was responsible for the reduced stability of FTO targets (Li, Weng et al. 2017).

However, there are several caveats to the conclusions of this initial paper. Firstly, in a CRISPR-based screen designed to identify genes essential for cell survival, the depletion of *FTO* did not show a substantial effect on AML cell viability across most of the 14 AML cell lines studied (Wang, Yu et al. 2017). Secondly, although FTO was originally thought to demethylate m^6A, it has since been shown to act primarily as a demethylase of m^6A_m (the N^6 -2'-O-dimethyladenosine modification in mRNA 5' caps) (Mauer, Luo et al. 2017). Thirdly, it has been pointed out that FTO is an α-ketoglutarate (α-KG)-dependent dioxygenase, and as such will be competitively inhibited by the structurally related metabolite D-2-hydorxyglutarate (D2-HG), which accumulates in *isocitrate dehydrogenase 1* or *2* (*IDH1/2*)-mutant tumours, including 20% of AMLs. For this reason, any effect of FTO has to be determined based on the *IDH* mutation status of an AML sample (Elkashef, Lin et al. 2017).

Whilst the requirement for m^6A demethylases in AML is less well defined at present than that of m^6A writers, the role of m^6A readers remains completely unexplored. With this in mind, and building on our findings in normal haematopoiesis (see Chapter 3) we examined the role of YTHDF2 in acute myeloid leukaemia. The results of this work are presented in this chapter.

4.1.2 Leukaemia models

In this chapter, a retroviral transduction/transformation assay (RTTA) was used to study the effect of *Ythdf2* deficiency in acute myeloid leukaemia driven by the co-expression of *Meis1/Hoxa9* oncogenes, or by expression of an oncogenic fusion (*Mll-AF9*, *PML-RARA, MOZ-TIF2*).

In RTTA, HSPCs are transduced with oncogenes or oncogenic fusion proteins, and serially re-plated in cytokine-supplemented semi-solid media prior to selection and transplantation to irradiated recipient mice (Lavau, Szilvassy et al. 1997).

RTTA has been used successfully for several decades to generate pathological AML from a variety of oncogenic drivers in mice (Lavau, Szilvassy et al. 1997, Thorsteinsdottir, Sauvageau et al. 1997, Kroon, Krosl et al. 1998, Lavau, Luo et al. 2000, Kroon, Thorsteinsdottir et al. 2001). Advantages of the technique over

transgenic models include the ability to evaluate the action of an oncogene in a specific subset of murine HSPCs, to study leukaemic transformation using human HSPCs in xenograft models, or to evaluate multiple oncogenes in parallel experiments using HSPCs from one mouse strain of genetic interest. Furthermore, retrovirally transduced cells can be tracked based on expression of reporter markers (for example GFP), facilitating monitoring of AML development and propagation. Nevertheless, there are also limitations to RTTA, most notably the potential for uncontrolled and potentially supra-physiological levels of oncogene expression. This is an important consideration given that the transforming effects of cellular oncogenes, including *MLL* fusions, *MYC*, *BCR-ABL* and *CEBPA*, may differ significantly depending on their expression levels (Caslini, Serna et al. 2004, Ren 2004, Chapiro, Russell et al. 2006, Chen, Kumar et al. 2008). Furthermore, limited control over the retroviral integration site during RTTA can lead to insertional mutagenesis, which means that the MSCV retroviral vector itself is associated with leukaemogenesis (Du, Jenkins et al. 2005).

4.1.2.1 Meis1/Hoxa9

The *Meis1/Hoxa9* retroviral AML mouse model is well characterised and has been widely used in leukaemic studies (Kroon, Krosl et al. 1998, Thorsteinsdottir, Kroon et al. 2001, Lessard and Sauvageau 2003, Zeisig, Milne et al. 2004, Vukovic, Guitart et al. 2015, Guitart, Panagopoulou et al. 2017).

Forced expression of *Hoxa9* in murine HSPCs is sufficient to induce leukaemic transformation in murine HSPCs, albeit with a long latency (Thorsteinsdottir, Kroon et al. 2001). Whilst retroviral overexpression of *Meis1* in murine HSPCs does not induce proliferation or leukaemic transformation in isolation, co-expression of *Meis1* and *Hoxa9* significantly reduces the latency of leukaemia induced by *Hoxa9* alone (median survival 54 days *Meis1/Hoxa9* versus 185 days *Hoxa9* alone) (Kroon, Krosl et al. 1998, Thorsteinsdottir, Kroon et al. 2001). Affected mice succumb to a myeloid leukaemia composed of approximately 77% blast cells versus 23% more mature myeloid cells (consistent with FAB M2 classification), with infiltration of spleen, lymph nodes and thymus in addition to BM (Thorsteinsdottir, Kroon et al. 2001).

Co-activation of *MEIS1* and *HOXA9* is a common feature of human AML of all subtypes except promyelocytic leukaemia (Lawrence, Rozenfeld et al. 1999) and is

associated with high-risk AML subtypes (Drabkin, Parsy et al. 2002). This, in combination with its high penetrance and short latency, makes the *Meis1/Hoxa9* retroviral AML mouse model an effective tool for studying AML *in vivo*.

4.1.2.2 MII-AF9

MLL-AF9 has been successfully used in the RTTA in several publications (Krivtsov, Twomey et al. 2006, Somervaille and Cleary 2006, Chen, Kumar et al. 2008, Thiel, Blessington et al. 2010), and a high correlation of CFC activity with leukaemogenic potential has been reported in this model of AML (Somervaille and Cleary 2006). Mice transplanted with *MLL-AF9* transduced cells develop AML at a high frequency (100% reported), with a median latency of 84.5 days (range 60-121) (Somervaille and Cleary 2006). MLL-AF9 leukaemia has been shown to follow a stem cell model (Krivtsov, Twomey et al. 2006, Somervaille and Cleary 2006), in which the bulk of leukaemic cells are derived from a rare population of cells (LSCs) capable of the limitless self-renewal necessary for cancer initiation and maintenance. It has been demonstrated that retroviral delivery of *MLL-AF9* can be used to transform both early haematopoietic progenitors (Somervaille and Cleary 2006) and more committed haematopoietic progenitors (Krivtsov, Twomey et al. 2006), although this indiscriminate transformation capacity may simply be a gene dosage effect, given the supra-physiological levels of *MLL-AF9* expression in this model (Chen, Kumar et al. 2008). Transformation by *MLL-AF9* induces aberrant expression of the MLL-AF9 target genes *HOXA9* and *MEIS1*, whose continued expression is essential for maintaining MLL-fusion mediated immortalisation (Ayton and Cleary 2003, Zeisig, Milne et al. 2004).

4.1.2.3 PML-RARA

Retroviral transduction of murine HSPCs with *PML-RARA* induces retinoic acid-sensitive promyelocytic leukaemias at a high frequency (>80%) with a latency of approximately 4 months (Minucci, Monestiroli et al. 2002). Retroviral *PML-RARA* is believed to be a ‘multiple-hit’ murine AML model, in which the fusion protein causes a “preleukaemic” phase and leukaemia occurs after additional genetic lesions (Minucci, Monestiroli et al. 2002).

4.1.2.4 MOZ-TIF2

Retroviral transduction of murine HSPCs with *MOZ-TIF2* generates AML at a high frequency (100% penetrance), with a short latency of approximately 3 months (Deguchi, Ayton et al. 2003). *MOZ-TIF2* has been identified as a leukaemia oncogene with the capacity to transform committed myeloid progenitor cells, which would otherwise be destined to undergo apoptotic cell death (Huntly, Shigematsu et al. 2004).

4.2 Aims

Based on the evidence presented in this introduction, we hypothesised that YTHDF2 might play a role in the development and maintenance of acute myeloid leukaemia.

The aim of this chapter was therefore to investigate the requirement for YTHDF2 at different stages of leukaemic transformation.

4.3 Outline of experiments described in Chapter 4

To investigate the functional requirement for YTHDF2 in leukaemogenesis, a retroviral transduction and transformation assay was used to generate pre-leukaemic stem cells (pre-LSCs) transformed with *Meis1/Hoxa9* oncogenes, or with an oncogenic fusion (*Mll-AF9*, *PML-RARA* or *MOZ-TIF2*), and these cells were transplanted to irradiated primary recipient mice. Upon development of leukaemia in these mice, leukaemic stem cells (LSCs) were harvested and transplanted to irradiated secondary recipient mice. The effect of *Ythdf2* deficiency was studied using *Ythdf2*$^{fl/fl}$*;Vav-iCre* conditional knock out mice, in which *Ythdf2* is specifically ablated within the hematopoietic system shortly after the emergence of definitive HSCs (de Boer, Williams et al. 2003). The effect of acute *Ythdf2* deletion was studied using *Ythdf2*$^{fl/fl}$;*Mx1-Cre* inducible conditional knock out mice, in which *Ythdf2* deletion is induced by polyinosinic:polycytidylic acid (pIpC) administration (Kuhn, Schwenk et al. 1995). In both cases, *Ythdf2*$^{fl/fl}$ mice acted as controls.

4.4 Results

4.4.1 Ythdf2 is required for leukaemic transformation in vitro

In order to assess the effect of *Ythdf2*-deficiency on leukaemic transformation *in vitro*, a retroviral transduction and transformation assay (RTTA) was employed. The *Vav-iCre* system was used to generate mice lacking *Ythdf2* specifically within the haematopoietic system, as previously described (see section **3.4.2**).

HSPCs (c-Kit$^+$ cells) were harvested from the FL of E14.5dpc *Ythdf2$^{fl/fl}$;Vav-iCre* and *Ythdf2$^{fl/fl}$* (control) embryos, and transduced with retroviruses co-expressing *Meis1* and *Hoxa9* oncogenes, or expressing chromosomal translocations known to be involved in leukaemogenesis (*Mll-AF9*, *MOZ-TIF2*, *PML-RARA*), as described in sections **2.11** and **2.12**. In the case of *Mll-AF9* and *MOZ-TIF2*, whose vectors contain a GFP selection cassette, C57BL/6 HSPCs (which are GFP$^-$) were transformed as controls in place of *Ythdf2$^{fl/fl}$* HSPCs (which are GFP$^+$), to facilitate FACS sorting of transformed (GFP$^+$) cells.

Transduced cells were serially re-plated using the colony forming assay (see section **2.13.2**) as an *in-vitro* measure of self-renewal capacity.

Both *Ythdf2$^{fl/fl}$* and *Ythdf2$^{fl/fl}$;Vav-iCre* cells were able to form colonies after transduction with *Meis1*/*Hoxa9*, or with any one of the three oncogenic fusions studied (*Mll-AF9*, *MOZ-TIF2*, *PML-RARA*). However, *Ythdf2$^{fl/fl}$;Vav-iCre* pre-LSCs generated significantly fewer colonies compared with *Ythdf2$^{fl/fl}$* pre-LSCs in all cases (**Figure 4.4.1 A-D**), although this effect was less marked in the case of *Mll-AF9* (**Figure 4.4.1 C**). Furthermore, there was a clear difference in the morphology of colonies derived from *Ythdf2*-deficient pre-LSCs, when compared to control pre-LSCs (**Figure 4.4.1 E-F**). Control colonies were predominantly compact and dense, whereas *Ythdf2*-deficient colonies were smaller, looser and less well defined. Colony morphology is reported to reflect cell differentiation status (Lavau, Szilvassy et al. 1997). Lavau et al. showed that HRX-ENL transformed cells generated three types of colonies in serial replating assays. Most (50–80%) were very compact and resembled colonies generated by primitive hematopoietic cells. A smaller subset (20–40%) had a compact centre with a diffuse halo of differentiating cells, and a third minor subset (15%) was comprised of large diffuse colonies. They went on to show that the compact colonies contained immature myeloid cells, whereas the diffuse colonies also included differentiated macrophages. Consistent with this observation, diffuse colonies had a

lower frequency of replating (only 1 in 5 diffuse colonies replated) compared with compact colonies (Lavau, Szilvassy et al. 1997). The colony morphology and replating capacity we observed in *Ythdf2*-deficient cells therefore suggested that pre-LSC differentiation might be increased in the absence of *Ythdf2*.

Overall, our results indicated that *Ythdf2* is required for leukaemic transformation *in vitro* induced by a variety of oncogenes and oncogenic fusions.

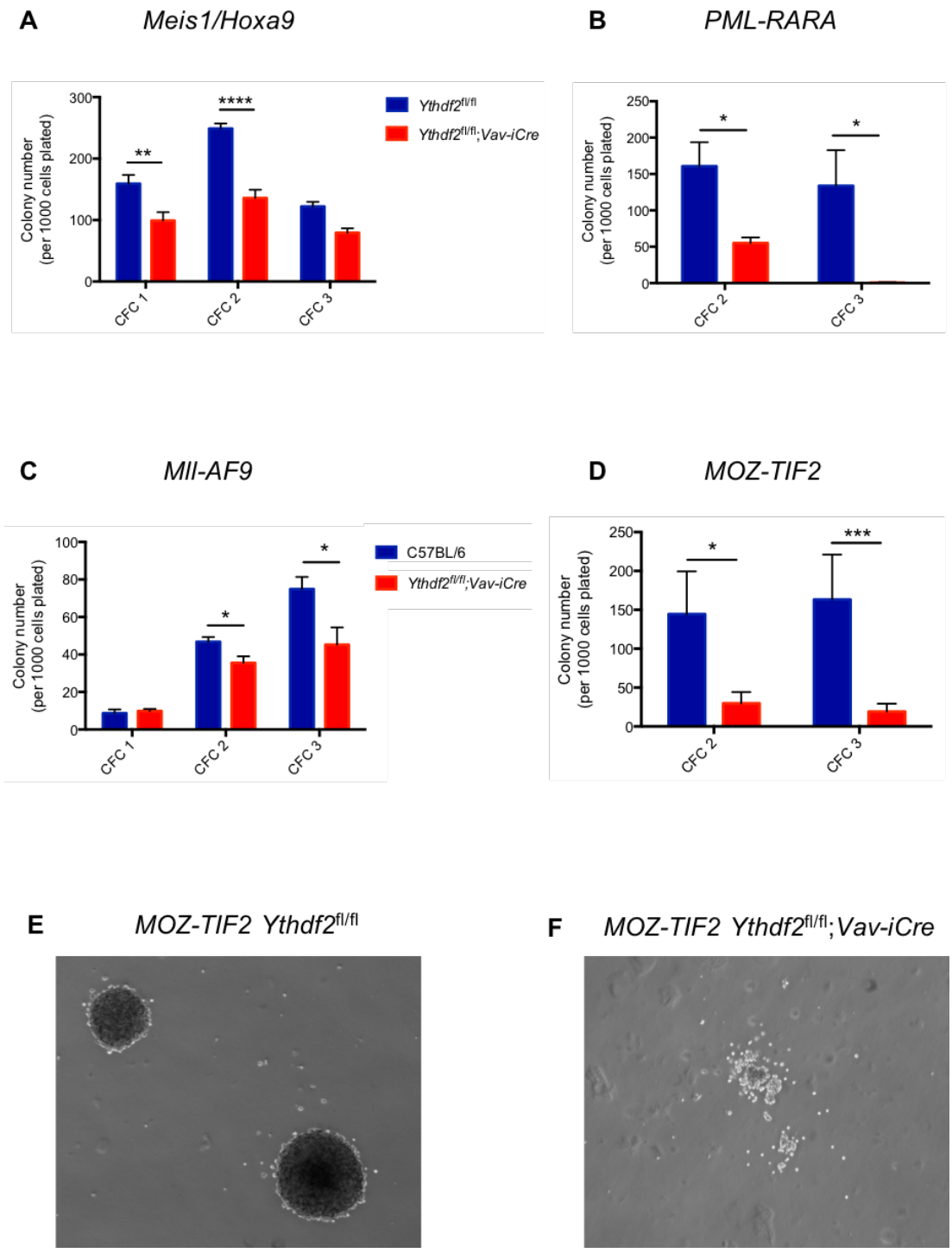

Figure 4.4.1 *Ythdf2*-deficient c-Kit^{+} cells show reduced transformation capacity *in vitro*. (**A-D**) Serial re-plating colony counts for HSPCs transformed with (**A**) *Meis1/Hoxa9* (**B**) *PML-RARA* (C) *Mll-AF9* (D) *MOZ-TIF2*. (**E-F**) Representative colony

images (10X magnification) for (**E**) *Ythdf2*$^{fl/fl}$ and (**F**) *Ythdf2*$^{fl/fl}$*;Vav-iCre* HSPCs transformed with *MOZ-TIF2*. Data are mean ± s.e.m, *n* = 4-6. Unpaired t-test.

4.4.2 Immunophenotypic characterisation of transformed colonies

In order to further explore the reduced transformation capacity of *Ythdf2*-deficient cells compared to control cells, immunophenotypic characterisation of pre-LSCs was carried out. *Meis1/Hoxa9* transformed pre-LSCs were harvested from CFC3 colonies and cultured in liquid media (see section **2.5**) prior to evaluation. Cells were stained with antibodies against mature myeloid markers (Gr-1 and CD11b) and the immature cell marker c-Kit, then analysed by flow cytometry (see section **2.8**). Both *Ythdf2*$^{fl/fl}$ and *Ythdf2*$^{fl/fl}$*;Vav-iCre* pre-LSCs expressed c-Kit and the myeloid markers Gr-1 and CD11b (**Figure 4.4.2**). There was a trend towards reduced monocytic differentiation (Gr-1^{-} CD11b^{+}) and greater granulocytic differentiation (Gr-1^{+} CD11b^{+}) in *Ythdf2*-deficient pre-LSCs, but it was not statistically significant. No other differences were observed when evaluating the immunophenotype of *Ythdf2*-deficient and control pre-LSCs.

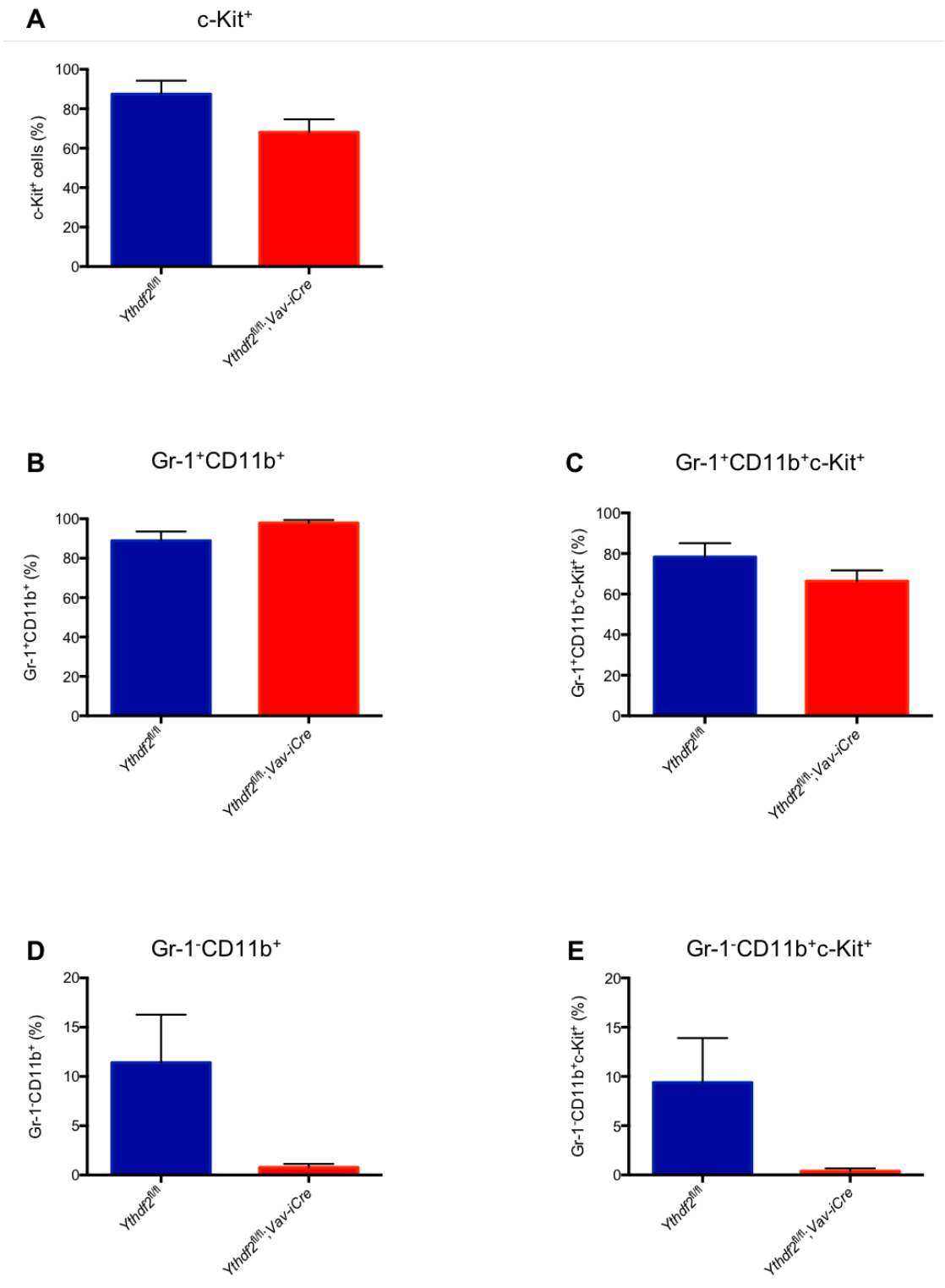

Figure 4.4.2 Immunophenotypic characterisation reveals no differences between *Ythdf2*-deficient and control *Meis1/Hoxa9* transformed pre-LSCs. Percentage of (**A**) c-Kit$^+$ cells (**B**) Gr-1$^+$ CD11b$^+$ cells (**C**) Gr-1$^+$ CD11b$^+$ c-Kit$^+$ cells (**D**)

Gr-1$^-$ CD11b$^+$ cells (**E**) Gr-1$^-$ CD11b$^+$ c-Kit$^+$ cells from *Ythdf2*-deficient and control *Meis1/Hoxa9* transformed pre-LSCs. Data are mean ± s.e.m, *n* = 5. Mann-Whitney U test.

4.4.3. *Ythdf2* inactivation compromises development of *Meis1/Hoxa9* leukaemia *in vivo*

In order to assess the role of *Ythdf2* in development of leukaemia *in vivo*, *Meis1/Hoxa9* pre-LSCs generated by RTTA (see sections **2.11-2.13**) were transplanted to irradiated recipient mice, as described in section **2.15.2**, and as shown in **Figure 4.4.3 A**. HSPCs were harvested from FL of *Ythdf2*$^{fl/fl}$ (control), *Ythdf2*$^{+/fl}$;*Vav-iCre* (heterozygote) and *Ythdf2*$^{fl/fl}$*;Vav-iCre* (*Ythdf2*-deficient) E14.5dpc embryos and transformed with *Meis1/Hoxa9* prior to serial re-plating *in vitro*. Pre-LSCs were harvested at CFC3 and 100 000 cells (CD45.2$^+$) were transplanted via the tail vein into lethally irradiated (11 Gy) recipient mice (CD45.1$^+$ CD45.2$^+$), together with 200 000 unfractionated bone marrow support (CD45.1$^+$). Leukaemic monitoring was carried out as described in section **2.15.4**, with CD45.1 and CD45.2 staining used to monitor engraftment of leukaemic cells against the background of recipient and support bone marrow cells.

Serial peripheral blood analysis showed slower engraftment of leukaemic cells in recipients of *Ythdf2*-deficient pre-LSCs (**Figure 4.4.3 B**) compared to control cells. At 20 days post transplantation, donor-derived chimerism in the peripheral blood was 5% for recipients transplanted with *Ythdf2*-deficient pre-LSCs and 43% for those transplanted with control pre-LSCs. By 60 days, chimerism was 81% compared with 2%, for *Ythdf2*-deficient pre-LSCs and control pre-LSCs respectively. Interestingly, engraftment in recipients of heterozygous (*Ythdf2*$^{+/fl}$;*Vav-iCre)* pre-LSCs was midway between that of control and Ythdf2-deficient cells at all time points, consistent with a dose dependent phenotype.

When recipient mice started to show signs of sickness, such as shortness of breath, hunched posture, pale paws, weight loss and reduced motion, they were culled and date of death was registered. Predictably, the slower engraftment of *Ythdf2*-deficient cells was reflected in the final Kaplan Meier survival curve (**Figure 4.4.3 C**), which showed a significantly longer median survival in recipients of *Ythdf2*-deficient pre-

LSCs (147.5 days) compared to control pre-LSCs (68 days), and heterozygous pre-LSCs (103 days).

Since this initial pilot experiment was carried out with one biological replicate (transplanted to 6 recipients each) per genotype, a follow up experiment was performed, this time with 3 biological replicates (transplanted to 3-5 recipients each) for both *Ythdf2*$^{fl/fl}$ and *Ythdf2*$^{fl/fl}$*;Vav-iCre* genotypes. This experiment confirmed the reproducibility of the preliminary result, with the Kaplan Meier survival curve showing a significantly longer survival for recipients of *Ythdf2*-deficient cells (97 days) compared with control cells (48 days) (**Figure 4.4.3 D**).

Post mortem examination of culled leukaemic mice revealed pale bones and grossly enlarged spleens (**Figure 4.4.3 E**) compared to healthy mice. However, spleen weight did not differ between leukaemic mice transplanted with control or *Ythdf2*-deficient cells (**Figure 4.4.3 F**).

Bone marrow of culled leukaemic mice was analysed by flow cytometry (see sections **2.7** and **2.8**). This showed a complete absence of GFP expression in *Ythdf2*$^{fl/fl}$*;Vav-iCre* LSCs, confirming continued lack of *Ythdf2* expression in these cells (**Figure 4.4.3 G**). Consistent with the clinical picture, the bone marrow was almost entirely effaced by CD45.2$^+$ LSCs (**Figure 4.4.3 H**), the majority of which were Gr-1$^+$ CD11b$^+$ or Gr-1$^-$ CD11b$^+$, consistent with myeloid leukaemia (**Figure 4.4.3 I**). A moderate proportion of LSCs was also c-Kit$^+$ (**Figure 4.4.3 J**). Notably, in spite of the longer latency of *Ythdf2*-deficient leukaemia, and consistent with the findings in pre-LSC cells, there was no significant difference in the immunophenotype of *Ythdf2*-deficient and control LSCs.

A

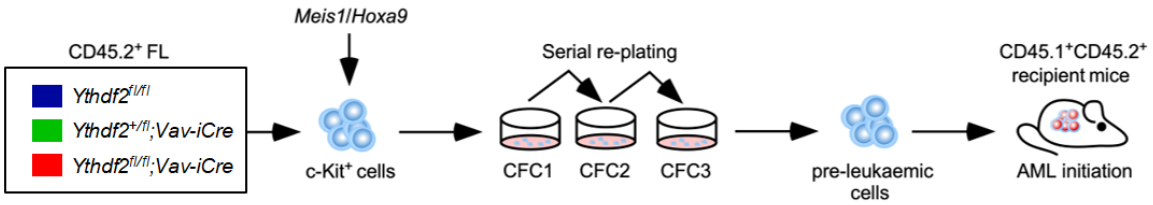
CD45.2+ FL
Ythdf2fl/fl
Ythdf2+/fl;Vav-iCre
Ythdf2fl/fl;Vav-iCre
Meis1/Hoxa9
c-Kit+ cells
Serial re-plating
CFC1
CFC2
CFC3
pre-leukaemic cells
CD45.1+CD45.2+ recipient mice
AML initiation

B

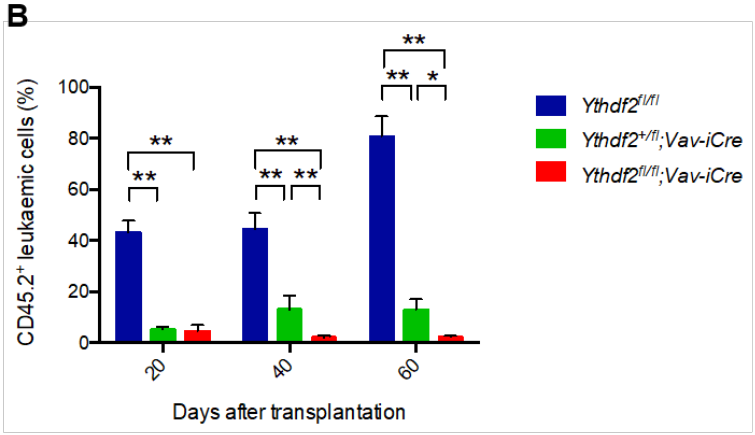
CD45.2+ leukaemic cells (%)
Days after transplantation
Ythdf2fl/fl
Ythdf2+/fl;Vav-iCre
Ythdf2fl/fl;Vav-iCre

C

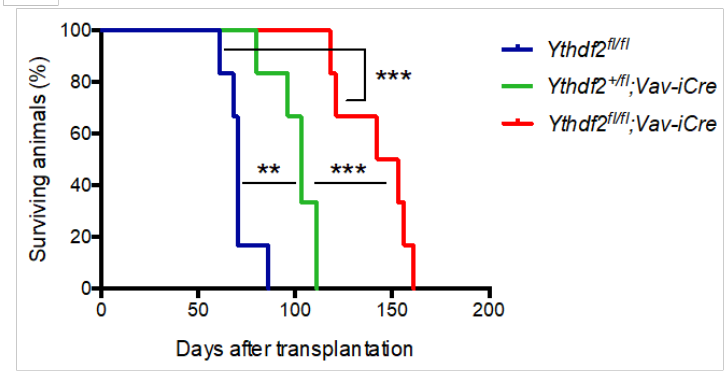
Surviving animals (%)
Days after transplantation
Ythdf2fl/fl
Ythdf2+/fl;Vav-iCre
Ythdf2fl/fl;Vav-iCre

D

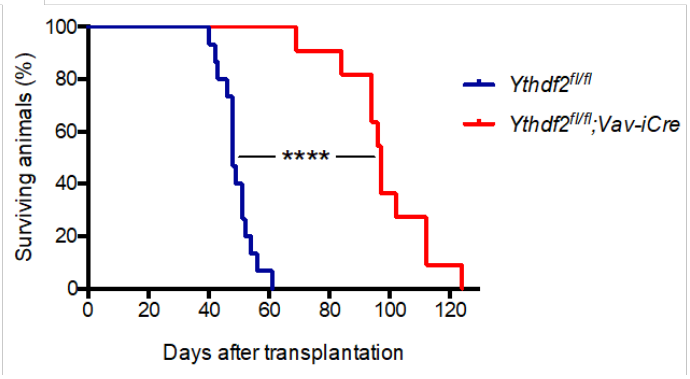
Surviving animals (%)
Days after transplantation
Ythdf2fl/fl
Ythdf2fl/fl;Vav-iCre

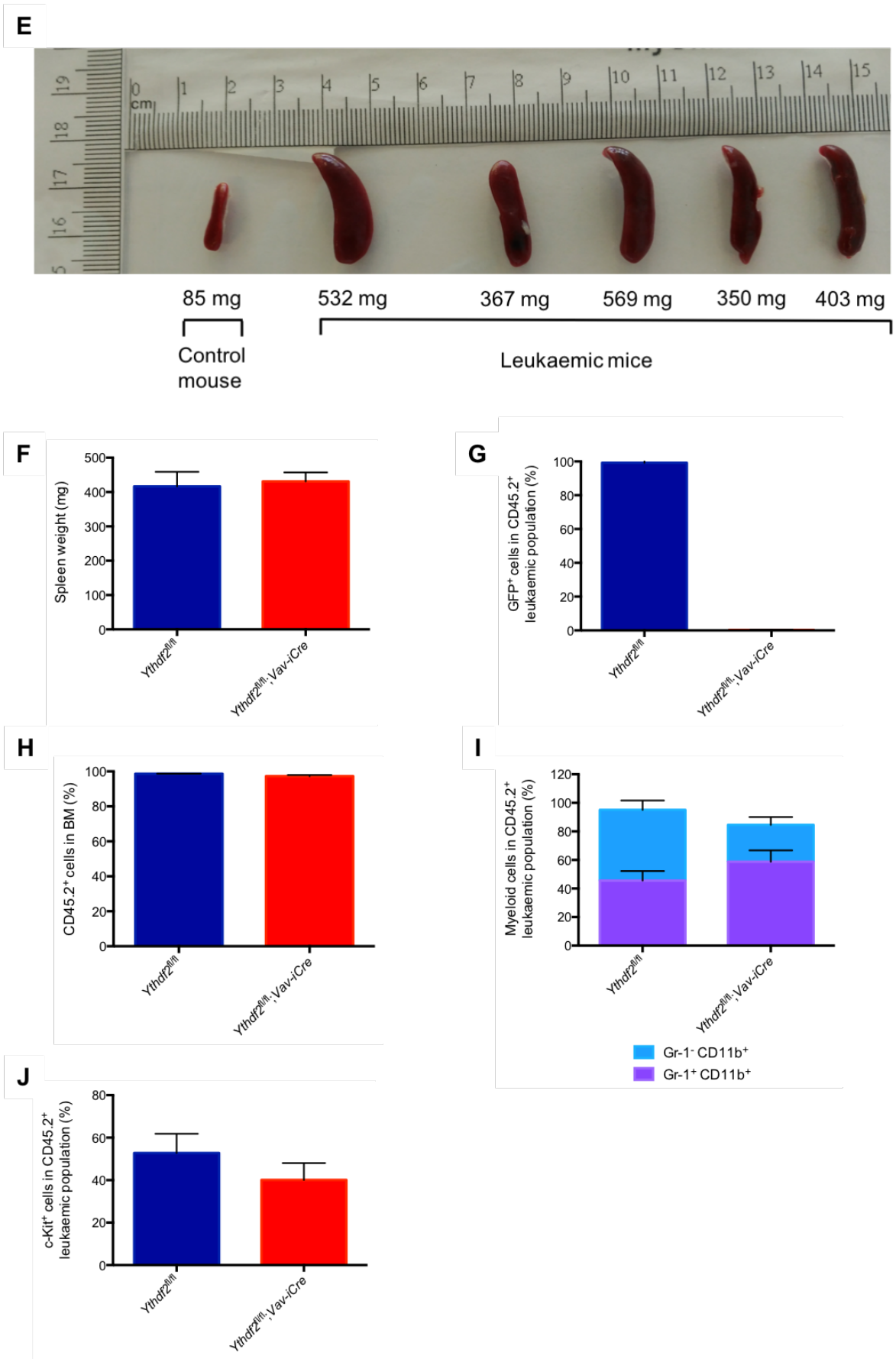
E
85 mg
532 mg
367 mg
569 mg
350 mg
403 mg
Control mouse
Leukaemic mice
F
Spleen weight (mg)
Ythdf2fl/fl
Ythdf2fl/fl;Vav-iCre
G
GFP+ cells in CD45.2+ leukaemic population (%)
H
CD45.2+ cells in BM (%)
I
Myeloid cells in CD45.2+ leukaemic population (%)
Gr-1- CD11b+
Gr-1+ CD11b+
J
c-Kit+ cells in CD45.2+ leukaemic population (%)

Figure 4.4.3 *Ythdf2* inactivation compromises development of leukaemia in a *Meis1/Hoxa9* murine AML model (**A**) *Ythdf2*$^{fl/fl}$ (control), *Ythdf2*$^{+/fl}$;*Vav-iCre* (heterozygote) and *Ythdf2*$^{fl/fl}$*;Vav-iCre* (*Ythdf2*-deficient) FL c-Kit^{+} cells were co-transduced with *Meis1* and *Hoxa9* retroviruses and serially re-plated. 100,000 c-Kit^{+} pre-leukaemic cells were transplanted into lethally irradiated recipient mice (*n* = 6 per genotype) together with 200,000 BM support cells. (**B**) Percentage of CD45.2^{+} leukaemic cells in the peripheral blood of the recipient mice 20-60 days after transplantation. Data are mean ± s.e.m, *n* = 6. *, P < 0.05; **, P<0.01. Mann-Whitney U test. (**C**) Kaplan-Meier survival curve of the recipient mice (*n* = 6 per genotype), **, P<0.01; ***, P < 0.001. Log-rank (Mantel-Cox test). (**D**) Repeat experiment Kaplan Meier survival curve (*n* = 11-15 per genotype), ****, P < 0.0001 Log-rank (Mantel-Cox test). (**E**) Appearance of spleens from culled leukaemic mice, and a healthy control. (**F**) Speen weights from culled leukaemic mice transplanted with *Ythdf2*$^{fl/fl}$ and *Ythdf2*$^{fl/fl}$*;Vav-iCre* cells. Data are mean ± s.e.m, *n* = 9-17 recipients per genotype. (**G**) Percentage of GFP-expressing cells as a measure of YTHDF2 expression in *Ythdf2*$^{fl/fl}$ and *Ythdf2*$^{fl/fl}$*;Vav-iCre* leukaemic cells within the bone marrow of culled recipient mice, *n* = 5-6 per genotype. (**H**) Percentage of leukaemic (CD45.2^{+}) cells within total bone marrow of culled recipient mice, *n* = 5-6 per genotype. (**I-J**) Percentage of (**I**) myeloid cells (CD11b^{+}± Gr-1^{+}) and (**J**) c-Kit^{+} cells within CD45.2^{+} leukaemic bone marrow cells of culled recipient mice, *n* = 5-6 per genotype.

4.4.4. *Ythdf2* inactivation may compromise development of *MII-AF9* leukaemia *in vivo*

Having established that *Ythdf2* inactivation compromises the development of *Meis1/Hoxa9* leukaemia in a murine retroviral model *in vivo*, we next sought to corroborate this in another retroviral murine AML model. Initially, we attempted to do so using pre-LSCs generated through RTTA with *MOZ-TIF2* retrovirus. However, due to the small numbers of *Ythdf2*-deficient colonies generated by serial replating *in vitro* (see section **4.4.1**), it was only possible to transplant 10 000 CFC3 pre-LSCs per mouse (to 6 mice in total per genotype), despite the use of 3 biological replicates, each of which was plated in duplicate. Sequential peripheral blood analysis over the following 6 months showed no evidence of leukaemic engraftment by either control, or *Ythdf2*-deficient pre-LSCs, therefore this experiment was discontinued. Next, we

attempted to study the effect of *Ythdf2* deficiency in a separate model of AML by using pre-LSCs generated through RTTA with *Mll-AF9* retrovirus (see section **4.4.1**). *Mll-AF9* transformed C57BL/6 and *Ythdf2$^{fl/fl}$;Vav-iCre* pre-LSCs were harvested at CFC3, and 100 000 cells (CD45.2^{+}) were transplanted via the tail vein into lethally irradiated (11 Gy) recipient mice (CD45.1^{+} CD45.2^{+}), together with 200 000 unfractionated bone marrow support cells (CD45.1^{+}). Leukaemic monitoring was carried out as previously described (see section **2.15.4**).

Analysis of the transplanted population showed no difference in surface marker expression between control and *Ythdf2$^{fl/fl}$;Vav-iCre* pre-LSCs (**Figure 4.4.4 A-B**). *Mll-AF9* pre LSCs were mostly myeloid (CD11b^{+}±Gr-1^{+}) (**Figure 4.4.4 A**), and approximately 20% expressed c-Kit **(Figure 4.4.4 B)**.

Peripheral blood analysis 3 weeks after transplantation showed lower engraftment of leukaemic cells in recipients of *Ythdf2*-deficient pre-LSCs compared to control pre-LSCs (**Figure 4.4.4 C**). Donor-derived chimerism in the peripheral blood was 3% for recipients transplanted with *Ythdf2*-deficient pre-LSCs and 11% for those transplanted with control pre-LSCs. However, this difference was no longer significant at 6 and 9 weeks (**Figure 4.4.4 C**), and the Kaplan Meir survival curves for recipients of *Ythdf2*-deficient and control pre-LSCs are also relatively similar to date (**Figure 4.4.4 D**). The role of Ythdf2 in Mll-AF9 leukaemia is therefore still unclear. For further discussion, please see section **4.5.**

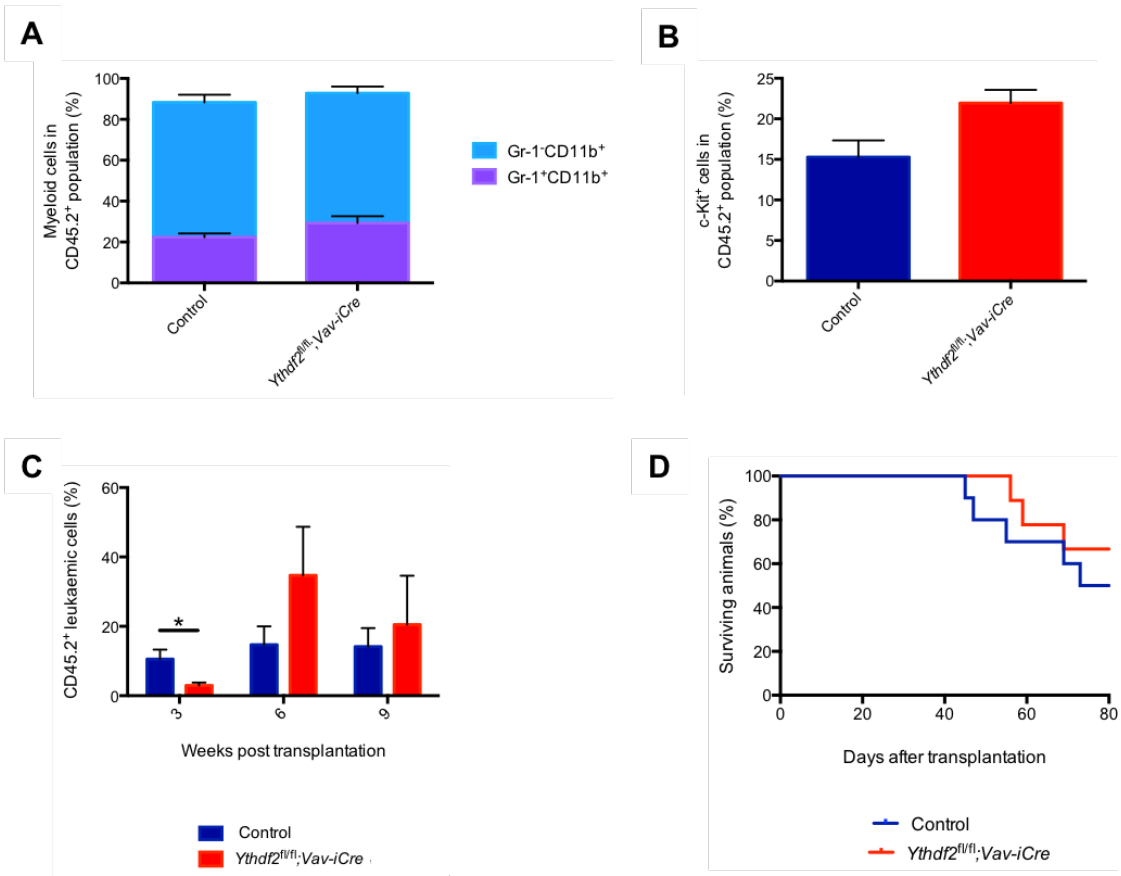

Figure 4.4.4 *Ythdf2* inactivation may compromise development of leukaemia in a *Mll-AF9* murine AML model. Percentage of (**A**) myeloid cells (CD11b$^+$± Gr-1$^+$) and (**B**) c-Kit$^+$ cells within CD45.2$^+$ pre-LSC population at the time of transplantation. Data are mean ± s.e.m, *n* = 5. (**C**) Percentage of CD45.2$^+$ leukemic cells in the peripheral blood of the recipient mice 3, 6 and 9 weeks after transplantation. Data are mean ± s.e.m, *n* = 10 per genotype. *, P < 0.05. Mann-Whitney U test. (**D**) Kaplan-Meier survival curve of the recipient mice (*n* = 10 per genotype).

4.4.5 Acute deletion of *Ythdf2* impairs LSC development and AML propagation in mice

Having established that *Ythdf2* is required for the development of *Meis1/Hoxa9* leukaemia using the *Vav-iCre* system, we next sought to establish the effect of acute *Ythdf2* deletion using an inducible model. To do so, we made use of the *Mx1-Cre* model (Kuhn, Schwenk et al. 1995), which has been widely used in experimental haematology by numerous groups (Gao, Graves et al. 2009, Gozdecka, Meduri et al. 2018) including our own (Kranc, Schepers et al. 2009, Guitart, Subramani et al. 2013,

Vukovic, Sepulveda et al. 2016, Guitart, Panagopoulou et al. 2017). The *Mx dynamin-like GTPase 1* (*Mx1*) promoter, which is part of the viral response to infection, is minimally active in healthy mice. However, the *Mx1* promoter can be transiently activated to high levels of transcription in multiple tissues upon treatment with interferon α (IFN-α), interferon ß (IFN-ß), or pIpC (which induces interferon signalling) (Kuhn, Schwenk et al. 1995), thus activating Cre recombinase. Upon pIpC treatment of *Mx1-Cre* mice, Cre mediated "floxed" target gene deletion occurs in many tissues, but is particularly efficient in the liver and immune system, with 98% deletion reported after one dose of pIpC, and complete deletion after 3 doses (Kuhn, Schwenk et al. 1995).

For the purposes of our study, *Ythdf2*$^{fl/fl}$ mice were crossed with *Mx1-Cre* mice to generate *Ythdf2*$^{fl/fl}$*;Mx1-Cre* and control *Ythdf2*$^{fl/fl}$ mice. *Meis1/Hoxa9* transformed *Ythdf2*$^{fl/fl}$ and *Ythdf2*$^{fl/fl}$*;Mx1-Cre* pre-LSCs were generated using RTTA as described previously (see sections **2.11-2.13**). Pre-LSCs were harvested at CFC3 and GFP expression (which indicates YTHDF2 expression) was checked by flow cytometry, as a means of ruling out spontaneous activation of *Mx1-Cre in-vitro*. GFP expression was greater than 90% in all samples, and there was no significant difference in GFP expression between *Ythdf2*$^{fl/fl}$ and *Ythdf2*$^{fl/fl}$*;Mx1-Cre* pre-LSCs, indicating comparable levels of YTHDF2 expression at this stage (**Figure 4.4.5 A**). Next, *Ythdf2*$^{fl/fl}$ and *Ythdf2*$^{fl/fl}$*;Mx1-Cre* pre-LSCs were transplanted to irradiated primary recipient mice, as described previously (see section **2.15.2**). Briefly, 50 000 pre-LSCs (CD45.2^{+}) were transplanted via the tail vein into lethally irradiated (11 Gy) recipient mice (CD45.1^{+} CD45.2^{+}), together with 200 000 unfractionated bone marrow support (CD45.1^{+}). Three weeks after transplantation, peripheral blood was obtained from the tail vein and analysed by flow cytometry to establish leukaemic engraftment levels. The results showed a mean engraftment of 5% for both *Ythdf2*$^{fl/fl}$ and *Ythdf2*$^{fl/fl}$*;Mx1-Cre* pre-LSCs (**Figure 4.4.5 B**). The mice were subsequently divided into two cohorts based on leukaemic engraftment levels (**Figure 4.4.5 C**).

4.4.5.1 Acute deletion of *Ythdf2* in pre-LSCs slows leukaemic engraftment

The first cohort of mice (hence termed 'Pre-LSC group', all with engraftment < 6%) received 300 μg pIpC by intraperitoneal injection every other day for a total of 6 doses to induce *Mx1-Cre* mediated deletion of *Ythdf2* from the transplanted pre-LSC

population. Peripheral blood analysis was carried out 3 days after the final pIpC injection (week 5) and every 3 weeks thereafter (**Figures 4.4.5 D-E**). This showed a dramatic and sustained drop in GFP expression by *Ythdf2*$^{fl/fl}$*;Mx1-Cre* pre-LSCs following pIpC treatment, indicating effective deletion of *Ythdf2* (**Figure 4.4.5 D**). Simultaneously, leukaemic engraftment was slower in recipients of *Ythdf2*$^{fl/fl}$*;Mx1-Cre* pre-LSCs compared with recipients of control pre-LSCs, although the difference only achieved statistical significance at week 11 (**Figure 4.4.5 E**). The Kaplan Meier survival curve (**Figure 4.4.5 F**) showed a trend towards increased survival in recipients of *Ythdf2*$^{fl/fl}$*;Mx1-Cre* pre-LSCs (median 104 days) compared with control pre-LSCs (median 93 days), although this did not achieve statistical significance.

Bone marrow of culled leukaemic mice was analysed by flow cytometry (see section **2.8**). This showed almost complete absence of GFP expression in *Ythdf2*$^{fl/fl}$*;Mx1-Cre* LSCs, confirming continued lack of *Ythdf2* expression in these cells (**Figure 4.4.5 G**). Consistent with the clinical picture, the bone marrow was almost entirely effaced by CD45.2$^+$ LSCs (**Figure 4.4.5 H**), the majority of which were Gr-1$^+$ CD11b$^+$ or Gr-1$^-$ CD11b$^+$, consistent with myeloid leukaemia (**Figure 4.4.5 I**). Approximately 20% of LSCs were also c-Kit$^+$ (**Figure 4.4.5 J**). Notably there was no significant difference in the immunophenotype of *Ythdf2*-deleted and control LSCs.

4.4.5.2 Acute deletion of Ythdf2 in LSCs impairs maintenance and propagation of AML

The second cohort of mice (hence termed 'LSC group') were left to develop leukaemia without pIpC treatment, but were monitored alongside the 'Pre-LSC group' by serial peripheral blood analysis during this time. Interestingly, at the 3 week analysis time point, a reduction in GFP expression, indicating spontaneous *Ythdf2* deletion, was observed in the 'LSC group' *Ythdf2*$^{fl/fl}$*;Mx1-Cre* recipient mice, despite the fact that they had received no pIpC treatment (**Figure 4.4.5 K**). This observation was consistent with spontaneous *Mx1-Cre*-activation (and thus "floxed" gene deletion), which has been reported previously at levels ranging from 2-3% (Kuhn, Schwenk et al. 1995), to 30-50% post transplantation (Velasco-Hernandez, Sawen et al. 2016).

The 'LSC group' mice were culled when they showed clinical signs compatible with leukaemia, as described previously. CD45.2$^+$ LSCs obtained from the BM of these mice were sorted for GFP$^+$ cells (those without *Ythdf2* deletion), and plated through

one round of CFC in preparation for transplantation. GFP expression at this stage was greater than 90% in all samples, and there was no significant difference between *Ythdf2*$^{fl/fl}$ and *Ythdf2*$^{fl/fl}$*;Mx1-Cre* LSCs, indicating comparable levels of *Ythdf2* expression before secondary transplantation (**Figure 4.4.5 L**). Next, 50 000 *Ythdf2*$^{fl/fl}$ and *Ythdf2*$^{fl/fl}$*;Mx1-Cre* LSCs (CD45.2^{+}) were transplanted via the tail vein into lethally irradiated (11 Gy) recipient mice (CD45.1^{+} CD45.2^{+}), together with 200 000 unfractionated bone marrow support (CD45.1^{+}), as previously described (section **2.15.2**). Three weeks after transplantation, peripheral blood was obtained from the tail vein and analysed by flow cytometry to establish engraftment levels (**Figure 4.4.5 M**). Whilst *Ythdf2*$^{fl/fl}$ GFP^{+} cells engrafted rapidly and caused aggressive AML upon transplantation to secondary recipients (**Figure 4.4.5 N**), *Ythdf2*$^{fl/fl}$*;Mx1-Cre* GFP^{+} cells lost YTHDF2 expression (**Figure 4.4.5 O)**, presumably due to spontaneous *Mx1-Cre* activation upon LSC transplantation (Velasco-Hernandez, Sawen et al. 2016), and failed to efficiently propagate the disease (**Figure 4.4.5 N**).

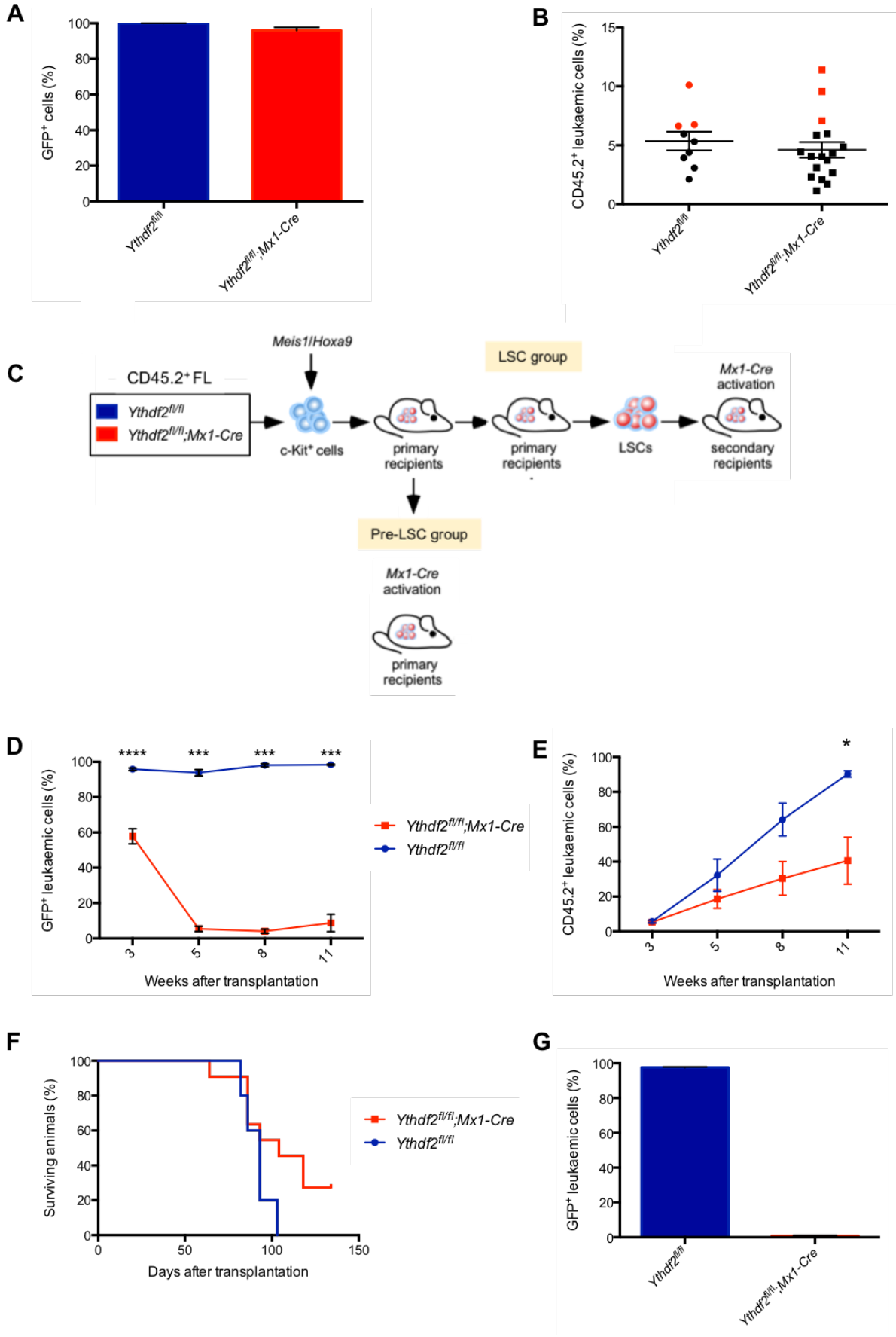
A
GFP+ cells (%)
Ythdf2fl/fl
Ythdf2fl/fl;Mx1-Cre
B
CD45.2+ leukaemic cells (%)
C
CD45.2+ FL
Ythdf2fl/fl
Ythdf2fl/fl;Mx1-Cre
Meis1/Hoxa9
c-Kit+ cells
primary recipients
LSC group
primary recipients
LSCs
Mx1-Cre activation
secondary recipients
Pre-LSC group
Mx1-Cre activation
primary recipients
D
GFP+ leukaemic cells (%)
****
***
***
***
Ythdf2fl/fl;Mx1-Cre
Ythdf2fl/fl
Weeks after transplantation
E
CD45.2+ leukaemic cells (%)
*
Weeks after transplantation
F
Surviving animals (%)
Ythdf2fl/fl;Mx1-Cre
Ythdf2fl/fl
Days after transplantation
G
GFP+ leukaemic cells (%)
Ythdf2fl/fl
Ythdf2fl/fl;Mx1-Cre

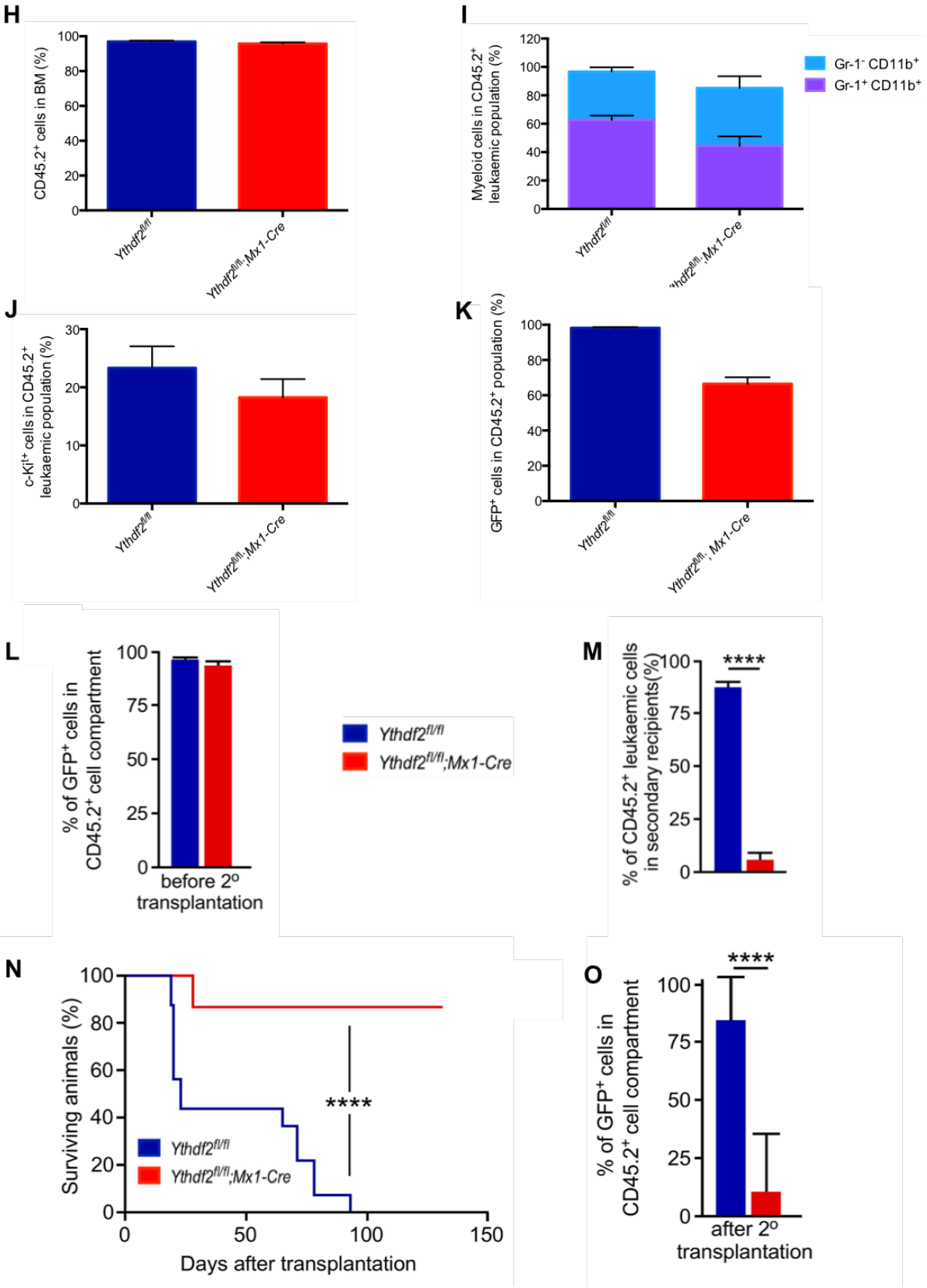
H
CD45.2+ cells in BM (%)
Ythdf2fl/fl
Ythdf2fl/fl;Mx1-Cre
I
Myeloid cells in CD45.2+ leukaemic population (%)
Gr-1- CD11b+
Gr-1+ CD11b+
J
c-Kit+ cells in CD45.2+ leukaemic population (%)
K
GFP+ cells in CD45.2+ population (%)
L
% of GFP+ cells in CD45.2+ cell compartment
before 2o transplantation
Ythdf2fl/fl
Ythdf2fl/fl;Mx1-Cre
M
% of CD45.2+ leukaemic cells in secondary recipients(%)
****
N
Surviving animals (%)
Days after transplantation
****
O
% of GFP+ cells in CD45.2+ cell compartment
after 2o transplantation
****

Figure 4.4.5 Acute deletion of *Ythdf2* impairs LSC development and AML propagation in mice. (**A**) Percentage of GFP-expressing cells as a measure of YTHDF2 expression in *Ythdf2*$^{fl/fl}$ and *Ythdf2*$^{fl/fl}$*;Mx1-Cre* pre-LSCs prior to transplantation. Data are mean ± s.e.m, *n* = 3. (**B**) Percentage of CD45.2^{+} leukaemic cells in the peripheral blood of primary recipient mice 3 weeks after transplantation. Data are mean ± s.e.m, *n* = 9-17 recipients per genotype. (**C**) Schematic of *Mx1-Cre* experiments. *Ythdf2*$^{fl/fl}$ and *Ythdf2*$^{fl/fl}$;*Mx1-Cre* FL c-Kit^{+} cells were co-transduced with *Meis1* and *Hoxa9* retroviruses, serially re-plated and transplanted into primary recipient mice, which were either treated with pIpC (Pre-LSC group) or left to develop AML (LSC group). GFP^{+} CD45.2^{+} cells sorted from LSC group leukemic primary recipients were re-transplanted into secondary recipient mice (*n* = 14-16 mice per genotype). (**D**) Percentage of CD45.2^{+} leukaemic cells in the peripheral blood of pIpC treated primary recipient mice 3-11 weeks after transplantation. Data are mean ± s.e.m, *n* = 6-14. *, P < 0.05. Mann-Whitney U test. (**E**) Percentage of GFP-expressing cells in the peripheral blood CD45.2^{+} cell compartment of pIpC treated primary recipient mice 3-11 weeks after transplantation. Data are mean ± s.e.m, *n* = 6-14. ***, P < 0.001; ****, P < 0.0001. Mann-Whitney U test. (**F**) Kaplan-Meier survival curve of primary recipient mice transplanted with *Ythdf2*$^{fl/fl}$ and *Ythdf2*$^{fl/fl}$;*Mx1-Cre* pre-LSCs. Data are mean ± s.e.m, *n* = 6-14 per genotype. (**G**) Percentage of GFP-expressing cells as a measure of YTHDF2 expression in *Ythdf2*$^{fl/fl}$ and *Ythdf2*$^{fl/fl}$;*Mx1-Cre* leukemic cells within the bone marrow of culled recipient mice, *n* = 5-6 per genotype. (**H**) Percentage of leukaemic (CD45.2^{+}) cells within total bone marrow of culled recipient mice, *n* = 5-6 per genotype. (**I-J**) Percentage of (**I**) myeloid cells (CD11b^{+}± Gr-1^{+}) and (**J**) c-Kit^{+} cells within CD45.2^{+} leukaemic bone marrow cells of culled recipient mice, *n* = 5-6 per genotype. (**K**) Percentage of GFP-expressing cells in the peripheral blood CD45.2^{+} cell compartment of non pIpC treated (i.e. LSC group) primary recipient mice 3 weeks after transplantation. (**L**) Percentage of GFP-expressing cells as a measure of YTHDF2 expression in *Ythdf2*$^{fl/fl}$ and *Ythdf2*$^{fl/fl}$;*Mx1-Cre* leukaemic cells prior to secondary transplantation (**M**) Percentage of CD45.2^{+} leukaemic cells in the peripheral blood of the secondary recipient mice 3 weeks after transplantation (*n* = 14-16 recipients per genotype). ****, P < 0.001. Mann-Whitney U test. (**N**) Kaplan-Meier survival curve of mice transplanted with *Ythdf2*$^{fl/fl}$ and *Ythdf2*$^{fl/fl}$;*Mx1-Cre* leukaemic cells. (*n* = 14-16 mice per genotype). ****, P<0.001 Log-rank (Mantel-Cox test). (**O**) Percentage of GFP-expressing cells in PB CD45.2^{+} cell compartment of

secondary recipient mice. Data are mean ± s.e.m.; ****, P < 0.001. Mann-Whitney U test.

4.5 Discussion

The work presented in this chapter demonstrates an important role for *Ythdf2* in development and maintenance of AML. First, we demonstrated the requirement for *Ythdf2* during *in vitro* leukaemic transformation with a variety of oncogenes and oncogenic fusions. Next, we showed that *Meis1/Hoxa9* transformed *Ythdf2*-deficient pre-LSCs initiate leukaemia *in vivo* with a significant delay compared to their control counterparts. Finally, we used the inducible *Mx1-Cre* system to show that acute *Ythdf2* deletion impairs LSC development and AML propagation in mice.

The role of *Ythdf2* has not previously been reported in AML. *YTHDF2* has been studied in solid cancers of humans, including those affecting the stomach, pancreas, liver and prostate (Yang, Li et al. 2017, Zhang, Pi et al. 2017, Chen, Wei et al. 2018, Li, Meng et al. 2018, Zhong, Liao et al. 2019). However, the role of *YTHDF2* in these tumours is controversial. In hepatocellular cancer, *YTHDF2* has been reported to function as an oncogene (Yang, Li et al. 2017), and also as a tumour suppressor (Zhong, Liao et al. 2019). Similarly, in pancreatic cancer *YTHDF2* has been shown to promote proliferation, whilst inhibiting migration and invasion (so called 'migration proliferation dichotomy') (Chen, Sun et al. 2017). Our study is the first to report the role of *Ythdf2* in AML. Previously, multiple groups have shown an essential requirement for the m^6A writers METTL3 and/or METTL14, as well the m^6A eraser FTO, in AML development and maintenance (Barbieri, Tzelepis et al. 2017, Li, Weng et al. 2017, Vu, Pickering et al. 2017, Su, Dong et al. 2018, Weng, Huang et al. 2018). However, the proposed oncogenic mechanism has varied between studies. Some studies have reported decreased target mRNA stability upon loss of m^6A (through inhibition of METTL14, or overexpression of FTO), suggesting a YTHDF2-independent mechanism of oncogenesis (Li, Weng et al. 2017, Weng, Huang et al. 2018). Others have identified an m^6A dependent alteration in translation, as opposed to degradation, as the driving mechanism (Barbieri, Tzelepis et al. 2017, Vu, Pickering et al. 2017). Our work demonstrated that *Ythdf2* is critically required for AML development and maintenance. Our studies to establish the mechanism for this are described in Chapter 5.

A high correlation of CFC activity with leukaemogenic potential has been reported using the RTTA model of AML (Lavau, Szilvassy et al. 1997, Somervaille and Cleary 2006). Consistent with this, we observed a reduction in the number and size of colonies generated from *Ythdf2*-deficient pre-LSCs transformed with *Meis1/Hoxa9*, *Mll-AF9*, *PML-RARA* and *MOZ-TIF2*, and prolonged survival in mice transplanted with *Ythdf2*-deficient *Meis1/Hoxa9* pre-LSCs. These findings are consistent with previous studies highlighting the importance of m^6A modification in AML (Barbieri, Tzelepis et al. 2017, Li, Weng et al. 2017, Vu, Pickering et al. 2017, Weng, Huang et al. 2018).

Although the survival curve has not been completed, the *Mll-AF9* transplant results obtained thus far are less convincing than those of *Meis1/Hoxa9*, with no observable survival advantage for mice receiving *Mll-AF9 Ythdf2*-deficient pre-LSCs compared with *Mll-AF9* control pre-LSCs. This result is surprising, given that *Meis1* and *Hoxa9* are key targets of Mll-AF9, which mediate the effects of this oncogenic fusion in AML (Armstrong, Staunton et al. 2001, Ayton and Cleary 2003, Kumar, Hudson et al. 2004, Zeisig, Milne et al. 2004, Krivtsov, Twomey et al. 2006). There are several possible explanations for the discrepancy. Firstly, considering that gene dosage has been reported to influence the target cell specificity of *Mll-AF9* (Chen, Kumar et al. 2008), it is possible that supra-physiological levels of *Mll-AF9* expression are masking the effect of *Ythdf2* deficiency in this retroviral model. To investigate this further, it would be useful to re-evaluate the effect of *Ythdf2* deficiency in an transgenic *Mll-AF9* model, for example in mice with doxycycline inducible *Mll-AF9* transgene expression (Stavropoulou, Kaspar et al. 2016). Another approach would be to better characterise the pre-LSCs (control and *Ythdf2*-deficient) in the *Mll-AF9* retroviral model, by performing a limiting dilution assay (Chen, Kumar et al. 2008, Hays 2009, Shlush, Zandi et al. 2014). Finally, given the heterogeneity of AML (Hays 2009, Meacham and Morrison 2013), it is perhaps not surprising that a range of mouse AML models may not all demonstrate the same genetic susceptibility (Velasco-Hernandez, Hyrenius-Wittsten et al. 2014), which further supports our decision to evaluate multiple oncogenes and oncogenic fusions when studying the role of *Ythdf2* in malignant haematopoiesis.

The results of our *Meis1/Hoxa9*, *MOZ-TIF2* and *PML-RARA* retroviral models suggested that YTHDF2 inhibition might be a therapeutic strategy in the treatment of human AML. For this to become a realistic proposition, we needed to establish

whether acute deletion of *Ythdf2* in established AML would be sufficient to delay or abolish leukaemic progression. To do so, we made use of the inducible *Mx1-Cre* system, in which *Cre* is expressed upon treatment with pIpC (Kuhn, Schwenk et al. 1995). We evaluated the effects of acute *Ythdf2* deletion in pre-LSCs (primary recipients) and in LSCs (secondary recipients).

In primary recipient mice, acute deletion of *Ythdf2* from pre-LSCs resulted in significantly reduced leukaemic engraftment 11 weeks after transplantation (**Figure 4.4.5 E**), and a trend towards a longer survival, although this did not reach statistical significance (**Figure 4.4.5 F**). However, it is worth noting that four mice had to be culled around the time of pIpC injections (all within a week of the last injection), owing to progressive anaemia, lethargy and weight loss. Antibody staining and flow cytometric BM analysis of these mice ruled out leukaemic progression as a cause of their clinical signs. Although mice were left to recover for 3 weeks following irradiation/transplantation prior to the initiation of pIpC injections, it is possible that this time period was insufficient. Following irradiation, transplanted animals undergo a 5 to 10 day irradiation sickness period from which they generally recover within 14 days (Duran-Struuck and Dysko 2009), providing that donor and residual host HSCs rapidly enter the cell cycle and proliferate to repopulate the BM with progenitor cells. However, pIpC, a synthetic double stranded RNA used to mimic viral infections *in vivo*, acts through its receptor TLR3 (Matsumoto and Seya 2008) to stimulate an IFN dependent response, ultimately forcing quiescent HSCs into the cell cycle (Essers, Offner et al. 2009). Treatment with pIpC increases HSC cycling six- to seven-fold for up to 3 days, leading to the accumulation of reactive oxygen species and DNA damage in remaining HSCs (Walter, Lier et al. 2015). DNA damage itself induces type I IFN-mediated stem cell senescence (Yu, Katlinskaya et al. 2015). It is therefore possible that the combination of recent irradiation, and then repeated doses of pIpC (200-300 μl poly(I:C) (1 μg/μl) by intraperitoneal injection every 48 hours for 6 doses), exhausted the HSC repopulation capacity of some mice, ultimately leading to progressive anaemia. Unfortunately, the loss of these mice, together with the prior division of the cohort to also provide LSCs for the secondary experiment (**Figure 4.4.5 C**) meant that this primary experiment may have been underpowered to detect a difference in survival following *Ythdf2* deletion in pre-LSCs.

In secondary recipient mice, spontaneous activation of *Mx1-Cre* occurred following transplantation, in the absence of pIpC treatment. As a result, *Ythdf2*$^{fl/fl}$; *Mx1-Cre* LSCs lost *Ythdf2* expression (**Figure 4.4.5 O**), and subsequently failed to initiate leukaemia in their recipient mice (**Figure 4.4.5 N**). Spontaneous activation of *Mx1-Cre* has been reported previously, at levels of 2-10% under homeostatic conditions (Kuhn, Schwenk et al. 1995), and increasing to around 40% following BM transplantation (Velasco-Hernandez, Sawen et al. 2016). In our study, spontaneous *Mx1-Cre* activation occurred after transplantation of pre-LSCs to primary recipients (**Figure 4.4.5 D** week 3), but was more marked following transplantation of LSCs to secondary recipients (**Figure 4.4.5 O**). As a result, engraftment was only delayed in primary recipients (even after pIpC treatment), but was abolished in secondary recipients. The reason for the differential *Mx1-Cre* activation in pre-LSCs and LSCs is not clear, but could reflect a difference in the behaviour, or host response to, the stage of leukaemic cell transplanted. To further investigate this, pre-LSCs and LSCs could be transplanted to parallel cohorts of mice in one experiment, ensuring all other variables are kept constant, to determine whether the effect is dependent on cell type or other factors. To circumnavigate the problem of spontaneous *Mx1-Cre* activation, future experiments could involve one of the alternative models described in the literature for inducible gene deletion, such as *Cre-ERT* (Hayashi and McMahon 2002) *or* Ah-*Cre*/Mx1-*Cre* together with *Cre-ERT* (Kemp, Ireland et al. 2004).

In summary, the results presented in this chapter show that *Ythdf2* is required for the development and propagation of AML, making *Ythdf2* inhibition an exciting potential novel therapeutic strategy for treatment of this aggressive disease. Investigations into the mechanism through which *Ythdf2* is required for AML are presented in the next chapter.

Chapter 5: Mechanisms of YTHDF2 function in leukaemogenesis

5.1 Introduction

5.1.1 Mechanisms of m^{6}A machinery in AML

Several studies have documented the important role of m^{6}A in AML, and this has been discussed in Chapter 1 (including **Table 1.3.5**) and Chapter 4. Although ours is the first study to focus on the role of YTHDF2 in AML, other groups have reported a requirement for the writer METTL3, and for members of the complex it forms together with METTL14, WTAP, KIAA1429, and ZFP217. The m^{6}A eraser FTO is also known to play an important role in AML. Three recent studies have identified the m^{6}A RNA modifying enzymes METTL3 and METTL14 as critical regulators of differentiation in both normal haematopoiesis and AML pathogenesis (Barbieri, Tzelepis et al. 2017, Vu, Pickering et al. 2017, Weng, Huang et al. 2018).

Vu et al., who showed that METTL3 controls myeloid differentiation of normal haematopoietic and leukaemia cells, used a combination of single nucleotide resolution mapping of m^{6}A coupled with ribosome profiling to demonstrate that m^{6}A promotes the translation of *c-MYC*, *BCL2* and *PTEN* mRNAs, whilst loss of *METTL3* leads to increased phosphorylated AKT, which contributes to induction of differentiation (Vu, Pickering et al. 2017).

Barbieri et al. also reported that METTL3 maintains myeloid leukaemia by m^{6}A dependent translational control (Barbieri, Tzelepis et al. 2017). This study carried out anti-METTL3 ChIP-Seq (chromatin immunoprecipitation followed by next-generation sequencing) and found that METTL3 associates with chromatin and localises to the transcriptional start site (TSS) of active genes. They showed that most of these genes have CEBPZ protein present at the TSS, and confirmed that this is required for METTL3 recruitment. Using a combination of m^{6}A meRIP-Seq and ribosome footprinting, they went on to show that promoter-bound METTL3 induces m^{6}A modification in the coding region of the associated mRNA and enhances its translation by relieving ribosome stalling. They showed that METTL3 binds the promoters of the

transcription factors *SP1* and *SP2*, which in turn bind the promoter of *c-MYC*. In support of this mechanistic pathway, overexpression of *SP1* was able to rescue the effect of *METTL3* knock down on the growth of a human AML cell line *in vitro* (Barbieri, Tzelepis et al. 2017).

METTL14 has also been shown to promote leukaemogenesis via mRNA m^6A modification (Weng, Huang et al. 2018). Using a combination of m^6A meRIP-Seq, RNA-Seq and CLIP assays, Weng et al. identified METTL14 targets, including *MYB* and *MYC*. Using actinomycin D to inhibit transcription and elucidate mRNA decay kinetics, and polysome profiling to characterise the translating pool of mRNAs, they showed that *METTL14* knock down affects both the half-lives and translation of *MYC* and *MYB* mRNAs. Interestingly, in this study, the majority of identified METTL14 targets (m^6A peaks with decreased abundance upon *METTL14* knock down) were associated with decreased mRNA levels in knock down cells, suggesting an alternative, non-YTHDF2 based mechanism for decreased mRNA stability in this case (Weng, Huang et al. 2018).

The demethylase FTO has also been shown to play an oncogenic role in AML (Li, Weng et al. 2017). Li et al. used a combination of RNA-Seq and m^6A meRIP-Seq in control and *FTO*-overexpressing cell lines, to identify potential FTO targets, including *ASB2* and *RARA*. Of note, the mRNA levels of these targets decreased upon *FTO* overexpression, once again suggesting the involvement of another, non-YTHDF2 dependent mechanism in determining mRNA stability (Li, Weng et al. 2017).

5.1.2 Molecular methods used to investigate the mechanism of YTHDF2 in AML

In order to investigate the mechanism of YTHDF2 requirement in AML we employed a variety of molecular techniques to evaluate the transcriptome overall, mRNA methylation, and the intracellular dynamics of mRNA transcription, processing, translation and decay.

5.1.2.1 RNA microarray

Gene microarray technology depends on the ability to deposit large numbers of DNA sequences in an ordered fashion on a small surface, typically referred to as a ‘chip’.

DNA arrays are used to probe a solution of labelled nucleic acids, with the final hybridization pattern reflecting the relative concentrations of nucleic acid species present in the sample (Lockhart, Dong et al. 1996).

For the purposes of our study, we used the GeneChip™ Mouse Gene 2.0 ST Array, which is a whole-transcript array that includes probes to measure both mRNA (>28,000 coding transcripts) and long intergenic non-coding RNA transcripts.

5.1.2.2 m^6A meRIP-Seq

N(6)-methyladenosine-sequencing (m^6A meRIP-Seq) is an immunocapturing approach for the unbiased transcriptome-wide localization of m^6A in high resolution (Dominissini, Moshitch-Moshkovitz et al. 2013). The method relies upon antibody-mediated enrichment of methylated RNA fragments followed by massively parallel sequencing. Subsequently, read densities are compared between immunoprecipitated RNA and untreated input control to identify methylated sites.

5.1.2.3 SLAM-Seq

Thiol (SH)-Linked Alkylation for the Metabolic Sequencing of RNA (SLAM-Seq) is an RNA sequencing technology that detects 4-thiouridine (S4U) incorporation in RNA species at single-nucleotide resolution (Herzog, Reichholf et al. 2017). Unlike standard RNA-Seq methods, which only measure RNA species at a single time point, SLAM-Seq can provide information about the intracellular dynamics of RNA transcription, processing and decay.

The SLAM-Seq technique was developed from pre-existing protocols for metabolic labelling of RNA using S4U (Rabani, Levin et al. 2011). These protocols relied upon S4U incorporation into newly transcribed RNA in place of uridine, allowing quantification of RNA synthesis with no detrimental effect on cell growth and survival. S4U containing RNA was separated out on the basis of biotin binding, and hybridized to microarrays, or subjected to RNA sequencing technologies.

The key distinguishing feature of the SLAM-Seq technique is an alkylation step after S4U labelling, during which iodoacetamide (IAA) covalently attaches a carboxyamidomethyl group to S4U by nucleophilic substitution (**Figure 5.1.2.3**).

During the subsequent cDNA library preparation step, the presence of a carboxyamidomethyl group causes reverse transcriptase to incorporate Guanine (G) instead of Adenine (A) in any position where a reduced S4U modified nucleotide is encountered. Analysis of T>C mutations can then be used to identify nascent RNA (Herzog, Reichholf et al. 2017). The technique has the advantage of enabling quantitative analysis of nascent and existing RNA in a single sample without the need for biochemical isolation (no biotin-dependent RNA pull-down required), thus reducing cost, labour, RNA input requirements and background noise.

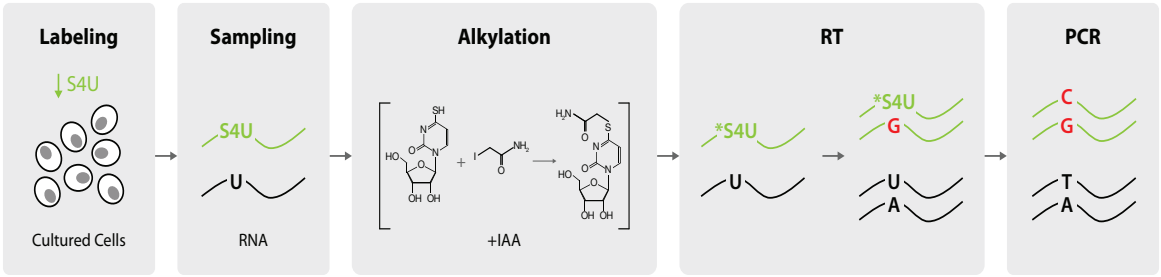

Figure 5.1.2.3 SLAM-Seq workflow. Cultured cells are treated with S4U to label nascent RNA (green), then total RNA is purified (sampling) and iodoacetamide (IAA) is added to induce alkylation of S4U. During reverse transcription (RT), the resulting carboxyamidomethyl group causes a G to be added instead of an A wherever a reduced S4U modified nucleotide is encountered. Second strand synthesis and PCR complete the protocol, and the presence of T>C mutations can then be used to identify nascent RNA. Taken from Lexogen SLAM-Seq kit protocol.

In this chapter, we describe use of SLAM-Seq specifically to look at RNA turnover (catabolic kinetics). Because S4U uptake is variable depending on the cell type studied, it is critical to first assess toxicity in the cells of interest, and determine the optimal S4U concentration for further experiments. Based on the results of this optimisation assay (see **2.21.1**), we used 2.91 μM S4U (the limiting IC_{10}, as determined in the cytotoxicity assay) for SLAM-Seq.

5.1.2.4 RIBO-Seq

RIBO-Seq is a technique which relies on deep sequencing of ribosome-protected mRNA fragments (generated by treatment of polyribosomes with exogenous nucleases) to provide a transcriptome-wide assessment of mRNA translation (Ingolia,

Ghaemmaghami et al. 2009). For the purpose of our study, we employed a recently described ribosome profiling technique based on micrococcal nuclease (MNase) (Reid, Shenolikar et al. 2015). In contrast to previous ribosome profiling methods (which typically use RNAse1), this method avoids the need for ribosome purification prior to extraction of ribosome-protected mRNA fragments (RPFs). This is because MNase activity can be tightly controlled under the reaction conditions specified, avoiding significant rRNA degradation. The RPFs generated can then be purified by gel electrophoresis based on size selection alone (Reid, Shenolikar et al. 2015).

5.2 Aims

The aims of this chapter were to understand the mechanism by which *Ythdf2* loss impedes the development and maintenance of acute myeloid leukaemia.

5.3 Outline of experiments described in Chapter 5

Experiments in this chapter were carried out jointly with colleagues. Samples were prepared and processed to the stage of RNA extraction (TRIzol™ method) by Jasmin Paris for Affymetrix, m^{6}A meRIP-Seq, SLAM-Seq and Ribo-Seq, and the remainder of these experiments, including data analyses, were performed by Marcos Morgan. Experiments in section **5.4.6** were carried out jointly with other collaborators (Joana Campos, Alena Shmakova, David Wotherspoon, Tim Sommervaille, Gary Spencer, Ivayla Ivanova, Junho Choe, Hannah Lawson & Richard Gregory) and are presented for completeness, and to explain the work carried out in section **5.4.7**, which was completed solely by Jasmin Paris.

This chapter describes the experiments carried out to investigate the mechanism by which *Ythdf2* loss impedes the development and maintenance of acute myeloid leukaemia. A combination of transcriptome profiling (Affymetrix™) and m^{6}A meRIP-Seq were used to identify deregulated gene sets upon loss of *Ythdf2*, and their relationship with m^{6}A occupancy. Subsequently, SLAM-Seq and RIBO-Seq were used to investigate how these changes might relate to a role for YTHDF2 in mRNA degradation and translation respectively. Finally, since combined data analyses identified *Tnfrsf1b* upregulation as a potential mechanism for impaired

leukaemogenesis in *Ythdf2*-deficient cells, an attempt to rescue the phenotype *in vitro* and *in vivo* using shRNA knockdown of *Tnfrsf1b* is described.

5.4 Results

5.4.1 Loss of *Ythdf2* results in deregulated gene expression

YTHDF2 is known to target methylated transcripts for decay through deadenylation (Wang, Lu et al. 2014, Du, Zhao et al. 2016). We therefore hypothesised that *Ythdf2* loss might result in altered transcript levels, which could in turn explain the impaired leukaemogenesis observed. To investigate this we submitted *Meis1/Hoxa9* transformed *Ythdf2*$^{fl/fl}$ and *Ythdf2*$^{fl/fl}$;*Vav-iCre* pre-LSCs (*n* = 5 for each genotype) for transcriptome profiling using the GeneChip™ Mouse Gene 2.0 ST Assay (see Affymetrix™, sections **2.18** and **2.19**). This is a whole-transcript array that includes probes to measure both mRNA and long intergenic non-coding RNA transcripts.

In order to minimise variability due to gender differences, pre-LSCs were generated from sex-matched (all female) HSPCs for this purpose (see section **2.3.2.4**), as shown in **Figure 5.4.1 A**. The Affymetrix data are deposited under the accession number E-MTAB-6783.

As predicted, the microarray results showed deregulated gene expression upon loss of *Ythdf2*, with 754 upregulated and 582 downregulated genes respectively ($P < 0.05$), in *Ythdf2*$^{fl/fl}$;*Vav-iCre* compared to *Ythdf2*$^{fl/fl}$ pre-leukaemic cells (**Figure 5.4.1 B** and **Appendix 1**).

In order to functionally profile the up- and down-regulated genes, Gene Ontology (GO) term enrichment was performed (Ashburner, Ball et al. 2000). GO term enrichment is a computational technique for interpreting gene sets based on the Gene Ontology system of classification. The Gene Ontology Consortium began in 1998, as a joint project based on three model organisms *Drosophila melanogaster* (fruit fly), *Mus musculus* (mouse), and *Saccharomyces cerevisiae* (yeast) (Ashburner, Ball et al. 2000). The number of different organisms represented in GO is now in the thousands (http://geneontology.org). The GO describes the current knowledge of biology with

respect to three aspects; molecular function, cellular component, and biological processes.

GO term enrichment of deregulated genes in *Ythdf2*$^{fl/fl}$;*Vav-iCre* pre-LSCs compared to *Ythdf2*$^{fl/fl}$ pre-LSCs revealed mostly generic metabolic processes in the upregulated genes and immune response processes in the down regulated genes (**Figure 5.4.1 C**). Interestingly, the enrichment for metabolic processes is also found in upregulated genes in *Ythdf2*-deficient oocytes (Ivanova, Much et al. 2017). Furthermore, down-regulation of immune response processes may be linked to the reduction in $CD8^+$ T cells observed in the peripheral blood and spleens of *Ythdf2*$^{fl/fl}$;*Vav-iCre* mice, and the compromised $CD4^+$ and $CD8^+$ T cell reconstitution by *Ythdf2*$^{fl/fl}$;*Vav-iCre* deficient HSCs, all of which are described and discussed in Chapter 3.

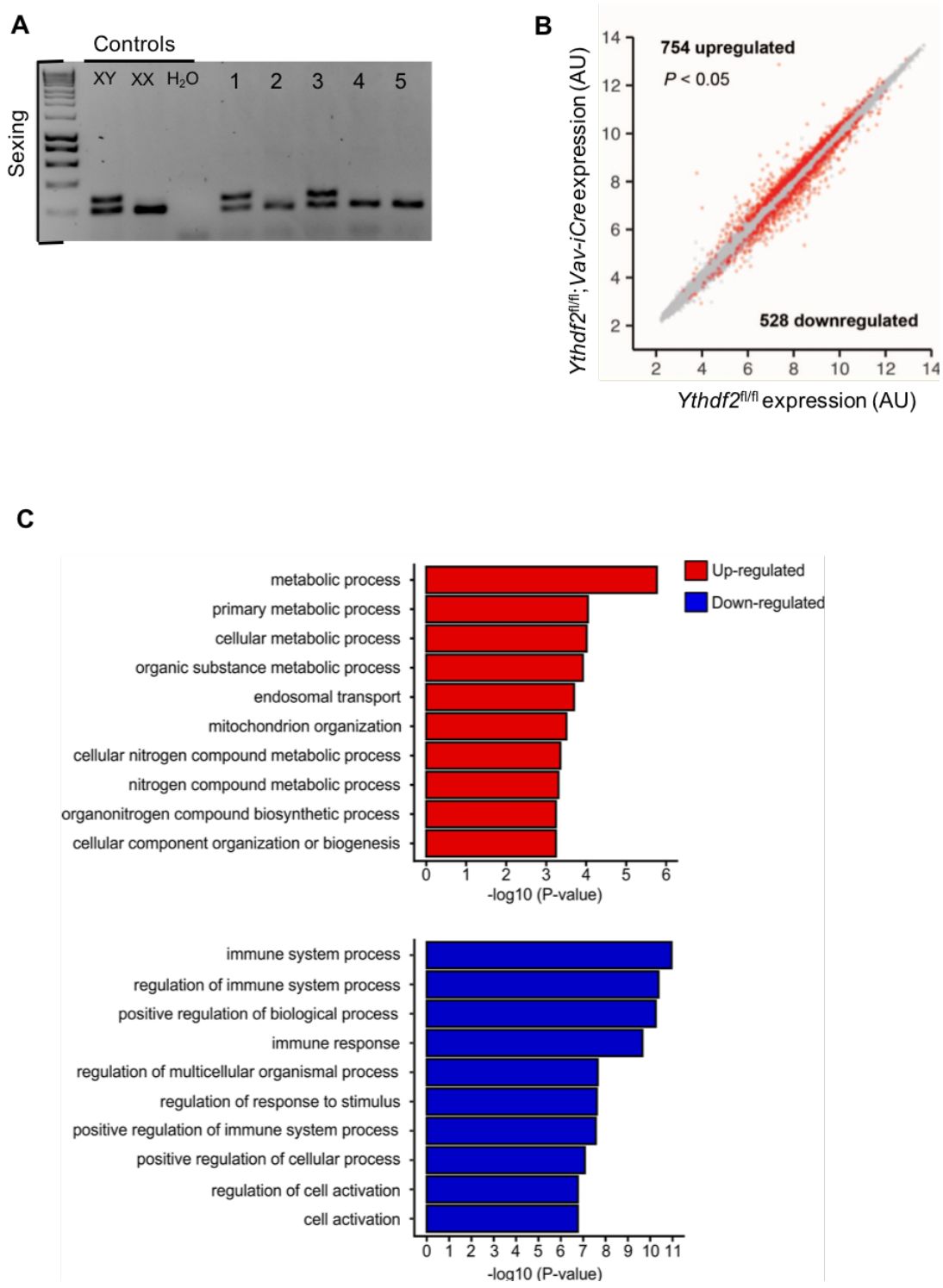

Figure 5.4.1 Loss of *Ythdf2* results in deregulated gene expression in *Ythdf2*$^{fl/fl;}$*Vav-iCre* pre-leukaemic cells. (**A**) Representative 'Sexing PCR' gel showing PCR amplification of genomic DNA from foetal liver c-Kit^{+} cells. Generated

genotypes were XX (female) or XY (male). (**B**) Transcript expression scatter plot from *Ythdf2*$^{fl/fl}$ and *Ythdf2*$^{fl/fl;}$*Vav-iCre* pre-leukaemic cells. Significantly upregulated or downregulated transcripts are highlighted in red (adjusted moderate t-student test, $P < 0.05$ corresponding to a fold change of ≧ 1.2). Five biological replicates were used for each condition. (**C**) Gene ontology analysis for the upregulated and downregulated genes in *Ythdf2*$^{fl/fl;}$*Vav-iCre* pre-leukaemic cells. The enrichment is presented as –log10 (*P*-value).

5.4.2 m^{6}A methylated transcripts are upregulated in *Ythdf2*-deficient pre-leukaemic cells

Having identified up- and down-regulated genes associated with *Ythdf2*-deficiency, we next sought to understand which of the deregulated transcripts could be direct targets of YTHDF2. For this purpose, m^{6}A meRIP-Seq was carried out to determine transcriptome-wide mRNA m^{6}A in *Ythdf2*$^{fl/fl}$;*Vav-iCre* compared to *Ythdf2*$^{fl/fl}$ pre-leukaemic cells (see sections **2.18** and **2.20**). This revealed the expected distribution of m^{6}A within the transcriptome, with highest m^{6}A peak occupancy around the stop codon in both genotypes (**Figure 5.4.2 A**). The consensus motif (**Figure 5.4.2 B**), and the overlap of m^{6}A peaks with separate transcript regions (5'UTR; start codon; coding sequence; stop codon; 3'UTR) (**Figure 5.4.2 C**) was as expected based on previous studies (Meyer, Saletore et al. 2012, Dominissini, Moshitch-Moshkovitz et al. 2013). Importantly, *Ythdf2* deficiency did not alter any of these parameters, and there was no significant difference in m^{6}A methylation between control and *Ythdf2*-deficient pre-LSCs. This finding was not unexpected, since *Ythdf2* functions as a 'reader' of m^{6}A, as opposed to a 'writer' or 'eraser' responsible for m^{6}A deposition or removal respectively.

Since YTHDF2 binds methylated transcripts and targets them for degradation, we predicted that loss of *Ythdf2* would be significantly associated with an upregulation of methylated transcripts. Indeed, a comparison of mRNA microarray and m^{6}A meRIP-Seq results revealed a significant enrichment for m^{6}A occupancy in the upregulated genes ($P < 0.05$, 754 genes) in *Ythdf2*$^{fl/fl}$;*Vav-iCre* pre-LSCs compared to the corresponding unchanged or downregulated gene sets (**Figure 5.4.2 D**).

Reciprocally, we analysed the transcriptome based on RNA m^{6}A modification, and found that methylated transcripts were more likely to be upregulated in *Ythdf2*$^{fl/fl}$;*Vav-iCre* pre-LSCs compared with *Ythdf2*$^{fl/fl}$ pre-LSCs (**Figure 5.4.2 E**). In fact, the level of methylation was correlated with degree of transcript upregulation (**Figure 5.4.2 F**).

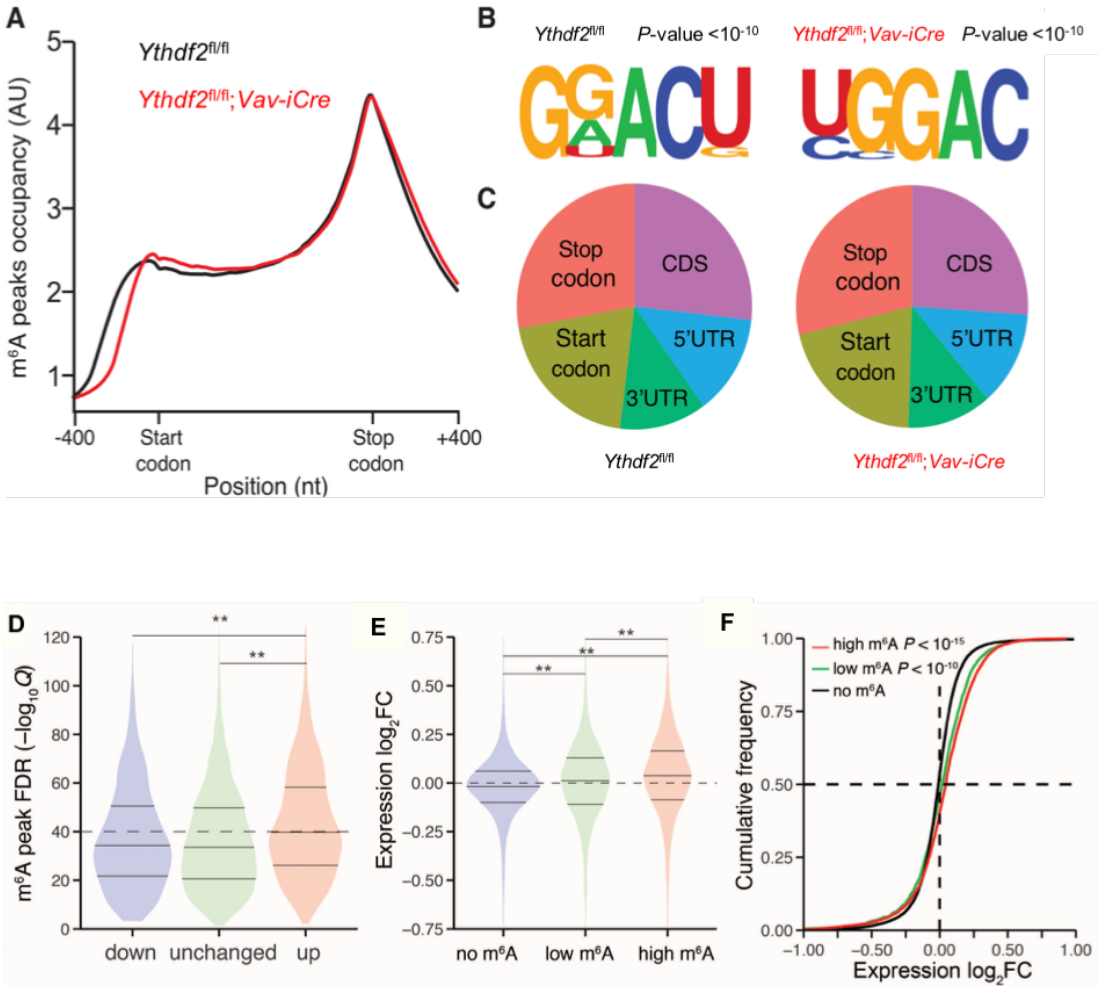

Figure 5.4.2 m^{6}A methylated transcripts are upregulated in *Ythdf2*-deficient pre-leukaemic cells. (**A**) m^{6}A peak occupancy along a transcript body model is shown for *Ythdf2*$^{fl/fl}$ (black) and *Ythdf2*$^{fl/fl;}$*Vav-iCre* (red) pre-leukaemic cells. One representative sample of three biological replicates is shown for each genotype. Transcripts models were extended 400 nucleotides upstream and downstream of the start and stop codons, respectively. (**B**) m^{6}A-seq motif enrichments and associated *P*-values are shown for each genotype. (**C**) m^{6}A peaks overlaps with different transcript regions (5'UTR; start codon; coding sequence, CDS; stop codon; 3'UTR)

are shown for each condition. (**D**) m^6A peak strength ($-\log_{10}Q$) in *Ythdf2*$^{fl/fl}$ pre-leukaemic cells for transcripts grouped according to expression changes between *Ythdf2*$^{fl/fl}$ and *Ythdf2*$^{fl/fl;}$*Vav-iCre* pre-leukaemic cells is shown (down, genes significantly downregulated in *Ythdf2*$^{fl/fl;}$*Vav-iCre* ($P < 0.05$); unchanged, genes not significantly changing in *Ythdf2*$^{fl/fl;}$*Vav-iCre*; up, genes significantly upregulated in *Ythdf2*$^{fl/fl;}$*Vav-iCre* ($P < 0.05$). ** indicates $P < 0.01$, Mann-Whitney, two-sided test). The upper and lower quartiles and the median are shown for each group. (**E**) Violin plots showing expression change between *Ythdf2*$^{fl/fl}$ and *Ythdf2*$^{fl/fl;}$*Vav-iCre* pre-leukaemic cells for not methylated (no m^6A), methylated (m^6A, $-\log_{10}Q \leq 25$) and highly methylated (m^6A high, $-\log_{10}Q > 25$) transcripts (** indicates $P < 0.01$, Mann-Whitney, two-sided test). The upper and lower quartiles and the median are indicated for each group. (**F**) Cumulative distributions of transcripts' expression change in *Ythdf2*$^{fl/fl}$ and *Ythdf2*$^{fl/fl;}$*Vav-iCre* pre-leukaemic cells for not methylated, methylated and highly methylated transcripts as in **E**.

5.4.3 m^6A methylated transcripts in pre-leukaemic cells are also upregulated in *Ythdf2*-deficient leukaemic cells

To understand whether the observations made in pre-leukaemic cells also extended to AML *in vivo*, we isolated LSCs from mice with *Meis1/Hoxa9* AML derived from *Ythdf2*$^{fl/fl}$ and *Ythdf2*$^{fl/fl}$;*Vav-iCre* pre-LSCs (culled mice, section **2.15.4**), and repeated the Affymetrix™ gene expression analyses. As in pre-leukaemic cells, LSC microarray results showed deregulated gene expression upon loss of *Ythdf2*, with 381 upregulated and 221 downregulated genes respectively ($P < 0.05$), in *Ythdf2*$^{fl/fl}$;*Vav-iCre* compared to *Ythdf2*$^{fl/fl}$ leukaemic cells (**Figure 5.4.3 A**). Furthermore, mirroring the observations made in pre-leukaemic cells, a significant enrichment for transcripts methylated in pre-LSCs was observed in upregulated genes of *Ythdf2*$^{fl/fl}$;*Vav-iCre* LSCs compared to the corresponding unchanged or downregulated gene sets (**Figure 5.4.3 B**). When analysing the leukaemic cell transcriptome based on pre-LSC RNA m^6A modification, we found that pre-LSC methylated transcripts were more likely to be upregulated in *Ythdf2*$^{fl/fl}$;*Vav-iCre* LSCs compared with *Ythdf2*$^{fl/fl}$ LSCs (**Figure 5.4.3 C**), and once again showed that methylation was correlated with degree of transcript upregulation (**Figure 5.4.3 D**).

Based on these results, we concluded that the relationship between m^{6}A occupancy and increased transcript dosage was present in both pre-leukaemic and leukaemic *Ythdf2*$^{fl/fl}$;*Vav-iCre* cells.

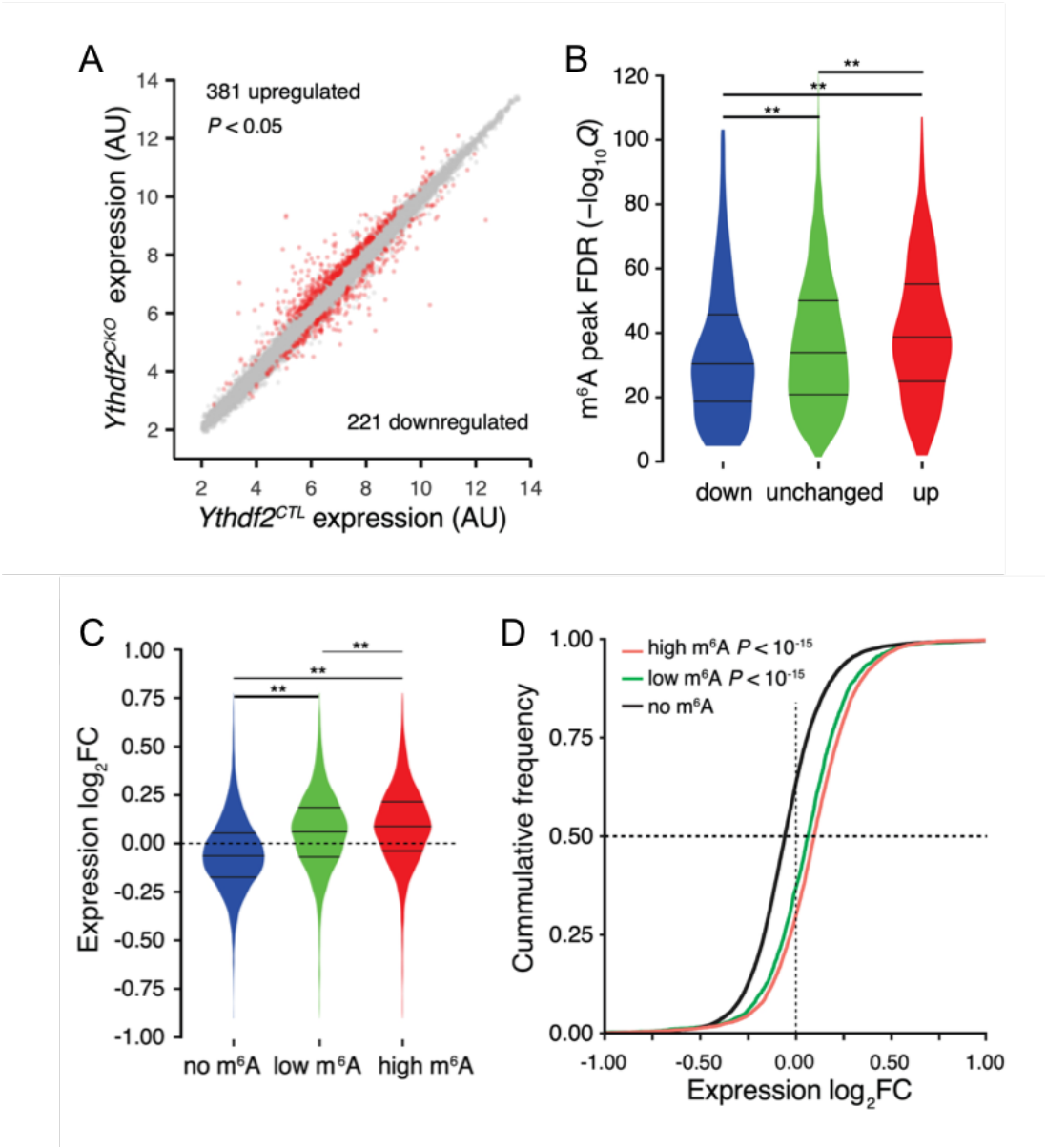

Figure 5.4.3 m^{6}A methylated transcripts in pre-leukaemic cells are also upregulated in *Ythdf2*-deficient leukaemic cells. (**A**) Transcript expression scatter plot from *Ythdf2*$^{fl/fl}$ and *Ythdf2*$^{fl/fl;}$*Vav-iCre* leukaemic cells. Significantly upregulated or downregulated transcripts are highlighted in red (Adjusted moderate t-student test, $P < 0.05$). Four biological replicates were used for each condition. (**B**) m^{6}A peak significance (-log$_{10}$Q) in pre-leukaemic cells for transcripts grouped according to

expression changes between *Ythdf2*$^{fl/fl}$ and *Ythdf2*$^{fl/fl;}$*Vav-iCre* leukaemic cells is shown (down, genes significantly downregulated in *Ythdf2*$^{fl/fl;}$*Vav-iCre* ($P < 0.05$); unchanged, genes not significantly changing in *Ythdf2*$^{fl/fl;}$*Vav-iCre*; up, genes significantly upregulated in *Ythdf2*$^{fl/fl;}$*Vav-iCre* ($P < 0.05$). ** indicates $P < 0.01$, Mann-Whitney, two-sided test). The upper and lower quartiles and the median are shown for each group. (**C**) Violin plots showing expression change between *Ythdf2*$^{fl/fl}$ and *Ythdf2*$^{fl/fl;}$*Vav-iCre* leukaemic cells for pre-leukaemic cells not methylated (no m^{6}A), methylated (m^{6}A, $-\log_{10}Q \leq 25$) and highly methylated (m^{6}A high, $-\log_{10}Q > 25$) transcripts (** indicates $P < 0.01$, Mann-Whitney, two-sided test). The upper and lower quartiles and the median are shown for each group. (**D**) Cumulative distribution of transcripts' expression change in *Ythdf2*$^{fl/fl}$ and *Ythdf2*$^{fl/fl;}$*Vav-iCre* pre-leukaemic cells for not methylated, methylated and highly methylated transcripts as in **C**.

5.4.4 *Ythdf2* loss increases half-life of methylated transcripts

Since YTHDF2 is responsible for targeting methylated transcripts for decay, we predicted that the upregulation of m^{6}A-containing transcripts in the absence of *Ythdf2* was likely to be due to an increase in their half-life. We therefore measured mRNA half-life transcriptome-wide in pre-leukaemic cells using SLAM-Seq (Herzog, Reichholf et al. 2017), as described in sections **2.21** and **5.1.2.3**.

SLAM-Seq revealed an overall modest increase in mRNA half-life in *Ythdf2*$^{fl/fl}$;*Vav-iCre* pre-LSCs (**Figure 5.4.4 A**) when compared to *Ythdf2*$^{fl/fl}$ pre-LSCs. Reassuringly, when evaluating *Ythdf2*$^{fl/fl}$ pre-LSCs, the half-lives of m^{6}A-containing transcripts were shorter than the half-lives of transcripts not containing m^{6}A (**Figure 5.4.4 B**), an observation which underscores the important role m^{6}A plays in mRNA decay under normal circumstances. The loss of *Ythdf2* extended the half-life of m^{6}A containing transcripts but not that of unmethylated transcripts (**Figure 5.4.4 C** and **D**). These findings were consistent with the theory that transcript upregulation upon loss of *Ythdf2* is through modulation of mRNA decay, specifically through an increased half-life of methylated transcripts.

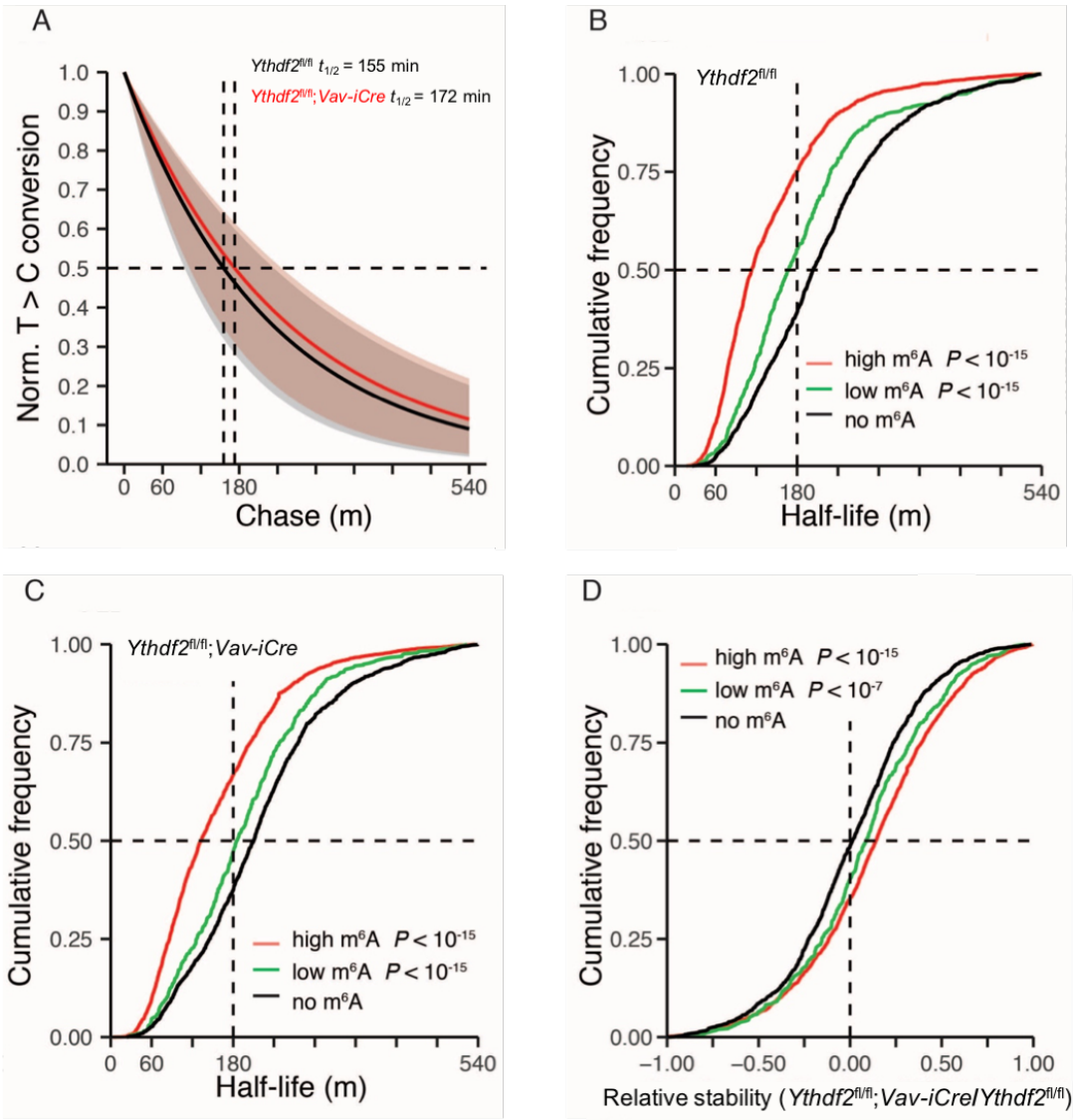

Figure 5.4.4 *Ythdf2* loss increases half-life of methylated transcripts. (**A**) Mode decay curves for *Ythdf2*$^{fl/fl}$ (black) and *Ythdf2*$^{fl/fl;}$*Vav-iCre* (red) pre-leukaemic cell transcriptomes are shown. The shaded areas indicate the first and third quantile decay curves range for each genotype. Transcript decay was estimated by the normalized cDNA T to C conversion rate at 0, 60, 180 and 540 minutes after S4U removal. Transcripts half-life modes for each genotype are indicated with horizontal dotted lines and are also shown at the panel top. (**B-C**) Cumulative distributions of transcripts' half-life in (**B**) *Ythdf2*$^{fl/fl}$ and (**C**) *Ythdf2*$^{fl/fl;}$*Vav-iCre* pre-leukaemic cells are shown for not methylated, methylated and highly methylated transcripts (as in **Figure 5.4.2 E**). The half-life change significance between the methylated and not methylated transcripts are indicated (Mann-Whitney, two-sided test). (**D**) Cumulative distributions of relative stability change between *Ythdf2*$^{fl/fl}$ and *Ythdf2*$^{fl/fl;}$*Vav-iCre* pre-leukaemic

cells are shown for not methylated, methylated and highly methylated transcripts. The relative stability change significances between the methylated and not methylated transcripts are indicated (Mann-Whitney, two-sided test).

5.4.5 *Ythdf2* loss does not alter translational efficiency

YTH domain family proteins (YTHDF1 and YTHDF3) are known to mediate m^6A dependent changes in translational efficiency. Furthermore, the tumour promoting effects of METTL enzymes in AML have been largely ascribed to m^6A dependent translational control (Barbieri, Tzelepis et al. 2017, Vu, Pickering et al. 2017). With this in mind, we sought to investigate whether the effect of *Ythdf2*-deficiency in this context might also be mediated in part by changes in translational efficiency. To do so, we employed RIBO-Seq (Reid, Shenolikar et al. 2015), as described in sections **2.22** and **5.1.2.4**.

Our results indicated that loss of *Ythdf2* does not affect translational efficiency. There was no gross difference in translational efficiency between *Ythdf2*$^{fl/fl}$ and *Ythdf2*$^{fl/fl}$;*Vav-iCre* pre-LSCs (**Figure 5.4.5 A**). Based on a cut-off defined as a significant two-fold reduction in translational efficiency, approximately 19 of 9474 analysed transcripts were less efficiently translated in *Ythdf2*$^{fl/fl}$;*Vav-iCre* pre-LSCs compared to *Ythdf2*$^{fl/fl}$ pre-LSCs, but this did not correlate with the presence of absence of m^6A. Indeed, the loss of *Ythdf2* did not alter the translational efficiency of either m^6A or non-m^6A- containing transcripts (**Figure 5.4.5 B**), for either *Ythdf2*$^{fl/fl}$ or *Ythdf2*$^{fl/fl}$;*Vav-iCre* pre-LSCs.

The combination of results obtained by SLAM-Seq (section **5.4.4**) and RIBO-Seq demonstrate that YTHDF2 regulates the leukaemic transcriptome through modulation of mRNA decay, and not via modulating mRNA translation efficiency.

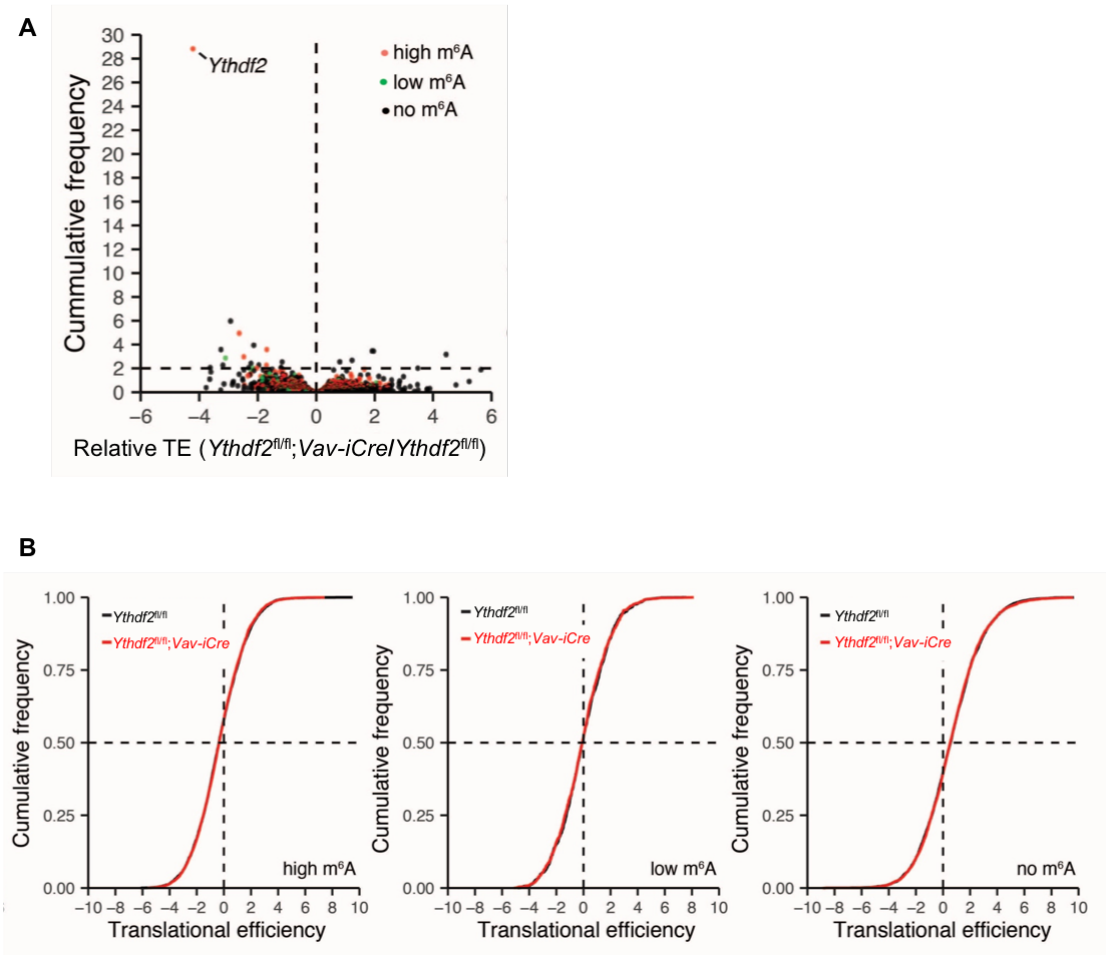

Figure 5.4.5 *Ythdf2* loss does not alter translational efficiency. (**A**) Volcano plot of translational efficiency change between *Ythdf2*$^{fl/fl}$ and *Ythdf2*$^{fl/fl;}$*Vav-iCre* pre-leukaemic cells. Not methylated, methylated and highly methylated transcripts (defined as in **Figure 6.4.2 E**), are shown in black, green and red, respectively. The number of transcripts with a significant two-fold reduction in translational efficiency is indicated for each group. (**B**) Cumulative distributions of translational efficiency of not methylated (right panel), methylated (centre panel) and highly methylated transcripts (left panel) are shown for *Ythdf2*$^{fl/fl}$ (black) and *Ythdf2*$^{fl/fl;}$*Vav-iCre* (red) pre-leukaemic cells.

5.4.6 Interrogation of *Ythdf2* molecular pathways

The work described in this section was carried out in collaboration with colleagues (see **5.3**), and is described for completeness, and in order to explain the experiments performed in section **5.4.7**.

We next sought to understand if the m^{6}A and *Ythdf2*-deregulated transcripts in our mouse AML model are also relevant to human AML. We found that the population of transcripts which were significantly upregulated in the *Ythdf2*$^{fl/fl}$;*Vav-iCre* pre-leukaemic cells were also preferentially methylated in the NOMO-1 and MA9.3ITD human AML cell lines (**Figure 5.4.6 A**). In order to focus our mechanistic studies, we defined selection criteria with which to group genes for further study. Upregulated genes in *Ythdf2*$^{fl/fl}$;*Vav-iCre* pre-leukaemic cells, which were also highly methylated in *Ythdf2*$^{fl/fl}$ pre-leukaemic cells and methylated in human MA9.3ITD and NOMO-1 cells were selected for further study (**Figure 5.4.6 B** and **Appendix 2**). There were 754 genes upregulated in *Ythdf2*$^{fl/fl}$;*Vav-iCre* pre-leukaemic cells, and of these 344 genes were high in m^{6}A, but only 292 genes were also methylated in MA9.3ITD and NOMO-1 cells. These 292 genes were selected for further study.

To understand the molecular pathways that these common mouse and human m^{6}A transcripts underpin, we performed ConcensusPathDB (CPDB) network analysis. CPDB is a meta-database (human, mouse and yeast) which integrates a physical protein interactions, metabolic and signalling reactions, and gene regulatory interactions in a functional association network (Kamburov, Pentchev et al. 2010, Kamburov, Pentchev et al. 2011, Kamburov, Stelzl et al. 2012). The results of our CPDB network analysis showed enrichment for RNA processing, mitochondrial function, ubiquitination, and also TNF signalling (**Figure 5.4.6 C**).

To understand why the loss of *Ythdf2* is correlated with a weak leukaemogenic potential, we interrogated gene sets from human AML samples associated with different leukaemogenic potential upon xenotransplantation. The LSC signature gene set we employed was a 17-gene stemness score for rapid determination of risk in AML, published in Nature by Ng S., et al. (Ng, Mitchell et al. 2016). In this study Ng et al. used samples from 78 human patients to identify 17 genes associated with LSC activity in AML, and validated their findings by xenotransplantation. Using this LSC signature gene set to analyse the gene lists, we performed a Gene Set Enrichment Analysis (GSEA) study of genes positively or negatively correlated with *YTHDF2* across more than 1732 human AML samples (see **2.23)**. GSEA is an analytical method for interpreting gene expression data in order to determine biological relevance from genome-wide sequencing data. The method works by focusing on

gene sets i.e. groups of genes that share common biological function, chromosomal location, or regulation (Subramanian, Tamayo et al. 2005).

The results of our GSEA are illustrated in the right panel of **Figure 5.4.6 B** and are listed in **Appendix 3**. We found that transcripts which negatively correlate with *YTHDF2* expression are highly associated with the loss of leukaemogenic potential (**Figure 5.4.6 D**). In this way, when an AML sample expresses low amounts of *YTHDF2*, transcripts associated with the loss of leukaemogenic potential have greater expression. In contrast, transcripts whose expression correlates with that of *YTHDF2* are depleted from the pool of transcripts associated with weak LSC activity (**Figure 5.4.6 B**). In summary therefore, *YTHDF2* negatively regulates transcripts whose expression limits LSC activity.

Inspecting the genes that negatively correlate with *YTHDF2* expression in human AML, contain m^6A in both mouse and human AML, are upregulated in *Ythdf2*$^{fl/fl}$;*Vav-iCre* LSCs, and are associated with weak LSC function, we identified TNF receptor 2 (TNFR2) encoded by the *Tnfrsf1b* (*Tnfrsf2*) gene (**Figure 5.4.6 D**). We focused our subsequent experiments on TNFR2 as TNF signalling was also identified as a node in the CPDB network analysis (**Figure 5.4.6 C**). Furthermore, TNFR2 together with TNFR1 has been shown previously to restrict the proliferation and survival of leukaemic cells (Hockendorf, Yabal et al. 2016). Notably, *TNFRSF1B* is highly methylated in both mouse pre-leukaemic cells and human AML cell lines (**Figure 5.4.6 E**). Furthermore, *TNFRSF1B* expression is significantly decreased in AML patient samples compared to non-leukaemic controls (**Figure 5.4.6 F**), and its expression negatively correlates with LSC activity (**Figure 5.4.6 G**). In addition, RIP-qPCR (carried out by David Wotherspoon, (Paris, Morgan et al. 2019)) revealed co-precipitation of the *Tnfrsf1b* transcript with YTHDF2 in mouse pre-leukaemic cells (**Figure 5.4.6 H**). Finally, concurrent with the increased half-life of *Tnfrsf1b* transcript (**Figure 5.4.6 I**), the surface expression of TNFR2 is upregulated on mouse *Ythdf2*$^{fl/fl}$;*Vav-iCre* pre-leukaemic cells (**Figure 5.4.6 J**). We therefore tested whether TNF stimulation had a differential impact on *Ythdf2*$^{fl/fl}$ and *Ythdf2*$^{fl/fl}$;*Vav-iCre* pre-leukaemic cells. Indeed, the loss of *Ythdf2* rendered cells more sensitive to TNF-induced apoptosis (**Figure 5.4.6 K**). Based on these findings, we concluded that the TNFR2 pathway contributes at least one molecular mechanism by which the loss of *Ythdf2* negatively impacts on AML.

Further work therefore focused on the TNFR2 pathway (*Tnfrsf1b* transcript) in *Ythdf2*$^{fl/fl}$ and *Ythdf2*$^{fl/fl}$;*Vav-iCre* pre-leukaemic cells.

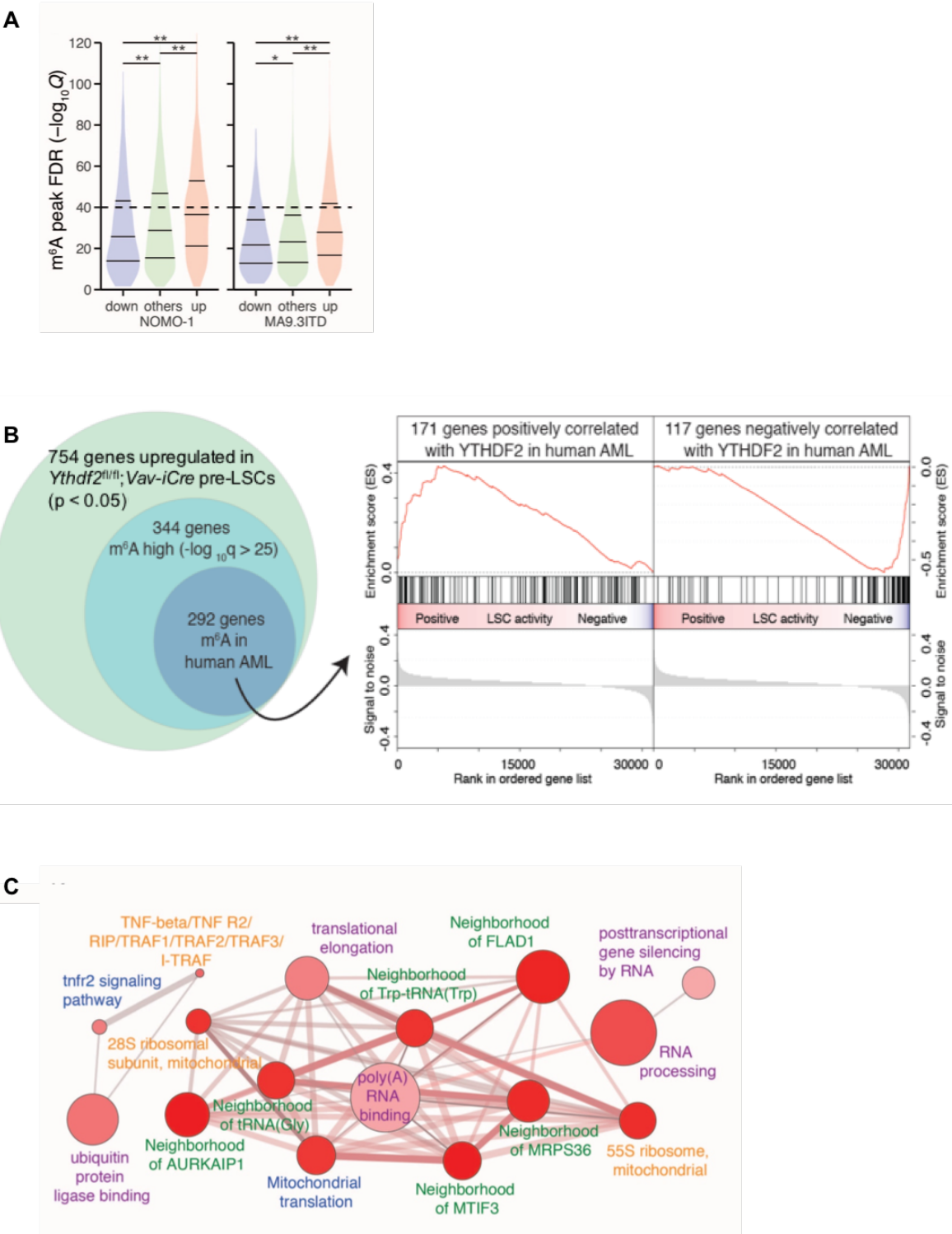

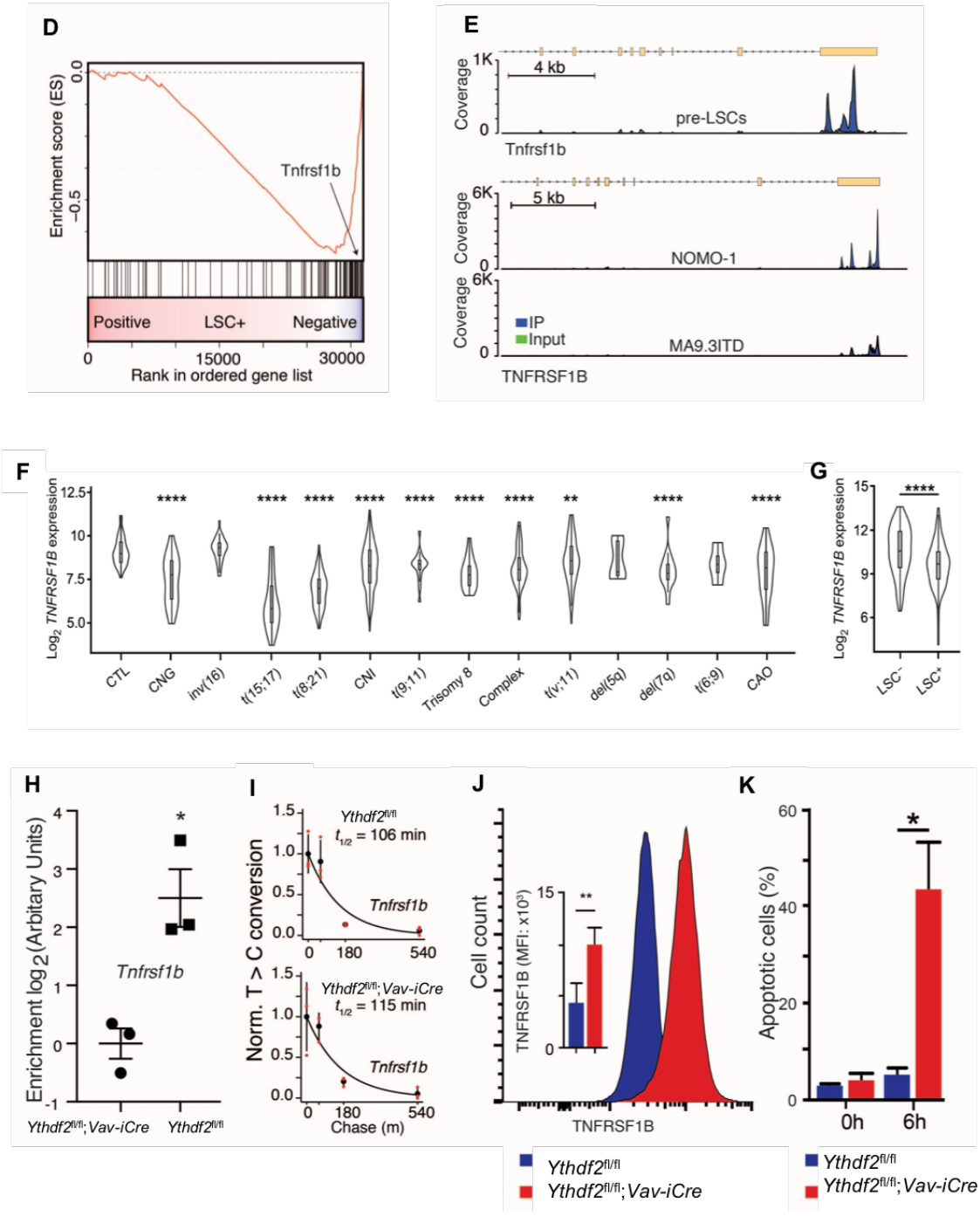

Figure 5.4.6 *TNFRSF1B* gene expression is decreased in different AML subtypes and negatively correlates with LSC activity. (**A**) Violin plots of m^{6}A peak strength (-log$_{10}$Q) in MA9.3ITD and NOMO-1 cells for transcripts grouped according to expression changes between *Ythdf2*$^{fl/fl}$ and *Ythdf2*$^{fl/fl;}$*Vav-iCre* pre-leukaemic cells (defined as in **Figure 5.4.2 E**) are shown. (*, $P < 0.05$, **, $P < 0.01$, Mann-Whitney, two-sided test). The upper and lower quartiles and the median are indicated for each group. (**B**) Left, overview of gene selection criteria for this study. Upregulated genes

in *Ythdf2*$^{fl/fl;}$*Vav-iCre* pre-leukaemic cells, highly methylated in *Ythdf2*$^{fl/fl}$ pre-leukaemic cells and methylated in human MA9.3ITD and NOMO-1 cells were further analyzed. Right, GSEA study of genes positively or negatively correlated with *YTHDF2* across more than 1732 human AML samples. The LSC signature (Ng, Mitchell et al. 2016) gene set was used to analyze the gene lists. (**C**) CPDB analysis of genes significantly upregulated in *Ythdf2*$^{fl/fl;}$*Vav-iCre* pre-leukaemic cells ($P < 0.05$) with high m^{6}A levels ($-\log_{10}Q > 25$) in mouse pre-leukaemic cells and also methylated in human AML (MA9.3ITD and NOMO-1) cell lines. (**D**) GSEA using LSC signature gene set for genes defined in (**C**) and that negatively correlate with *YTHDF2* expression in human AML samples (**E**) m^{6}A IP read coverage (blue) from *Ythdf2*$^{fl/fl}$ pre-leukaemic cells along the *Trnfrs1b* genomic locus (upper panel) and m^{6}A IP read coverage from NOMO-1, and MA9.3ITD cells along *TNFRSF1B* genomic locus (lower panels) are shown. Input coverage is shown in green. Gene models are depicted on top. (**F**) *TNFRSF1B* gene expression in control (CTL) and different cytogenetic subgroups of human AML bone marrow samples. Violin plots show the distribution of $\log_2$ expression values. Horizontal line in the boxplots indicates median. **, P<0.01; ****, P<0.0001. CNG, cytologically normal with good prognosis; CNI, cytologically normal with intermediate prognosis; CAO, cytologically abnormal not otherwise specified. (**G**) *TNFRSF1B* gene expression in primitive AML cell compartments with (LSC$^+$) and without (LSC$^-$) leukaemic engraftment potential. ****, P<0.0001. (**H**) *Tnfrsf1b* enrichment in YTHDF2 immuno-precipitates from *Ythdf2*$^{fl/fl}$ pre-leukaemic cells is shown. Tnfrsf1b background levels were determined using *Ythdf2*$^{fl/fl;}$*Vav-iCre* pre-leukaemic cells. Data are mean ± s.e.m., n = 3. *, P < 0.05. (**I**) Decay curves for *Trnfrs1b* in *Ythdf2*$^{fl/fl}$ (top panel) and *Ythdf2*$^{fl/fl;}$*Vav-iCre* (bottom panel) pre-leukaemic cells transcriptomes are shown. Transcript decay was estimated by the normalized cDNA T to C conversion rate at 0, 60, 180 and 540 minutes after S4U removal. The centre value and the error bars at each time point indicate the conversion rate mean and standard deviation, respectively. The conversion rates for each biological replicate are indicated with dots. For each genotype, the *Trnfrs1b* half-life is also shown. (**J**) Representative FACS plots showing the expression of TNFRSF1B on the cell surface of *Ythdf2*$^{fl/fl}$ and *Ythdf2*$^{fl/fl;}$*Vav-iCre* pre-leukaemic cells. The inner graph displays the quantification of TNFRSF1B expression. Data are mean ± s.e.m, n = 4 per genotype. **, $P < 0.01$. (**K**) Percentage of Annexin V$^+$DAPI$^-$ *Ythdf2*$^{fl/fl}$ and *Ythdf2*$^{fl/fl;}$*Vav-iCre* pre-leukaemic cells treated with 10 ng/ml TNF-α at 0 and 6-hour timepoints are shown. Data are mean ± s.e.m., n = 3. *, $P < 0.05$.

5.4.7 *Tnfrsf1b* knockdown does not fully rescue impaired leukaemic transformation potential of *Ythdf2*-deficient cells *in vitro*, or delayed leukaemic development *in vivo*

In order to test the hypothesis that TNFR2 upregulation contributes to the impaired leukaemic potential of *Ythdf2*$^{fl/fl}$;*Vav-iCre* pre-LSCs, we attempted to rescue the phenotype through short hairpin RNA (shRNA) mediated knockdown of *Tnfrsf1b.* This is a method of RNA silencing based on expression of shRNAs from the RNA polymerase III promoter (Paddison, Caudy et al. 2002). In our case, we used the HIV-based third generation transfer plasmid *pLKO.1 puro* for cloning and expressing the shRNA sequences with which to knockdown *Tnfrsf1b* (Stewart, Dykxhoorn et al. 2003).

Meis1/Hoxa9 transformed *Ythdf2*$^{fl/fl}$ and *Ythdf2*$^{fl/fl}$;*Vav-iCre* pre-LSCs were generated as previously described (see sections **2.11- 2.13**). Control *Ythdf2*$^{fl/fl}$ pre-LSCs (*n*=2 biological replicates) were then transduced with lentivirus carrying one of three *Tnfrsf1b* knockdown shRNAs (KD shRNA1-3), or control shRNA (CTL) (see sections **2.12** and **2.17**). Transduced cells were selected based on puromycin resistance, and subsequently stained with antibody against TNFR2 and analysed by flow cytometry (see section **2.8**). When compared with CTL-transduced pre-LSCs (CTL pre-LSCs), surface expression of TNFR2 was significantly reduced following *Tnfrsf1b* knockdown with shRNA3, but not with shRNA1 and shRNA2 (**Figure 5.4.7 A**). Further experiments were therefore carried out with shRNA3 transduced cells only, hence referred to as 'knockdown' pre-LSCs (KD pre-LSCs).

Ythdf2$^{fl/fl}$ and *Ythdf2*$^{fl/fl}$;*Vav-iCre* pre-LSCs (*n* = 5 biological replicates each) were transduced with lentivirus carrying *Tnfrsf1b* knockdown shRNA3 (validated as described above) or control shRNA (CTL). Transduced cells were selected based on puromycin resistance, and subsequently stained with antibody against TNFR2 and analysed by flow cytometry. As demonstrated previously (**Figure 5.4.6 J)**, the surface expression of TNFR2 was upregulated on *Ythdf2*$^{fl/fl}$;*Vav-iCre* pre-LSCs when compared with *Ythdf2*$^{fl/fl}$ pre-LSCs. (**Figure 5.4.7 B)**. Following knockdown with shRNA3, surface expression of TNFR2 was reduced in *Ythdf2*$^{fl/fl}$;*Vav-iCre* pre-LSCs, and although this reduction did not attain significance at this stage (CTL *Ythdf2*$^{fl/fl}$;*Vav-*

iCre pre-LSCs versus KD *Ythdf2*$^{fl/fl}$;*Vav-iCre* pre-LSCs p = 0.0556), the difference between CTL *Ythdf2*$^{fl/fl}$ pre-LSCs and KD *Ythdf2*$^{fl/fl}$;*Vav-iCre* pre-LSCs was no longer present (CTL *Ythdf2*$^{fl/fl}$ pre-LSCs versus CTL *Ythdf2*$^{fl/fl}$;*Vav-iCre* pre-LSCs p = 0.0079, whereas CTL *Ythdf2*$^{fl/fl}$ pre-LSCs versus KD *Ythdf2*$^{fl/fl}$;*Vav-iCre* pre-LSCs p = 0.0952 (**Figure 5.4.7 B)**.

CTL and KD pre-LSCs (both *Ythdf2*$^{fl/fl}$ and *Ythdf2*$^{fl/fl}$;*Vav-iCre* genotypes of each) were serially re-plated as described previously (see section **2.13.2**) as an *in vitro* measure of self-renewal capacity. Colony counts at CFC1, CFC2 and CFC3 showed no significant differences between CTL and KD pre-LSCs for either *Ythdf2*$^{fl/fl}$ or *Ythdf2*$^{fl/fl}$;*Vav-iCre* genotypes (**Figure 5.4.7 C**). There was a trend towards increased colony numbers at CFC3 in *Ythdf2*$^{fl/fl}$;*Vav-iCre* pre-LSCs following *Tnfrsf1b* knockdown, but this was not significant. Repeated antibody staining and flow cytometric analysis of CFC3 pre-LSCs (**Figure 5.4.7 D**) showed a significant reduction of surface expression of TNFR2 in *Ythdf2*$^{fl/fl}$;*Vav-iCre* pre-LSCs following shRNA-mediated *Tnfrsf1b* knockdown (CTL *Ythdf2*$^{fl/fl}$;*Vav-iCre* pre-LSCs versus KD *Ythdf2*$^{fl/fl}$;*Vav-iCre* pre-LSCs p = 0.0159), ruling out escape from knockdown as a cause of the failure to demonstrate a significant rescue effect.

In order to investigate the effect of *Tnfrsf1b* knockdown *in vivo*, *Meis1/Hoxa9* transformed CTL and KD pre-LSCs (both *Ythdf2*$^{fl/fl}$ and *Ythdf2*$^{fl/fl}$;*Vav-iCre* genotypes of each), were transplanted to irradiated primary recipients, exactly as described previously (see section **2.15.2**).

Serial peripheral blood analysis showed no difference in the engraftment of KD pre-LSCs compared with their CTL counterpart, for both *Ythdf2*$^{fl/fl}$ and *Ythdf2*$^{fl/fl}$;*Vav-iCre* genotypes (**Figure 5.4.7 E**), and subsequently no difference in the Kaplan Meier survival curve (**Figure 5.4.7 F**). As observed previously, there was a significant difference in both engraftment and overall survival between *Ythdf2*$^{fl/fl}$ and *Ythdf2*$^{fl/fl}$;*Vav-iCre* pre-LSCs (**Figures 5.4.7 E-F**), which knock down of *Tnfrsf1b* failed to rescue.

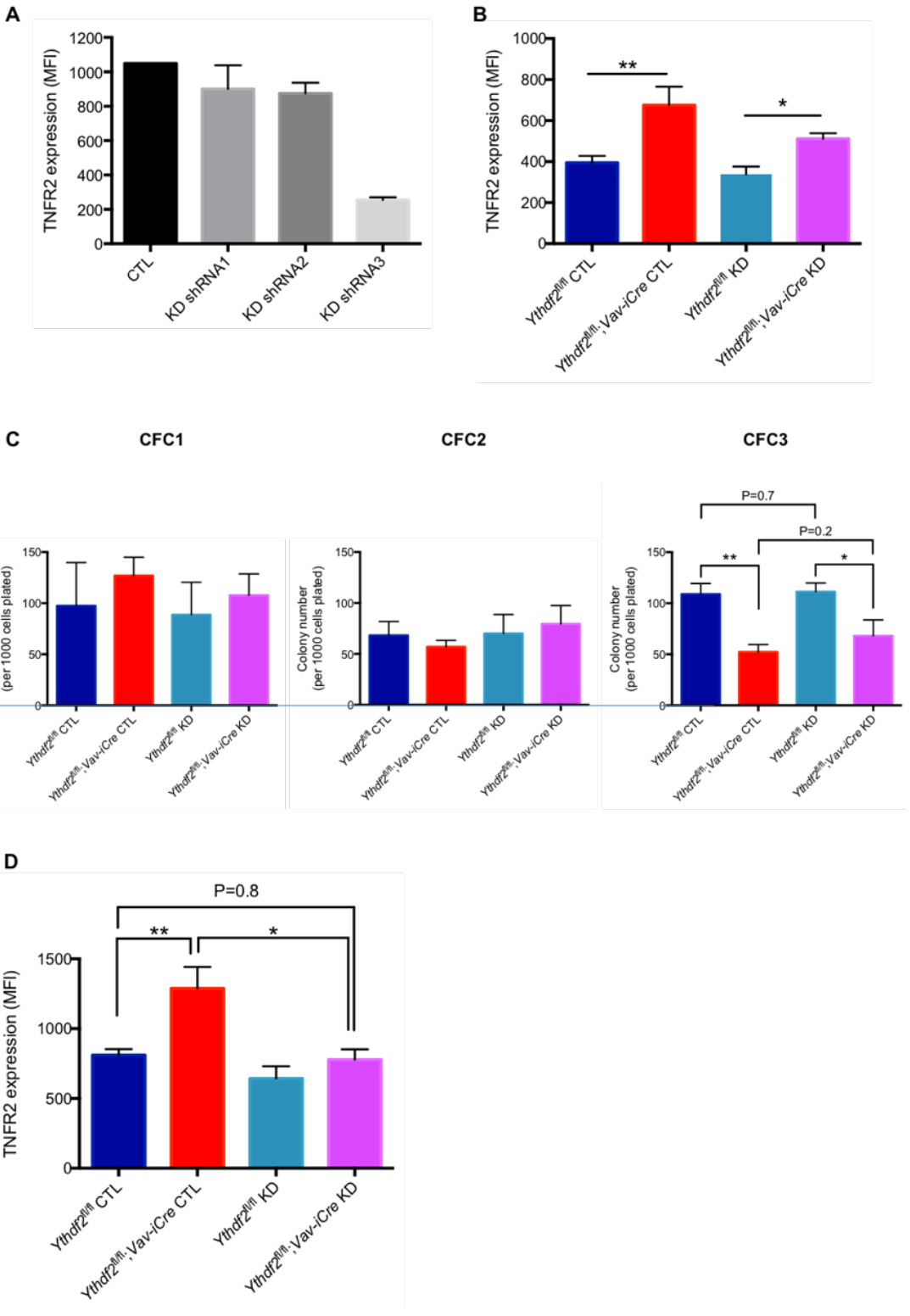
A
TNFR2 expression (MFI)
1200
1000
800
600
400
200
0
CTL
KD shRNA1
KD shRNA2
KD shRNA3
B
TNFR2 expression (MFI)
1000
800
600
400
200
0
**
*
Ythdf2fl/fl CTL
Ythdf2fl/fl;Vav-iCre CTL
Ythdf2fl/fl KD
Ythdf2fl/fl;Vav-iCre KD
C
CFC1
CFC2
CFC3
Colony number (per 1000 cells plated)
150
100
50
0
P=0.7
P=0.2
**
*
Ythdf2fl/fl CTL
Ythdf2fl/fl;Vav-iCre CTL
Ythdf2fl/fl KD
Ythdf2fl/fl;Vav-iCre KD
D
P=0.8
**
*
TNFR2 expression (MFI)
1500
1000
500
0
Ythdf2fl/fl CTL
Ythdf2fl/fl;Vav-iCre CTL
Ythdf2fl/fl KD
Ythdf2fl/fl;Vav-iCre KD

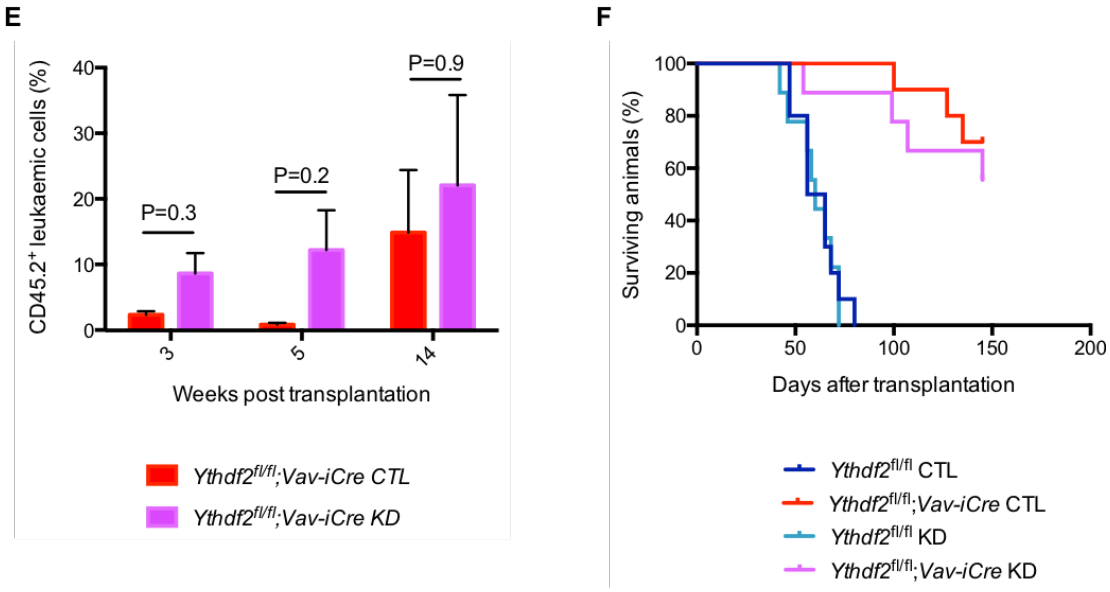

Figure 5.4.7 The impact of *Tnfrsf1b* knockdown on *Ythdf2*-deficient pre-leukaemic cell colony formation *in vitro* and engraftment *in vivo*. (**A**) TNFR2 cell surface protein expression in *Meis1*/*Hoxa9*-transduced pre-leukaemic cells co-transduced with lentiviruses expressing scrambled shRNA (CTL) or shRNAs targeting *Tnfrsf1b* (KD shRNA1-3). Data are mean ± s.e.m., *n* = 2. (**B**) TNFR2 cell surface protein expression in *Meis1*/*Hoxa9*-transduced pre-leukaemic cells co-transduced with lentiviruses expressing scrambled shRNA (CTL) or shRNA targeting *Tnfrsf1b* (KD). Data are mean ± s.e.m., *n* = 5. *, P < 0.05; **, P<0.01. (**C**) Number of CFC1-3 colonies generated by cells shown in panel B. (**D**) TNFR2 cell surface protein expression of CFC3 cells shown in panel C. Data are mean ± s.e.m., *n* = 5. *, P < 0.05; **, P<0.01. (**E**) Pre-leukaemic cells shown in panels C-D were transplanted into recipient mice. The graphs show leukaemic engraftment 3, 5 and 14 weeks after transplantation. Data are mean ± s.e.m., *n* = 8 recipients per genotype. (**F**) In progress Kaplan-Meier survival curve of the recipient mice (*n* = 8 per genotype) (experiment still underway).

5.5 Discussion

This chapter describes the results of our mechanistic studies into the requirement for YTHDF2 in AML. Using a combination of transcriptome profiling and m^{6}A meRIP-Seq, we identified YTHDF2 targets, including *Tnfrsf1b*. SLAM-Seq and RIBO-Seq were then carried out to investigate mRNA decay kinetics and translation respectively. Unlike results of studies into m^{6}A dependent METTL enzyme functions in AML (Lin,

Choe et al. 2016, Barbieri, Tzelepis et al. 2017, Vu, Pickering et al. 2017, Weng, Huang et al. 2018), our RIBO-Seq results indicated that YTHDF2 does not significantly impact mRNA translation. In contrast, SLAM-Seq results showed that m^6A-directed YTHDF2-mediated mRNA decay regulates the leukaemic transcriptome.

Our results are consistent with those of Wang et al. who used a combination of ribosome profiling and RNA-Seq on *YTHDF2* knock down and control cells to show that YTHDF2 is primarily involved in RNA degradation, not translation (Wang, Lu et al. 2014). In this study, Wang et al. used two independent methods (PAR-CLIP and RIP-Seq) to look at YTHDF2 binding sites, as well as m^6A meRIP-Seq to determine transcriptome wide methylation. They identified over 3000 YTHDF2 targets, mostly mRNA (but also non coding RNAs) with a conserved core motif of G(m^6A)C, predominantly around the stop codon and 3'UTR of mRNAs. The subsequently showed that the carboxy (C) terminal of YTHDF2 selectively binds methylated mRNA, whilst the amino (N) terminal localises the mRNA to RNA decay sites (Wang, Lu et al. 2014), known as processing (P) bodies.

Du et al. then reported that methylated mRNAs show accelerated YTHDF2-dependent deadenylation, mediated by the CCR4-NOT complex (Du, Zhao et al. 2016). They showed that YTHDF2 recruits the CCR4-NOT complex by a direct interaction between the YTHDF2 N terminus and the SH domain of the CNOT1 subunit, which is essential for the deadenylation of m^6A containing RNAs by CAF1 and CCR4 (Du, Zhao et al. 2016). Deadenylation is the commonest pathway by which eukaryotic mRNA degradation occurs, initiated by shortening of the protective 3' polyA tail (Garneau, Wilusz et al. 2007)

Wang et al. and Du et al. used non leukaemic cell lines (HeLa) to show that YTHDF2 regulates the stability of m^6A modified mRNAs (Wang, Lu et al. 2014, Du, Zhao et al. 2016). In our study, we confirmed that the same is true in the context of AML.

Our microarray results identified a large number of deregulated genes in *Ythdf2*-deficient pre-LSCs compared to wild type controls, including 754 upregulated and 528 downregulated genes. Subsequently, m^6A meRIP-Seq showed that methylated transcripts were more likely to be upregulated in *Ythdf2*$^{fl/fl}$;*Vav-iCre* pre-LSCs

compared with *Ythdf2*$^{fl/fl}$ pre-LSCs. To direct our investigations towards the most promising of these candidate genes, we employed several techniques to stratify and refine our results. Firstly, although there were 754 genes upregulated in *Ythdf2*$^{fl/fl}$;*Vav-iCre* pre-leukaemic cells, only 344 of these genes were high in m^{6}A, and only 292 genes were also methylated in MA9.3ITD and NOMO-1 cells (human AML cell lines). These 292 genes were chosen for further study. CPDB network analysis showed enrichment for RNA processing, mitochondrial function, ubiquitination, and also TNF signalling. Next, GSEA was carried out as another means of interpreting gene expression data, using a 17 essential gene set signature derived from human AML cases to establish YTHDF2 target transcripts associated with weak LSC function. The combination of these analyses, and human AML data sets, identified TNF receptor 2 (TNFR2) encoded by the *Tnfrsf1b* gene, as a strong YTHDF2 target in AML.

TNF is a pleiotropic cytokine signals which plays an important role in immune and inflammatory responses (Sedger and McDermott 2014). TNF signals through two receptors, TNFRSF1A (TNFR1) and TNFRSF1B (TNFR2), which have been reported as having differing roles. TNFR1 has an intracellular death domain and is involved in apoptosis signalling, whilst TNFR2 is implicated in the promotion of cellular proliferation (Aggarwal 2003). However, given the documented cross talk, including ligand passing between the receptors (Tartaglia, Pennica et al. 1993), it is likely that some of the functions of TNF may be dependent on expression of both receptors simultaneously.

TNF has been implicated previously in the control of both normal and malignant haematopoiesis. Several groups have shown that TNF has the ability to suppress mouse and human HSC maintenance *in vitro* (Broxmeyer, Williams et al. 1986, Zhang, Harada et al. 1995, Bryder, Ramsfjell et al. 2001, Dybedal, Bryder et al. 2001). More recently, Pronk et al. reported that both TNFR1 and TNFR2 restrict the self-renewal capacity of healthy HSPCs *in vivo* (Pronk, Veiby et al. 2011). These authors showed that BM cells deficient for both TNFR1 (*Tnfrsf1a*$^{-/-}$) and TNFR2 (*Tnfrsf1b*$^{-/-}$) receptors, hereafter referred to as TNFR double KO (*Tnfrsf1-dKO),* exhibited a significant competitive advantage over control BM cells in their ability to reconstitute myeloid and lymphoid cell lineages in myeloablated wild type recipients. A less pronounced, but still significant, competitive advantage was also seen for BM cells deficient in either *Tnfrsf1a* or *Tnfrsf1b* (Pronk, Veiby et al. 2011).

However, other groups have shown contrasting effects of TNF on HSCs. *In vitro*, Caux et al. reported a stimulatory role for TNF-α on human HSPCs (Caux, Saeland et al. 1990). *In vivo*, Rebel at al showed a fourfold decrease in the number of *Tnfrsf1a*-deficient HSCs in a competitive repopulating assay, and impaired self-renewal ability of *Tnfrsf1a*-deficient HSCs in secondary BM transplantation experiments (Rebel, Hartnett et al. 1999). In this study, adult *Tnfrsf1a*-deficient mice had increased marrow cellularity and increased numbers of myeloid and erythroid colony forming progenitor cells, paralleled by elevated peripheral blood cell counts. In contrast to the increased myeloid compartment, pre-B CFCs were deficient in older *Tnfrsf1a*-deficient mice (Rebel, Hartnett et al. 1999). More recent work by Pearl-Yafe et al. also indicated a supportive role for TNFRs in murine HSPC function in the early stages of engraftment following BM transplantation (Pearl-Yafe, Mizrahi et al. 2010).

Very recently, Yamashita and Passegué reported a complex role for TNF-α in haematopoietic regeneration (Yamashita and Passegué 2019). They showed that TNF-α has different effects on HSCs and progenitor cells, which facilitates haematopoietic clearance and regeneration in an inflammatory context. Their studies indicated that TNF-α induces myeloid progenitor cell apoptosis, but simultaneously promotes HSC survival and myeloid differentiation through a p65-NF-κB-dependent gene program (Yamashita and Passegué 2019).

The role of TNF signalling in leukaemia is similarly complex. Constitutive NF-κB activity has been described as a contributor to leukaemic progression in mouse models of AML, and has been attributed to autocrine TNF-α secretion by leukaemia initiating cells (Kagoya, Yoshimi et al. 2014). A correlation between TNF-α and NF-κB activity has also been documented in human AML samples (Kagoya, Yoshimi et al. 2014). In contrast, knock out of both *Tnfrsf1a* and *Tnfrsf1b* in a *FLT3-ITD* driven AML mouse model resulted in a strong increase in the overall leukaemic burden compared with wild type mice, which was attributed to a reduction in RIPK3-dependent cell death and differentiation (Hockendorf, Yabal et al. 2016).

We attempted to confirm the role of the YTHDF2-TNFR2 axis in AML through shRNA mediated knock down of *Tnfrsf1b* in *Ythdf2*$^{fl/fl}$ and *Ythdf2*$^{fl/fl}$;*Vav-iCre* pre-LSCs. Despite achieving a significant level of knock down using one construct (**Figure 5.4.7 D**), this did not translate to a survival advantage following transplantation to irradiated mice. There are several possible explanations for this. Firstly, it is unlikely that the

supporting role of *Ythdf2* in development and propagation of AML is dependent on a single pathway. More probably, multiple interacting pathways are contributing. Secondly, it may be that in the context of TNF, knock down of both *Tnfrsf1a* and *Tnfrsf1b* would be preferable in order to rule out potential compenstation in the system, particularly as the two receptors have been shown to have a synergistic effect in mediating TNF signalling in HSPCs (Pronk, Veiby et al. 2011).

In summary, our mechanistic studies showed that the critical role of *Ythdf2* in AML development and propagation depends on m^6A-directed *Ythdf2*-mediated mRNA decay, and we demonstrated that *Tnfrsf1b* upregulation represents one specific molecular mechanism by which the loss of *Ythdf2* may negatively impact on AML.

Chapter 6: Conclusions and future work

The work presented in this thesis identifies YTHDF2 as a critical regulator of normal and malignant haematopoiesis. Previous studies of METTL3/14 methyltransferases, and the demethylase FTO, have shown a key role for m^6A in AML pathogenesis (Barbieri, Tzelepis et al. 2017, Li, Weng et al. 2017, Weng, Huang et al. 2018). Whilst modification of mRNA with m^6A can have multiple outcomes on the respective transcript (Zhao, Roundtree et al. 2017), we demonstrate here that the YTHDF2-mediated m^6A-dependent mRNA degradation pathway is essential for cancer stem cells in AML. Using mouse models, we find that deletion of *Ythdf2* specifically compromises LSC development and propagation. Furthermore, consistent with recent findings in mouse and human HSCs (Li, Qian et al. 2018, Wang, Zuo et al. 2018), we demonstrate that targeting *Ythdf2* expands HSCs and enhances their myeloid reconstitution potential in lethally irradiated mice (**Figure 6**).

These unique properties of YTHDF2 highlight the therapeutic potential of YTHDF2 inhibition as a strategy for AML treatment. Such an intervention would have the dual benefits of eradicating malignant LSCs while bestowing a competitive advantage to normal HSCs. Standard AML therapies are non-specific, and are therefore associated with significant side effects. Whilst the survival of young people with AML has improved significantly in the last 30 years, the prognosis for older patients remains stubbornly poor (Döhner, Estey et al. 2017). Whilst this is partly due to older patients having higher cytogenetic risk disease, many of these patients are also unable to tolerate high intensity cytarabine/anthracycline therapy, or HSCT. At present, treatment options for these patients are limited, and are associated with a poor response. The median survival time for patients > 60 years is only 6-9 months. In this group of patients therefore, YTHDF2-inhibition would be a particularly promising treatment strategy.

In a separate context, YTHDF2 inhibition might offer a novel strategy with which to expand HSCs *in vitro* for therapeutic purposes. Given their unique dual capacity for self-renewal and multipotency, HSCs are a valuable therapeutic commodity for the purposes of HSCT, which can be used to treat a variety of diseases, including cancer, congenital or acquired BM failure, immunodeficiency states, and autoimmunity (Copelan 2006). At present, HSCT is hampered by an inability to isolate HSCs in

sufficient quantities, and a failure to expand them *in vitro* (Dahlberg, Delaney et al. 2011). HSC self-renewal, differentiation and quiescence is determined by signals from the microenvironment, as well as stem cell intrinsic regulators (Nakamura-Ishizu, Takizawa et al. 2014). The primary limiting factor for the use of HSCT is the limited number of HSCs that can be obtained from donors, and the poor efficacy of expanding these HSCs *in vitro*. For *ex-vivo* HSC expansion, approaches that potentiate HSC symmetrical division without further differentiation are required (Morrison and Kimble 2006). However, cytokine cocktails currently used to potentiate HSC proliferation *in vitro* (such as SCF, Flt3, TPO, IL-3 and IL-6) may only regulate short term (4 day) HSC survival(Knapp, Hammond et al. 2017). More recently, high throughput screens have identified several new compounds with the potential to improve HSC expansion *in vitro*, but their efficacy in a clinical setting remains to be proven (Tajer, Pike-Overzet et al. 2019). Based on our findings, YTHDF2 inhibition is another candidate strategy with which to expand functional HSCs *in vitro* or *in vivo* for the purposes of therapeutic HSCT.

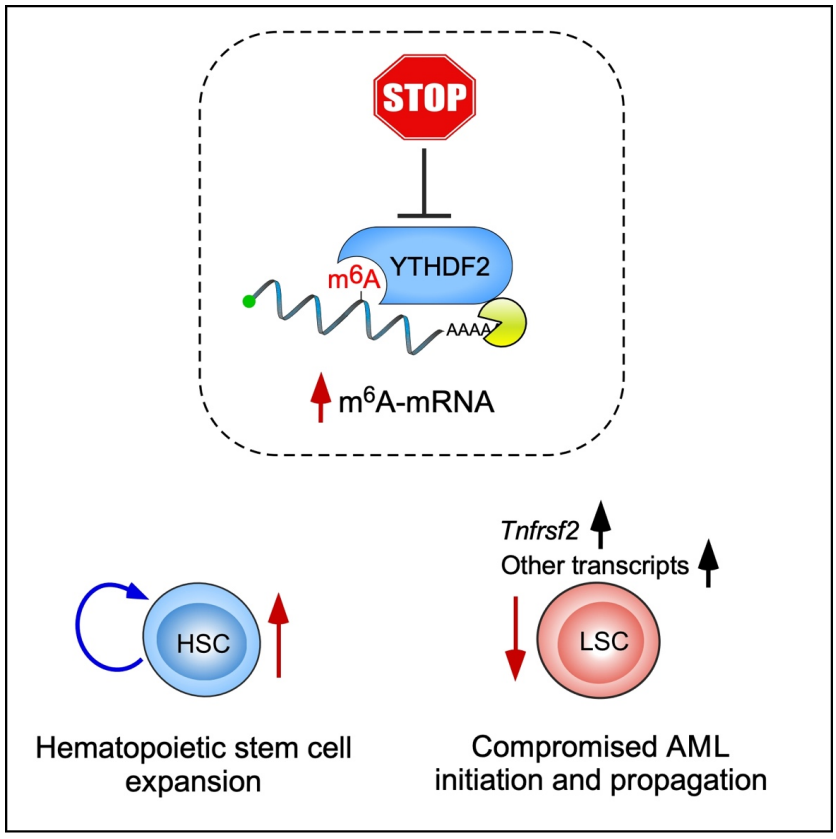

Figure 6 The effect of targeting *Ythdf2* on normal and malignant haematopoiesis. *Ythdf2* inhibition inhibits degradation of m^{6}A-modified mRNA,

resulting in an accumulation of m^{6}A-modified transcripts. As a result, HSC expansion occurs, and AML initiation and propagation are compromised, in part through *Tnfrsf2* (*Tnfrsf1b*). Adapted from Paris, Morgan et al. 2019 (Paris, Morgan et al. 2019).

Whilst undeniably positive, the reason for the differential outcomes of targeting *Ythdf2* in HSCs and LSCs is not clear. However, several previous studies have shown that the effect of m^{6}A is context dependent, varying according to cell type and stage. For example, Geula et al. showed that depletion of *Mettl3* in embryonic stem cells (ESCs) compromised their ability to transform into a primed epiblast state *in vitro.* However, upon examining a later stage of differentiation, the same group found that depletion of *Mettl3* actually hastened differentiation. They concluded that the effect of *Mettl3* was stage dependent, probably reflecting the background switch between pluripotency and differentiation genes (Geula, Moshitch-Moshkovitz et al. 2015).
There is evidence to suggest that *Mettl3* may also have varying effects in normal and malignant haematopoiesis. Using two independent CRISPR genetic screens, Barbieri et al. showed that that *METTL3* was essential for growth of AML cells, but was not required by primary haematopoietic cells (Barbieri, Tzelepis et al. 2017). Subsequently, Yao et al. and Lee et al. both used a *Mx1-Cre* conditional genetic deletion strategy to target *Mettl3* in adult mice, and reported a large increase in HSCs, albeit lacking reconstitution capacity in transplantation experiments (Yao, Sang et al. 2018, Lee, Bao et al. 2019). In contrast, *METTL3* depletion in human AML samples has been shown to result in apoptosis and differentiation, and delayed leukaemia *in vivo* (Vu, Pickering et al. 2017). These findings suggest that m^{6}A can have differing functions in haematopoietic cells under normal and malignant conditions, therefore supporting our own findings, that targeting *Ythdf2* expands HSCs and compromises AML initiation and propagation.

Although mechanistic investigations presented in this thesis only focused on LSCs, further work is underway by other members of the group to characterise the mechanism for YTHDF2 in a non-malignant context. It will be interesting to assess the similarities or differences between the two, when considering the contrasting phenotypes.

Looking to the future as a group, we hope to develop small molecule inhibitors with which to target YTHDF2, initially in mouse models of AML, and later in human cell

lines and primary AML cells. If these results prove to be promising, we will work with collaborators to bring these treatments into the clinical field. Meanwhile, we will extend our murine studies to include a transgenic model of AML, to complement the RTTA transplantation studies conducted to date.

With regards to YTHDF2 targeting in the context of non-malignant haematopoiesis, we plan to collaborate with groups working to expand HSCs *in vitro* for therapeutic purposes. Finally, I plan to look more closely at the immune system of the *Ythdf2*-deficient mice, in particular the lymphocyte lineages which are compromised upon *Ythdf2* deletion, to better characterise the phenotypic and functional effects of *Ythdf2* deficiency within the adaptive immune system.

Appendix: Supplementary tables relating to Chapter 5

Symbol	log_2(FC)	adj. P Value
Csn2	5,51	0,00004099
Sva	4,57	0,00000001
Gm595	2,90	0,02040276
Cpne2	2,55	0,00000048
Mrgpra2a	1,92	0,00100306
Dlk1	1,90	0,04005395
Nrp2	1,88	0,01201683
Il1rl2	1,85	0,00657882
Laptm4b	1,83	0,04615550
Scarf1	1,82	0,00227636
Il1f9	1,81	0,02953698
Lair1	1,68	0,00055642
Gatm	1,64	0,01129324
Pmp22	1,54	0,00978065
Eng	1,39	0,01382162
Npl	1,37	0,02225112
Hspa1b	1,33	0,00715852
Kcnk12	1,33	0,02697286
Glyat	1,31	0,00267415
Chst15	1,27	0,01082185
0610040J01Rik	1,27	0,00648365
Slc16a7	1,22	0,00892191
Lrg1	1,20	0,00617104
Slc40a1	1,19	0,01259119
Cpne8	1,18	0,02930489
Ccl6	1,15	0,04678231
Ly6g5b	1,15	0,03334376
Lpl	1,14	0,01277766
Myo1e	1,12	0,02775427
Afap1	1,11	0,00142512
Rxra	1,10	0,00048341
Rnf144b	1,08	0,00999466
Mycn	1,08	0,01772719
Plxna2	1,08	0,00393508
Slc39a4	1,07	0,03829813
Ak3	1,07	0,00108212
Ces2g	1,06	0,00280342
Pde2a	1,03	0,00165227
Bai1	1,01	0,00417171
Zmat3	1,00	0,00327908
Cd55	0,98	0,00690838
Cd79b	0,97	0,00722837
Zfp943	0,93	0,00264831
Pla2g5	0,92	0,00897905
Adrbk2	0,91	0,01832420
Fen1	0,90	0,03609294

Ptk7	0,90	0,00719714
Pik3r5	0,90	0,00033087
Dio2	0,90	0,00722837
Hpgds	0,88	0,01028171
1810011H11Rik	0,87	0,02127968
Ecm1	0,84	0,01305287
Ogdhl	0,84	0,04255846
Nid2	0,83	0,02241511
Plcg1	0,80	0,00424456
NA	0,78	0,01407804
Pik3r6	0,77	0,00955344
Olfr56	0,75	0,00712944
Tanc1	0,75	0,00293324
Myo7a	0,74	0,01211048
Ppap2b	0,73	0,02847224
Dock9	0,72	0,03556259
Wwc2	0,72	0,00711345
Gpr84	0,72	0,00393508
Gkap1	0,72	0,02625104
Snx7	0,71	0,00995127
H2afy2	0,71	0,00845127
Gatsl2	0,71	0,00534147
Nanp	0,71	0,01209590
Gp9	0,70	0,04776381
Vamp5	0,69	0,00374844
Arsb	0,69	0,01368656
Cbr1	0,69	0,02953698
Mospd3	0,68	0,03257628
Tusc1	0,68	0,00844962
Tbc1d30	0,67	0,01186164
Chd3	0,66	0,00401669
Tmc7	0,66	0,01642187
Lima1	0,66	0,00089937
Trp53inp1	0,66	0,04946880
Rab3il1	0,66	0,00293324
Srxn1	0,65	0,00690838
Tnfaip8l1	0,65	0,00621088
Cpped1	0,65	0,00357674
Dock10	0,65	0,02020948
Ubash3a	0,65	0,01002245
Gm364	0,64	0,02075986
Mrpl46	0,64	0,00849760
Ppfibp1	0,64	0,02102952
Renbp	0,64	0,00074506
2310028H24Rik	0,64	0,00293324
Hebp1	0,64	0,00176940
Als2	0,64	0,00231350
Mrpl16	0,63	0,00074506
Chchd10	0,63	0,00691575
Plxna1	0,63	0,02190816
Olfr51	0,62	0,03092340

Psd3	0,62	0,00844962
Pgp	0,62	0,04580074
Emid1	0,62	0,02374741
Hnmt	0,62	0,02023394
Irak1bp1	0,61	0,01034518
Sh3tc1	0,61	0,00628337
Nlgn2	0,61	0,02618829
Exoc3l	0,61	0,03559810
Ephx1	0,61	0,01129324
Plscr3	0,61	0,03054057
Clmn	0,61	0,00773601
Emilin1	0,60	0,03107530
Rpusd1	0,60	0,00143744
Commd5	0,60	0,00185915
Fam115a	0,60	0,04490563
Batf	0,60	0,00534147
Arl4a	0,60	0,00730580
2810432D09Rik	0,60	0,02023394
Pak1	0,59	0,00621088
Csf3r	0,59	0,03364364
Ubtd2	0,59	0,01481064
Tbc1d16	0,59	0,00629381
9030617O03Rik	0,59	0,01757521
Kctd6	0,59	0,00231350
Scamp5	0,58	0,01348771
Abhd6	0,58	0,02068986
Gmppb	0,58	0,02673716
Btg2	0,58	0,02865139
Extl3	0,58	0,01248263
Cdc42bpb	0,58	0,00392058
Plekha1	0,58	0,03062262
Prodh	0,58	0,00231350
Tacc2	0,58	0,01324153
Klhl8	0,57	0,02775427
Acy3	0,57	0,01089479
Mfsd5	0,57	0,00064919
BC003266	0,57	0,00374844
Tanc2	0,57	0,02731743
Mrpl51	0,57	0,00888400
Ubtd1	0,56	0,00789830
Abt1	0,56	0,00713144
Tsku	0,56	0,00825478
Hyal2	0,56	0,00709176
Tmem53	0,56	0,02080605
Mrpl43	0,56	0,00169303
Als2cl	0,56	0,03221455
Fam195a	0,56	0,00691575
Spryd4	0,56	0,00393508
Plekho1	0,55	0,04433043
Wdr55	0,55	0,03121408
Fam69a	0,55	0,00621088

E130012A19Rik	0,54	0,00282906
Tysnd1	0,54	0,02787096
H2-DMb1	0,54	0,01145623
Pqlc2	0,54	0,02010105
Tomm5	0,54	0,02043170
Nfatc2	0,54	0,00641007
Znhit2	0,54	0,02374741
N6amt2	0,54	0,01950134
Gnb1l	0,54	0,00940835
Phlda3	0,54	0,00844962
Trmt5	0,53	0,00296933
Dusp9	0,53	0,00690838
Siah1b	0,53	0,02403610
Tk1	0,53	0,02526871
Atg12	0,53	0,00148083
Nlrx1	0,53	0,01563641
Grwd1	0,53	0,00357270
Irgm1	0,53	0,01090952
Zbtb45	0,53	0,01797250
Rab7l1	0,53	0,00721282
Tuba4a	0,53	0,02977308
Shroom4	0,53	0,01229685
Frmd6	0,53	0,01234749
Hfe	0,52	0,03283321
D330045A20Rik	0,52	0,00789830
Mpzl1	0,52	0,03852733
Lpar5	0,52	0,00789830
Kbtbd4	0,52	0,01279567
Mrps7	0,52	0,01015088
Ccdc23	0,52	0,02391575
Chpf2	0,52	0,00995127
Zcchc17	0,52	0,02149877
Slc16a13	0,51	0,00888064
Mrpl12	0,51	0,01002245
Pik3c2b	0,51	0,01779216
Dok4	0,51	0,01096282
Fkrp	0,51	0,00293324
Bmpr1a	0,51	0,01089479
Cables2	0,51	0,00116418
Nxt1	0,51	0,01348771
Slc10a3	0,51	0,01642155
6230427J02Rik	0,51	0,00407070
Wdr81	0,50	0,00363305
Nubp2	0,50	0,02177819
Ece2	0,50	0,00325600
Nav2	0,50	0,01715493
Bcl9	0,50	0,00393508
5031439G07Rik	0,50	0,01563641
Cdk18	0,50	0,00371773
Oas2	0,50	0,03790564
Srl	0,50	0,04867220

Rbmxl1	0,50	0,01568725
Sep-08	0,50	0,01514006
Rps6ka3	0,50	0,01457843
Pter	0,50	0,01421999
Itpk1	0,50	0,00940978
Slc35a4	0,50	0,02190816
Slc28a2	0,50	0,01062891
Med29	0,49	0,03801022
Trim65	0,49	0,00845127
2410017P09Rik	0,49	0,00730580
Phospho1	0,49	0,00610476
4933430I17Rik	0,49	0,02225940
Ece1	0,49	0,02115083
Scd4	0,48	0,01015088
Rgs8	0,48	0,02587636
Fam105b	0,48	0,01530697
Zswim1	0,48	0,01404115
Impdh1	0,48	0,02667670
Slc46a1	0,47	0,00593388
Tnf	0,47	0,01832420
Wdr66	0,47	0,01019248
Trappc3	0,47	0,00417171
Ndufaf4	0,47	0,00712944
Spn	0,47	0,01810627
Elof1	0,47	0,03234970
Nupl2	0,47	0,00540659
Fastkd2	0,47	0,02377744
Tle1	0,47	0,02618829
Alad	0,47	0,01816129
Hsd3b7	0,47	0,00958761
Bbs7	0,47	0,03875079
Ldlrap1	0,47	0,02190816
Spr	0,47	0,00995127
Gmpr	0,46	0,01014895
Asb8	0,46	0,01283398
Fam110a	0,46	0,00986858
Ndufaf1	0,46	0,02046304
Tulp4	0,46	0,01258700
Agap2	0,46	0,01650406
Mmp19	0,46	0,00280342
Mical3	0,46	0,01722702
Ppfibp2	0,46	0,01028171
Fam69b	0,46	0,01563641
Tprn	0,46	0,02547456
Rbpms2	0,46	0,03109627
Elmod3	0,46	0,00417171
Smad1	0,46	0,02595223
0610011L14Rik	0,45	0,01327013
Urgcp	0,45	0,00988236
Rbm19	0,45	0,01129324
Gclm	0,45	0,00357674

Atp6v0a2	0,45	0,00200253
Gltp	0,45	0,00657882
2810453I06Rik	0,45	0,02010105
C2cd2	0,45	0,00779129
Vps18	0,45	0,01248263
Ywhag	0,45	0,00789830
Khk	0,45	0,01715493
Neu1	0,45	0,02190816
Smpd2	0,45	0,00424451
Plekho2	0,44	0,02771148
Map2k3	0,44	0,01463136
Slc19a2	0,44	0,01898743
2410022L05Rik	0,44	0,00921589
Ttyh2	0,44	0,01607309
Gjb3	0,44	0,01463136
Acer3	0,44	0,02697286
Bysl	0,44	0,01151293
B4galt4	0,44	0,04887601
Igsf6	0,44	0,00425725
B3gnt1	0,44	0,00598630
Mpv17l2	0,44	0,00690838
Phospho2	0,44	0,00267113
Agpat2	0,43	0,00779615
Gm962	0,43	0,01832420
Dip2c	0,43	0,03756514
Omg	0,43	0,00921589
Gtdc2	0,43	0,03093125
B230120H23Rik	0,43	0,00162838
Poln	0,43	0,00995127
Otud3	0,43	0,01301677
Nudt19	0,43	0,04226806
Ywhah	0,43	0,01425066
Rpusd2	0,43	0,02602277
Ccng1	0,43	0,00921589
Ppp2r5b	0,43	0,02119237
Sf3b4	0,43	0,03801022
Nme6	0,43	0,01283398
Tesk1	0,43	0,01018596
Ano6	0,43	0,01326052
B3gnt8	0,43	0,02296086
Rhod	0,43	0,04893778
Pinx1	0,43	0,00621088
Mrpl50	0,43	0,00548984
App	0,43	0,01984757
Dnase2a	0,43	0,00452959
Xrcc6bp1	0,42	0,00845127
Nop2	0,42	0,03340482
Tex264	0,42	0,00238538
Zw10	0,42	0,02195807
Ccne1	0,42	0,02075986
Tnfrsf1b	0,42	0,01867878

Suox	0,42	0,00545505
Phactr2	0,42	0,03084616
Mgat4b	0,42	0,00480937
Mrps25	0,42	0,02662149
Oas1a	0,42	0,01299779
Panx1	0,42	0,00709176
Tmem8	0,42	0,03623233
Erf	0,42	0,01607410
Cyth4	0,42	0,01299577
Mad2l1bp	0,42	0,01347608
Gpr160	0,42	0,01543779
Mrps30	0,42	0,02697286
Naa40	0,41	0,01010354
Mrps2	0,41	0,00512495
Rapgef5	0,41	0,04963493
Rgnef	0,41	0,02402526
Thg1l	0,41	0,00713144
Sipa1	0,41	0,01945030
Bax	0,41	0,03280118
Chpt1	0,41	0,00711345
Clp1	0,41	0,01421999
Hspa13	0,41	0,01070472
Dhrs4	0,41	0,00940978
Gria3	0,41	0,03036671
Dgcr14	0,41	0,02010105
Steap3	0,41	0,04725833
Mgmt	0,41	0,01466073
Pcyox1	0,41	0,03437566
Ccrl2	0,41	0,02325173
Fhod1	0,41	0,04238165
Psmd7	0,41	0,04087968
St6galnac4	0,41	0,00713144
Tlr3	0,41	0,04892498
1810055G02Rik	0,41	0,03906522
Narfl	0,41	0,00534650
Brms1	0,40	0,02595223
Snord4a	0,40	0,04561035
Ralb	0,40	0,01904211
Grpel1	0,40	0,02980247
Gsn	0,40	0,03406618
Gfm1	0,40	0,04369755
Nup50	0,40	0,01832420
1110012L19Rik	0,40	0,01923240
Ssbp4	0,40	0,00779615
Timm8a1	0,40	0,01005398
Ccdc59	0,40	0,04949090
Pop7	0,40	0,01548282
2010321M09Rik	0,40	0,01201683
Uap1l1	0,40	0,04751215
Mrto4	0,40	0,02142457
Ppp1r13b	0,40	0,03045546

D230037D09Rik	0,40	0,03588580
Rnmtl1	0,39	0,02783163
Bcl9l	0,39	0,02099877
C230052I12Rik	0,39	0,01028171
Metrn	0,39	0,02930489
Inpp4b	0,39	0,01541556
Jmjd4	0,39	0,02403610
Pde12	0,39	0,01201683
Ripk1	0,39	0,01603693
Zbtb41	0,39	0,00690838
Exo1	0,39	0,02611982
Def8	0,39	0,02798783
0610010K14Rik	0,39	0,03082667
Galnt7	0,39	0,03836688
Foxp4	0,39	0,01120179
Ctns	0,39	0,00773601
Orai1	0,39	0,00845127
Ipo13	0,38	0,01670152
Slc12a7	0,38	0,03970393
Bdh1	0,38	0,00743313
Trmt61a	0,38	0,02918481
Sac3d1	0,38	0,01935250
Nagpa	0,38	0,02697286
Xylb	0,38	0,02080605
Sap30bp	0,38	0,00621088
Sssca1	0,38	0,03036671
Snx33	0,38	0,01348771
Stard8	0,38	0,02930489
Eif2b1	0,38	0,04238165
1810063B05Rik	0,38	0,03169648
Klhdc4	0,38	0,04933377
Ndst1	0,38	0,01352362
Gm10495	0,38	0,04544722
Brp44	0,37	0,00621088
Gemin4	0,37	0,04186192
Gpsm2	0,37	0,00713144
Kif21a	0,37	0,04523665
Nudt18	0,37	0,03356401
Pgd	0,37	0,03670644
Chst12	0,37	0,01779216
Mrpl15	0,37	0,02225940
1500001M20Rik	0,37	0,01326052
Cables1	0,37	0,03283321
Mrps23	0,37	0,02147747
Polr3g	0,37	0,02941507
Hmox2	0,37	0,02325173
Fkbpl	0,37	0,01028171
Mrpl55	0,37	0,03641255
Eif2ak1	0,37	0,02847224
Osbpl11	0,37	0,00690838
Jagn1	0,37	0,03556259

Dnajc15	0,37	0,02114312
Tmem184b	0,37	0,02149877
Ssh3	0,37	0,01216521
Zfp507	0,37	0,02697286
Snx8	0,37	0,00921589
Cdyl2	0,37	0,03713034
Nfam1	0,37	0,03556259
D1Ertd622e	0,37	0,04347554
Plcb2	0,36	0,03765366
Nif3l1	0,36	0,01234749
Mcat	0,36	0,01372618
Vamp8	0,36	0,02225940
Rps19bp1	0,36	0,02999950
Tspan4	0,36	0,00908657
Letm1	0,36	0,02115083
Fam20b	0,36	0,02639957
Ptpn12	0,36	0,01096282
Rragc	0,36	0,01305287
Bpnt1	0,36	0,02773164
Snx20	0,36	0,02753860
Rab11fip1	0,36	0,00920791
Fzd9	0,36	0,04483083
Fnip2	0,36	0,03924987
Ptp4a3	0,36	0,01779216
C1galt1	0,36	0,02726428
D8Ertd738e	0,36	0,02677388
Wdr18	0,36	0,03233268
S1pr2	0,36	0,01589189
Utp15	0,36	0,02010105
D330012F22Rik	0,36	0,02190816
2210016L21Rik	0,36	0,00690838
1300001I01Rik	0,36	0,04657515
Elovl1	0,35	0,03569713
Ccdc22	0,35	0,01650406
Gstp1	0,35	0,02241511
Zdhhc8	0,35	0,02582792
Thap7	0,35	0,01182005
Gng7	0,35	0,02081778
1110038F14Rik	0,35	0,03479415
Zfp36l2	0,35	0,01483949
Comtd1	0,35	0,02767841
Pdhx	0,35	0,00789830
Cstf1	0,35	0,03755982
Gcdh	0,35	0,01034518
Baz1a	0,35	0,02753802
Zfp771	0,35	0,01921388
Aen	0,35	0,02049003
Cyb561	0,35	0,04806947
Ankrd40	0,35	0,02225940
Tada2b	0,35	0,00691575
Cgrrf1	0,35	0,02199502

Rogdi	0,35	0,04235515
Cog8	0,35	0,03019283
Ncor2	0,35	0,00964336
Usp46	0,35	0,02479955
Usp54	0,35	0,01556181
9430016H08Rik	0,35	0,00921589
Taf5l	0,35	0,00713144
Pstpip1	0,35	0,02940043
Depdc7	0,35	0,03641048
Akr7a5	0,35	0,03609294
Pip4k2b	0,35	0,01028171
Tymp	0,35	0,03935789
Cyp3a59	0,35	0,01585454
Med21	0,35	0,01422985
2310079F23Rik	0,35	0,04771581
Gpr125	0,35	0,03364364
Jtb	0,35	0,00844962
1700123O20Rik	0,35	0,04946880
Atp5e	0,35	0,02353486
Ggct	0,35	0,01863124
Nat15	0,34	0,00879460
Lrrc14	0,34	0,04447683
Nln	0,34	0,01547374
Ccdc86	0,34	0,03641255
Bzrap1	0,34	0,03469313
Lsm10	0,34	0,01327013
Txnl4a	0,34	0,01305287
Ccnyl1	0,34	0,03342003
Rhou	0,34	0,03107530
Isg20l2	0,34	0,01898743
4933403F05Rik	0,34	0,01233038
Apeh	0,34	0,01040613
Orai3	0,34	0,02183621
Ftsjd1	0,34	0,02183621
Ehd4	0,34	0,01151293
9030625A04Rik	0,34	0,04238165
Tmem115	0,34	0,02738620
Puf60	0,34	0,02673716
Setd6	0,34	0,01382338
Mprip	0,34	0,00888400
Nol6	0,34	0,04725833
Pgpep1	0,34	0,03484916
Crat	0,34	0,01351343
Rai14	0,34	0,01485115
Senp3	0,34	0,03394171
Cops8	0,33	0,03878083
Zfp282	0,33	0,02445213
Rybp	0,33	0,02325173
Rnpepl1	0,33	0,03556259
Syngr1	0,33	0,01072270
Hps4	0,33	0,01329059

E130218I03Rik	0,33	0,04054128
9130401M01Rik	0,33	0,02190816
Dtnbp1	0,33	0,02190816
2510039O18Rik	0,33	0,04124861
Ints5	0,33	0,04660266
Fbxo6	0,33	0,01715493
Rrp12	0,33	0,02119237
Mrps17	0,33	0,03148539
BC023829	0,33	0,03052097
Mtmr10	0,33	0,02450124
Hrh2	0,33	0,04976677
Pdpr	0,33	0,01234749
Mrpl36	0,33	0,04608961
4930453N24Rik	0,33	0,02190816
Olfr1360	0,33	0,01848341
Tmem214	0,33	0,04893778
LOC674846	0,33	0,04279566
Pus1	0,33	0,03933416
Supt7l	0,33	0,03257628
Oxnad1	0,33	0,01670852
1110008P14Rik	0,33	0,00964336
Sdhaf2	0,33	0,01129324
Dhx33	0,33	0,02400225
Tm2d2	0,32	0,02359196
Dbf4	0,32	0,03400765
Cep68	0,32	0,03037567
Bcl3	0,32	0,03641255
Chrac1	0,32	0,02385398
Nt5c	0,32	0,02278446
Klhl12	0,32	0,03019283
Zdhhc3	0,32	0,00956603
Chaf1b	0,32	0,01348771
Dtwd2	0,32	0,01881617
Dnajc30	0,32	0,02885172
Llph	0,32	0,03549780
Max	0,32	0,04469221
Slc35b4	0,32	0,03975578
Ufsp1	0,32	0,01877036
Il21r	0,32	0,04226806
Srrd	0,32	0,00884534
Tssc4	0,32	0,01326312
Ccdc91	0,32	0,02834419
Sphk2	0,32	0,01284027
Sgsm3	0,32	0,04492646
Uspl1	0,32	0,04925869
Zfp746	0,32	0,03022302
Efhd2	0,32	0,04948625
Tram2	0,32	0,02353486
Mesdc2	0,32	0,02804935
Snap29	0,32	0,03938804
Pikfyve	0,32	0,03623233

Tbc1d13	0,32	0,02190816
Bag5	0,32	0,01642155
Adap1	0,32	0,03926480
Def6	0,32	0,01945030
Fam118b	0,32	0,02088732
Ccdc56	0,32	0,02206416
Dpp7	0,32	0,04217340
2510012J08Rik	0,32	0,04164029
Rab35	0,32	0,03850942
Bend3	0,32	0,03082667
Zfp259	0,32	0,01822229
2010012O05Rik	0,31	0,03556259
Snx15	0,31	0,04434335
Taf1c	0,31	0,01327013
Anxa11	0,31	0,03267723
Mrps18b	0,31	0,02582792
Wrap53	0,31	0,01481064
Rnf8	0,31	0,01904211
9630033F20Rik	0,31	0,01348771
Cox10	0,31	0,01348771
Ythdf1	0,31	0,02658308
Fanca	0,31	0,04890944
Mrps34	0,31	0,02046304
Lrr1	0,31	0,04648836
Ifrd2	0,31	0,03069264
Tnrc6c	0,31	0,03109627
Acacb	0,31	0,04725833
Hras1	0,31	0,03023608
Ftsj2	0,31	0,03121408
Zdhhc1	0,31	0,04027854
Ptcd2	0,31	0,03935789
Pip4k2a	0,31	0,01946451
Mfn2	0,31	0,02074663
Mms19	0,31	0,01242175
Stx2	0,31	0,01327013
Tnfrsf21	0,31	0,03667541
Fut4	0,31	0,02625104
Zscan22	0,31	0,03926480
4930534B04Rik	0,31	0,03294780
Bcr	0,31	0,01832420
Lrrc41	0,30	0,02798783
Rhobtb2	0,30	0,01466230
Snap47	0,30	0,01360734
Nit1	0,30	0,02742213
Trappc5	0,30	0,01279567
Tmco7	0,30	0,03979223
Lonrf3	0,30	0,03221455
2700078E11Rik	0,30	0,02636142
Spsb3	0,30	0,04567470
Zfp628	0,30	0,02677388
Ube2f	0,30	0,02639957

Shq1	0,30	0,01696034
Ext2	0,30	0,01283398
Ptplb	0,30	0,02798783
Mllt1	0,30	0,02440558
Crtc1	0,30	0,04867220
Txndc15	0,30	0,03125136
Rpp14	0,30	0,04542172
Btd	0,30	0,04544722
Elac2	0,30	0,02296327
Dtx4	0,30	0,03447792
Mtf1	0,30	0,01867480
Gm16517	0,30	0,04725833
Tgfbrap1	0,30	0,01755408
Thap11	0,30	0,02447607
Ppip5k1	0,30	0,00964336
Pdk2	0,30	0,04186192
Gclc	0,29	0,03434549
Clpp	0,29	0,03082667
Serac1	0,29	0,04946880
Ptrh2	0,29	0,02149877
Tapt1	0,29	0,01002382
Flad1	0,29	0,02751109
Fam89b	0,29	0,01362013
Sec14l1	0,29	0,03609294
Agpat6	0,29	0,03280118
Dcun1d2	0,29	0,03962952
Traf6	0,29	0,00940978
2410016O06Rik	0,29	0,03405626
Ccdc32	0,29	0,02190816
Gnptab	0,29	0,02646819
Tpst2	0,29	0,03462218
Cdh4	0,28	0,04186192
Commd7	0,28	0,01372618
Ehd1	0,28	0,02877450
Traf3	0,28	0,02669824
Herc2	0,28	0,04445136
Yipf5	0,28	0,02931718
Fam50a	0,28	0,04219583
Ndufaf3	0,28	0,03862010
Rela	0,28	0,03825770
H6pd	0,28	0,03623233
Ubox5	0,28	0,02190816
Yars2	0,28	0,03233793
Fem1b	0,28	0,03221455
Ubiad1	0,28	0,03589848
Tgfbr1	0,28	0,04976541
Ccdc93	0,28	0,02088199
Prmt10	0,28	0,01963059
Rnf25	0,28	0,02325173
Kctd1	0,28	0,03922586
2310022A10Rik	0,27	0,03406618

Aste1	0,27	0,03882155
Cln5	0,27	0,03875079
Hes6	0,27	0,04725833
Dot1l	0,27	0,01361750
Suds3	0,27	0,02858574
C1rl	0,27	0,03566335
Dicer1	0,27	0,02667670
Cln8	0,27	0,04170296
Clcn4-2	0,27	0,03233268
Tmem216	0,27	0,03609294
Ppif	0,27	0,04951116
Aak1	0,27	0,04280188
Stk16	0,27	0,02183621
Prl4a1	0,27	0,04678231
Patz1	0,27	0,04849433
Fbxw9	0,27	0,04893778
Kdm2b	0,27	0,04751215
Cdca4	0,27	0,02799211
Fitm2	0,27	0,02595223
Ttc1	0,26	0,02861142
Bud31	0,26	0,02246936
Csrp2bp	0,26	0,04326930
Ltbr	0,26	0,04751215
E130309D02Rik	0,26	0,01945030
Gemin7	0,26	0,02190816
Pi4kb	0,26	0,04130175
Rsl24d1	0,26	0,02931718
Npas3	0,26	0,04238165
Cat	0,26	0,03623233
Phf23	0,26	0,03452207
Fes	0,26	0,02750440
Ammecr1l	0,26	0,02475394
Cela3b	0,26	0,03933416
Jam3	0,26	0,03213064
Map2k2	0,26	0,04238165
Rbm28	0,26	0,04475580
Scaf1	0,26	0,02695018
C1qbp	0,26	0,04238165
Chmp1a	0,26	0,02998360
Nacc1	0,26	0,02263495
Pcbp1	0,26	0,04893778
Gng12	0,26	0,01444040
Prep	0,26	0,02119237
Cdk9	0,26	0,01305287
Cog2	0,26	0,04544722
Ctsz	0,26	0,04284466
1110057K04Rik	0,26	0,04648836
Naif1	0,26	0,03400765
Rev1	0,26	0,03144574
Mrps18a	0,26	0,04430945
Eme2	0,25	0,03601115

Mpp1	0,25	0,02753860
Extl2	0,25	0,03926480
Gne	0,25	0,03641255
Cmtm7	0,25	0,02783163
Plekhm2	0,25	0,04235515
AI317395	0,25	0,03636136
Fam53b	0,25	0,03556259
Dnajb14	0,25	0,02346214
4831426I19Rik	0,25	0,04648836
Acad9	0,25	0,04576472
Slc48a1	0,25	0,03559810
Rapgef1	0,25	0,04751215
Stk11	0,25	0,02659283
Slc25a45	0,24	0,02318130
Vrk2	0,24	0,04161791
Pigq	0,24	0,04940302
Brap	0,24	0,03618319
Rab13	0,24	0,03756514
Mif4gd	0,24	0,04036948
Mon1a	0,24	0,02436120
Klhl26	0,24	0,02658308
Prosc	0,24	0,02861142
Kti12	0,24	0,03087063
Sharpin	0,24	0,04238165
Dcaf13	0,24	0,04648836
Akap1	0,24	0,02917611
Klhdc3	0,23	0,02064972
Rps6kb2	0,23	0,04235515
Muted	0,23	0,02582792
4930471M23Rik	0,23	0,04939795
Mettl8	0,23	0,04849433
Ecd	0,23	0,04946880
1700017B05Rik	0,23	0,04232360
Cdk13	0,23	0,04946880
Vat1	0,23	0,04430945
Eci2	0,22	0,02392065
Crkl	0,22	0,02930489
Stx6	0,22	0,03588580
Spin1	0,22	0,04445136
Xrcc1	0,21	0,04935024
Mrpl17	0,21	0,04129087
Tfec	0,21	0,02667670
Fiz1	0,21	0,03641255
Klhl15	0,21	0,04959157
Trim27	0,21	0,03850942

Appendix 1 List of significantly upregulated genes ($p<0.05$) in *Ythdf2*$^{fl/fl}$;*Vav-iCre* compared to *Ythdf2*$^{fl/fl}$ pre-leukaemic cells. Symbol, gene symbol; log_2(FC), expression fold change (log_2); adj. P Value, moderated t-statistics adjusted P value.

Symbol	log_2(FC)	adj. P Val	$-log_{10}$(q)
Rxra	1,10	0,0005	27,55
Fen1	0,90	0,0361	31,16
1810011H11Rik	0,87	0,0213	36,94
Gpr84	0,72	0,0039	30,26
Nanp	0,71	0,0121	52,65
Srxn1	0,65	0,0069	41,52
Tnfaip8l1	0,65	0,0062	55,03
Mrpl46	0,64	0,0085	29,58
Sh3tc1	0,61	0,0063	50,29
Emilin1	0,60	0,0311	28,61
Rpusd1	0,60	0,0014	30,27
Commd5	0,60	0,0019	32,81
Batf	0,60	0,0053	41,01
Arl4a	0,60	0,0073	42,69
Ubtd2	0,59	0,0148	32,08
Kctd6	0,59	0,0023	33,13
Gmppb	0,58	0,0267	44,13
Extl3	0,58	0,0125	59,72
Mfsd5	0,57	0,0006	48,33
Ubtd1	0,56	0,0079	45,11
Abt1	0,56	0,0071	41,13
Hyal2	0,56	0,0071	36,51
Mrpl43	0,56	0,0017	32,79
Spryd4	0,56	0,0039	30,83
Plekho1	0,55	0,0443	37,31
Nfatc2	0,54	0,0064	37,97
Znhit2	0,54	0,0237	52,25
Gnb1l	0,54	0,0094	65,28
Phlda3	0,54	0,0084	70,01
Siah1b	0,53	0,0240	25,39
Tk1	0,53	0,0253	43,34
Nlrx1	0,53	0,0156	93,14
Grwd1	0,53	0,0036	69,33
Irgm1	0,53	0,0109	72,50
Zbtb45	0,53	0,0180	53,28
Kbtbd4	0,52	0,0128	31,50
Mrps7	0,52	0,0101	27,72
Chpf2	0,52	0,0099	70,54
Zcchc17	0,52	0,0215	26,54
Slc16a13	0,51	0,0089	38,17
Fkrp	0,51	0,0029	66,09
Bmpr1a	0,51	0,0109	34,22
Cables2	0,51	0,0012	64,91
Nxt1	0,51	0,0135	51,55
Slc10a3	0,51	0,0164	32,69
Wdr81	0,50	0,0036	65,61
Bcl9	0,50	0,0039	42,20
Itpk1	0,50	0,0094	93,49
Slc35a4	0,50	0,0219	41,79

Trim65	0,49	0,0084	60,72
Spn	0,47	0,0181	39,18
Nupl2	0,47	0,0054	31,52
Asb8	0,46	0,0128	51,33
Fam110a	0,46	0,0099	65,89
Tulp4	0,46	0,0126	35,07
Agap2	0,46	0,0165	53,50
Fam69b	0,46	0,0156	67,32
Tprn	0,46	0,0255	35,14
Elmod3	0,46	0,0042	47,28
Urgcp	0,45	0,0099	98,09
Rbm19	0,45	0,0113	37,25
C2cd2	0,45	0,0078	48,63
Vps18	0,45	0,0125	60,07
Neu1	0,45	0,0219	29,59
Plekho2	0,44	0,0277	37,65
Map2k3	0,44	0,0146	41,39
Bysl	0,44	0,0115	68,52
B4galt4	0,44	0,0488	54,45
Phospho2	0,44	0,0027	41,73
Agpat2	0,43	0,0078	53,26
Poln	0,43	0,0099	28,81
Rpusd2	0,43	0,0260	63,97
Sf3b4	0,43	0,0380	32,11
Tesk1	0,43	0,0102	44,42
B3gnt8	0,43	0,0229	43,13
Tex264	0,42	0,0024	33,95
Zw10	0,42	0,0219	25,33
Tnfrsf1b	0,42	0,0187	63,53
Phactr2	0,42	0,0308	26,69
Mrps25	0,42	0,0266	30,01
Panx1	0,42	0,0071	26,71
Cyth4	0,42	0,0130	31,42
Mad2l1bp	0,42	0,0135	35,19
Gpr160	0,42	0,0154	47,65
Mrps30	0,42	0,0270	27,55
Naa40	0,41	0,0101	49,97
Mrps2	0,41	0,0051	52,21
Sipa1	0,41	0,0194	42,50
Clp1	0,41	0,0142	35,96
Hspa13	0,41	0,0107	45,76
Dgcr14	0,41	0,0201	28,33
Steap3	0,41	0,0472	27,08
St6galnac4	0,41	0,0071	37,58
1810055G02Rik	0,41	0,0390	48,60
Narfl	0,41	0,0053	53,73
Brms1	0,40	0,0259	31,33
Ralb	0,40	0,0190	28,47
Grpel1	0,40	0,0298	30,11
Nup50	0,40	0,0183	41,11
1110012L19Rik	0,40	0,0192	26,14

Timm8a1	0,40	0,0100	60,61
Ccdc59	0,40	0,0495	39,19
Pop7	0,40	0,0155	39,61
Mrto4	0,40	0,0214	28,12
Bcl9l	0,39	0,0210	37,83
Jmjd4	0,39	0,0240	38,90
Pde12	0,39	0,0120	25,26
Ripk1	0,39	0,0160	34,90
Exo1	0,39	0,0261	42,85
Def8	0,39	0,0280	27,19
Foxp4	0,39	0,0112	55,81
Ctns	0,39	0,0077	54,59
Ipo13	0,38	0,0167	35,31
Bdh1	0,38	0,0074	42,87
Trmt61a	0,38	0,0292	30,14
Sac3d1	0,38	0,0193	66,51
Sap30bp	0,38	0,0062	31,03
Sssca1	0,38	0,0303	33,31
Snx33	0,38	0,0135	66,34
Eif2b1	0,38	0,0424	27,44
Gemin4	0,37	0,0418	60,33
Nudt18	0,37	0,0335	28,07
Mrpl15	0,37	0,0222	74,61
Cables1	0,37	0,0328	39,75
Fkbpl	0,37	0,0103	71,23
Eif2ak1	0,37	0,0285	35,44
Osbpl11	0,37	0,0069	94,17
Jagn1	0,37	0,0355	31,16
Zfp507	0,37	0,0270	51,29
D1Ertd622e	0,37	0,0434	57,59
Nif3l1	0,36	0,0123	65,62
Mcat	0,36	0,0137	70,10
Rps19bp1	0,36	0,0300	71,66
Fam20b	0,36	0,0264	50,28
Ptpn12	0,36	0,0110	49,32
Snx20	0,36	0,0275	103,10
C1galt1	0,36	0,0272	56,42
D8Ertd738e	0,36	0,0268	28,84
S1pr2	0,36	0,0159	36,95
2210016L21Rik	0,36	0,0069	32,46
Zdhhc8	0,35	0,0258	30,62
Thap7	0,35	0,0118	64,16
Zfp36l2	0,35	0,0148	47,23
Cstf1	0,35	0,0375	48,87
Zfp771	0,35	0,0192	38,21
Aen	0,35	0,0205	52,49
Ankrd40	0,35	0,0222	74,23
Tada2b	0,35	0,0069	55,46
Cgrrf1	0,35	0,0220	55,66
Cog8	0,35	0,0302	64,92
Ncor2	0,35	0,0096	58,12

Taf5l	0,35	0,0071	52,89
Akr7a5	0,35	0,0361	26,29
Pip4k2b	0,35	0,0103	41,99
Tymp	0,35	0,0393	63,24
Lrrc14	0,34	0,0445	61,74
Lsm10	0,34	0,0133	46,51
Txnl4a	0,34	0,0130	55,40
Rhou	0,34	0,0311	41,05
Isg20l2	0,34	0,0190	40,47
Orai3	0,34	0,0218	32,89
Tmem115	0,34	0,0274	69,23
Nol6	0,34	0,0472	48,75
Pgpep1	0,34	0,0348	86,83
Zfp282	0,33	0,0244	77,31
Rybp	0,33	0,0232	26,19
Rnpepl1	0,33	0,0355	45,23
Hps4	0,33	0,0133	81,02
2510039O18Rik	0,33	0,0412	48,99
Ints5	0,33	0,0466	63,17
Mtmr10	0,33	0,0245	62,41
Pdpr	0,33	0,0123	49,47
4930453N24Rik	0,33	0,0219	42,67
Supt7l	0,33	0,0326	39,20
Sdhaf2	0,33	0,0113	51,13
Dhx33	0,33	0,0240	59,50
Dbf4	0,32	0,0340	34,20
Cep68	0,32	0,0304	46,90
Chrac1	0,32	0,0238	38,12
Zdhhc3	0,32	0,0096	35,85
Chaf1b	0,32	0,0135	30,12
Dnajc30	0,32	0,0288	53,28
Max	0,32	0,0447	28,78
Slc35b4	0,32	0,0397	41,18
Il21r	0,32	0,0422	92,33
Srrd	0,32	0,0088	60,78
Sphk2	0,32	0,0128	36,92
Uspl1	0,32	0,0492	53,08
Zfp746	0,32	0,0302	68,12
Pikfyve	0,32	0,0362	30,44
Bag5	0,32	0,0164	27,62
Adap1	0,32	0,0392	38,00
Def6	0,32	0,0194	33,74
Rab35	0,32	0,0385	43,49
Bend3	0,32	0,0308	54,12
Taf1c	0,31	0,0133	47,96
Mrps18b	0,31	0,0258	26,11
Rnf8	0,31	0,0190	49,03
Cox10	0,31	0,0135	35,19
Ythdf1	0,31	0,0266	26,27
Mrps34	0,31	0,0204	39,27
Lrr1	0,31	0,0465	27,32

Ifrd2	0,31	0,0307	32,69
Tnrc6c	0,31	0,0311	59,22
Pip4k2a	0,31	0,0194	51,00
Mfn2	0,31	0,0207	34,94
Tnfrsf21	0,31	0,0366	43,10
Fut4	0,31	0,0262	38,09
Zscan22	0,31	0,0392	63,99
Bcr	0,31	0,0183	33,53
Lrrc41	0,30	0,0280	29,20
Rhobtb2	0,30	0,0146	38,73
Snap47	0,30	0,0136	38,34
Nit1	0,30	0,0274	38,83
Trappc5	0,30	0,0128	46,45
Spsb3	0,30	0,0456	60,87
Zfp628	0,30	0,0268	30,90
Shq1	0,30	0,0170	57,62
Ext2	0,30	0,0128	34,78
Mllt1	0,30	0,0244	59,26
Txndc15	0,30	0,0312	44,55
Btd	0,30	0,0454	76,41
Dtx4	0,30	0,0344	33,01
Mtf1	0,30	0,0187	54,48
Tgfbrap1	0,30	0,0175	58,93
Thap11	0,30	0,0245	35,59
Serac1	0,29	0,0494	35,17
Ptrh2	0,29	0,0215	41,29
Tapt1	0,29	0,0100	49,44
Dcun1d2	0,29	0,0396	72,24
Traf6	0,29	0,0094	41,12
Ccdc32	0,29	0,0219	47,74
Gnptab	0,29	0,0264	42,27
Tpst2	0,29	0,0346	57,97
Traf3	0,28	0,0267	26,37
Herc2	0,28	0,0444	84,51
H6pd	0,28	0,0362	53,14
Ubox5	0,28	0,0219	60,08
Fem1b	0,28	0,0322	71,23
Ubiad1	0,28	0,0359	28,66
Ccdc93	0,28	0,0209	33,21
Rnf25	0,28	0,0232	32,83
Kctd1	0,28	0,0392	42,12
2310022A10Rik	0,27	0,0340	46,76
Aste1	0,27	0,0388	34,20
Cln5	0,27	0,0387	38,70
Hes6	0,27	0,0472	34,07
Dot1l	0,27	0,0136	64,36
Dicer1	0,27	0,0266	58,47
Cln8	0,27	0,0417	62,95
Tmem216	0,27	0,0361	64,51
Aak1	0,27	0,0428	37,46
Patz1	0,27	0,0485	76,12

Kdm2b	0,27	0,0475	31,53
Cdca4	0,27	0,0280	39,06
Fitm2	0,27	0,0259	35,40
Ttc1	0,26	0,0286	30,80
Ltbr	0,26	0,0475	56,10
E130309D02Rik	0,26	0,0194	64,53
Gemin7	0,26	0,0219	42,00
Pi4kb	0,26	0,0413	31,60
Phf23	0,26	0,0345	29,59
Fes	0,26	0,0275	39,88
Ammecr1l	0,26	0,0247	36,73
Rbm28	0,26	0,0447	25,13
Scaf1	0,26	0,0269	47,72
Nacc1	0,26	0,0226	35,17
Pcbp1	0,26	0,0489	46,38
Cdk9	0,26	0,0130	39,91
Ctsz	0,26	0,0428	28,95
Naif1	0,26	0,0340	43,04
Rev1	0,26	0,0314	67,80
Eme2	0,25	0,0360	60,87
Gne	0,25	0,0364	45,93
Plekhm2	0,25	0,0423	55,24
Fam53b	0,25	0,0355	73,98
Stk11	0,25	0,0266	73,26
Brap	0,24	0,0361	28,22
Mif4gd	0,24	0,0403	31,14
Mon1a	0,24	0,0243	28,36
Klhl26	0,24	0,0266	82,66
Sharpin	0,24	0,0424	34,88
Akap1	0,24	0,0291	28,59
Mettl8	0,23	0,0485	31,71
Ecd	0,23	0,0494	27,67
1700017B05Rik	0,23	0,0423	62,24
Cdk13	0,23	0,0494	78,12
Crkl	0,22	0,0293	78,36
Stx6	0,22	0,0359	26,88
Spin1	0,22	0,0444	35,19
Fiz1	0,21	0,0364	33,08
Trim27	0,21	0,0385	58,48

Appendix 2 List of significantly upregulated genes ($p<0.05$) in *Ythdf2*$^{fl/fl}$;*Vav-iCre* pre-leukaemic cells that are highly methylated in *Ythdf2*$^{fl/fl}$ pre-leukaemic cells ($-\log_{10}q>25$) and methylated in MA9.3ITD and NOMO-1 cells. Symbol, gene symbol; $\log_2$(FC), expression fold change ($\log_2$); adj. P Value, moderated t-statistics adjusted P value for the expression change; $-\log_{10}$(q), peak calling false discovery rate ($-\log_{10}$).

Symbol	Pearson coef.
DEF8	-0,466
TNFRSF1B	-0,452
GPR84	-0,428
RXRA	-0,423
B3GNT8	-0,379
RHOU	-0,361
TADA2B	-0,326
OSBPL11	-0,324
B4GALT4	-0,323
SNX20	-0,321
TXNDC15	-0,310
TYMP	-0,308
ITPK1	-0,306
NIF3L1	-0,295
FAM110A	-0,288
IL21R	-0,285
LSM10	-0,284
CTSZ	-0,282
EXO1	-0,282
NIT1	-0,281
BATF	-0,274
GPR160	-0,272
ADAP1	-0,269
FEN1	-0,269
DEF6	-0,266
UBTD1	-0,262
RALB	-0,261
CABLES2	-0,261
KIAA2013	-0,245
ZCCHC17	-0,239
TPST2	-0,237
PIP4K2A	-0,227
TTC1	-0,227
C10orf128	-0,220
FITM2	-0,218
NUPL2	-0,211
NLRX1	-0,203
RNPEPL1	-0,196
TRIM27	-0,189
MTF1	-0,189
SIPA1	-0,188
LRR1	-0,184
ZSCAN22	-0,182
STEAP3	-0,176
PLEKHO2	-0,172
IPO13	-0,172
ELMOD3	-0,168
C19orf47	-0,166
WDR81	-0,165

CTNS	-0,162
STX6	-0,159
ASB8	-0,154
C11orf24	-0,150
SPRYD4	-0,148
DICER1	-0,147
C5orf30	-0,143
AGAP2	-0,142
MFN2	-0,138
MAX	-0,128
BTD	-0,126
BCL9L	-0,123
FKBPL	-0,122
SRXN1	-0,120
STK11	-0,120
SHARPIN	-0,119
COMMD5	-0,117
TRAPPC5	-0,112
PHF23	-0,108
CYTH4	-0,108
ST6GALNAC4	-0,107
EIF2AK1	-0,106
TMEM216	-0,106
ZW10	-0,104
TRAF3	-0,101
SLC35A4	-0,100
SAC3D1	-0,100
FES	-0,100
ZDHHC3	-0,099
SH3TC1	-0,098
ZNF507	-0,096
REV1	-0,091
SHQ1	-0,087
TULP4	-0,087
EXTL3	-0,083
CDK13	-0,081
SRRD	-0,081
TK1	-0,081
DTX4	-0,079
SPSB3	-0,079
NUP50	-0,078
MRPS18B	-0,077
INTS5	-0,077
MIF4GD	-0,073
PCBP1	-0,073
BMPR1A	-0,069
POLN	-0,062
PTPN12	-0,062
ZNF771	-0,060
HES6	-0,056
AKAP1	-0,054

ZBTB45	-0,052
MLLT1	-0,045
FIZ1	-0,042
H6PD	-0,041
UBOX5	-0,038
PHACTR2	-0,035
GRPEL1	-0,032
EME2	-0,022
MRPL46	-0,021
SDHAF2	-0,012
ARL4A	-0,010
POP7	-0,010
AAK1	-0,006
FAM53B	-0,006
SCAF1	-0,002
SERAC1	-0,001
NUDT18	0,000
COX10	0,001
PHLDA3	0,006
ZFP36L2	0,006
ORAI3	0,011
FUT4	0,011
TAF1C	0,012
RNF8	0,015
NFATC2	0,022
SLC35B4	0,023
COG8	0,024
CLN8	0,025
TNRC6C	0,031
MTMR10	0,036
GEMIN7	0,037
BDH1	0,038
ZNF282	0,039
TIMM8A	0,039
RNF25	0,042
GRWD1	0,046
PHOSPHO2	0,049
NAA40	0,050
ASTE1	0,052
SPHK2	0,054
MRPS34	0,054
JAGN1	0,055
LRRC14	0,056
LTBR	0,058
S1PR2	0,060
MRPS25	0,061
THAP11	0,064
MRPS7	0,068
FAM20B	0,074
PTRH2	0,080
C1GALT1	0,080

RIPK1	0,082
AKR7A2	0,083
VPS18	0,093
BCL9	0,095
PGPEP1	0,096
NARFL	0,099
DOT1L	0,102
SLC10A3	0,102
HYAL2	0,104
CSTF1	0,112
THAP7	0,112
MCAT	0,116
TAF5L	0,117
CCDC93	0,119
TRIM65	0,120
MON1A	0,122
RHOBTB2	0,127
AEN	0,131
KCTD1	0,132
MRPL15	0,133
CEP68	0,135
NCOR2	0,140
TAPT1	0,141
PIP4K2B	0,141
TESK1	0,142
EIF2B1	0,144
AKR7A3	0,145
RYBP	0,146
GNPTAB	0,147
NOL6	0,147
EMILIN1	0,147
RBM28	0,151
NACC1	0,159
SSSCA1	0,160
UBTD2	0,160
RAB35	0,162
TEX264	0,163
RBM19	0,165
TPRN	0,166
TNFAIP8L1	0,166
JMJD4	0,168
HPS4	0,169
AGPAT2	0,169
LRRC41	0,171
PANX1	0,177
SPN	0,178
PDE12	0,182
PIKFYVE	0,183
UBIAD1	0,184
BRAP	0,185
ANKRD40	0,186

GNB1L	0,188
C15orf39	0,190
NANP	0,192
URGCP	0,197
METTL8	0,197
GEMIN4	0,201
PDPR	0,205
BYSL	0,206
ZNHIT2	0,209
CHAF1B	0,214
FOXP4	0,215
NEU1	0,217
MRTO4	0,218
MRPL43	0,224
DCUN1D2	0,224
SNX33	0,230
TMEM115	0,231
IFRD2	0,231
C19orf53	0,232
CXorf40A	0,233
SAP30BP	0,242
C2CD2	0,246
DHX33	0,249
NAIF1	0,253
CXorf40B	0,259
ZNF746	0,259
ZDHHC8	0,260
CDCA4	0,261
TXNL4A	0,262
RPUSD1	0,265
FKRP	0,265
TNFRSF21	0,266
DNAJC30	0,267
PI4KB	0,270
HERC2	0,271
MFSD5	0,276
PLEKHO1	0,277
SUPT7L	0,282
CABLES1	0,284
IRGM	0,286
EXT2	0,289
SF3B4	0,293
KCTD6	0,302
RPS19BP1	0,302
TRMT61A	0,314
BEND3	0,318
C12orf43	0,319
BRMS1	0,323
CDK9	0,323
FAM69B	0,334
CHPF2	0,347

HSPA13	0,349
KDM2B	0,349
CGRRF1	0,352
DBF4	0,356
ISG20L2	0,356
PLEKHM2	0,358
ECD	0,365
KLHL26	0,377
C7orf26	0,377
ZNF628	0,379
SIAH1	0,400
MRPS2	0,413
CLN5	0,422
RPUSD2	0,423
ABT1	0,425
SPIN1	0,426
CRKL	0,428
TRAF6	0,429
NXT1	0,438
AMMECR1L	0,441
CHRAC1	0,444
MAD2L1BP	0,445
CLP1	0,453
USPL1	0,466
GNE	0,486
C3orf38	0,489
BCR	0,490
FEM1B	0,508
TGFBRAP1	0,528
CCDC59	0,547
PATZ1	0,553
KBTBD4	0,572
YTHDF1	0,590
BAG5	0,596
MRPS30	0,680

Appendix 3 Correlation with YTHDF2 expression levels across human AML samples for genes significantly upregulated ($p<0.05$) in *Ythdf2*$^{fl/fl}$;*Vav-iCre* pre-leukaemic cells that are highly methylated in *Ythdf2*$^{fl/fl}$ pre-leukaemic cells ($-\log_{10}q > 25$) and methylated in MA9.3ITD and NOMO-1 cells. Symbol, gene symbol; Pearson coef., Pearson correlation coefficient.

References

Acar, M., K. S. Kocherlakota, M. M. Murphy, J. G. Peyer, H. Oguro, C. N. Inra, C. Jaiyeola, Z. Zhao, K. Luby-Phelps and S. J. Morrison (2015). "Deep imaging of bone marrow shows non-dividing stem cells are mainly perisinusoidal." Nature **526**(7571): 126.

Adolfsson, J., O. J. Borge, D. Bryder, K. Theilgaard-Mönch, I. Åstrand-Grundström, E. Sitnicka, Y. Sasaki and S. E. Jacobsen (2001). "Upregulation of Flt3 expression within the bone marrow Lin− Sca1+ c-kit+ stem cell compartment is accompanied by loss of self-renewal capacity." Immunity **15**(4): 659-669.

Adolfsson, J., R. Månsson, N. Buza-Vidas, A. Hultquist, K. Liuba, C. T. Jensen, D. Bryder, L. Yang, O.-J. Borge and L. A. Thoren (2005). "Identification of Flt3+ lympho-myeloid stem cells lacking erythro-megakaryocytic potential: a revised road map for adult blood lineage commitment." Cell **121**(2): 295-306.

Aggarwal, B. B. (2003). "Signalling pathways of the TNF superfamily: a double-edged sword." Nature reviews immunology **3**(9): 745.

Akashi, K., D. Traver, T. Miyamoto and I. L. Weissman (2000). "A clonogenic common myeloid progenitor that gives rise to all myeloid lineages." Nature **404**(6774): 193.

Al-Anazi, K. A. (2012). "Autologous hematopoietic stem cell transplantation for multiple myeloma without cryopreservation." Bone marrow research **2012**.

Alarcón, C. R., H. Goodarzi, H. Lee, X. Liu, S. Tavazoie and S. F. Tavazoie (2015). "HNRNPA2B1 is a mediator of m6A-dependent nuclear RNA processing events." Cell **162**(6): 1299-1308.

Alarcón, C. R., H. Lee, H. Goodarzi, N. Halberg and S. F. Tavazoie (2015). "N 6-methyladenosine marks primary microRNAs for processing." Nature **519**(7544): 482.

Arber, D. A., A. Orazi, R. Hasserjian, J. Thiele, M. J. Borowitz, M. M. Le Beau, C. D. Bloomfield, M. Cazzola and J. W. Vardiman (2016). "The 2016 revision to the World Health Organization classification of myeloid neoplasms and acute leukemia." Blood **127**(20): 2391-2405.

Armstrong, S. A., J. E. Staunton, L. B. Silverman, R. Pieters, M. L. den Boer, M. D. Minden, S. E. Sallan, E. S. Lander, T. R. Golub and S. J. Korsmeyer (2001). "MLL translocations specify a distinct gene expression profile that distinguishes a unique leukemia." Nature genetics **30**(1): 41.

Ashburner, M., C. A. Ball, J. A. Blake, D. Botstein, H. Butler, J. M. Cherry, A. P. Davis, K. Dolinski, S. S. Dwight and J. T. Eppig (2000). "Gene ontology: tool for the unification of biology." Nature genetics **25**(1): 25.

Avellino, R. and R. Delwel (2017). "Expression and regulation of C/EBPα in normal myelopoiesis and in malignant transformation." Blood **129**(15): 2083-2091.

Ayton, P. M. and M. L. Cleary (2003). "Transformation of myeloid progenitors by MLL oncoproteins is dependent on Hoxa7 and Hoxa9." Genes & development **17**(18): 2298-2307.

Bachas, C., G. J. Schuurhuis, C. M. Zwaan, M. M. van den Heuvel-Eibrink, M. L. den Boer, E. S. de Bont, Z. J. Kwidama, D. Reinhardt, U. Creutzig, V. de Haas, G. J. Kaspers and J. Cloos (2015). "Gene expression profiles associated with pediatric relapsed AML." PLoS One **10**(4): e0121730.

Bailey, A. S., P. J. Batista, R. S. Gold, Y. G. Chen, D. G. de Rooij, H. Y. Chang and M. T. Fuller (2017). "The conserved RNA helicase YTHDC2 regulates the transition from proliferation to differentiation in the germline." Elife **6**: e26116.
Bansal, H., Q. Yihua, S. P. Iyer, S. Ganapathy, D. Proia, L. Penalva, P. Uren, U. Suresh, J. Carew and A. Karnad (2014). "WTAP is a novel oncogenic protein in acute myeloid leukemia." Leukemia **28**(5): 1171.
Barbieri, I., K. Tzelepis, L. Pandolfini, J. Shi, G. Millán-Zambrano, S. C. Robson, D. Aspris, V. Migliori, A. J. Bannister and N. Han (2017). "Promoter-bound METTL3 maintains myeloid leukaemia by m 6 A-dependent translation control." Nature **552**(7683): 126.
Baron, M. H., J. Isern and S. T. Fraser (2012). "The embryonic origins of erythropoiesis in mammals." Blood **119**(21): 4828-4837.
Batista, P. J., B. Molinie, J. Wang, K. Qu, J. Zhang, L. Li, D. M. Bouley, E. Lujan, B. Haddad, K. Daneshvar, A. C. Carter, R. A. Flynn, C. Zhou, K. S. Lim, P. Dedon, M. Wernig, A. C. Mullen, Y. Xing, C. C. Giallourakis and H. Y. Chang (2014). "m(6)A RNA modification controls cell fate transition in mammalian embryonic stem cells." Cell Stem Cell **15**(6): 707-719.
Becker, A. J., E. A. McCulloch and J. E. Till (1963). "Cytological demonstration of the clonal nature of spleen colonies derived from transplanted mouse marrow cells."
Beerman, I., D. Bhattacharya, S. Zandi, M. Sigvardsson, I. L. Weissman, D. Bryder and D. J. Rossi (2010). "Functionally distinct hematopoietic stem cells modulate hematopoietic lineage potential during aging by a mechanism of clonal expansion." Proceedings of the National Academy of Sciences **107**(12): 5465-5470.
Bene, M., G. Castoldi, W. Knapp, W. Ludwig, E. Matutes, A. Orfao and M. Veer van't (1995). "Proposals for the immunological classification of acute leukemias. European Group for the Immunological Characterization of Leukemias (EGIL)." Leukemia **9**(10): 1783-1786.
Benjamin, D. Y., J. L. Hess, S. E. Horning, G. A. Brown and S. J. Korsmeyer (1995). "Altered Hox expression and segmental identity in Mll-mutant mice." Nature **378**(6556): 505.
Benjamini, Y. and Y. Hochberg (1995). "Controlling the False Discovery Rate: A Practical and Powerful Approach to Multiple Testing." Journal of the Royal Statistical Society. Series B (Methodological) **57**(1): 289-300.
Bennett, J. M., D. Catovsky, M. T. Daniel, G. Flandrin, D. A. Galton, H. R. Gralnick and C. Sultan (1976). "Proposals for the classification of the acute leukaemias French-American-British (FAB) co-operative group." British journal of haematology **33**(4): 451-458.
Benveniste, P., C. Frelin, S. Janmohamed, M. Barbara, R. Herrington, D. Hyam and N. N. Iscove (2010). "Intermediate-term hematopoietic stem cells with extended but time-limited reconstitution potential." Cell stem cell **6**(1): 48-58.
Biosciences, B. and S. Jose (2012). "Studying Mouse Thymocyte Development using Multiparametric Flow Cytometry: An Efficient Method to Improve an 8-Color Panel on the BD FACSVerse™ System."
Blank, U., G. Karlsson and S. Karlsson (2008). "Signaling pathways governing stem-cell fate." Blood **111**(2): 492-503.

Boccaletto, P., M. A. Machnicka, E. Purta, P. Piątkowski, B. Bagiński, T. K. Wirecki, V. de Crécy-Lagard, R. Ross, P. A. Limbach and A. Kotter (2017). "MODOMICS: a database of RNA modification pathways. 2017 update." Nucleic acids research **46**(D1): D303-D307.
Bokar, J., M. Shambaugh, D. Polayes, A. Matera and F. Rottman (1997). "Purification and cDNA cloning of the AdoMet-binding subunit of the human mRNA (N6-adenosine)-methyltransferase." Rna **3**(11): 1233-1247.
Bornstein, C., S. Nevo, A. Giladi, N. Kadouri, M. Pouzolles, F. Gerbe, E. David, A. Machado, A. Chuprin and B. Tóth (2018). "Single-cell mapping of the thymic stroma identifies IL-25-producing tuft epithelial cells." Nature **559**(7715): 622.
Borrow, J., V. P. Stanton, J. M. Andresen, R. Becher, F. G. Behm, R. S. Chaganti, C. I. Civin, C. Disteche, I. Dubé and A. M. Frischauf (1996). "The translocation t (8; 16)(p11; p13) of acute myeloid leukaemia fuses a putative acetyltransferase to the CREB–binding protein." Nature genetics **14**(1): 33.
Boulais, P. E. and P. S. Frenette (2015). "Making sense of hematopoietic stem cell niches." Blood **125**(17): 2621-2629.
Boyer, S. W., A. V. Schroeder, S. Smith-Berdan and E. C. Forsberg (2011). "All hematopoietic cells develop from hematopoietic stem cells through Flk2/Flt3-positive progenitor cells." Cell stem cell **9**(1): 64-73.
Broxmeyer, H., D. Williams, L. Lu, S. Cooper, S. Anderson, G. Beyer, R. Hoffman and B. Rubin (1986). "The suppressive influences of human tumor necrosis factors on bone marrow hematopoietic progenitor cells from normal donors and patients with leukemia: synergism of tumor necrosis factor and interferon-gamma." The Journal of Immunology **136**(12): 4487-4495.
Bruns, I., D. Lucas, S. Pinho, J. Ahmed, M. P. Lambert, Y. Kunisaki, C. Scheiermann, L. Schiff, M. Poncz and A. Bergman (2014). "Megakaryocytes regulate hematopoietic stem cell quiescence through CXCL4 secretion." Nature medicine **20**(11): 1315.
Bryder, D., V. Ramsfjell, I. Dybedal, K. Theilgaard-Mönch, C.-M. Högerkorp, J. Adolfsson, O. J. Borge and S. E. W. Jacobsen (2001). "Self-renewal of multipotent long-term repopulating hematopoietic stem cells is negatively regulated by Fas and tumor necrosis factor receptor activation." Journal of Experimental Medicine **194**(7): 941-952.
Buenrostro, J. D., M. R. Corces, C. A. Lareau, B. Wu, A. N. Schep, M. J. Aryee, R. Majeti, H. Y. Chang and W. J. Greenleaf (2018). "Integrated single-cell analysis maps the continuous regulatory landscape of human hematopoietic differentiation." Cell **173**(6): 1535-1548. e1516.
Bueso-Ramos, C. E., R. Kanagal-Shamanna, M. J. Routbort and C. A. Hanson (2015). "Therapy-related myeloid neoplasms." American journal of clinical pathology **144**(2): 207-218.
Burnett, A. K., N. H. Russell, A. E. Hunter, D. Milligan, S. Knapper, K. Wheatley, J. Yin, M. F. McMullin, S. Ali and D. Bowen (2013). "Clofarabine doubles the response rate in older patients with acute myeloid leukemia but does not improve survival." Blood **122**(8): 1384-1394.

Busch, K., K. Klapproth, M. Barile, M. Flossdorf, T. Holland-Letz, S. M. Schlenner, M. Reth, T. Höfer and H.-R. Rodewald (2015). "Fundamental properties of unperturbed haematopoiesis from stem cells in vivo." Nature **518**(7540): 542.
Byrd, J. C., K. Mrózek, R. K. Dodge, A. J. Carroll, C. G. Edwards, D. C. Arthur, M. J. Pettenati, S. R. Patil, K. W. Rao and M. S. Watson (2002). "Pretreatment cytogenetic abnormalities are predictive of induction success, cumulative incidence of relapse, and overall survival in adult patients with de novo acute myeloid leukemia: results from Cancer and Leukemia Group B (CALGB 8461): presented in part at the 43rd annual meeting of the American Society of Hematology, Orlando, FL, December 10, 2001, and published in abstract form. 59." Blood **100**(13): 4325-4336.
Carapeti, M., R. C. Aguiar, J. M. Goldman and N. C. Cross (1998). "A novel fusion between MOZ and the nuclear receptor coactivator TIF2 in acute myeloid leukemia." Blood **91**(9): 3127-3133.
Carapeti, M., R. C. Aguiar, A. E. Watmore, J. M. Goldman and N. C. Cross (1999). "Consistent fusion of MOZ and TIF2 in AML with inv (8)(p11q13)." Cancer genetics and cytogenetics **113**(1): 70-72.
Cardelli, M., F. Marchegiani, L. Cavallone, F. Olivieri, S. Giovagnetti, E. Mugianesi, R. Moresi, R. Lisa and C. Franceschi (2006). "A polymorphism of the YTHDF2 gene (1p35) located in an Alu-rich genomic domain is associated with human longevity." The Journals of Gerontology Series A: Biological Sciences and Medical Sciences **61**(6): 547-556.
Carlile, T. M., M. F. Rojas-Duran, B. Zinshteyn, H. Shin, K. M. Bartoli and W. V. Gilbert (2014). "Pseudouridine profiling reveals regulated mRNA pseudouridylation in yeast and human cells." Nature **515**(7525): 143.
Carrelha, J., Y. Meng, L. M. Kettyle, T. C. Luis, R. Norfo, V. Alcolea, H. Boukarabila, F. Grasso, A. Gambardella and A. Grover (2018). "Hierarchically related lineage-restricted fates of multipotent haematopoietic stem cells." Nature **554**(7690): 106.
Caslini, C., A. Serna, V. Rossi, M. Introna and A. Biondi (2004). "Modulation of cell cycle by graded expression of MLL-AF4 fusion oncoprotein." Leukemia **18**(6): 1064.
Castilla, L. H., L. Garrett, N. Adya, D. Orlic, A. Dutra, S. Anderson, J. Owens, M. Eckhaus, D. Bodine and P. P. Liu (1999). "The fusion gene Cbfb-MYH11 blocks myeloid differentiation and predisposes mice to acute myelomonocytic leukaemia." Nature genetics **23**(2): 144.
Caux, C., S. Saeland, C. Favre, V. Duvert, P. Mannoni and J. Banchereau (1990). "Tumor necrosis factor-alpha strongly potentiates interleukin-3 and granulocyte-macrophage colony-stimulating factor-induced proliferation of human CD34+ hematopoietic progenitor cells." Blood **75**(12): 2292-2298.
Cazzola, M., M. G. Della Porta and L. Malcovati (2013). "The genetic basis of myelodysplasia and its clinical relevance." Blood **122**(25): 4021-4034.
Cerami, E., J. Gao, U. Dogrusoz, B. E. Gross, S. O. Sumer, B. A. Aksoy, A. Jacobsen, C. J. Byrne, M. L. Heuer and E. Larsson (2012). The cBio cancer genomics portal: an open platform for exploring multidimensional cancer genomics data, AACR.
Chan, C. K., C.-C. Chen, C. A. Luppen, J.-B. Kim, A. T. DeBoer, K. Wei, J. A. Helms, C. J. Kuo, D. L. Kraft and I. L. Weissman (2009). "Endochondral ossification is required for haematopoietic stem-cell niche formation." Nature **457**(7228): 490.

Chapiro, E., L. Russell, I. Radford-Weiss, C. Bastard, M. Lessard, S. Struski, H. Cave, S. Fert-Ferrer, C. Barin and O. Maarek (2006). "Overexpression of CEBPA resulting from the translocation t (14; 19)(q32; q13) of human precursor B acute lymphoblastic leukemia." Blood **108**(10): 3560-3563.
Chen, J., Y. Sun, X. Xu, D. Wang, J. He, H. Zhou, Y. Lu, J. Zeng, F. Du and A. Gong (2017). "YTH domain family 2 orchestrates epithelial-mesenchymal transition/proliferation dichotomy in pancreatic cancer cells." Cell Cycle **16**(23): 2259-2271.
Chen, M., L. Wei, C. T. Law, F. H. C. Tsang, J. Shen, C. L. H. Cheng, L. H. Tsang, D. W. H. Ho, D. K. C. Chiu and J. M. F. Lee (2018). "RNA N6-methyladenosine methyltransferase-like 3 promotes liver cancer progression through YTHDF2-dependent posttranscriptional silencing of SOCS2." Hepatology **67**(6): 2254-2270.
Chen, W., A. R. Kumar, W. A. Hudson, Q. Li, B. Wu, R. A. Staggs, E. A. Lund, T. N. Sam and J. H. Kersey (2008). "Malignant transformation initiated by Mll-AF9: gene dosage and critical target cells." Cancer cell **13**(5): 432-440.
Chen, X., H. Deng, M. J. Churchill, L. L. Luchsinger, X. Du, T. H. Chu, R. A. Friedman, M. Middelhoff, H. Ding and Y. H. Tailor (2017). "Bone marrow myeloid cells regulate myeloid-biased hematopoietic stem cells via a histamine-dependent feedback loop." Cell Stem Cell **21**(6): 747-760. e747.
Chen, X., H. Xie, B. L. Wood, R. B. Walter, J. M. Pagel, P. S. Becker, V. K. Sandhu, J. L. Abkowitz, F. R. Appelbaum and E. H. Estey (2015). "Relation of clinical response and minimal residual disease and their prognostic impact on outcome in acute myeloid leukemia." Journal of Clinical Oncology **33**(11): 1258-1264.
Cheson, B., J. Bennett, K. Kopecky, T. Büchner, C. Willman, E. Estey, C. Schiffer, H. Doehner, M. Tallman and T. Lister (2003). "International Working Group for Diagnosis, Standardization of Response Criteria, Treatment Outcomes, and Reporting Standards for Therapeutic Trials in Acute Myeloid Leukemia. Revised recommendations of the International Working Group for Diagnosis, standardization of response criteria, treatment outcomes, and reporting standards for therapeutic trials in acute myeloid leukemia." J Clin Oncol **21**(24): 4642-4649.
Clancy, M. J., M. E. Shambaugh, C. S. Timpte and J. A. Bokar (2002). "Induction of sporulation in Saccharomyces cerevisiae leads to the formation of N 6-methyladenosine in mRNA: a potential mechanism for the activity of the IME4 gene." Nucleic acids research **30**(20): 4509-4518.
Clapp, D. W., B. Freie, W. H. Lee and Y. Y. Zhang (1995). "Molecular evidence that in situ-transduced fetal liver hematopoietic stem/progenitor cells give rise to medullary hematopoiesis in adult rats." Blood **86**(6): 2113-2122.
Cohn, W. E. (1960). "Pseudouridine, a carbon-carbon linked ribonucleoside in ribonucleic acids: isolation, structure, and chemical characteristics." Journal of Biological Chemistry **235**(5): 1488-1498.
Cohn, W. E. and E. Volkin (1951). "Nucleoside-5'-phosphates from ribonucleic acid." Nature **167**(4247): 483.
Copelan, E. A. (2006). "Hematopoietic stem-cell transplantation." New England Journal of Medicine **354**(17): 1813-1826.
Creutzig, U., M. Zimmermann, D. Reinhardt, M. Rasche, C. von Neuhoff, T. Alpermann, M. Dworzak, K. Perglerová, Z. Zemanova and J. Tchinda (2016). "Changes

in cytogenetics and molecular genetics in acute myeloid leukemia from childhood to adult age groups." Cancer **122**(24): 3821-3830.
Croker, B. A., D. Metcalf, L. Robb, W. Wei, S. Mifsud, L. DiRago, L. A. Cluse, K. D. Sutherland, L. Hartley and E. Williams (2004). "SOCS3 is a critical physiological negative regulator of G-CSF signaling and emergency granulopoiesis." Immunity **20**(2): 153-165.
Cui, Q., H. Shi, P. Ye, L. Li, Q. Qu, G. Sun, G. Sun, Z. Lu, Y. Huang and C.-G. Yang (2017). "m6A RNA methylation regulates the self-renewal and tumorigenesis of glioblastoma stem cells." Cell reports **18**(11): 2622-2634.
Dahlberg, A., C. Delaney and I. D. Bernstein (2011). "Ex vivo expansion of human hematopoietic stem and progenitor cells." Blood **117**(23): 6083-6090.
Davis, D. R. (1995). "Stabilization of RNA stacking by pseudouridine." Nucleic acids research **23**(24): 5020-5026.
de Boer, J., A. Williams, G. Skavdis, N. Harker, M. Coles, M. Tolaini, T. Norton, K. Williams, K. Roderick and A. J. Potocnik (2003). "Transgenic mice with hematopoietic and lymphoid specific expression of Cre." European journal of immunology **33**(2): 314-325.
de Bruijn, M. and E. Dzierzak (2017). "Runx transcription factors in the development and function of the definitive hematopoietic system." Blood **129**(15): 2061-2069.
De Bruijn, M. F., X. Ma, C. Robin, K. Ottersbach, M.-J. Sanchez and E. Dzierzak (2002). "Hematopoietic stem cells localize to the endothelial cell layer in the midgestation mouse aorta." Immunity **16**(5): 673-683.
De Kouchkovsky, I. and M. Abdul-Hay (2016). "Acute myeloid leukemia: a comprehensive review and 2016 update." Blood cancer journal **6**(7): e441.
De Lima, M., I. McNiece, S. N. Robinson, M. Munsell, M. Eapen, M. Horowitz, A. Alousi, R. Saliba, J. D. McMannis and I. Kaur (2012). "Cord-blood engraftment with ex vivo mesenchymal-cell coculture." New England Journal of Medicine **367**(24): 2305-2315.
de Sauvage, F. J., K. Carver-Moore, S.-M. Luoh, A. Ryan, M. Dowd, D. L. Eaton and M. W. Moore (1996). "Physiological regulation of early and late stages of megakaryocytopoiesis by thrombopoietin." Journal of Experimental Medicine **183**(2): 651-656.
de Thé, H., C. Chomienne, M. Lanotte, L. Degos and A. Dejean (1990). "The t (15; 17) translocation of acute promyelocytic leukaemia fuses the retinoic acid receptor α gene to a novel transcribed locus." Nature **347**(6293): 558.
Deguchi, K., P. M. Ayton, M. Carapeti, J. L. Kutok, C. S. Snyder, I. R. Williams, N. C. Cross, C. K. Glass, M. L. Cleary and D. G. Gilliland (2003). "MOZ-TIF2-induced acute myeloid leukemia requires the MOZ nucleosome binding motif and TIF2-mediated recruitment of CBP." Cancer cell **3**(3): 259-271.
den Braber, I., T. Mugwagwa, N. Vrisekoop, L. Westera, R. Mögling, A. B. de Boer, N. Willems, E. H. Schrijver, G. Spierenburg and K. Gaiser (2012). "Maintenance of peripheral naive T cells is sustained by thymus output in mice but not humans." Immunity **36**(2): 288-297.

Desrosiers, R., K. Friderici and F. Rottman (1974). "Identification of methylated nucleosides in messenger RNA from Novikoff hepatoma cells." Proceedings of the National Academy of Sciences **71**(10): 3971-3975.
Dimitrova, D. G., L. Teysset and C. Carré (2019). "RNA 2'-O-Methylation (Nm) Modification in human diseases." Genes **10**(2): 117.
Ding, L. and S. J. Morrison (2013). "Haematopoietic stem cells and early lymphoid progenitors occupy distinct bone marrow niches." Nature **495**(7440): 231.
Ding, L., T. L. Saunders, G. Enikolopov and S. J. Morrison (2012). "Endothelial and perivascular cells maintain haematopoietic stem cells." Nature **481**(7382): 457.
Döhner, H., E. Estey, D. Grimwade, S. Amadori, F. R. Appelbaum, T. Büchner, H. Dombret, B. L. Ebert, P. Fenaux and R. A. Larson (2017). "Diagnosis and management of AML in adults: 2017 ELN recommendations from an international expert panel." Blood **129**(4): 424-447.
Döhner, H., E. H. Estey, S. Amadori, F. R. Appelbaum, T. Büchner, A. K. Burnett, H. Dombret, P. Fenaux, D. Grimwade and R. A. Larson (2010). "Diagnosis and management of acute myeloid leukemia in adults: recommendations from an international expert panel, on behalf of the European LeukemiaNet." Blood **115**(3): 453-474.
Döhner, H., D. J. Weisdorf and C. D. Bloomfield (2015). "Acute myeloid leukemia." New England Journal of Medicine **373**(12): 1136-1152.
Dombret, H., J. F. Seymour, A. Butrym, A. Wierzbowska, D. Selleslag, J. H. Jang, R. Kumar, J. Cavenagh, A. C. Schuh and A. Candoni (2015). "International phase 3 study of azacitidine vs conventional care regimens in older patients with newly diagnosed AML with> 30% blasts." Blood **126**(3): 291-299.
Dominissini, D., S. Moshitch-Moshkovitz, M. Salmon-Divon, N. Amariglio and G. Rechavi (2013). "Transcriptome-wide mapping of N 6-methyladenosine by m 6 A-seq based on immunocapturing and massively parallel sequencing." Nature protocols **8**(1): 176.
Dominissini, D., S. Nachtergaele, S. Moshitch-Moshkovitz, E. Peer, N. Kol, M. S. Ben-Haim, Q. Dai, A. Di Segni, M. Salmon-Divon and W. C. Clark (2016). "The dynamic N 1-methyladenosine methylome in eukaryotic messenger RNA." Nature **530**(7591): 441.
Dores, G. M., S. S. Devesa, R. E. Curtis, M. S. Linet and L. M. Morton (2012). "Acute leukemia incidence and patient survival among children and adults in the United States, 2001-2007." Blood **119**(1): 34-43.
Doulatov, S., F. Notta, E. Laurenti and J. E. Dick (2012). "Hematopoiesis: a human perspective." Cell stem cell **10**(2): 120-136.
Drabkin, H., C. Parsy, K. Ferguson, F. Guilhot, L. Lacotte, L. Roy, C. Zeng, A. Baron, S. Hunger and M. Varella-Garcia (2002). "Quantitative HOX expression in chromosomally defined subsets of acute myelogenous leukemia." Leukemia **16**(2): 186.
Du, H., Y. Zhao, J. He, Y. Zhang, H. Xi, M. Liu, J. Ma and L. Wu (2016). "YTHDF2 destabilizes m 6 A-containing RNA through direct recruitment of the CCR4–NOT deadenylase complex." Nature communications **7**: 12626.

Du, H., Y. Zhao, J. He, Y. Zhang, H. Xi, M. Liu, J. Ma and L. Wu (2016). "YTHDF2 destabilizes m(6)A-containing RNA through direct recruitment of the CCR4-NOT deadenylase complex." Nat Commun **7**: 12626.
Du, Y., N. A. Jenkins and N. G. Copeland (2005). "Insertional mutagenesis identifies genes that promote the immortalization of primary bone marrow progenitor cells." Blood **106**(12): 3932-3939.
Dubin, D. T. and R. H. Taylor (1975). "The methylation state of poly A-containing-messenger RNA from cultured hamster cells." Nucleic acids research **2**(10): 1653-1668.
Duran-Struuck, R. and R. C. Dysko (2009). "Principles of bone marrow transplantation (BMT): providing optimal veterinary and husbandry care to irradiated mice in BMT studies." Journal of the American Association for Laboratory Animal Science **48**(1): 11-22.
Dybedal, I., D. Bryder, A. Fossum, L. S. Rusten and S. E. W. Jacobsen (2001). "Tumor necrosis factor (TNF)–mediated activation of the p55 TNF receptor negatively regulates maintenance of cycling reconstituting human hematopoietic stem cells." Blood **98**(6): 1782-1791.
Edupuganti, R. R., S. Geiger, R. G. Lindeboom, H. Shi, P. J. Hsu, Z. Lu, S.-Y. Wang, M. P. Baltissen, P. W. Jansen and M. Rossa (2017). "N 6-methyladenosine (m 6 A) recruits and repels proteins to regulate mRNA homeostasis." Nature structural & molecular biology **24**(10): 870.
Elagib, K. E. and A. N. Goldfarb (2007). "Oncogenic pathways of AML1-ETO in acute myeloid leukemia: multifaceted manipulation of marrow maturation." Cancer letters **251**(2): 179-186.
Elkashef, S. M., A.-P. Lin, J. Myers, H. Sill, D. Jiang, P. L. Dahia and R. C. Aguiar (2017). "IDH mutation, competitive inhibition of FTO, and RNA methylation." Cancer cell **31**(5): 619-620.
Engel, M. and A. Chen (2018). "The emerging role of mRNA methylation in normal and pathological behavior." Genes, Brain and Behavior **17**(3): e12428.
Ernst, P., M. Mabon, A. J. Davidson, L. I. Zon and S. J. Korsmeyer (2004). "An Mll-dependent Hox program drives hematopoietic progenitor expansion." Current biology **14**(22): 2063-2069.
Esposito, M. T., L. Zhao, T. K. Fung, J. K. Rane, A. Wilson, N. Martin, J. Gil, A. Y. Leung, A. Ashworth and C. W. E. So (2015). "Synthetic lethal targeting of oncogenic transcription factors in acute leukemia by PARP inhibitors." Nature medicine **21**(12): 1481.
Essers, M. A., S. Offner, W. E. Blanco-Bose, Z. Waibler, U. Kalinke, M. A. Duchosal and A. Trumpp (2009). "IFNα activates dormant haematopoietic stem cells in vivo." Nature **458**(7240): 904.
Estey, E. H. (2013). "Acute myeloid leukemia: 2013 update on risk-stratification and management." American journal of hematology **88**(4): 317-327.
Etchin, J., Q. Sun, A. Kentsis, A. Farmer, Z. Zhang, T. Sanda, M. Mansour, C. Barcelo, D. McCauley and M. Kauffman (2013). "Antileukemic activity of nuclear export inhibitors that spare normal hematopoietic cells." Leukemia **27**(1): 66.

Fares, I., J. Chagraoui, Y. Gareau, S. Gingras, R. Ruel, N. Mayotte, E. Csaszar, D. J. Knapp, P. Miller and M. Ngom (2014). "Pyrimidoindole derivatives are agonists of human hematopoietic stem cell self-renewal." Science **345**(6203): 1509-1512.
Fernández, I. S., C. L. Ng, A. C. Kelley, G. Wu, Y.-T. Yu and V. Ramakrishnan (2013). "Unusual base pairing during the decoding of a stop codon by the ribosome." Nature **500**(7460): 107.
Fitzsimmons, C. M. and P. J. Batista (2018). "It's complicated… m6A-dependent regulation of gene expression in cancer." Biochimica et Biophysica Acta (BBA)-Gene Regulatory Mechanisms.
Forsberg, E. C., T. Serwold, S. Kogan, I. L. Weissman and E. Passegué (2006). "New evidence supporting megakaryocyte-erythrocyte potential of flk2/flt3+ multipotent hematopoietic progenitors." Cell **126**(2): 415-426.
Frenette, P. S., S. Pinho, D. Lucas and C. Scheiermann (2013). "Mesenchymal stem cell: keystone of the hematopoietic stem cell niche and a stepping-stone for regenerative medicine." Annual review of immunology **31**: 285-316.
Fu, L., C. R. Guerrero, N. Zhong, N. J. Amato, Y. Liu, S. Liu, Q. Cai, D. Ji, S.-G. Jin and L. J. Niedernhofer (2014). "Tet-mediated formation of 5-hydroxymethylcytosine in RNA." Journal of the American Chemical Society **136**(33): 11582-11585.
Fu, Y., G. Jia, X. Pang, R. Wang, X. Wang, C. Li, S. Smemo, Q. Dai, K. Bailey and M. Nobrega (2013). FTO-mediated formation of N6-hydroxymethyladenosine and N6-formyladenosine in mammalian RNA. Nat Commun 4: 1798.
Fustin, J.-M., M. Doi, Y. Yamaguchi, H. Hida, S. Nishimura, M. Yoshida, T. Isagawa, M. S. Morioka, H. Kakeya and I. Manabe (2013). "RNA-methylation-dependent RNA processing controls the speed of the circadian clock." Cell **155**(4): 793-806.
Gao, J., B. A. Aksoy, U. Dogrusoz, G. Dresdner, B. Gross, S. O. Sumer, Y. Sun, A. Jacobsen, R. Sinha and E. Larsson (2013). "Integrative analysis of complex cancer genomics and clinical profiles using the cBioPortal." Sci. Signal. **6**(269): pl1-pl1.
Gao, J., S. Graves, U. Koch, S. Liu, V. Jankovic, S. Buonamici, A. El Andaloussi, S. D. Nimer, B. L. Kee and R. Taichman (2009). "Hedgehog signaling is dispensable for adult hematopoietic stem cell function." Cell stem cell **4**(6): 548-558.
Garneau, N. L., J. Wilusz and C. J. Wilusz (2007). "The highways and byways of mRNA decay." Nature reviews Molecular cell biology **8**(2): 113.
Gekas, C., F. Dieterlen-Lièvre, S. H. Orkin and H. K. Mikkola (2005). "The placenta is a niche for hematopoietic stem cells." Developmental cell **8**(3): 365-375.
Gentleman, R. C., V. J. Carey, D. M. Bates, B. Bolstad, M. Dettling, S. Dudoit, B. Ellis, L. Gautier, Y. Ge, J. Gentry, K. Hornik, T. Hothorn, W. Huber, S. Iacus, R. Irizarry, F. Leisch, C. Li, M. Maechler, A. J. Rossini, G. Sawitzki, C. Smith, G. Smyth, L. Tierney, J. Y. Yang and J. Zhang (2004). "Bioconductor: open software development for computational biology and bioinformatics." Genome Biol **5**(10): R80.
Geula, S., S. Moshitch-Moshkovitz, D. Dominissini, A. A. Mansour, N. Kol, M. Salmon-Divon, V. Hershkovitz, E. Peer, N. Mor and Y. S. Manor (2015). "m6A mRNA methylation facilitates resolution of naïve pluripotency toward differentiation." Science **347**(6225): 1002-1006.
Ghosh, A. and C. D. Lima (2010). "Enzymology of RNA cap synthesis." Wiley Interdisciplinary Reviews: RNA **1**(1): 152-172.

Gill, S., S. K. Tasian, M. Ruella, O. Shestova, Y. Li, D. L. Porter, M. Carroll, G. Danet-Desnoyers, J. Scholler and S. A. Grupp (2014). "Preclinical targeting of human acute myeloid leukemia and myeloablation using chimeric antigen receptor–modified T cells." Blood **123**(15): 2343-2354.
Ginhoux, F., M. Greter, M. Leboeuf, S. Nandi, P. See, S. Gokhan, M. F. Mehler, S. J. Conway, L. G. Ng and E. R. Stanley (2010). "Fate mapping analysis reveals that adult microglia derive from primitive macrophages." Science **330**(6005): 841-845.
Ginhoux, F. and M. Guilliams (2016). "Tissue-resident macrophage ontogeny and homeostasis." Immunity **44**(3): 439-449.
Glass, C. K., D. W. Rose and M. G. Rosenfeld (1997). "Nuclear receptor coactivators." Current opinion in cell biology **9**(2): 222-232.
Godwin, C., R. Gale and R. Walter (2017). "Gemtuzumab ozogamicin in acute myeloid leukemia." Leukemia **31**(9): 1855.
Golub, T. R., D. K. Slonim, P. Tamayo, C. Huard, M. Gaasenbeek, J. P. Mesirov, H. Coller, M. L. Loh, J. R. Downing and M. A. Caligiuri (1999). "Molecular classification of cancer: class discovery and class prediction by gene expression monitoring." science **286**(5439): 531-537.
Goodell, M. A., K. Brose, G. Paradis, A. S. Conner and R. C. Mulligan (1996). "Isolation and functional properties of murine hematopoietic stem cells that are replicating in vivo." Journal of Experimental Medicine **183**(4): 1797-1806.
Gozdecka, M., E. Meduri, M. Mazan, K. Tzelepis, M. Dudek, A. J. Knights, M. Pardo, L. Yu, J. S. Choudhary and E. Metzakopian (2018). "UTX-mediated enhancer and chromatin remodeling suppresses myeloid leukemogenesis through noncatalytic inverse regulation of ETS and GATA programs." Nature genetics **50**(6): 883.
Gray, D. H., N. Seach, T. Ueno, M. K. Milton, A. Liston, A. M. Lew, C. C. Goodnow and R. L. Boyd (2006). "Developmental kinetics, turnover, and stimulatory capacity of thymic epithelial cells." Blood **108**(12): 3777-3785.
Greenbaum, A., Y.-M. S. Hsu, R. B. Day, L. G. Schuettpelz, M. J. Christopher, J. N. Borgerding, T. Nagasawa and D. C. Link (2013). "CXCL12 in early mesenchymal progenitors is required for haematopoietic stem-cell maintenance." Nature **495**(7440): 227.
Grosso, D. A., R. C. Hess and M. A. Weiss (2015). "Immunotherapy in acute myeloid leukemia." Cancer **121**(16): 2689-2704.
Gruber, T. A. and J. R. Downing (2015). "The biology of pediatric acute megakaryoblastic leukemia." Blood **126**(8): 943-949.
Guillouf, C., I. Gallais and F. Moreau-Gachelin (2006). "Spi-1/PU. 1 oncoprotein affects splicing decisions in a promoter binding-dependent manner." Journal of Biological Chemistry **281**(28): 19145-19155.
Guitart, A. V., T. I. Panagopoulou, A. Villacreces, M. Vukovic, C. Sepulveda, L. Allen, R. N. Carter, L. N. van de Lagemaat, M. Morgan and P. Giles (2017). "Fumarate hydratase is a critical metabolic regulator of hematopoietic stem cell functions." Journal of Experimental Medicine **214**(3): 719-735.
Guitart, A. V., C. Subramani, A. Armesilla-Diaz, G. Smith, C. Sepulveda, D. Gezer, M. Vukovic, K. Dunn, P. Pollard and T. L. Holyoake (2013). "Hif-2α is not essential for cell-autonomous hematopoietic stem cell maintenance." Blood **122**(10): 1741-1745.

Gupta, P., G. U. Gurudutta, D. Saluja and R. P. Tripathi (2009). "PU. 1 and partners: regulation of haematopoietic stem cell fate in normal and malignant haematopoiesis." Journal of cellular and molecular medicine **13**(11-12): 4349-4363.
Gupta, V., M. S. Tallman and D. J. Weisdorf (2011). "Allogeneic hematopoietic cell transplantation for adults with acute myeloid leukemia: myths, controversies, and unknowns." Blood **117**(8): 2307-2318.
Haferlach, C., C. Mecucci, S. Schnittger, A. Kohlmann, M. Mancini, A. Cuneo, N. Testoni, G. Rege-Cambrin, A. Santucci, M. Vignetti, P. Fazi, M. P. Martelli, T. Haferlach and B. Falini (2009). "AML with mutated NPM1 carrying a normal or aberrant karyotype show overlapping biologic, pathologic, immunophenotypic, and prognostic features." Blood **114**(14): 3024-3032.
Haferlach, T., A. Kohlmann, L. Wieczorek, G. Basso, G. T. Kronnie, M. C. Bene, J. De Vos, J. M. Hernandez, W. K. Hofmann, K. I. Mills, A. Gilkes, S. Chiaretti, S. A. Shurtleff, T. J. Kipps, L. Z. Rassenti, A. E. Yeoh, P. R. Papenhausen, W. M. Liu, P. M. Williams and R. Foa (2010). "Clinical utility of microarray-based gene expression profiling in the diagnosis and subclassification of leukemia: report from the International Microarray Innovations in Leukemia Study Group." J Clin Oncol **28**(15): 2529-2537.
Hahne, F. and R. Ivanek (2016). Visualizing genomic data using Gviz and bioconductor. Statistical Genomics, Springer**:** 335-351.
Han, D., J. Liu, C. Chen, L. Dong, Y. Liu, R. Chang, X. Huang, Y. Liu, J. Wang and U. Dougherty (2019). "Anti-tumour immunity controlled through mRNA m 6 A methylation and YTHDF1 in dendritic cells." Nature: 1.
Hanenberg, H., X. L. Xiao, D. Dilloo, K. Hashino, I. Kato and D. A. Williams (1996). "Colocalization of retrovirus and target cells on specific fibronectin fragments increases genetic transduction of mammalian cells." Nature medicine **2**(8): 876.
Harrison, D. E. (1980). "Competitive repopulation: a new assay for long-term stem cell functional capacity." Blood **55**(1): 77-81.
Haussmann, I. U., Z. Bodi, E. Sanchez-Moran, N. P. Mongan, N. Archer, R. G. Fray and M. Soller (2016). "m 6 A potentiates Sxl alternative pre-mRNA splicing for robust Drosophila sex determination." Nature **540**(7632): 301.
Hay, S. B., K. Ferchen, K. Chetal, H. L. Grimes and N. Salomonis (2018). "The Human Cell Atlas bone marrow single-cell interactive web portal." Experimental hematology **68**: 51-61.
Hayashi, S. and A. P. McMahon (2002). "Efficient recombination in diverse tissues by a tamoxifen-inducible form of Cre: a tool for temporally regulated gene activation/inactivation in the mouse." Developmental biology **244**(2): 305-318.
Hays, L. E. (2009). "Heterogeneity in the AML stem cell pool." Blood **114**(19): 3976-3977.
Herzog, V. A., B. Reichholf, T. Neumann, P. Rescheneder, P. Bhat, T. R. Burkard, W. Wlotzka, A. von Haeseler, J. Zuber and S. L. Ameres (2017). "Thiol-linked alkylation of RNA to assess expression dynamics." Nat Methods **14**(12): 1198-1204.
Hess, J. L. (2004). "MLL: a histone methyltransferase disrupted in leukemia." Trends in molecular medicine **10**(10): 500-507.
Hockendorf, U., M. Yabal, T. Herold, E. Munkhbaatar, S. Rott, S. Jilg, J. Kauschinger, G. Magnani, F. Reisinger, M. Heuser, H. Kreipe, K. Sotlar, T. Engleitner, R. Rad, W.

Weichert, C. Peschel, J. Ruland, M. Heikenwalder, K. Spiekermann, J. Slotta-Huspenina, O. Gross and P. J. Jost (2016). "RIPK3 Restricts Myeloid Leukemogenesis by Promoting Cell Death and Differentiation of Leukemia Initiating Cells." Cancer Cell **30**(1): 75-91.
Horiuchi, K., T. Kawamura, H. Iwanari, R. Ohashi, M. Naito, T. Kodama and T. Hamakubo (2013). "Identification of Wilms' tumor 1-associating protein complex and its role in alternative splicing and the cell cycle." Journal of Biological Chemistry **288**(46): 33292-33302.
Hsu, P. J., Y. Zhu, H. Ma, Y. Guo, X. Shi, Y. Liu, M. Qi, Z. Lu, H. Shi and J. Wang (2017). "Ythdc2 is an N 6-methyladenosine binding protein that regulates mammalian spermatogenesis." Cell research **27**(9): 1115.
Huang, H., H. Weng, W. Sun, X. Qin, H. Shi, H. Wu, B. S. Zhao, A. Mesquita, C. Liu and C. L. Yuan (2018). "Recognition of RNA N 6-methyladenosine by IGF2BP proteins enhances mRNA stability and translation." Nature cell biology **20**(3): 285.
Huntly, B. J., H. Shigematsu, K. Deguchi, B. H. Lee, S. Mizuno, N. Duclos, R. Rowan, S. Amaral, D. Curley and I. R. Williams (2004). "MOZ-TIF2, but not BCR-ABL, confers properties of leukemic stem cells to committed murine hematopoietic progenitors." Cancer cell **6**(6): 587-596.
Ikuta, K. and I. L. Weissman (1992). "Evidence that hematopoietic stem cells express mouse c-kit but do not depend on steel factor for their generation." Proceedings of the National Academy of Sciences **89**(4): 1502-1506.
Ingolia, N. T., S. Ghaemmaghami, J. R. Newman and J. S. Weissman (2009). "Genome-wide analysis in vivo of translation with nucleotide resolution using ribosome profiling." science **324**(5924): 218-223.
Ishikawa, E. T., K. Chang, R. Nayak, H. Olsson, A. Ficker, S. Dunn, M. Madhu, A. Sengupta, J. Whitsett and H. Grimes (2013). "Klf5 controls bone marrow homing of stem cells and progenitors through Rab5-mediated β1/β2-integrin trafficking." Nature communications **4**: 1660.
Ito, K., R. Turcotte, J. Cui, S. E. Zimmerman, S. Pinho, T. Mizoguchi, F. Arai, J. M. Runnels, C. Alt and J. Teruya-Feldstein (2016). "Self-renewal of a purified Tie2+ hematopoietic stem cell population relies on mitochondrial clearance." Science **354**(6316): 1156-1160.
Ivanova, I., C. Much, M. Di Giacomo, C. Azzi, M. Morgan, P. N. Moreira, J. Monahan, C. Carrieri, A. J. Enright and D. O'Carroll (2017). "The RNA m(6)A Reader YTHDF2 Is Essential for the Post-transcriptional Regulation of the Maternal Transcriptome and Oocyte Competence." Mol Cell **67**(6): 1059-1067 e1054.
Jacobson, L., E. Simmons, E. Marks and J. Eldredge (1951). "Recovery from radiation injury." Science (Washington): 510-511.
Jaffredo, T., R. Gautier, A. Eichmann and F. Dieterlen-Lièvre (1998). "Intraaortic hemopoietic cells are derived from endothelial cells during ontogeny." Development **125**(22): 4575-4583.
Jain, D., M. R. Puno, C. Meydan, N. Lailler, C. E. Mason, C. D. Lima, K. V. Anderson and S. Keeney (2018). "ketu mutant mice uncover an essential meiotic function for the ancient RNA helicase YTHDC2." Elife **7**: e30919.

Jaiswal, S., P. Fontanillas, J. Flannick, A. Manning, P. V. Grauman, B. G. Mar, R. C. Lindsley, C. H. Mermel, N. Burtt and A. Chavez (2014). "Age-related clonal hematopoiesis associated with adverse outcomes." New England Journal of Medicine **371**(26): 2488-2498.
Jia, G., Y. Fu, X. Zhao, Q. Dai, G. Zheng, Y. Yang, C. Yi, T. Lindahl, T. Pan and Y.-G. Yang (2011). "N6-methyladenosine in nuclear RNA is a major substrate of the obesity-associated FTO." Nature chemical biology **7**(12): 885.
Jude, C. D., L. Climer, D. Xu, E. Artinger, J. K. Fisher and P. Ernst (2007). "Unique and independent roles for MLL in adult hematopoietic stem cells and progenitors." Cell stem cell **1**(3): 324-337.
Juliusson, G., P. Antunovic, Å. Derolf, S. Lehmann, L. Möllgård, D. Stockelberg, U. Tidefelt, A. Wahlin and M. Höglund (2009). "Age and acute myeloid leukemia: real world data on decision to treat and outcomes from the Swedish Acute Leukemia Registry." Blood **113**(18): 4179-4187.
Kadrmas, J. L. and M. C. Beckerle (2004). "The LIM domain: from the cytoskeleton to the nucleus." Nature reviews Molecular cell biology **5**(11): 920.
Kagoya, Y., A. Yoshimi, K. Kataoka, M. Nakagawa, K. Kumano, S. Arai, H. Kobayashi, T. Saito, Y. Iwakura and M. Kurokawa (2014). "Positive feedback between NF-κB and TNF-α promotes leukemia-initiating cell capacity." The Journal of clinical investigation **124**(2): 528-542.
Kamburov, A., K. Pentchev, H. Galicka, C. Wierling, H. Lehrach and R. Herwig (2010). "ConsensusPathDB: toward a more complete picture of cell biology." Nucleic acids research **39**(suppl_1): D712-D717.
Kamburov, A., K. Pentchev, H. Galicka, C. Wierling, H. Lehrach and R. Herwig (2011). "ConsensusPathDB: toward a more complete picture of cell biology." Nucleic Acids Res **39**(Database issue): D712-717.
Kamburov, A., U. Stelzl, H. Lehrach and R. Herwig (2012). "The ConsensusPathDB interaction database: 2013 update." Nucleic acids research **41**(D1): D793-D800.
Kantarjian, H. M., H. P. Erba, D. Claxton, M. Arellano, R. M. Lyons, T. Kovascovics, J. Gabrilove, M. Craig, D. Douer and M. Maris (2009). "Phase II study of clofarabine monotherapy in previously untreated older adults with acute myeloid leukemia and unfavorable prognostic factors." Journal of Clinical Oncology **28**(4): 549-555.
Kantarjian, H. M., X. G. Thomas, A. Dmoszynska, A. Wierzbowska, G. Mazur, J. Mayer, J.-P. Gau, W.-C. Chou, R. Buckstein and J. Cermak (2012). "Multicenter, randomized, open-label, phase III trial of decitabine versus patient choice, with physician advice, of either supportive care or low-dose cytarabine for the treatment of older patients with newly diagnosed acute myeloid leukemia." Journal of clinical oncology **30**(21): 2670.
Karamitros, D., B. Stoilova, Z. Aboukhalil, F. Hamey, A. Reinisch, M. Samitsch, L. Quek, G. Otto, E. Repapi and J. Doondeea (2018). "Single-cell analysis reveals the continuum of human lympho-myeloid progenitor cells." Nature immunology **19**(1): 85.
Karijolich, J. and Y.-T. Yu (2011). "Converting nonsense codons into sense codons by targeted pseudouridylation." Nature **474**(7351): 395.

Kauffmann, A., R. Gentleman and W. Huber (2009). "arrayQualityMetrics--a bioconductor package for quality assessment of microarray data." Bioinformatics **25**(3): 415-416.
Kawagoe, H., R. Humphries, A. Blair, H. Sutherland and D. Hogge (1999). "Expression of HOX genes, HOX cofactors, and MLL in phenotypically and functionally defined subpopulations of leukemic and normal human hematopoietic cells." Leukemia **13**(5): 687.
Kelly, L. M. and D. G. Gilliland (2002). "Genetics of myeloid leukemias." Annual review of genomics and human genetics **3**(1): 179-198.
Kemp, R., H. Ireland, E. Clayton, C. Houghton, L. Howard and D. J. Winton (2004). "Elimination of background recombination: somatic induction of Cre by combined transcriptional regulation and hormone binding affinity." Nucleic acids research **32**(11): e92-e92.
Kent, D. G., M. R. Copley, C. Benz, S. Wöhrer, B. J. Dykstra, E. Ma, J. Cheyne, Y. Zhao, M. B. Bowie and Y. Zhao (2009). "Prospective isolation and molecular characterization of hematopoietic stem cells with durable self-renewal potential." Blood **113**(25): 6342-6350.
Kern, W., C. Haferlach, T. Haferlach and S. Schnittger (2008). "Monitoring of minimal residual disease in acute myeloid leukemia." Cancer: Interdisciplinary International Journal of the American Cancer Society **112**(1): 4-16.
Khwaja, A., M. Bjorkholm, R. E. Gale, R. L. Levine, C. T. Jordan, G. Ehninger, C. D. Bloomfield, E. Estey, A. Burnett and J. J. Cornelissen (2016). "Acute myeloid leukaemia." Nature reviews Disease primers **2**: 16010.
Kiel, M. J., G. L. Radice and S. J. Morrison (2007). "Lack of evidence that hematopoietic stem cells depend on N-cadherin-mediated adhesion to osteoblasts for their maintenance." Cell stem cell **1**(2): 204-217.
Kiel, M. J., Ö. H. Yilmaz, T. Iwashita, O. H. Yilmaz, C. Terhorst and S. J. Morrison (2005). "SLAM family receptors distinguish hematopoietic stem and progenitor cells and reveal endothelial niches for stem cells." Cell **121**(7): 1109-1121.
Kim, D., B. Langmead and S. L. Salzberg (2015). "HISAT: a fast spliced aligner with low memory requirements." Nature methods **12**(4): 357.
Kim, I., S. He, Ö. H. Yilmaz, M. J. Kiel and S. J. Morrison (2006). "Enhanced purification of fetal liver hematopoietic stem cells using SLAM family receptors." Blood **108**(2): 737-744.
Kim, I., T. L. Saunders and S. J. Morrison (2007). "Sox17 dependence distinguishes the transcriptional regulation of fetal from adult hematopoietic stem cells." Cell **130**(3): 470-483.
Kingston, R. E., C. A. Chen and J. K. Rose (2003). "Calcium phosphate transfection." Current protocols in molecular biology **63**(1): 9.1. 1-9.1. 11.
Klein, H. U., C. Ruckert, A. Kohlmann, L. Bullinger, C. Thiede, T. Haferlach and M. Dugas (2009). "Quantitative comparison of microarray experiments with published leukemia related gene expression signatures." BMC Bioinformatics **10**: 422.
Klein-Hitpass, L., S. Y. Tsai, N. L. Weigel, G. F. Allan, D. Riley, R. Rodriguez, W. T. Schrader, M.-l. Tsai and B. W. O'Malley (1990). "The progesterone receptor

stimulates cell-free transcription by enhancing the formation of a stable preinitiation complex." Cell **60**(2): 247-257.
Knapp, D. J., C. A. Hammond, T. Hui, M. T. van Loenhout, F. Wang, N. Aghaeepour, P. H. Miller, M. Moksa, G. M. Rabu and P. A. Beer (2018). "Single-cell analysis identifies a CD33+ subset of human cord blood cells with high regenerative potential." Nature cell biology **20**(6): 710.
Knapp, D. J., C. A. Hammond, P. H. Miller, G. M. Rabu, P. A. Beer, M. Ricicova, V. Lecault, D. Da Costa, M. VanInsberghe and A. M. Cheung (2017). "Dissociation of survival, proliferation, and state control in human hematopoietic stem cells." Stem cell reports **8**(1): 152-162.
Knuckles, P., S. H. Carl, M. Musheev, C. Niehrs, A. Wenger and M. Bühler (2017). "RNA fate determination through cotranscriptional adenosine methylation and microprocessor binding." Nature structural & molecular biology **24**(7): 561.
Kobayashi, H., J. M. Butler, R. O'donnell, M. Kobayashi, B.-S. Ding, B. Bonner, V. K. Chiu, D. J. Nolan, K. Shido and L. Benjamin (2010). "Angiocrine factors from Akt-activated endothelial cells balance self-renewal and differentiation of haematopoietic stem cells." Nature cell biology **12**(11): 1046.
Kolb, E. A. and S. Meshinchi (2015). "Acute myeloid leukemia in children and adolescents: identification of new molecular targets brings promise of new therapies." ASH Education Program Book **2015**(1): 507-513.
Kondo, M., I. L. Weissman and K. Akashi (1997). "Identification of clonogenic common lymphoid progenitors in mouse bone marrow." Cell **91**(5): 661-672.
Kranc, K. R., H. Schepers, N. P. Rodrigues, S. Bamforth, E. Villadsen, H. Ferry, T. Bouriez-Jones, M. Sigvardsson, S. Bhattacharya and S. E. Jacobsen (2009). "Cited2 is an essential regulator of adult hematopoietic stem cells." Cell stem cell **5**(6): 659-665.
Krivtsov, A. V. and S. A. Armstrong (2007). "MLL translocations, histone modifications and leukaemia stem-cell development." Nature Reviews Cancer **7**(11): 823.
Krivtsov, A. V., D. Twomey, Z. Feng, M. C. Stubbs, Y. Wang, J. Faber, J. E. Levine, J. Wang, W. C. Hahn and D. G. Gilliland (2006). "Transformation from committed progenitor to leukaemia stem cell initiated by MLL–AF9." Nature **442**(7104): 818.
Kroon, E., J. Krosl, U. Thorsteinsdottir, S. Baban, A. M. Buchberg and G. Sauvageau (1998). "Hoxa9 transforms primary bone marrow cells through specific collaboration with Meis1a but not Pbx1b." The EMBO journal **17**(13): 3714-3725.
Kroon, E., U. Thorsteinsdottir, N. Mayotte, T. Nakamura and G. Sauvageau (2001). "NUP98–HOXA9 expression in hemopoietic stem cells induces chronic and acute myeloid leukemias in mice." The EMBO journal **20**(3): 350-361.
Krumlauf, R. (1994). "Hox genes in vertebrate development." Cell **78**(2): 191-201.
Kuhn, R., F. Schwenk, M. Aguet and K. Rajewsky (1995). "Inducible gene targeting in mice." Science **269**(5229): 1427-1429.
Kulessa, H., J. Frampton and T. Graf (1995). "GATA-1 reprograms avian myelomonocytic cell lines into eosinophils, thromboblasts, and erythroblasts." Genes & development **9**(10): 1250-1262.
Kumar, A. R., W. A. Hudson, W. Chen, R. Nishiuchi, Q. Yao and J. H. Kersey (2004). "Hoxa9 influences the phenotype but not the incidence of Mll-AF9 fusion gene leukemia." Blood **103**(5): 1823-1828.

Kumar, S. and H. Geiger (2017). "HSC niche biology and HSC expansion ex vivo." Trends in molecular medicine **23**(9): 799-819.
Kumaravelu, P., L. Hook, A. M. Morrison, J. Ure, S. Zhao, S. Zuyev, J. Ansell and A. Medvinsky (2002). "Quantitative developmental anatomy of definitive haematopoietic stem cells/long-term repopulating units (HSC/RUs): role of the aorta-gonad-mesonephros (AGM) region and the yolk sac in colonisation of the mouse embryonic liver." Development **129**(21): 4891-4899.
Kunisaki, Y., I. Bruns, C. Scheiermann, J. Ahmed, S. Pinho, D. Zhang, T. Mizoguchi, Q. Wei, D. Lucas and K. Ito (2013). "Arteriolar niches maintain haematopoietic stem cell quiescence." Nature **502**(7473): 637.
Kwok, C.-T., A. D. Marshall, J. E. Rasko and J. J. Wong (2017). "Genetic alterations of m 6 A regulators predict poorer survival in acute myeloid leukemia." Journal of hematology & oncology **10**(1): 39.
Lacaud, G. and V. Kouskoff (2017). "Hemangioblast, hemogenic endothelium, and primitive versus definitive hematopoiesis." Experimental Hematology **49**: 19-24.
Lapidot, T., A. Dar and O. Kollet (2005). "How do stem cells find their way home?" Blood **106**(6): 1901-1910.
Laslo, P., C. J. Spooner, A. Warmflash, D. W. Lancki, H.-J. Lee, R. Sciammas, B. N. Gantner, A. R. Dinner and H. Singh (2006). "Multilineage transcriptional priming and determination of alternate hematopoietic cell fates." Cell **126**(4): 755-766.
Laurenti, E. and B. Göttgens (2018). "From haematopoietic stem cells to complex differentiation landscapes." Nature **553**(7689): 418.
Lavau, C., R. T. Luo, C. Du and M. J. Thirman (2000). "Retrovirus-mediated gene transfer of MLL-ELL transforms primary myeloid progenitors and causes acute myeloid leukemias in mice." Proceedings of the National Academy of Sciences **97**(20): 10984-10989.
Lavau, C., S. J. Szilvassy, R. Slany and M. L. Cleary (1997). "Immortalization and leukemic transformation of a myelomonocytic precursor by retrovirally transduced HRX–ENL." The EMBO journal **16**(14): 4226-4237.
Lawrence, H., S. Rozenfeld, C. Cruz, K. Matsukuma, A. Kwong, L. Kömüves, A. Buchberg and C. Largman (1999). "Frequent co-expression of the HOXA9 and MEIS1 homeobox genes in human myeloid leukemias." Leukemia **13**(12): 1993.
Lee, E. J., A. Pollak, R. D. Leavitt, J. R. Testa and C. A. Schiffer (1987). "Minimally differentiated acute nonlymphocytic leukemia: a distinct entity." Blood **70**(5): 1400-1406.
Lee, H., S. Bao, Y. Qian, S. Geula, J. Leslie, C. Zhang, J. H. Hanna and L. Ding (2019). "Stage-specific requirement for Mettl3-dependent m 6 A mRNA methylation during haematopoietic stem cell differentiation." Nature cell biology: 1.
Lessard, J. and G. Sauvageau (2003). "Bmi-1 determines the proliferative capacity of normal and leukaemic stem cells." nature **423**(6937): 255.
Li, F., D. Zhao, J. Wu and Y. Shi (2014). "Structure of the YTH domain of human YTHDF2 in complex with an m 6 A mononucleotide reveals an aromatic cage for m 6 A recognition." Cell research **24**(12): 1490.

Li, H.-B., J. Tong, S. Zhu, P. J. Batista, E. E. Duffy, J. Zhao, W. Bailis, G. Cao, L. Kroehling and Y. Chen (2017). "m 6 A mRNA methylation controls T cell homeostasis by targeting the IL-7/STAT5/SOCS pathways." Nature **548**(7667): 338.
Li, J., S. Meng, M. Xu, S. Wang, L. He, X. Xu, X. Wang and L. Xie (2018). "Downregulation of N6-methyladenosine binding YTHDF2 protein mediated by miR-493-3p suppresses prostate cancer by elevating N6-methyladenosine levels." Oncotarget **9**(3): 3752.
Li, M., X. Zhao, W. Wang, H. Shi, Q. Pan, Z. Lu, S. P. Perez, R. Suganthan, C. He and M. Bjørås (2018). "Ythdf2-mediated m 6 A mRNA clearance modulates neural development in mice." Genome biology **19**(1): 69.
Li, X., X. Xiong, K. Wang, L. Wang, X. Shu, S. Ma and C. Yi (2016). "Transcriptome-wide mapping reveals reversible and dynamic N 1-methyladenosine methylome." Nature chemical biology **12**(5): 311.
Li, X., P. Zhu, S. Ma, J. Song, J. Bai, F. Sun and C. Yi (2015). "Chemical pulldown reveals dynamic pseudouridylation of the mammalian transcriptome." Nature chemical biology **11**(8): 592.
Li, Z., P. Qian, W. Shao, H. Shi, X. C. He, M. Gogol, Z. Yu, Y. Wang, M. Qi and Y. Zhu (2018). "Suppression of m 6 A reader Ythdf2 promotes hematopoietic stem cell expansion." Cell research **28**(9): 904.
Li, Z., H. Weng, R. Su, X. Weng, Z. Zuo, C. Li, H. Huang, S. Nachtergaele, L. Dong and C. Hu (2017). "FTO plays an oncogenic role in acute myeloid leukemia as a N6-methyladenosine RNA demethylase." Cancer cell **31**(1): 127-141.
Liang, Y., G. Van Zant and S. J. Szilvassy (2005). "Effects of aging on the homing and engraftment of murine hematopoietic stem and progenitor cells." Blood **106**(4): 1479-1487.
Lin, S., J. Choe, P. Du, R. Triboulet and R. I. Gregory (2016). "The m6A methyltransferase METTL3 promotes translation in human cancer cells." Molecular cell **62**(3): 335-345.
Lin, S., J. Liu, W. Jiang, P. Wang, C. Sun, X. Wang, Y. Chen and H. Wang (2019). "METTL3 promotes the proliferation and mobility of gastric cancer cells." Open Medicine **14**(1): 25-31.
Lindsley, R. C., B. G. Mar, E. Mazzola, P. V. Grauman, S. Shareef, S. L. Allen, A. Pigneux, M. Wetzler, R. K. Stuart and H. P. Erba (2015). "Acute myeloid leukemia ontogeny is defined by distinct somatic mutations." Blood **125**(9): 1367-1376.
Ling, K.-W., K. Ottersbach, J. P. Van Hamburg, A. Oziemlak, F.-Y. Tsai, S. H. Orkin, R. Ploemacher, R. W. Hendriks and E. Dzierzak (2004). "GATA-2 plays two functionally distinct roles during the ontogeny of hematopoietic stem cells." Journal of Experimental Medicine **200**(7): 871-882.
Little, N. A., N. D. Hastie and R. C. Davies (2000). "Identification of WTAP, a novel Wilms' tumour 1-associating protein." Human molecular genetics **9**(15): 2231-2239.
Liu, F., W. Clark, G. Luo, X. Wang, Y. Fu, J. Wei, X. Wang, Z. Hao, Q. Dai and G. Zheng (2016). "ALKBH1-mediated tRNA demethylation regulates translation." Cell **167**(3): 816-828. e816.
Liu, J., M. A. Eckert, B. T. Harada, S.-M. Liu, Z. Lu, K. Yu, S. M. Tienda, A. Chryplewicz, A. C. Zhu and Y. Yang (2018). "m 6 A mRNA methylation regulates AKT activity to

promote the proliferation and tumorigenicity of endometrial cancer." Nature cell biology **20**(9): 1074.
Liu, J., Y. Yue, D. Han, X. Wang, Y. Fu, L. Zhang, G. Jia, M. Yu, Z. Lu and X. Deng (2014). "A METTL3–METTL14 complex mediates mammalian nuclear RNA N 6-adenosine methylation." Nature chemical biology **10**(2): 93.
Liu, N., Q. Dai, G. Zheng, C. He, M. Parisien and T. Pan (2015). "N 6-methyladenosine-dependent RNA structural switches regulate RNA–protein interactions." Nature **518**(7540): 560.
Liu, N., K. I. Zhou, M. Parisien, Q. Dai, L. Diatchenko and T. Pan (2017). "N6-methyladenosine alters RNA structure to regulate binding of a low-complexity protein." Nucleic acids research **45**(10): 6051-6063.
Liu, P., S. A. Tarle, A. Hajra, D. F. Claxton, P. Marlton, M. Freedman, M. J. Siciliano and F. S. Collins (1993). "Fusion between transcription factor CBF beta/PEBP2 beta and a myosin heavy chain in acute myeloid leukemia." Science **261**(5124): 1041-1044.
Liu, X., H. Zheng, W.-M. Yu, T. M. Cooper, K. D. Bunting and C.-K. Qu (2015). "Maintenance of mouse hematopoietic stem cells ex vivo by reprogramming cellular metabolism." Blood **125**(10): 1562-1565.
Lo-Coco, F., G. Avvisati, M. Vignetti, C. Thiede, S. M. Orlando, S. Iacobelli, F. Ferrara, P. Fazi, L. Cicconi and E. Di Bona (2013). "Retinoic acid and arsenic trioxide for acute promyelocytic leukemia." New England Journal of Medicine **369**(2): 111-121.
Lockhart, D. J., H. Dong, M. C. Byrne, M. T. Follettie, M. V. Gallo, M. S. Chee, M. Mittmann, C. Wang, M. Kobayashi and H. Norton (1996). "Expression monitoring by hybridization to high-density oligonucleotide arrays." Nature biotechnology **14**(13): 1675.
Lorenz, E., C. Congdon and D. Uphoff (1952). "Modification of acute irradiation injury in mice and guinea-pigs by bone marrow injections." Radiology **58**(6): 863-877.
Luthman, H. and G. Magnusson (1983). "High efficiency polyoma DNA transfection of chloroquine treated cells." Nucleic acids research **11**(5): 1295-1308.
Lutterbach, B., Y. Hou, K. L. Durst and S. W. Hiebert (1999). "The inv (16) encodes an acute myeloid leukemia 1 transcriptional corepressor." Proceedings of the National Academy of Sciences **96**(22): 12822-12827.
Lv, J., Y. Zhang, S. Gao, C. Zhang, Y. Chen, W. Li, Y.-G. Yang, Q. Zhou and F. Liu (2018). "Endothelial-specific m 6 A modulates mouse hematopoietic stem and progenitor cell development via Notch signaling." Cell research **28**(2): 249.
Ma, J. z., F. Yang, C. c. Zhou, F. Liu, J. h. Yuan, F. Wang, T. t. Wang, Q. g. Xu, W. p. Zhou and S. h. Sun (2017). "METTL14 suppresses the metastatic potential of hepatocellular carcinoma by modulating N6-methyladenosine-dependent primary MicroRNA processing." Hepatology **65**(2): 529-543.
Majeti, R., C. Y. Park and I. L. Weissman (2007). "Identification of a hierarchy of multipotent hematopoietic progenitors in human cord blood." Cell stem cell **1**(6): 635-645.
Månsson, R., A. Hultquist, S. Luc, L. Yang, K. Anderson, S. Kharazi, S. Al-Hashmi, K. Liuba, L. Thorén and J. Adolfsson (2007). "Molecular evidence for hierarchical transcriptional lineage priming in fetal and adult stem cells and multipotent progenitors." Immunity **26**(4): 407-419.

Mansson, R., P. Tsapogas, M. Akerlund, A. Lagergren, R. Gisler and M. Sigvardsson (2004). "Pearson correlation analysis of microarray data allows for the identification of genetic targets for early B-cell factor." J Biol Chem **279**(17): 17905-17913.
Martens, J. H. and H. G. Stunnenberg (2010). "The molecular signature of oncofusion proteins in acute myeloid leukemia." FEBS letters **584**(12): 2662-2669.
Mathiyalagan, P., M. Adamiak, J. Mayourian, Y. Sassi, Y. Liang, N. Agarwal, D. Jha, S. Zhang, E. Kohlbrenner and E. Chepurko (2019). "FTO-dependent N6-methyladenosine regulates cardiac function during remodeling and repair." Circulation **139**(4): 518-532.
Matsumoto, M. and T. Seya (2008). "TLR3: interferon induction by double-stranded RNA including poly (I: C)." Advanced drug delivery reviews **60**(7): 805-812.
Mauer, J., X. Luo, A. Blanjoie, X. Jiao, A. V. Grozhik, D. P. Patil, B. Linder, B. F. Pickering, J.-J. Vasseur and Q. Chen (2017). "Reversible methylation of m 6 A m in the 5' cap controls mRNA stability." Nature **541**(7637): 371.
McCall, M. N., P. N. Murakami, M. Lukk, W. Huber and R. A. Irizarry (2011). "Assessing affymetrix GeneChip microarray quality." BMC Bioinformatics **12**: 137.
McDevitt, M. A., R. A. Shivdasani, Y. Fujiwara, H. Yang and S. H. Orkin (1997). "A "knockdown" mutation created by cis-element gene targeting reveals the dependence of erythroid cell maturation on the level of transcription factor GATA-1." Proceedings of the National Academy of Sciences **94**(13): 6781-6785.
McMahon, K. A., S. Y. Hiew, S. Hadjur, H. Veiga-Fernandes, U. Menzel, A. J. Price, D. Kioussis, O. Williams and H. J. Brady (2007). "Mll has a critical role in fetal and adult hematopoietic stem cell self-renewal." Cell Stem Cell **1**(3): 338-345.
Meacham, C. E. and S. J. Morrison (2013). "Tumour heterogeneity and cancer cell plasticity." Nature **501**(7467): 328.
Medvinsky, A. and E. Dzierzak (1996). "Definitive hematopoiesis is autonomously initiated by the AGM region." Cell **86**(6): 897-906.
Méndez-Ferrer, S., T. V. Michurina, F. Ferraro, A. R. Mazloom, B. D. MacArthur, S. A. Lira, D. T. Scadden, A. Ma'ayan, G. N. Enikolopov and P. S. Frenette (2010). "Mesenchymal and haematopoietic stem cells form a unique bone marrow niche." Nature **466**(7308): 829.
Metzelder, S. K., C. Michel, M. von Bonin, M. Rehberger, E. Hessmann, S. Inselmann, M. Solovey, Y. Wang, K. Sohlbach, C. Brendel, T. Stiewe, J. Charles, A. Ten Haaf, V. Ellenrieder, A. Neubauer, S. Gattenlohner, M. Bornhauser and A. Burchert (2015). "NFATc1 as a therapeutic target in FLT3-ITD-positive AML." Leukemia **29**(7): 1470-1477.
Metzeler, K. H., T. Herold, M. Rothenberg-Thurley, S. Amler, M. C. Sauerland, D. Görlich, S. Schneider, N. P. Konstandin, A. Dufour and K. Bräundl (2016). "Spectrum and prognostic relevance of driver gene mutations in acute myeloid leukemia." Blood **128**(5): 686-698.
Metzeler, K. H., M. Hummel, C. D. Bloomfield, K. Spiekermann, J. Braess, M. C. Sauerland, A. Heinecke, M. Radmacher, G. Marcucci, S. P. Whitman, K. Maharry, P. Paschka, R. A. Larson, W. E. Berdel, T. Buchner, B. Wormann, U. Mansmann, W. Hiddemann, S. K. Bohlander, C. Buske, Cancer, B. Leukemia Group and A. M. L. C. G.

German (2008). "An 86-probe-set gene-expression signature predicts survival in cytogenetically normal acute myeloid leukemia." Blood **112**(10): 4193-4201.
Meyer, K. D., D. P. Patil, J. Zhou, A. Zinoviev, M. A. Skabkin, O. Elemento, T. V. Pestova, S.-B. Qian and S. R. Jaffrey (2015). "5′ UTR m6A promotes cap-independent translation." Cell **163**(4): 999-1010.
Meyer, K. D., Y. Saletore, P. Zumbo, O. Elemento, C. E. Mason and S. R. Jaffrey (2012). "Comprehensive analysis of mRNA methylation reveals enrichment in 3′ UTRs and near stop codons." Cell **149**(7): 1635-1646.
Miharada, K., V. Sigurdsson and S. Karlsson (2014). "Dppa5 improves hematopoietic stem cell activity by reducing endoplasmic reticulum stress." Cell reports **7**(5): 1381-1392.
Miller, C. L. and B. Lai (2005). Human and mouse hematopoietic colony-forming cell assays. Basic Cell Culture Protocols, Springer**:** 71-89.
Mills, K. I., A. Kohlmann, P. M. Williams, L. Wieczorek, W.-m. Liu, R. Li, W. Wei, D. T. Bowen, H. Loeffler, J. M. Hernandez, W.-K. Hofmann and T. Haferlach (2009). "Microarray-based classifiers and prognosis models identify subgroups with distinct clinical outcomes and high risk of AML transformation of myelodysplastic syndrome." Blood **114**(5): 1063-1072.
Milne, T. A., S. D. Briggs, H. W. Brock, M. E. Martin, D. Gibbs, C. D. Allis and J. L. Hess (2002). "MLL targets SET domain methyltransferase activity to Hox gene promoters." Molecular cell **10**(5): 1107-1117.
Minucci, S., S. Monestiroli, S. Giavara, S. Ronzoni, F. Marchesi, A. Insinga, D. Diverio, P. Gasparini, M. Capillo and E. Colombo (2002). "PML-RAR induces promyelocytic leukemias with high efficiency following retroviral gene transfer into purified murine hematopoietic progenitors." Blood **100**(8): 2989-2995.
Mitelman, F., B. Johansson and F. Mertens (2002). "Mitelman Database of Chromosome Aberrations in Cancer http://cgap. nci. nih. gov/Chromosomes." Mitelman (Access on November 27, 2009).
Mochizuki, Y., J. He, S. Kulkarni, M. Bessler and P. J. Mason (2004). "Mouse dyskerin mutations affect accumulation of telomerase RNA and small nucleolar RNA, telomerase activity, and ribosomal RNA processing." Proceedings of the National Academy of Sciences **101**(29): 10756-10761.
Moens, C. B. and L. Selleri (2006). "Hox cofactors in vertebrate development." Developmental biology **291**(2): 193-206.
Montesinos, P., I. Lorenzo, G. Martín, J. Sanz, M. L. Pérez-Sirvent, D. Martínez, G. Ortí, L. Algarra, J. Martínez and F. Moscardó (2008). "Tumor lysis syndrome in patients with acute myeloid leukemia: identification of risk factors and development of a predictive model." Haematologica **93**(1): 67-74.
Morita, Y., H. Ema and H. Nakauchi (2010). "Heterogeneity and hierarchy within the most primitive hematopoietic stem cell compartment." Journal of Experimental Medicine **207**(6): 1173-1182.
Morrison, S. J., H. D. Hemmati, A. M. Wandycz and I. L. Weissman (1995). "The purification and characterization of fetal liver hematopoietic stem cells." Proceedings of the National Academy of Sciences **92**(22): 10302-10306.

Morrison, S. J. and J. Kimble (2006). "Asymmetric and symmetric stem-cell divisions in development and cancer." nature **441**(7097): 1068-1074.
Morrison, S. J. and D. T. Scadden (2014). "The bone marrow niche for haematopoietic stem cells." Nature **505**(7483): 327.
Morrison, S. J., A. M. Wandycz, H. D. Hemmati, D. E. Wright and I. L. Weissman (1997). "Identification of a lineage of multipotent hematopoietic progenitors." Development **124**(10): 1929-1939.
Moskow, J. J., F. Bullrich, K. Huebner, I. O. Daar and A. M. Buchberg (1995). "Meis1, a PBX1-related homeobox gene involved in myeloid leukemia in BXH-2 mice." Molecular and cellular biology **15**(10): 5434-5443.
Mrózek, K., G. Marcucci, D. Nicolet, K. S. Maharry, H. Becker, S. P. Whitman, K. H. Metzeler, S. Schwind, Y.-Z. Wu and J. Kohlschmidt (2012). "Prognostic significance of the European LeukemiaNet standardized system for reporting cytogenetic and molecular alterations in adults with acute myeloid leukemia." Journal of clinical oncology **30**(36): 4515.
Müller, A. M., A. Medvinsky, J. Strouboulis, F. Grosveld and E. Dzierzakt (1994). "Development of hematopoietic stem cell activity in the mouse embryo." Immunity **1**(4): 291-301.
Muntean, A. G. and J. L. Hess (2012). "The pathogenesis of mixed-lineage leukemia." Annual Review of Pathology: Mechanisms of Disease **7**: 283-301.
Nakamura, T., T. Mori, S. Tada, W. Krajewski, T. Rozovskaia, R. Wassell, G. Dubois, A. Mazo, C. M. Croce and E. Canaani (2002). "ALL-1 is a histone methyltransferase that assembles a supercomplex of proteins involved in transcriptional regulation." Molecular cell **10**(5): 1119-1128.
Nakamura-Ishizu, A., H. Takizawa and T. Suda (2014). "The analysis, roles and regulation of quiescence in hematopoietic stem cells." Development **141**(24): 4656-4666.
Nakamura-Ishizu, A., K. Takubo, M. Fujioka and T. Suda (2014). "Megakaryocytes are essential for HSC quiescence through the production of thrombopoietin." Biochemical and biophysical research communications **454**(2): 353-357.
Nerlov, C. and T. Graf (1998). "PU. 1 induces myeloid lineage commitment in multipotent hematopoietic progenitors." Genes & development **12**(15): 2403-2412.
Nerlov, C., K. M. McNagny, G. Döderlein, E. Kowenz-Leutz and T. Graf (1998). "Distinct C/EBP functions are required for eosinophil lineage commitment and maturation." Genes & development **12**(15): 2413-2423.
Network, C. G. A. R. (2013). "Genomic and epigenomic landscapes of adult de novo acute myeloid leukemia." New England Journal of Medicine **368**(22): 2059-2074.
Ng, S. W., A. Mitchell, J. A. Kennedy, W. C. Chen, J. McLeod, N. Ibrahimova, A. Arruda, A. Popescu, V. Gupta and A. D. Schimmer (2016). "A 17-gene stemness score for rapid determination of risk in acute leukaemia." Nature **540**(7633): 433.
Nguyen, T. T., L. N. Ma, M. L. Slovak, C. D. Bangs, A. M. Cherry and D. A. Arber (2006). "Identification of novel Runx1 (AML1) translocation partner genes SH3D19, YTHDf2, and ZNF687 in acute myeloid leukemia." Genes, Chromosomes and Cancer **45**(10): 918-932.

Nombela-Arrieta, C., G. Pivarnik, B. Winkel, K. J. Canty, B. Harley, J. E. Mahoney, S.-Y. Park, J. Lu, A. Protopopov and L. E. Silberstein (2013). "Quantitative imaging of haematopoietic stem and progenitor cell localization and hypoxic status in the bone marrow microenvironment." Nature cell biology **15**(5): 533.
North, T., T.-L. Gu, T. Stacy, Q. Wang, L. Howard, M. Binder, M. Marín-Padilla and N. A. Speck (1999). "Cbfa2 is required for the formation of intra-aortic hematopoietic clusters." Development **126**(11): 2563-2575.
North, T. E., M. F. De Bruijn, T. Stacy, L. Talebian, E. Lind, C. Robin, M. Binder, E. Dzierzak and N. A. Speck (2002). "Runx1 expression marks long-term repopulating hematopoietic stem cells in the midgestation mouse embryo." Immunity **16**(5): 661-672.
Notta, F., S. Doulatov, E. Laurenti, A. Poeppl, I. Jurisica and J. E. Dick (2011). "Isolation of single human hematopoietic stem cells capable of long-term multilineage engraftment." Science **333**(6039): 218-221.
Notta, F., S. Zandi, N. Takayama, S. Dobson, O. I. Gan, G. Wilson, K. B. Kaufmann, J. McLeod, E. Laurenti and C. F. Dunant (2016). "Distinct routes of lineage development reshape the human blood hierarchy across ontogeny." Science **351**(6269): aab2116.
Nutt, S. L., B. Heavey, A. G. Rolink and M. Busslinger (1999). "Commitment to the B-lymphoid lineage depends on the transcription factor Pax5." Nature **401**(6753): 556.
Oguro, H., L. Ding and S. J. Morrison (2013). "SLAM family markers resolve functionally distinct subpopulations of hematopoietic stem cells and multipotent progenitors." Cell stem cell **13**(1): 102-116.
Okada, S., H. Nakauchi, K. Nagayoshi, S.-I. Nishikawa, Y. Miura and T. Suda (1992). "In vivo and in vitro stem cell function of c-kit-and Sca-1-positive murine hematopoietic cells." Blood **80**(12): 3044-3050.
Okuda, T., J. Van Deursen, S. W. Hiebert, G. Grosveld and J. R. Downing (1996). "AML1, the target of multiple chromosomal translocations in human leukemia, is essential for normal fetal liver hematopoiesis." Cell **84**(2): 321-330.
Orkin, S. H. and L. I. Zon (2008). "Hematopoiesis: an evolving paradigm for stem cell biology." Cell **132**(4): 631-644.
Osawa, M., K.-i. Hanada, H. Hamada and H. Nakauchi (1996). "Long-term lymphohematopoietic reconstitution by a single CD34-low/negative hematopoietic stem cell." Science **273**(5272): 242-245.
Ottersbach, K. and E. Dzierzak (2005). "The murine placenta contains hematopoietic stem cells within the vascular labyrinth region." Developmental cell **8**(3): 377-387.
Paddison, P. J., A. A. Caudy, E. Bernstein, G. J. Hannon and D. S. Conklin (2002). "Short hairpin RNAs (shRNAs) induce sequence-specific silencing in mammalian cells." Genes & development **16**(8): 948-958.
Palis, J., S. Robertson, M. Kennedy, C. Wall and G. Keller (1999). "Development of erythroid and myeloid progenitors in the yolk sac and embryo proper of the mouse." Development **126**(22): 5073-5084.
Pan, T. (2018). "Modifications and functional genomics of human transfer RNA." Cell research **28**(4): 395.

Pang, J. W., L. S. Cook, S. M. Schwartz and N. S. Weiss (2002). "Incidence of leukemia in Asian migrants to the United States and their descendants." Cancer Causes & Control **13**(9): 791-795.
Papaemmanuil, E., M. Gerstung, L. Bullinger, V. I. Gaidzik, P. Paschka, N. D. Roberts, N. E. Potter, M. Heuser, F. Thol and N. Bolli (2016). "Genomic classification and prognosis in acute myeloid leukemia." New England Journal of Medicine **374**(23): 2209-2221.
Paris, J., M. Morgan, J. Campos, G. J. Spencer, A. Shmakova, I. Ivanova, C. Mapperley, H. Lawson, D. A. Wotherspoon and C. Sepulveda (2019). "Targeting the RNA m6A Reader YTHDF2 Selectively Compromises Cancer Stem Cells in Acute Myeloid Leukemia." Cell stem cell.
Patil, D. P., C.-K. Chen, B. F. Pickering, A. Chow, C. Jackson, M. Guttman and S. R. Jaffrey (2016). "m 6 A RNA methylation promotes XIST-mediated transcriptional repression." Nature **537**(7620): 369.
Pearl-Yafe, M., K. Mizrahi, J. Stein, E. S. Yolcu, O. Kaplan, H. Shirwan, I. Yaniv and N. Askenasy (2010). "Tumor necrosis factor receptors support murine hematopoietic progenitor function in the early stages of engraftment." Stem Cells **28**(7): 1270-1280.
Pellin, D., M. Loperfido, C. Baricordi, S. L. Wolock, A. Montepeloso, O. K. Weinberg, A. Biffi, A. M. Klein and L. Biasco (2019). "A comprehensive single cell transcriptional landscape of human hematopoietic progenitors." Nature communications **10**(1): 2395.
Pendleton, K. E., B. Chen, K. Liu, O. V. Hunter, Y. Xie, B. P. Tu and N. K. Conrad (2017). "The U6 snRNA m6A methyltransferase METTL16 regulates SAM synthetase intron retention." Cell **169**(5): 824-835. e814.
Perdiguero, E. G. and F. Geissmann (2016). "The development and maintenance of resident macrophages." Nature immunology **17**(1): 2.
Perry, R. and D. Kelley (1974). "Existence of methylated messenger RNA in mouse L cells." Cell **1**(1): 37-42.
Pietras, E. M., D. Reynaud, Y.-A. Kang, D. Carlin, F. J. Calero-Nieto, A. D. Leavitt, J. M. Stuart, B. Göttgens and E. Passegué (2015). "Functionally distinct subsets of lineage-biased multipotent progenitors control blood production in normal and regenerative conditions." Cell stem cell **17**(1): 35-46.
Pigazzi, M., R. Masetti, S. Bresolin, A. Beghin, A. Di Meglio, S. Gelain, L. Trentin, E. Baron, M. Giordan, A. Zangrando, B. Buldini, A. Leszl, M. C. Putti, C. Rizzari, F. Locatelli, A. Pession, G. Te Kronnie and G. Basso (2011). "MLL partner genes drive distinct gene expression profiles and genomic alterations in pediatric acute myeloid leukemia: an AIEOP study." Leukemia **25**(3): 560-563.
Pineault, N., C. D. Helgason, H. J. Lawrence and R. K. Humphries (2002). "Differential expression of Hox, Meis1, and Pbx1 genes in primitive cells throughout murine hematopoietic ontogeny." Experimental hematology **30**(1): 49-57.
Ping, X.-L., B.-F. Sun, L. Wang, W. Xiao, X. Yang, W.-J. Wang, S. Adhikari, Y. Shi, Y. Lv and Y.-S. Chen (2014). "Mammalian WTAP is a regulatory subunit of the RNA N6-methyladenosine methyltransferase." Cell research **24**(2): 177.
Pinho, S. and P. S. Frenette (2019). "Haematopoietic stem cell activity and interactions with the niche." Nature Reviews Molecular Cell Biology: 1.

Podoltsev, N. A., M. Stahl, A. M. Zeidan and S. D. Gore (2017). "Selecting initial treatment of acute myeloid leukaemia in older adults." Blood reviews **31**(2): 43-62.
Porcher, C., H. Chagraoui and M. S. Kristiansen (2017). "SCL/TAL1: a multifaceted regulator from blood development to disease." Blood **129**(15): 2051-2060.
Poulos, M. G., P. Guo, N. M. Kofler, S. Pinho, M. C. Gutkin, A. Tikhonova, I. Aifantis, P. S. Frenette, J. Kitajewski and S. Rafii (2013). "Endothelial Jagged-1 is necessary for homeostatic and regenerative hematopoiesis." Cell reports **4**(5): 1022-1034.
Pronk, C. J. and D. Bryder (2011). Flow cytometry-based identification of immature myeloerythroid development. Flow Cytometry Protocols, Springer**:** 275-293.
Pronk, C. J., D. J. Rossi, R. Månsson, J. L. Attema, G. L. Norddahl, C. K. F. Chan, M. Sigvardsson, I. L. Weissman and D. Bryder (2007). "Elucidation of the phenotypic, functional, and molecular topography of a myeloerythroid progenitor cell hierarchy." Cell stem cell **1**(4): 428-442.
Pronk, C. J., O. P. Veiby, D. Bryder and S. E. W. Jacobsen (2011). "Tumor necrosis factor restricts hematopoietic stem cell activity in mice: involvement of two distinct receptors." Journal of Experimental Medicine **208**(8): 1563-1570.
Puumala, S. E., J. A. Ross, R. Aplenc and L. G. Spector (2013). "Epidemiology of childhood acute myeloid leukemia." Pediatric blood & cancer **60**(5): 728-733.
Quinlan, A. R. and I. M. Hall (2010). "BEDTools: a flexible suite of utilities for comparing genomic features." Bioinformatics **26**(6): 841-842.
Rabani, M., J. Z. Levin, L. Fan, X. Adiconis, R. Raychowdhury, M. Garber, A. Gnirke, C. Nusbaum, N. Hacohen and N. Friedman (2011). "Metabolic labeling of RNA uncovers principles of RNA production and degradation dynamics in mammalian cells." Nature biotechnology **29**(5): 436.
Ramírez, F., F. Dündar, S. Diehl, B. A. Grüning and T. Manke (2014). "deepTools: a flexible platform for exploring deep-sequencing data." Nucleic acids research **42**(W1): W187-W191.
Ranganathan, P., X. Yu, C. Na, R. Santhanam, S. Shacham, M. Kauffman, A. Walker, R. Klisovic, W. Blum and M. Caligiuri (2012). "Preclinical activity of a novel CRM1 inhibitor in acute myeloid leukemia." Blood **120**(9): 1765-1773.
Rebel, V. I., S. Hartnett, G. R. Hill, S. B. Lazo-Kallanian, J. L. Ferrara and C. A. Sieff (1999). "Essential role for the p55 tumor necrosis factor receptor in regulating hematopoiesis at a stem cell level." Journal of Experimental Medicine **190**(10): 1493-1504.
Rebel, V. I., C. L. Miller, C. J. Eaves and P. M. Lansdorp (1996). "The repopulation potential of fetal liver hematopoietic stem cells in mice exceeds that of their liver adult bone marrow counterparts." Blood **87**(8): 3500-3507.
Reid, D. W., S. Shenolikar and C. V. Nicchitta (2015). "Simple and inexpensive ribosome profiling analysis of mRNA translation." Methods **91**: 69-74.
Remberger, M., J. Törlén, O. Ringdén, M. Engström, E. Watz, M. Uhlin and J. Mattsson (2015). "Effect of total nucleated and CD34+ cell dose on outcome after allogeneic hematopoietic stem cell transplantation." Biology of Blood and Marrow Transplantation **21**(5): 889-893.
Ren, R. (2004). "Modeling the dosage effect of oncogenes in leukemogenesis." Current opinion in hematology **11**(1): 25-34.

Ries, R. J., S. Zaccara, P. Klein, A. Olarerin-George, S. Namkoong, B. F. Pickering, D. P. Patil, H. Kwak, J. H. Lee and S. R. Jaffrey (2019). "m 6 A enhances the phase separation potential of mRNA." Nature: 1.
Ritchie, M. E., B. Phipson, D. Wu, Y. Hu, C. W. Law, W. Shi and G. K. Smyth (2015). "limma powers differential expression analyses for RNA-sequencing and microarray studies." Nucleic acids research **43**(7): e47-e47.
Röllig, C. and G. Ehninger (2015). "How I treat hyperleukocytosis in acute myeloid leukemia." Blood **125**(21): 3246-3252.
Roundtree, I. A., M. E. Evans, T. Pan and C. He (2017). "Dynamic RNA modifications in gene expression regulation." Cell **169**(7): 1187-1200.
Roundtree, I. A., G.-Z. Luo, Z. Zhang, X. Wang, T. Zhou, Y. Cui, J. Sha, X. Huang, L. Guerrero and P. Xie (2017). "YTHDC1 mediates nuclear export of N6-methyladenosine methylated mRNAs." Elife **6**: e31311.
Ruppert, R., M. Moser, M. Sperandio, E. Rognoni, M. Orban, W.-H. Liu, A. S. Schulz, R. A. Oostendorp, S. Massberg and R. Fässler (2015). "Kindlin-3–mediated integrin adhesion is dispensable for quiescent but essential for activated hematopoietic stem cells." Journal of Experimental Medicine **212**(9): 1415-1432.
Růžička, K., M. Zhang, A. Campilho, Z. Bodi, M. Kashif, M. Saleh, D. Eeckhout, S. El-Showk, H. Li and S. Zhong (2017). "Identification of factors required for m6A mRNA methylation in Arabidopsis reveals a role for the conserved E3 ubiquitin ligase HAKAI." New Phytologist **215**(1): 157-172.
Sachs, A. (1990). "The role of poly (A) in the translation and stability of mRNA." Current opinion in cell biology **2**(6): 1092-1098.
Sanjuan-Pla, A., I. C. Macaulay, C. T. Jensen, P. S. Woll, T. C. Luis, A. Mead, S. Moore, C. Carella, S. Matsuoka and T. B. Jones (2013). "Platelet-biased stem cells reside at the apex of the haematopoietic stem-cell hierarchy." Nature **502**(7470): 232.
Saultz, J. and R. Garzon (2016). "Acute myeloid leukemia: a concise review." Journal of clinical medicine **5**(3): 33.
Sauvageau, G., P. M. Lansdorp, C. J. Eaves, D. E. Hogge, W. H. Dragowska, D. S. Reid, C. Largman, H. J. Lawrence and R. K. Humphries (1994). "Differential expression of homeobox genes in functionally distinct CD34+ subpopulations of human bone marrow cells." Proceedings of the National Academy of Sciences **91**(25): 12223-12227.
Schlenk, R. F. (2014). "Post-remission therapy for acute myeloid leukemia." Haematologica **99**(11): 1663-1670.
Schluns, K. S., W. C. Kieper, S. C. Jameson and L. Lefrançois (2000). "Interleukin-7 mediates the homeostasis of naive and memory CD8 T cells in vivo." Nature immunology **1**(5): 426.
Schofield, R. (1978). "The relationship between the spleen colony-forming cell and the haemopoietic stem cell." Blood cells **4**(1-2): 7-25.
Schwartz, S., D. A. Bernstein, M. R. Mumbach, M. Jovanovic, R. H. Herbst, B. X. León-Ricardo, J. M. Engreitz, M. Guttman, R. Satija and E. S. Lander (2014). "Transcriptome-wide mapping reveals widespread dynamic-regulated pseudouridylation of ncRNA and mRNA." Cell **159**(1): 148-162.

Score, J., A. Chase, L. Forsberg, L. Feng, K. Waghorn, A. Jones, C. Rasi, D. Linch, J. Dumanski and R. Gale (2015). "Detection of leukemia-associated mutations in peripheral blood DNA of hematologically normal elderly individuals." Leukemia **29**(7): 1600.
Sedger, L. M. and M. F. McDermott (2014). "TNF and TNF-receptors: from mediators of cell death and inflammation to therapeutic giants–past, present and future." Cytokine & growth factor reviews **25**(4): 453-472.
Seif, A. E. (2011). "Pediatric leukemia predisposition syndromes: clues to understanding leukemogenesis." Cancer genetics **204**(5): 227-244.
Seita, J. and I. L. Weissman (2010). "Hematopoietic stem cell: self-renewal versus differentiation." Wiley Interdisciplinary Reviews: Systems Biology and Medicine **2**(6): 640-653.
Shen, X., Y. Liu, Y.-J. Hsu, Y. Fujiwara, J. Kim, X. Mao, G.-C. Yuan and S. H. Orkin (2008). "EZH1 mediates methylation on histone H3 lysine 27 and complements EZH2 in maintaining stem cell identity and executing pluripotency." Molecular cell **32**(4): 491-502.
Shi, H., X. Wang, Z. Lu, B. S. Zhao, H. Ma, P. J. Hsu, C. Liu and C. He (2017). "YTHDF3 facilitates translation and decay of N 6-methyladenosine-modified RNA." Cell research **27**(3): 315.
Shima, H., M. Matsumoto, Y. Ishigami, M. Ebina, A. Muto, Y. Sato, S. Kumagai, K. Ochiai, T. Suzuki and K. Igarashi (2017). "S-Adenosylmethionine synthesis is regulated by selective N6-adenosine methylation and mRNA degradation involving METTL16 and YTHDC1." Cell reports **21**(12): 3354-3363.
Shimshek, D. R., J. Kim, M. R. Hübner, D. J. Spergel, F. Buchholz, E. Casanova, A. F. Stewart, P. H. Seeburg and R. Sprengel (2002). "Codon-improved Cre recombinase (iCre) expression in the mouse." genesis **32**(1): 19-26.
Shlush, L. I., S. Zandi, A. Mitchell, W. C. Chen, J. M. Brandwein, V. Gupta, J. A. Kennedy, A. D. Schimmer, A. C. Schuh and K. W. Yee (2014). "Identification of pre-leukaemic haematopoietic stem cells in acute leukaemia." Nature **506**(7488): 328.
Short, N. J., M. E. Rytting and J. E. Cortes (2018). "Acute myeloid leukaemia." The Lancet.
Sigurdsson, V., H. Takei, S. Soboleva, V. Radulovic, R. Galeev, K. Siva, L. F. Leeb-Lundberg, T. Iida, H. Nittono and K. Miharada (2016). "Bile acids protect expanding hematopoietic stem cells from unfolded protein stress in fetal liver." Cell Stem Cell **18**(4): 522-532.
Silver, L. and J. Palis (1997). "Initiation of murine embryonic erythropoiesis: a spatial analysis." Blood **89**(4): 1154-1164.
Sive, J. I. and B. Göttgens (2014). "Transcriptional network control of normal and leukaemic haematopoiesis." Experimental cell research **329**(2): 255-264.
Sloan, K. E., A. S. Warda, S. Sharma, K.-D. Entian, D. L. Lafontaine and M. T. Bohnsack (2017). "Tuning the ribosome: The influence of rRNA modification on eukaryotic ribosome biogenesis and function." RNA biology **14**(9): 1138-1152.
Somervaille, T. C. and M. L. Cleary (2006). "Identification and characterization of leukemia stem cells in murine MLL-AF9 acute myeloid leukemia." Cancer cell **10**(4): 257-268.

Sorci, M., Z. Ianniello, S. Cruciani, S. Larivera, L. C. Ginistrelli, E. Capuano, M. Marchioni, F. Fazi and A. Fatica (2018). "METTL3 regulates WTAP protein homeostasis." Cell death & disease **9**(8): 796.
Spangrude, G. J. and D. M. Brooks (1992). "Phenotypic analysis of mouse hematopoietic stem cells shows a Thy-1-negative subset." Blood **80**(8): 1957-1964.
Spangrude, G. J., S. Heimfeld and I. L. Weissman (1988). "Purification and characterization of mouse hematopoietic stem cells." Science **241**(4861): 58-62.
Squires, J. E., H. R. Patel, M. Nousch, T. Sibbritt, D. T. Humphreys, B. J. Parker, C. M. Suter and T. Preiss (2012). "Widespread occurrence of 5-methylcytosine in human coding and non-coding RNA." Nucleic acids research **40**(11): 5023-5033.
Stavropoulou, V., S. Kaspar, L. Brault, M. A. Sanders, S. Juge, S. Morettini, A. Tzankov, M. Iacovino, I.-J. Lau and T. A. Milne (2016). "MLL-AF9 expression in hematopoietic stem cells drives a highly invasive AML expressing EMT-related genes linked to poor outcome." Cancer cell **30**(1): 43-58.
Stefanska, M., K. Batta, R. Patel, M. Florkowska, V. Kouskoff and G. Lacaud (2017). "Primitive erythrocytes are generated from hemogenic endothelial cells." Scientific reports **7**(1): 6401.
Stein, E. M., C. D. DiNardo, D. A. Pollyea, A. T. Fathi, G. J. Roboz, J. K. Altman, R. M. Stone, D. J. DeAngelo, R. L. Levine and I. W. Flinn (2017). "Enasidenib in mutant IDH2 relapsed or refractory acute myeloid leukemia." Blood **130**(6): 722-731.
Stewart, S. A., D. M. Dykxhoorn, D. Palliser, H. Mizuno, E. Y. Yu, D. S. An, D. M. Sabatini, I. S. Chen, W. C. Hahn and P. A. Sharp (2003). "Lentivirus-delivered stable gene silencing by RNAi in primary cells." Rna **9**(4): 493-501.
Stone, R. M., S. J. Mandrekar, B. L. Sanford, K. Laumann, S. Geyer, C. D. Bloomfield, C. Thiede, T. W. Prior, K. Döhner and G. Marcucci (2017). "Midostaurin plus chemotherapy for acute myeloid leukemia with a FLT3 mutation." New England Journal of Medicine **377**(5): 454-464.
Su, R., L. Dong, C. Li, S. Nachtergaele, M. Wunderlich, Y. Qing, X. Deng, Y. Wang, X. Weng and C. Hu (2018). "R-2HG exhibits anti-tumor activity by targeting FTO/m6A/MYC/CEBPA signaling." Cell **172**(1-2): 90-105. e123.
Subramanian, A., P. Tamayo, V. K. Mootha, S. Mukherjee, B. L. Ebert, M. A. Gillette, A. Paulovich, S. L. Pomeroy, T. R. Golub and E. S. Lander (2005). "Gene set enrichment analysis: a knowledge-based approach for interpreting genome-wide expression profiles." Proceedings of the National Academy of Sciences **102**(43): 15545-15550.
Sun, J., A. Ramos, B. Chapman, J. B. Johnnidis, L. Le, Y.-J. Ho, A. Klein, O. Hofmann and F. D. Camargo (2014). "Clonal dynamics of native haematopoiesis." Nature **514**(7522): 322.
Swansbury, G., R. Slater, B. Bain, A. Moorman and L. Secker-Walker (1998). Hematological malignancies with t (9; 11)(p21–22; q23)–a laboratory and clinical study of 125 cases, Nature Publishing Group.
Szilvassy, S. J., R. K. Humphries, P. M. Lansdorp, A. C. Eaves and C. J. Eaves (1990). "Quantitative assay for totipotent reconstituting hematopoietic stem cells by a competitive repopulation strategy." Proceedings of the National Academy of Sciences **87**(22): 8736-8740.

Szilvassy, S. J., P. M. Lansdorp, R. K. Humphries, A. C. Eaves and C. J. Eaves (1989). "Isolation in a single step of a highly enriched murine hematopoietic stem cell population with competitive long-term repopulating ability." Blood **74**(3): 930-939.
Szilvassy, S. J., T. E. Meyerrose, P. L. Ragland and B. Grimes (2001). "Differential homing and engraftment properties of hematopoietic progenitor cells from murine bone marrow, mobilized peripheral blood, and fetal liver." Blood **98**(7): 2108-2115.
Tajer, P., K. Pike-Overzet, S. Arias, M. Havenga and F. J. Staal (2019). "Ex vivo expansion of hematopoietic stem cells for therapeutic purposes: lessons from development and the niche." Cells **8**(2): 169.
Takubo, K., G. Nagamatsu, C. I. Kobayashi, A. Nakamura-Ishizu, H. Kobayashi, E. Ikeda, N. Goda, Y. Rahimi, R. S. Johnson and T. Soga (2013). "Regulation of glycolysis by Pdk functions as a metabolic checkpoint for cell cycle quiescence in hematopoietic stem cells." Cell stem cell **12**(1): 49-61.
Tan, A., Y. Dang, G. Chen and Z. Mo (2015). "Overexpression of the fat mass and obesity associated gene (FTO) in breast cancer and its clinical implications." International journal of clinical and experimental pathology **8**(10): 13405.
Tartaglia, L. A., D. Pennica and D. Goeddel (1993). "Ligand passing: the 75-kDa tumor necrosis factor (TNF) receptor recruits TNF for signaling by the 55-kDa TNF receptor." Journal of Biological Chemistry **268**(25): 18542-18548.
Taskesen, E., L. Bullinger, A. Corbacioglu, M. A. Sanders, C. A. Erpelinck, B. J. Wouters, S. C. van der Poel-van de Luytgaarde, F. Damm, J. Krauter, A. Ganser, R. F. Schlenk, B. Lowenberg, R. Delwel, H. Dohner, P. J. Valk and K. Dohner (2011). "Prognostic impact, concurrent genetic mutations, and gene expression features of AML with CEBPA mutations in a cohort of 1182 cytogenetically normal AML patients: further evidence for CEBPA double mutant AML as a distinctive disease entity." Blood **117**(8): 2469-2475.
Taswell, C. (1981). "Limiting dilution assays for the determination of immunocompetent cell frequencies. I. Data analysis." The Journal of Immunology **126**(4): 1614-1619.
Thiel, A. T., P. Blessington, T. Zou, D. Feather, X. Wu, J. Yan, H. Zhang, Z. Liu, P. Ernst and G. A. Koretzky (2010). "MLL-AF9-induced leukemogenesis requires coexpression of the wild-type Mll allele." Cancer cell **17**(2): 148-159.
Thorsteinsdottir, U., E. Kroon, L. Jerome, F. Blasi and G. Sauvageau (2001). "Defining roles for HOX and MEIS1 genes in induction of acute myeloid leukemia." Molecular and cellular biology **21**(1): 224-234.
Thorsteinsdottir, U., G. Sauvageau, M. R. Hough, W. Dragowska, P. M. Lansdorp, H. J. Lawrence, C. Largman and R. K. Humphries (1997). "Overexpression of HOXA10 in murine hematopoietic cells perturbs both myeloid and lymphoid differentiation and leads to acute myeloid leukemia." Molecular and cellular biology **17**(1): 495-505.
Thota, S., A. D. Viny, H. Makishima, B. Spitzer, T. Radivoyevitch, B. Przychodzen, M. A. Sekeres, R. L. Levine and J. P. Maciejewski (2014). "Genetic alterations of the cohesin complex genes in myeloid malignancies." Blood **124**(11): 1790-1798.
Till, J. E. and E. A. McCulloch (1961). "A direct measurement of the radiation sensitivity of normal mouse bone marrow cells." Radiation research **14**(2): 213-222.

Tober, J., A. Koniski, K. E. McGrath, R. Vemishetti, R. Emerson, K. K. de Mesy-Bentley, R. Waugh and J. Palis (2007). "The megakaryocyte lineage originates from hemangioblast precursors and is an integral component both of primitive and of definitive hematopoiesis." Blood **109**(4): 1433-1441.
Tomasson, M. H., Z. Xiang, R. Walgren, Y. Zhao, Y. Kasai, T. Miner, R. E. Ries, O. Lubman, D. H. Fremont, M. D. McLellan, J. E. Payton, P. Westervelt, J. F. DiPersio, D. C. Link, M. J. Walter, T. A. Graubert, M. Watson, J. Baty, S. Heath, W. D. Shannon, R. Nagarajan, C. D. Bloomfield, E. R. Mardis, R. K. Wilson and T. J. Ley (2008). "Somatic mutations and germline sequence variants in the expressed tyrosine kinase genes of patients with de novo acute myeloid leukemia." Blood **111**(9): 4797-4808.
Tong, J., G. Cao, T. Zhang, E. Sefik, M. C. A. Vesely, J. P. Broughton, S. Zhu, H. Li, B. Li and L. Chen (2018). "m 6 A mRNA methylation sustains Treg suppressive functions." Cell research **28**(2): 253.
Tsai, F.-Y., G. Keller, F. C. Kuo, M. Weiss, J. Chen, M. Rosenblatt, F. W. Alt and S. H. Orkin (1994). "An early haematopoietic defect in mice lacking the transcription factor GATA-2." Nature **371**(6494): 221.
Uchida, N. and I. L. Weissman (1992). "Searching for hematopoietic stem cells: evidence that Thy-1.1 lo Lin-Sca-1+ cells are the only stem cells in C57BL/Ka-Thy-1.1 bone marrow." Journal of Experimental Medicine **175**(1): 175-184.
Vardiman, J. W., N. L. Harris and R. D. Brunning (2002). "The World Health Organization (WHO) classification of the myeloid neoplasms." Blood **100**(7): 2292-2302.
Vardiman, J. W., J. Thiele, D. A. Arber, R. D. Brunning, M. J. Borowitz, A. Porwit, N. L. Harris, M. M. Le Beau, E. Hellström-Lindberg and A. Tefferi (2009). "The 2008 revision of the World Health Organization (WHO) classification of myeloid neoplasms and acute leukemia: rationale and important changes." Blood **114**(5): 937-951.
Velasco-Hernandez, T., A. Hyrenius-Wittsten, M. Rehn, D. Bryder and J. Cammenga (2014). "HIF-1α can act as a tumor suppressor gene in murine acute myeloid leukemia." Blood **124**(24): 3597-3607.
Velasco-Hernandez, T., P. Sawen, D. Bryder and J. Cammenga (2016). "Potential Pitfalls of the Mx1-Cre System: Implications for Experimental Modeling of Normal and Malignant Hematopoiesis." Stem Cell Reports **7**(1): 11-18.
Velten, L., S. F. Haas, S. Raffel, S. Blaszkiewicz, S. Islam, B. P. Hennig, C. Hirche, C. Lutz, E. C. Buss and D. Nowak (2017). "Human haematopoietic stem cell lineage commitment is a continuous process." Nature cell biology **19**(4): 271.
Visnjic, D., Z. Kalajzic, D. W. Rowe, V. Katavic, J. Lorenzo and H. L. Aguila (2004). "Hematopoiesis is severely altered in mice with an induced osteoblast deficiency." Blood **103**(9): 3258-3264.
Visvanathan, A., V. Patil, A. Arora, A. Hegde, A. Arivazhagan, V. Santosh and K. Somasundaram (2018). "Essential role of METTL3-mediated m 6 A modification in glioma stem-like cells maintenance and radioresistance." Oncogene **37**(4): 522.
Vo, L. T., M. A. Kinney, X. Liu, Y. Zhang, J. Barragan, P. M. Sousa, D. K. Jha, A. Han, M. Cesana and Z. Shao (2018). "Regulation of embryonic haematopoietic multipotency by EZH1." Nature **553**(7689): 506.

Vu, L. P., B. F. Pickering, Y. Cheng, S. Zaccara, D. Nguyen, G. Minuesa, T. Chou, A. Chow, Y. Saletore, M. MacKay, J. Schulman, C. Famulare, M. Patel, V. M. Klimek, F. E. Garrett-Bakelman, A. Melnick, M. Carroll, C. E. Mason, S. R. Jaffrey and M. G. Kharas (2017). "The N(6)-methyladenosine (m(6)A)-forming enzyme METTL3 controls myeloid differentiation of normal hematopoietic and leukemia cells." Nat Med **23**(11): 1369-1376.
Vukovic, M., A. V. Guitart, C. Sepulveda, A. Villacreces, E. O'duibhir, T. I. Panagopoulou, A. Ivens, J. Menendez-Gonzalez, J. M. Iglesias and L. Allen (2015). "Hif-1α and Hif-2α synergize to suppress AML development but are dispensable for disease maintenance." Journal of Experimental Medicine **212**(13): 2223-2234.
Vukovic, M., C. Sepulveda, C. Subramani, A. V. Guitart, J. Mohr, L. Allen, T. I. Panagopoulou, J. Paris, H. Lawson and A. Villacreces (2016). "Adult hematopoietic stem cells lacking Hif-1α self-renew normally." Blood **127**(23): 2841-2846.
Walter, D., A. Lier, A. Geiselhart, F. B. Thalheimer, S. Huntscha, M. C. Sobotta, B. Moehrle, D. Brocks, I. Bayindir and P. Kaschutnig (2015). "Exit from dormancy provokes DNA-damage-induced attrition in haematopoietic stem cells." Nature **520**(7548): 549.
Wang, H., H. Zuo, J. Liu, F. Wen, Y. Gao, X. Zhu, B. Liu, F. Xiao, W. Wang and G. Huang (2018). "Loss of YTHDF2-mediated m 6 A-dependent mRNA clearance facilitates hematopoietic stem cell regeneration." Cell research **28**(10): 1035.
Wang, P., K. A. Doxtader and Y. Nam (2016). "Structural basis for cooperative function of Mettl3 and Mettl14 methyltransferases." Molecular cell **63**(2): 306-317.
Wang, Q., T. Stacy, M. Binder, M. Marin-Padilla, A. H. Sharpe and N. A. Speck (1996). "Disruption of the Cbfa2 gene causes necrosis and hemorrhaging in the central nervous system and blocks definitive hematopoiesis." Proceedings of the National Academy of Sciences **93**(8): 3444-3449.
Wang, T., H. Yu, N. W. Hughes, B. Liu, A. Kendirli, K. Klein, W. W. Chen, E. S. Lander and D. M. Sabatini (2017). "Gene essentiality profiling reveals gene networks and synthetic lethal interactions with oncogenic Ras." Cell **168**(5): 890-903. e815.
Wang, X., J. Feng, Y. Xue, Z. Guan, D. Zhang, Z. Liu, Z. Gong, Q. Wang, J. Huang and C. Tang (2016). "Structural basis of N 6-adenosine methylation by the METTL3–METTL14 complex." Nature **534**(7608): 575.
Wang, X., Z. Li, B. Kong, C. Song, J. Cong, J. Hou and S. Wang (2017). "Reduced m6A mRNA methylation is correlated with the progression of human cervical cancer." Oncotarget **8**(58): 98918.
Wang, X., Z. Lu, A. Gomez, G. C. Hon, Y. Yue, D. Han, Y. Fu, M. Parisien, Q. Dai and G. Jia (2014). "N 6-methyladenosine-dependent regulation of messenger RNA stability." Nature **505**(7481): 117.
Wang, X., Z. Lu, A. Gomez, G. C. Hon, Y. Yue, D. Han, Y. Fu, M. Parisien, Q. Dai, G. Jia, B. Ren, T. Pan and C. He (2014). "N6-methyladenosine-dependent regulation of messenger RNA stability." Nature **505**(7481): 117-120.
Wang, X., B. S. Zhao, I. A. Roundtree, Z. Lu, D. Han, H. Ma, X. Weng, K. Chen, H. Shi and C. He (2015). "N6-methyladenosine modulates messenger RNA translation efficiency." Cell **161**(6): 1388-1399.

Warda, A. S., J. Kretschmer, P. Hackert, C. Lenz, H. Urlaub, C. Höbartner, K. E. Sloan and M. T. Bohnsack (2017). "Human METTL16 is a N6-methyladenosine (m6A) methyltransferase that targets pre-mRNAs and various non-coding RNAs." EMBO reports **18**(11): 2004-2014.
Wei, C.-M. and B. Moss (1977). "Nucleotide sequences at the N6-methyladenosine sites of HeLa cell messenger ribonucleic acid." Biochemistry **16**(8): 1672-1676.
Wei, J., F. Liu, Z. Lu, Q. Fei, Y. Ai, P. C. He, H. Shi, X. Cui, R. Su and A. Klungland (2018). "Differential m6A, m6Am, and m1A demethylation mediated by FTO in the cell nucleus and cytoplasm." Molecular cell **71**(6): 973-985. e975.
Wen, J., R. Lv, H. Ma, H. Shen, C. He, J. Wang, F. Jiao, H. Liu, P. Yang and L. Tan (2018). "Zc3h13 regulates nuclear RNA m6A methylation and mouse embryonic stem cell self-renewal." Molecular cell **69**(6): 1028-1038. e1026.
Weng, H., H. Huang, H. Wu, X. Qin, B. S. Zhao, L. Dong, H. Shi, J. Skibbe, C. Shen and C. Hu (2018). "METTL14 inhibits hematopoietic stem/progenitor differentiation and promotes leukemogenesis via mRNA m6A modification." Cell Stem Cell **22**(2): 191-205. e199.
Wilkinson, A. C., R. Ishida, M. Kikuchi, K. Sudo, M. Morita, R. V. Crisostomo, R. Yamamoto, K. M. Loh, Y. Nakamura and M. Watanabe (2019). "Long-term ex vivo haematopoietic-stem-cell expansion allows nonconditioned transplantation." Nature: 1.
Wilson, A., E. Laurenti, G. Oser, R. C. van der Wath, W. Blanco-Bose, M. Jaworski, S. Offner, C. F. Dunant, L. Eshkind and E. Bockamp (2008). "Hematopoietic stem cells reversibly switch from dormancy to self-renewal during homeostasis and repair." Cell **135**(6): 1118-1129.
Wilson, C. L. and C. J. Miller (2005). "Simpleaffy: a BioConductor package for Affymetrix Quality Control and data analysis." Bioinformatics **21**(18): 3683-3685.
Wilson, N. K., S. D. Foster, X. Wang, K. Knezevic, J. Schütte, P. Kaimakis, P. M. Chilarska, S. Kinston, W. H. Ouwehand and E. Dzierzak (2010). "Combinatorial transcriptional control in blood stem/progenitor cells: genome-wide analysis of ten major transcriptional regulators." Cell stem cell **7**(4): 532-544.
Wohrer, S., D. J. Knapp, M. R. Copley, C. Benz, D. G. Kent, K. Rowe, S. Babovic, H. Mader, R. A. Oostendorp and C. J. Eaves (2014). "Distinct stromal cell factor combinations can separately control hematopoietic stem cell survival, proliferation, and self-renewal." Cell reports **7**(6): 1956-1967.
Wojtas, M. N., R. R. Pandey, M. Mendel, D. Homolka, R. Sachidanandam and R. S. Pillai (2017). "Regulation of m6A transcripts by the 3'→ 5' RNA helicase YTHDC2 is essential for a successful meiotic program in the mammalian germline." Molecular cell **68**(2): 374-387. e312.
Wong, P., M. Iwasaki, T. C. Somervaille, C. W. E. So and M. L. Cleary (2007). "Meis1 is an essential and rate-limiting regulator of MLL leukemia stem cell potential." Genes & development **21**(21): 2762-2774.
Wu, A., J. Till, L. Siminovitch and E. McCulloch (1967). "A cytological study of the capacity for differentiation of normal hemopoietic colony-forming cells." Journal of cellular physiology **69**(2): 177-184.

Wu, B., S. Su, D. P. Patil, H. Liu, J. Gan, S. R. Jaffrey and J. Ma (2018). "Molecular basis for the specific and multivariant recognitions of RNA substrates by human hnRNP A2/B1." Nature communications **9**(1): 420.
Wu, R., A. Li, B. Sun, J.-G. Sun, J. Zhang, T. Zhang, Y. Chen, Y. Xiao, Y. Gao and Q. Zhang (2019). "A novel m 6 A reader Prrc2a controls oligodendroglial specification and myelination." Cell research **29**(1): 23.
Wu, R., Y. Liu, Y. Yao, Y. Zhao, Z. Bi, Q. Jiang, Q. Liu, M. Cai, F. Wang and Y. Wang (2018). "FTO regulates adipogenesis by controlling cell cycle progression via m6A-YTHDF2 dependent mechanism." Biochimica et Biophysica Acta (BBA)-Molecular and Cell Biology of Lipids **1863**(10): 1323-1330.
Xiang, Y., B. Laurent, C.-H. Hsu, S. Nachtergaele, Z. Lu, W. Sheng, C. Xu, H. Chen, J. Ouyang and S. Wang (2017). "RNA m 6 A methylation regulates the ultraviolet-induced DNA damage response." Nature **543**(7646): 573.
Xiao, W., S. Adhikari, U. Dahal, Y.-S. Chen, Y.-J. Hao, B.-F. Sun, H.-Y. Sun, A. Li, X.-L. Ping and W.-Y. Lai (2016). "Nuclear m6A reader YTHDC1 regulates mRNA splicing." Molecular cell **61**(4): 507-519.
Xie, M., C. Lu, J. Wang, M. D. McLellan, K. J. Johnson, M. C. Wendl, J. F. McMichael, H. K. Schmidt, V. Yellapantula and C. A. Miller (2014). "Age-related mutations associated with clonal hematopoietic expansion and malignancies." Nature medicine **20**(12): 1472.
Xu, C., X. Wang, K. Liu, I. A. Roundtree, W. Tempel, Y. Li, Z. Lu, C. He and J. Min (2014). "Structural basis for selective binding of m 6 A RNA by the YTHDC1 YTH domain." Nature chemical biology **10**(11): 927.
Xu, K., Y. Yang, G.-H. Feng, B.-F. Sun, J.-Q. Chen, Y.-F. Li, Y.-S. Chen, X.-X. Zhang, C.-X. Wang and L.-Y. Jiang (2017). "Mettl3-mediated m 6 A regulates spermatogonial differentiation and meiosis initiation." Cell research **27**(9): 1100.
Yagi, H., K. Deguchi, A. Aono, Y. Tani, T. Kishimoto and T. Komori (1998). "Growth disturbance in fetal liver hematopoiesis of Mll-mutant mice." Blood **92**(1): 108-117.
Yamada, Y., A. J. Warren, C. Dobson, A. Forster, R. Pannell and T. H. Rabbitts (1998). "The T cell leukemia LIM protein Lmo2 is necessary for adult mouse hematopoiesis." Proceedings of the National Academy of Sciences **95**(7): 3890-3895.
Yamamoto, J. F. and M. T. Goodman (2008). "Patterns of leukemia incidence in the United States by subtype and demographic characteristics, 1997–2002." Cancer Causes & Control **19**(4): 379-390.
Yamamoto, R., Y. Morita, J. Ooehara, S. Hamanaka, M. Onodera, K. L. Rudolph, H. Ema and H. Nakauchi (2013). "Clonal analysis unveils self-renewing lineage-restricted progenitors generated directly from hematopoietic stem cells." Cell **154**(5): 1112-1126.
Yamashita, M. and E. Passegué (2019). "TNF-α Coordinates Hematopoietic Stem Cell Survival and Myeloid Regeneration." Cell stem cell.
Yang, L., D. Bryder, J. Adolfsson, J. Nygren, R. Månsson, M. Sigvardsson and S. E. W. Jacobsen (2005). "Identification of Lin–Sca1+ kit+ CD34+ Flt3–short-term hematopoietic stem cells capable of rapidly reconstituting and rescuing myeloablated transplant recipients." Blood **105**(7): 2717-2723.

Yang, S., J. Wei, Y.-H. Cui, G. Park, P. Shah, Y. Deng, A. E. Aplin, Z. Lu, S. Hwang and C. He (2019). "m 6 A mRNA demethylase FTO regulates melanoma tumorigenicity and response to anti-PD-1 blockade." Nature communications **10**(1): 2782.
Yang, X., Y. Yang, B.-F. Sun, Y.-S. Chen, J.-W. Xu, W.-Y. Lai, A. Li, X. Wang, D. P. Bhattarai and W. Xiao (2017). "5-methylcytosine promotes mRNA export—NSUN2 as the methyltransferase and ALYREF as an m 5 C reader." Cell research **27**(5): 606.
Yang, Z., J. Li, G. Feng, S. Gao, Y. Wang, S. Zhang, Y. Liu, L. Ye, Y. Li and X. Zhang (2017). "MicroRNA-145 modulates N6-methyladenosine levels by targeting the 3'-untranslated mRNA region of the N6-methyladenosine binding YTH domain family 2 protein." Journal of Biological Chemistry **292**(9): 3614-3623.
Yao, Q. J., L. Sang, M. Lin, X. Yin, W. Dong, Y. Gong and B. O. Zhou (2018). "Mettl3–Mettl14 methyltransferase complex regulates the quiescence of adult hematopoietic stem cells." Cell research **28**(9): 952.
Yilmaz, Ö. H., M. J. Kiel and S. J. Morrison (2006). "SLAM family markers are conserved among hematopoietic stem cells from old and reconstituted mice and markedly increase their purity." Blood **107**(3): 924-930.
Yu, Q., Y. V. Katlinskaya, C. J. Carbone, B. Zhao, K. V. Katlinski, H. Zheng, M. Guha, N. Li, Q. Chen and T. Yang (2015). "DNA-damage-induced type I interferon promotes senescence and inhibits stem cell function." Cell reports **11**(5): 785-797.
Yue, Y., J. Liu, X. Cui, J. Cao, G. Luo, Z. Zhang, T. Cheng, M. Gao, X. Shu and H. Ma (2018). "VIRMA mediates preferential m 6 A mRNA methylation in 3' UTR and near stop codon and associates with alternative polyadenylation." Cell discovery **4**(1): 10.
Zanjani, E. D., J. L. Ascensao and M. Tavassoli (1993). "Liver-derived fetal hematopoietic stem cells selectively and preferentially home to the fetal bone marrow." Blood **81**(2): 399-404.
Zeisig, B. B., T. Milne, M.-P. García-Cuéllar, S. Schreiner, M.-E. Martin, U. Fuchs, A. Borkhardt, S. K. Chanda, J. Walker and R. Soden (2004). "Hoxa9 and Meis1 are key targets for MLL-ENL-mediated cellular immortalization." Molecular and cellular biology **24**(2): 617-628.
Zhang, C., Y. Chen, B. Sun, L. Wang, Y. Yang, D. Ma, J. Lv, J. Heng, Y. Ding and Y. Xue (2017). "m 6 A modulates haematopoietic stem and progenitor cell specification." Nature **549**(7671): 273.
Zhang, C., D. Samanta, H. Lu, J. W. Bullen, H. Zhang, I. Chen, X. He and G. L. Semenza (2016). "Hypoxia induces the breast cancer stem cell phenotype by HIF-dependent and ALKBH5-mediated m6A-demethylation of NANOG mRNA." Proceedings of the National Academy of Sciences **113**(14): E2047-E2056.
Zhang, F., Y. Kang, M. Wang, Y. Li, T. Xu, W. Yang, H. Song, H. Wu, Q. Shu and P. Jin (2018). "Fragile X mental retardation protein modulates the stability of its m6A-marked messenger RNA targets." Human molecular genetics **27**(22): 3936-3950.
Zhang, J., C. Niu, L. Ye, H. Huang, X. He, W.-G. Tong, J. Ross, J. Haug, T. Johnson and J. Q. Feng (2003). "Identification of the haematopoietic stem cell niche and control of the niche size." Nature **425**(6960): 836.
Zhang, J., J. Pi, Y. Liu, J. Yu and T. Feng (2017). "Knockdown of YTH N6-methyladenosine RNA binding protein 2 (YTHDF2) inhibits proliferation and promotes

apoptosis in MGC-803 gastric cancer cells." Xi bao yu fen zi mian yi xue za zhi= Chinese journal of cellular and molecular immunology **33**(12): 1628-1634.
Zhang, L., N.-T. Tran, H. Su, R. Wang, Y. Lu, H. Tang, S. Aoyagi, A. Guo, A. Khodadadi-Jamayran and D. Zhou (2015). "Cross-talk between PRMT1-mediated methylation and ubiquitylation on RBM15 controls RNA splicing." elife **4**: e07938.
Zhang, S., B. S. Zhao, A. Zhou, K. Lin, S. Zheng, Z. Lu, Y. Chen, E. P. Sulman, K. Xie and O. Bögler (2017). "m6A demethylase ALKBH5 maintains tumorigenicity of glioblastoma stem-like cells by sustaining FOXM1 expression and cell proliferation program." Cancer cell **31**(4): 591-606. e596.
Zhang, Y., S. Gao, J. Xia and F. Liu (2018). "Hematopoietic hierarchy–an updated roadmap." Trends in cell biology **28**(12): 976-986.
Zhang, Y., A. Harada, H. Bluethmann, J. Wang, S. Nakao, N. Mukaida and K. Matsushima (1995). "Tumor necrosis factor (TNF) is a physiologic regulator of hematopoietic progenitor cells: increase of early hematopoietic progenitor cells in TNF receptor p55-deficient mice in vivo and potent inhibition of progenitor cell proliferation by TNF alpha in vitro." Blood **86**(8): 2930-2937.
Zhang, Y., T. Liu, C. A. Meyer, J. Eeckhoute, D. S. Johnson, B. E. Bernstein, C. Nusbaum, R. M. Myers, M. Brown and W. Li (2008). "Model-based analysis of ChIP-Seq (MACS)." Genome biology **9**(9): R137.
Zhao, B. S., I. A. Roundtree and C. He (2017). "Post-transcriptional gene regulation by mRNA modifications." Nature reviews Molecular cell biology **18**(1): 31.
Zhao, B. S., X. Wang, A. V. Beadell, Z. Lu, H. Shi, A. Kuuspalu, R. K. Ho and C. He (2017). "m 6 A-dependent maternal mRNA clearance facilitates zebrafish maternal-to-zygotic transition." Nature **542**(7642): 475.
Zhao, M., J. M. Perry, H. Marshall, A. Venkatraman, P. Qian, X. C. He, J. Ahamed and L. Li (2014). "Megakaryocytes maintain homeostatic quiescence and promote post-injury regeneration of hematopoietic stem cells." Nature medicine **20**(11): 1321.
Zheng, G., J. A. Dahl, Y. Niu, P. Fedorcsak, C.-M. Huang, C. J. Li, C. B. Vågbø, Y. Shi, W.-L. Wang and S.-H. Song (2013). "ALKBH5 is a mammalian RNA demethylase that impacts RNA metabolism and mouse fertility." Molecular cell **49**(1): 18-29.
Zheng, S., E. Papalexi, A. Butler, W. Stephenson and R. Satija (2018). "Molecular transitions in early progenitors during human cord blood hematopoiesis." Molecular systems biology **14**(3).
Zhong, L., D. Liao, M. Zhang, C. Zeng, X. Li, R. Zhang, H. Ma and T. Kang (2019). "YTHDF2 suppresses cell proliferation and growth via destabilizing the EGFR mRNA in hepatocellular carcinoma." Cancer letters **442**: 252-261.
Zhou, J., J. Wan, X. Gao, X. Zhang, S. R. Jaffrey and S.-B. Qian (2015). "Dynamic m 6 A mRNA methylation directs translational control of heat shock response." Nature **526**(7574): 591.
Zhu, T., I. A. Roundtree, P. Wang, X. Wang, L. Wang, C. Sun, Y. Tian, J. Li, C. He and Y. Xu (2014). "Crystal structure of the YTH domain of YTHDF2 reveals mechanism for recognition of N6-methyladenosine." Cell research **24**(12): 1493.